Novel thermal error reduction techniques in temperature domain

Morishima, Takeshi

DOI
10.4233/uuid:ffdfd697-640c-419a-b39a-539d57b17d60

Publication date
2016

Document Version
Final published version

Citation (APA)
Morishima, T. (2016). *Novel thermal error reduction techniques in temperature domain*. [Dissertation (TU Delft), Delft University of Technology]. https://doi.org/10.4233/uuid:ffdfd697-640c-419a-b39a-539d57b17d60

Novel thermal error reduction techniques in temperature domain

PROEFSCHRIFT

ter verkrijging van de graad van doctor
aan de Technische Universiteit Delft,
op gezag van de Rector Magnificus prof.ir. K.C.A.M. Luyben;
voorzitter van het College voor Promoties,
in het openbaar te verdedigen op
maandag 5 decmber 2016 om 12:30 uur

door

Takeshi MORISHIMA

werktuigbouwkundig ingenieur
geboren te Hamakita, Shizuoka, JAPAN

This dissertation has been approved by the
Promotor: Prof.ir. R.H. Munnig Schmidt
Copromotor: Dr.ir. R.A.J. van Ostayen.

Composition of the doctoral committee:

Rector Magnificus	Chairman
Prof.ir. R.H. Munnig Schmidt	Delft University of Technology, promotor
Dr.ir. R.A.J. van Ostayen	Delft University of Technology, copromotor
Independent members:	
Prof.dr.ir. F. van Keulen	Delft University of Technology
Prof.dr.ir. M. Verhaegen	Delft University of Technology
Prof.dr.ir. W.M.J.M. Coene	Delft University of Technology, ASML Netherlands B.V.
Prof.dr. S. Weiland	Eindhoven University of Technology
Dr.ir. T.A.M. Ruijl	MI-partners BV
Prof.dr.ir. J.L. Herder	Delft University of Technology, reserved

This project is funded by the Dutch Ministry of Economic Affairs, the Province of Limburg, the Province of Overijssel, the Province of Noord-Brabant and the cityregion Eindhoven.

Océ and NTS mechatronics have supported this project in the expertise of high precision industrial inkjet printer.

ISBN: 978-94-028-0423-2

Printed in the Netherlands.
An electronic version of this dissertation is available at
http://repository.tudelft.nl/.

Acknowledgment

Six years and five months ago, I started my PhD study in the group of Mechatronic System Design. Many things have changed for and around me during this period. However, looking back at this six and half years period, sometimes I wonder how much wiser I have become. Maybe not at all, or hopefully at least a little bit. And if there is any positive change inside myself, that is attributed to the people who have interacted with me during this period. So I would like to give my sincere appreciation to all people who interacted with me both in and out of my PhD study.

First of all, I would like to express my appreciation for my supervisors. Professor Jan van Eijk shared his vision on this research with me. Initially, it was difficult for me to grasp how far he foresaw the direction of this project even from the beginning. As time went by, I realized more and more his splendid vision and was always impressed by that. Professor Robert Munnig Schmidt was always a great manager and critical thinker. His sharp analyses clarified the most critical points to find the way forward in the project and helped me keep focused on the subject. The daily supervisor Dr. Ron van Ostayen gave me a lot of thought provoking questions. After every meeting, I was a full of exciting questions to think about. Quite often, or almost every time, our discussion went into mathematics. However such mathematical discussions helped me a lot in developing ideas in a logical manner in this research.

This research project was supported by Océ and NTS mechatronics providing the expertise of high precision industrial inkjet printing. Dr. Theo Heeren and Ir. Jos Gunsing, and others from Océ and NTS group helped this project in obtaining practical information on industrial inkjet printers and in developing the experimental setup. Ir. Hylke Veenstra and his colleagues in High Tech Campus branch of Océ helped me a lot in experimental measurement of the printing error of an inkjet printing process.

Also many thanks to Professor Fred van Keulen and his PhD student Evert Hooijkamp for their corporation on thermal studies and thermal modal analysis, and the many useful discussions on subjects related to thermal issues. Professor M. Verhaegen provided a tremendous contribution to the development of the Modal Control technique by offering his knowledge in control theory. And thanks to Arturo Tejada Ruiz, Johan Vogel and Ruxandra Mustata for offering me a nice opportunity to use the experimental temperature control setup for different applications. It was very exciting to work with colleagues who study different subjects that have some important aspects in common.

Some master students from the group of MSD helped this research on the experimental side. Christan Teunissen developed an excellent experimental setup for temperature control by using a large video projector in his master thesis research. Paul Ouwehand and

Rens Berkhof developed and improved an in-plane thermal displacement measurement setup. I really enjoyed working with you guys and our daily discussions on the development of the experimental setups.

I would also like to thank to the staff and my colleagues, Professor Just Herder, Jo Spronck, Rob Luttjeboer, Jasper Wesselingh, Jeroen van Schieveen, Chris Valentin, Guido Delhaes, Rudolf Saathof, Ruijun Deng, Arjan Meskers, Phuc Vuong, Jan Schutten, Johan Vogel, Oscar van den Ven, Patrice Lambert, Pablo Estevez Castillo, Teun Hoevenaars, Saputra, Venkata Girish Kotnur, Maarten van der Seijs, Michael Kirschneck, Selman Tamer, Banafsheh Sajadi, Rob Eling, Rob Dedden, Yueting Liu, Wu Long and many others, for daily discussions and joyful coffee breaks.

I also would like to thank Corinne, Birgit, Marli, Marianne, and Gaby for supporting me with many of the required administrative tasks. Many times, I was helped by your kind support, even before coming to the university and even after leaving the university.

And my deepest appreciation to my wife Atsuko. Whole through my PhD study period, your devoted support helped me in all aspects of my life. It might be a mediocre expression to say "Without your support, I could not finish my PhD study and reach this very date". However, in my case, this was literally the case.

Finally, to our daughter Kaho. You were born just before I finished writing this thesis. Since then, my world has changed completely. Thanks to you, now I feel that I know the reason to be here in this world.

Veldhoven, Oct. 2016
Takeshi Morishima

Summary

The relative importance of thermal errors in precision machines has increased in recent years. The requirements on precision machines such as higher precision and higher productivity become more stringent over product generations. Improved precision of precision machines has increased the importance of thermal errors in precision machines. To increase the productivity of precision machines, more energy needs to be consumed in general, resulting in increased heat generation and thermal errors, and poorer precision performance. To further improve the precision of precision machines while achieving increased productivity at the same time, thermal errors in precision machines need to be studied and reduced further.

This thesis studies reduction techniques of thermal errors using an industrial inkjet printer with a hot melt ink as an example problem. Especially, the thermal displacement error in the printing substrate during the printing process is studied. In this example problem, a moving disturbance load from the hot melt ink and the hot printhead are applied to the substrate and the thermal displacement of the substrate at the moving location of the printhead is minimized to reduce the thermal error during the printing process. This problem is distinctive from other, more conventional, thermal error studies in that both the disturbance load and the point of interest in which the thermal error needs to be minimized are moving during the machine's operation.

Thermal Modal Analysis is used in this thesis to study thermal errors, create a reduced order thermal error model, and develop novel thermal error reduction techniques. Thermal Modal Analysis is a modal analysis technique applied to the temperature domain and thermal displacement domain. Using Thermal Modal Analysis, the temperature distribution of a structure is decomposed into a finite number of thermal modes. Each thermal mode represents a temperature distribution of the structure with a certain spatial frequency and with time-dependent amplitude. The thermal error model is constructed using the thermal displacement shapes associated with the selected thermal modes.

Based on the understanding of thermal errors using Thermal Modal Analysis, we propose two novel thermal error reduction techniques in this thesis. The proposed techniques reduce the thermal error of a structure by controlling the temperature distribution of the structure. The temperature distribution is controlled in these techniques by applying external control heat loads together with a uniform and constant strength cooling.

The first technique developed in the thesis is termed as Mode Cancellation. Mode Cancellation controls the same number of thermal modes in the temperature domain as the number of external control heat loads. Mode Cancellation eliminates a set of thermal modes from the temperature distribution of the structure and eliminates the thermal

displacement fields associated with the controlled thermal modes from the thermal displacement field of the structure. The selection of the thermal modes to be controlled is chosen such that the corresponding thermal displacement fields have the largest contribution to the thermal error. By controlling the temperature distribution of the structure in this way, the dominant thermal displacement fields in the thermal error are eliminated and the thermal error is reduced.

The second technique introduced in the thesis is termed Modal Control. Modal Control calculates the amplitudes of external control heat loads using Linear Quadratic Regulator. This method is developed to overcome the major limitations of Mode Cancellation. The number of controlled thermal modes using this method is not restricted to the number of the external control heat loads. This results in a better thermal error reduction capability compared to Mode Cancellation. Avoiding matrix singularity in the control sensitivity matrix is not required in Modal Control as opposed to the case of Mode Cancellation. This property of Modal Control eliminates the necessity of manual selection of the controlled modes in Mode Cancellation.

It is also shown that it is possible to extend the Modal Control method and implement moving external control heat loads. In the moving external control heat loads case, the control heat loads are placed closer to the moving disturbance heat load and move together with the disturbance load over the target structure. This results in a better thermal error reduction capability than when the external control heat loads are fixed to a target structure such as to each corner of the printing substrate.

An experimental setup has been then developed for conducting experimental Thermal Modal Analysis and experimental validation of the proposed novel thermal error reduction techniques. First, an experimental setup for conducting temperature control and measurement based on thermal modes has been developed and its performances evaluated and corrected. Then experimental measurement of thermal mode shapes of a test substrate has been conducted to validate the method of Thermal Modal Analysis.

After the evaluation of the experimental setup, experimental validation of Mode Cancellation and Modal Control have been conducted. In both experiments, only the temperature distribution of the substrate has been measured as the relation between the temperature distribution and the thermal displacement has already been well established and is not the main objective of the thesis. The results of experimental validation shows good agreement with simulation results, successfully validate the proposed thermal error reduction techniques.

Contents

Nomenclature

Model parameters, variables and functions

ρ	material density	[kg/m^3]
c	specific heat capacity	[J/(K·kg)]
k	thermal conductivity	[W/(K· m)]
α_{EXP}	thermal expansion coefficient	[−]
h	convection coefficient	[W/(K· m)]
L	length of 1D beam	[m]
A	cross sectional area of 1D beam	[m^2]
$L_{\mathrm{x}}, L_{\mathrm{y}}$	length of 2D plate	[m]
w	thickness of 2D plate	[m]
$\boldsymbol{x}$	space variable vector	[m]
x, y	space variable	[m]
t	time variable	[s]
t_k	discrete time step	[s]
$\boldsymbol{T}(\boldsymbol{x}, t)$	temperature field	[K]
$T_{\mathrm{ref}}, T_{\mathrm{nom}}, T_{\mathrm{room}}$	constant temperature value	[K]
$\boldsymbol{C}$	heat capacity matrix	[J/(K·kg)]
$\boldsymbol{K}$	thermal conductivity matrix	[W/(K· m)]
$\boldsymbol{q}(t)$	heat source vector	[W/m^2]
$q(t)$	heat source amplitude	[W/m^2]
$\tau, \tau_{\mathrm{i}}, \tau_{\mathrm{i,j}}$	time constant of a mode	[s]
$\boldsymbol{\phi}_{\mathrm{i}}, \boldsymbol{\phi}_{\mathrm{i,j}}$	thermal mode shape	[K]
$\boldsymbol{\Phi}$	thermal mode shape matrix	[K]
$\theta_{\mathrm{i}}(t), \theta_{\mathrm{i,j}}(t)$	modal amplitude	[−]
$\boldsymbol{\theta}(t)$	modal amplitude vector	[−]
$\boldsymbol{\psi}_{\mathrm{u,i}}, \boldsymbol{\psi}_{\mathrm{u,i,j}}$	thermal displacement field in x-direction corresponding to $\boldsymbol{\phi}_{\mathrm{i}}, \boldsymbol{\phi}_{\mathrm{i,j}}$	[m]
$\boldsymbol{\Psi}_{\mathrm{u}}$	matrix of thermal displacement fields $\boldsymbol{\psi}_{\mathrm{u,i}}, \boldsymbol{\psi}_{\mathrm{u,i,j}}$	[m]
$\boldsymbol{\psi}_{\mathrm{v,i}}, \boldsymbol{\psi}_{\mathrm{v,i,j}}$	thermal displacement field in y-direction corresponding to $\boldsymbol{\phi}_{\mathrm{i}}, \boldsymbol{\phi}_{\mathrm{i,j}}$	[m]
$\boldsymbol{\Psi}_{\mathrm{v}}$	matrix of thermal displacement fields $\boldsymbol{\psi}_{\mathrm{v,i}}, \boldsymbol{\psi}_{\mathrm{v,i,j}}$	[m]
$\boldsymbol{\psi}_{\mathrm{i}}$, $\boldsymbol{\psi}_{\mathrm{i,j}}$	total thermal displacement fields for each location $\boldsymbol{x}$ is defined as $\psi_{\mathrm{i}}(\boldsymbol{x}) = \sqrt{\psi_{\mathrm{u,i}}(\boldsymbol{x})^2 + \psi_{\mathrm{v,i}}(\boldsymbol{x})^2}$, $\psi_{\mathrm{i,j}}(\boldsymbol{x}) = \sqrt{\psi_{\mathrm{u,i,j}}(\boldsymbol{x})^2 + \psi_{\mathrm{v,i,j}}(\boldsymbol{x})^2}$	[m]
$\boldsymbol{\Psi}$	matrix of total thermal displacement fields $\boldsymbol{\psi}_{\mathrm{i}}$, $\boldsymbol{\psi}_{\mathrm{i,j}}$	[m]

$\boldsymbol{U}(t)$	thermal displacement field vector	[m]
$\boldsymbol{u}(t)$	thermal displacement field in x direction	[m]
$\boldsymbol{v}(t)$	thermal displacement field in y direction	[m]
$[C_\mathrm{r}]$	modal capacitance matrix	[(J·K)/kg]
$[K_\mathrm{r}]$	modal conductivity matrix	[(W·K)/m]
$[\frac{1}{\tau_\mathrm{r}}]$	diagonal matrix of inverse time constants	[1/s]
c_i	modal capacitance of mode i	[(J·K)/kg]

Control parameters

J	Objective function for LQR control	[−]
$\boldsymbol{Q}$	state weight matrix	[−]
$Q_\mathrm{i,j}$	(i,j)-th element of state weight matrix	[−]
$\boldsymbol{R}$	control load weight matrix	[−]
$\boldsymbol{I}$	unit matrix	[−]
K	feedback gain	[−]
$\boldsymbol{x}_\mathrm{s}$	state vector	[−]
$\boldsymbol{y}_\mathrm{s}$	output vector	[−]
$\boldsymbol{u}_\mathrm{s}$	input vector	[−]
$\boldsymbol{A}$	state matrix	[−]
$\boldsymbol{B}$	input matrix	[−]
$\boldsymbol{A}_\mathrm{d}$	discrete state matrix	[−]
$\boldsymbol{B}_\mathrm{d}$	discrete input matrix	[−]
$\boldsymbol{C}_\mathrm{d}$	discrete output matrix	[−]
$\boldsymbol{P}$	solution to a Riccati equation	[−]
$\bar{\boldsymbol{O}}$	state matrix for initial state values in static representation	[−]
$\bar{\boldsymbol{H}}_\mathrm{CT}$	input matrix in static representation	[−]
$\boldsymbol{L}$	triangular matrix in modified Cholesky decomposition	[−]
$\boldsymbol{D}$	diagonal matrix in modified Cholesky decomposition	[−]
$\boldsymbol{E}$	diagonal matrix in modified Cholesky decomposition	[−]

List of Figures

Chapter 1

Introduction

1.1 Thermal errors in precision machines

Precision and accuracy has led to a continuous improvement of the performance of a variety of machines, such as telescopes, machine tools, and optical lithography machines among others. The improved accuracy and precision of telescopes have enabled astronomers to study the motion of stars in the sky, which has resulted in the discovery of the laws of motion and put a start to the explosive development of science. Machine tools have enabled accurate metal cutting, which has resulted in a number of things, for example, the realization of the steam engine, which in turn led to the industrial revolution. Optical lithography machines have been continuously shrinking the minimum feature size the machine can produce in high volume, which has then resulted in billions of computers and mobile phones. Aiming for accuracy and precision has always created innovations in human history. Therefore, precision machines have been and will continue to be an important part of our society.

Accuracy requirements for precision machines, such as machine tools, optical lithography machines, and industrial inkjet printers, have been increasing together with the needs for increasing productivity and functionality. Accuracy of precision machines is degraded by multiple error sources, such as vibration, self-weight deformation, and measurement error. One of the dominant error sources which lowers the accuracy of precision machines is thermal deformation of the machine structure [16]. Heat loads inside the machine structure change the temperature distribution within the machine structure. This causes thermal expansion or thermal bending of the machine structure and results in the degradation of the machines functionality as expressed in positioning accuracy, measurement accuracy, and processing accuracy.

Heat generated in precision machines increases with increase in productivity, since increasing productivity requires machines to operate at a higher speed. In many cases this increase is obtained at the cost of an increase in dissipated power and thus heat. Therefore, increasing demands for accuracy and productivity in precision machines are fundamentally conflicting goals. To solve these conflicting issues, thermal errors in precision machines are becoming important issues, as the requirement for accuracy is becoming tighter, while the demand for productivity is increasing simultaneously.

To reduce thermal errors in precision machines, understanding the causes of thermal er-

rors and mechanisms that manifest them from the causes is useful. When machines are in operation, they heat up and become hotter than the surrounding atmosphere. Several components in precision machines such as electric motors and ball bearings produce heat inside the machine structure during its operation. Some machine processes, such as metal cutting or wafer exposure by light, produce heat inside the machine structure.

These heat loads inside the machine structure not only increase the heat of the machine structure themselves, but are also exchanged with the surrounding environment by conduction, convection, and radiation. Heat is transferred from a hot machine to the floor of a factory by thermal conduction through its supports. The temperature of the surrounding air changes over time due to a change of the factory temperature, an air conditioner or the heat produced by the machines on the floor. Convection between machines and the surrounding air mutually connects the temperature changes between the machines and the surrounding air. The sunlight radiating through factory windows warms up the machines. Radiation also emits heat from surfaces of machine parts and exchanges heat among machine parts surfaces. In this way, the temperature distribution within a machine structure has a complex interaction between itself and the surroundings [16].

This thesis aims to contribute to the reduction of thermal errors in precision machines, especially of a class of thermal problems expected in industrial inkjet printers and machines with similar processes in terms of thermal errors.

1.2 Thermal errors in inkjet printers

In this thesis, thermal errors in inkjet printers are studied, as the inkjet printers exhibit an interesting class of thermal error problem in precision machine field, which has not been studied much in the past.

In recent years, inkjet printers have begun to be used not only for graphic applications, but also for manufacturing purposes. One notable trend in recent years is 3D printing by ejecting and depositing materials to create a 3D structure. Other applications are printed electronics or solar cell manufacturing where etching material for PCB production process is printed using inkjet printers. Even more ambitious applications are direct printing of metal lines to print electric circuits directly on a substrate.

For these purposes, several types of ink materials are used other than conventional inks for graphic applications. One of the promising ink materials is known as hot-melt ink, which is solid at room temperature, but liquefies when heated up to around 130 C° [50]. Droplets of the hot liquid ink are ejected from inkjet printing nozzles on a substrate to build functional structures. These hot ink droplets increase the temperature of the substrate during printing. In addition, the inkjet printhead produces heat required to melt the ink, which is transferred to the rest of the machine structure through conduction, to the surrounding air by convection, and to the substrate through convection and radiation. This heat causes the thermal deformation of both, the inkjet printers machine structure and the printing substrate. The thermal deformation of the machine structure may cause an unwanted change of the relative distance between the printhead and the printing position where the droplets are to be ejected, causing degradation of droplet positioning accuracy with respect to the printing substrate. However, more directly, the

thermal deformation of the printing substrate causes the displacement of target printing region on the substrate stage.

As opposed to the conventional thermal error problems in precision machines, these thermal issues result in a new class of problems, which were not the main topics in the thermal error field in the past. The heat loads (the hot droplets and the printhead) move over the substrate; the point where the displacement error needs to be minimized also changes over time as the printing area moves within the substrate as the printing process continues. Therefore, in short, this is a moving load and moving point of interest problem, in contrast to the past when many of the precision machines studied for thermal errors had stationary heat sources and a stationary point of interest.

Optical lithography machines are another example of moving heat load and moving point of interest type of thermal problem.

Exposing a wafer with increasing heat energy causes larger thermal deformation of the wafer and results in thermal displacement error of the exposure region in the wafer [17]. In optical lithography machines, positioning accuracy of the exposure region in a wafer is controlled at increasing accuracy at nanometre level, while heat input to the wafer from exposure light is increased over machine generations to improve the throughput performance. To meet these conflicting demands of increased accuracy and throughput, thermal errors in a wafer under moving heat load need to be reduced at the position of the moving exposure region over the wafer.

1.3 Objectives and contributions of this thesis

By studying the moving heat load and moving point of interest problem, we aim to propose novel thermal error reduction techniques, especially suitable for this class of problems to contribute to the field.
Given the situation of the study on thermal errors in precision engineering context, the goals of this thesis are defined as follows:

- Propose novel thermal error reduction techniques
- Develop guidelines for thermal design

The thesis proposes novel techniques for thermal error reduction. The proposed techniques use Thermal Modal Analysis as a method to analyse the temperature distribution of a machine structure over space and time using thermal modes. In addition, the thermal deformation of the structure that is caused by the temperature distribution of the machine structure is expressed and analysed using the thermal modes. The proposed techniques aim to control the temperature distribution within the machine structure by controlling the thermal modes with large contribution to the thermal error at the point of interest. Its mathematical forms and characteristics are studied. Then, their performances are analysed using simulation. Experimental validation of the methods and development of an experimental setup for the validation are conducted. Design guidelines are developed based on the understanding of the thermal errors obtained through the development of the methods.

The proposed thermal error reduction techniques and thermal error analyses using Thermal Modal Analysis can contribute to the field in the following respects.

(1) The novel thermal error reduction techniques propose to reduce thermal displacement errors by controlling the temperature field by applying and controlling external heat loads rather than compensating for thermal displacement errors. This gives a new class of solutions for thermal error reduction. (2) These techniques can easily handle moving disturbance heat loads and/or moving point of interest problems. This has hardly been studied in the thermal error reduction field, as typical heat loads such as motors, bearings, and process heat are stationary in machine structures, and the point of interest to minimize the thermal displacement such as cutting tool tip or measurement probe position is also stationary. (3) Thermal modes can be used to create a concise dynamic model of temperature distribution and thermal displacement field. It is also possible to understand and control the temperature distribution or thermal displacement field using thermal modes.

1.4 Structure of this thesis

The structure of the thesis is as follows:

In Chapter 2, an overview of thermal errors in precision machines is provided, and the motivation to develop novel thermal error reduction techniques is described.

In Chapter 3, Thermal Modal Analysis is introduced as an analysis tool for temperature distribution and thermal deformation.

In Chapter 4, Mode Cancellation, one of the novel thermal error compensation techniques proposed in this thesis, is introduced based on the understanding of thermal errors in terms of thermal modes described in the previous chapter.

In Chapter 5, Modal Control and its extension to moving external control loads are introduced to solve the limitations of Mode Cancellation and further extend the method.

In Chapter 6, the three proposed novel thermal error compensation techniques are compared. Several issues common to these techniques are discussed.

In Chapter 7, the development and evaluation of an experimental setup for experimental validation of the proposed solutions are described.

In Chapter 8, the results of the experimental validation of the proposed techniques are shown, and the analysis is carried out for the results of the validation and the experimental Thermal Modal Analysis.

Finally in Chapter 9, this thesis has been summarized. It is described what has been achieved in this thesis and future research subjects are suggested.

In Appendix A, the method and a setup for experimental validation of the thermal displacement model based on Thermal Modal Analysis is described.

In Appendix B, the first 10*10 thermal mode shapes and thermal displacement fields that are used in the simulation study in this thesis are displayed.

In Appendix C, the thermal mode shapes and time constants of a 2D rectangular plate are derived analytically.

Chapter 2

Thermal errors in precision engineering

2.1 Introduction

Thermal displacement errors in precision machines can be defined as the change of the relative distance between two points in a machine, such as a tool and a target object caused by the temperature distribution of the machine. The tool and the target object can be a cutting tool and a workpiece to be cut by the tool [38], [19], [54], a measurement probe and an object to be measured [53], [6], [69] or exposure light and an exposure field on a wafer [17], [75], respectively.

Thermal displacement errors occur when a machine structure has a temperature field, which has a uniform but different temperature than the nominal operating temperature condition or the temperature field has a non-uniform spatial distribution. An example of this is a vertical temperature gradient within the machine structure due to the temperature difference between the floor and the ceiling in a factory. A uniform temperature field with a different temperature from its nominal temperature causes a uniform expansion of the machine structure and a shift of the functional point of the machine proportional to the temperature value difference. A non-uniform temperature field causes more complex thermal deformation within the machine structure. One simple example is the thermal bending, which is caused by a temperature gradient along one direction in the machine structure. For example, a horizontally supported cantilever beam with vertical temperature gradient has a different temperature in its upper and lower surfaces and, as a result has different amount of thermal expansion at the top and the bottom. Because of this difference in the amount of thermal expansion, the cantilever bends in vertical direction. Then, the free end point of the cantilever moves both in horizontal and vertical directions, which is a qualitatively different displacement of the point than is the case with a uniform, but different temperature value from the nominal [45].

The change of this relative distance is caused by, for example, a process heat such as cutting heat or absorption of exposure light. Other heat sources can be heat generating machine components (such as a motor or bearing) or environmental influences (such as temperature fluctuation of surrounding air or radiation of sun through factory windows).

The temperature distribution within a machine structure changes over time and space due to heat transfer within the machine structure and between the machine and the environment. Three types of heat transfer processes take place in heat transfer: thermal conduction, convection, and radiation. The heat sources and heat transfer processes are the causes of the temperature distribution and the corresponding thermal deformation of the structure.

Subsequent sections describe the causes of the temperature change, existing solutions to thermal errors, and the remaining challenges in the field. Thermal error compensation is described in more detail, as it is one of the most general and powerful methods to reduce thermal errors in precision machines. Later, the current limitations of these existing approaches are studied and novel thermal error reduction techniques to this class of problems are proposed to overcome some of the major challenges in the field.

2.2 Causes of thermal errors

Heat sources can be classified into several aspects such as either interior or exterior to the structure, static or dynamic, concentrated or distributed, or stationary or moving [16], [84]. Further, types of heat transportation to and from or within the machine structure can be classified into three kinds: conduction, convection, and radiation.

Examples of internal heat sources in precision machines are electric motors and linear motors [42] that convert electrical current into heat due to Joule heating or Eddy current losses losses, and ball bearings, [62] spindles [29], [10], and ball screws [59], [34], [25], [46], [2], [43], which convert mechanical friction in the bearings into heat. Moreover, the machines primal processes often produce heat such as metal cutting process, photo lithography exposure or inkjet printing of hot-melt ink.

Examples of external heat sources in precision machines are heat conduction between the machine and the factory floor, heat convection between the machine and the surrounding air, or the sunlight irradiating through the factory windows [16], [84].

These heat sources are generally dynamic, thus changing their intensity over time, and some sources are distributed over space like surrounding air in the factory or move within a machine like ball screw [2], [43], [46] or inkjet printhead. Generally, a machine structure uses many different materials with different thermal conductivity, heat capacity, and thermal expansion coefficients. This causes different heat conduction within the machine structure or different speed of heat exchange through convection or radiation with the environment. Further, a difference of thermal expansion coefficients within the structure causes thermal bending of the machine even at a uniform temperature different from the reference temperature and may result in large errors [37], [11].

2.3 Remedies for thermal errors

Many different kinds of solutions have been proposed and practiced to reduce thermal errors in precision machines [84], [51], [60], [37]. Major solutions are listed below:

- Reduction of heat source

- Isolation of heat source
- Thermal shielding
- Thermal design
- Forced cooling
- Room temperature control
- Thermal error compensation

These solutions can be categorized into preventive type (isolation of heat source, reduction of heat source, thermal shielding, and thermal design) or treatment type (forced cooling, room temperature control, and thermal error compensation). The preventive type of solutions can reduce thermal errors by removing the cause or reducing the impact of the cause to thermal errors. Even after reducing the impact of thermal sources, the heat that remains may still be too large and the thermal error as a result needs to be reduced. Then treatment type of solutions can further reduce thermal errors by adding counteractions to the thermal error such as cooling or position deviation compensation of the point of interest. Limitations of existing solutions of both types have been overviewed below.

Preventive type solutions

Reduction of a heat source reduces the heat generation inside a machine, and the most straightforward method is to choose components which generate less heat inside the machine. For example, motors with less energy dissipation or bearings with less friction are chosen to reduce heat generation inside the machine during its operation. If such a component is not available, developing a new component which generates less heat than the existing ones of the same kind can be pursued.

Isolation of the heat source surrounds the heat source with thermally insulating or highly resistive material, so that the heat produced in the source does not conduct to the rest of the structure, or at least to the temperature sensitive part of the machine. This approach is applicable when the major sources of heat are identified.

Thermal shielding encloses a machine structure, for example, using high heat conductivity material such as aluminium. Thermal shielding protects the machine from heat disturbances from the surroundings such as air flow in the room or sunlight radiation. In addition, the thermal shielding realizes a uniform temperature distribution within the shielding. Hence, thermal shielding acts as a spatial low pass filter to an external heat load [70], [69].

The purpose of thermal design is to reduce thermal errors of a machine by designing the machine in a way that it will exhibit reduced thermal errors [16], [36], [26], [37]. Material properties such as high thermal conductivity and low thermal expansion coefficient are chosen for reducing temperature non-uniformity and thermal deformation magnitude. The geometry of a machine is designed to reduce thermal deformation of the machine, for example by combining materials with well-chosen different thermal expansion coefficients or by making the machine symmetric along an axis.

Treatment type solutions

Forced cooling utilizes thermal convection and/or thermal conduction processes for the purpose of cooling [88], [7]. The typical media of convection used in high precision systems are air, water, and oil. A liquid medium has larger heat capacities than gaseous medium and thus has a stronger capacity of extracting heat from a machine and control the temperature. However, a liquid medium needs more facilities within the machine structure to handle these cooling media.

In room temperature control, a machine is situated within a temperature-controlled room so that the influence of ambient temperature variations on the machine temperature distribution is minimized. Also, the temperature controlled room works as an air convection cooling for the machine.

Thermal error compensation reduces thermal errors by usually controlling the position of a part of a machine. Compensation can be conducted in feedforward and feedback. Feedforward compensation uses a thermal error model of the target machine together with working conditions of the machine, such as the moving speed of the stage and rotating speed of the spindle. It calculates thermal errors from the model and the machine inputs [72], [76], [64] and compensates for the calculated errors. Feedback compensation is conducted from either direct measurement of the position of interest or prediction of the position from other quantities of the machine. As the direction measurement of the position of interest is not always available due to the difficulty to measure the position in real time [89], prediction of the position of interest from other measured quantities from the machine is more commonly practiced. Prediction of the position of interest requires a model of the machine as well. The model predicts the position change due to thermal errors from operation conditions such as motor speed of the machine or temperature measurements on and in the machine. It is also possible to control the temperature distribution of the machine to reduce thermal errors. However, this approach is less common than the position control approach.

Combination of above solutions

There are some solutions which are a combination of the above-mentioned solutions. One example is to use aluminium as a body frame material of an optical lithography tool [12]. Aluminium has a large thermal expansion coefficient, and therefore, it is not a preferable material for a body frame when considering thermal deformation of the machine. However, aluminium has high thermal conductivity which reduces non-uniformity of the temperature distribution of the machine. Therefore, when it is combined with a cooling system which extracts heat from the whole machine structure by circulating coolant within the machine, the temperature variation of the machine can be controlled well and kept uniform. Therefore, resultant thermal errors of the machine can be reduced by using an aluminium frame combined with a cooling system even though aluminium has large thermal expansion coefficient.

Therefore, as shown in this example, it is possible to solve thermal issues by combining two or more aspects of the existing solutions.

2.4 Major obstacles in reducing thermal errors

Although there have been many different kinds of approaches for the reduction of thermal errors, thermal error problems have not been solved sufficiently yet. This section overviews some of the main obstacles the thermal error issues face and the limitations of the existing solutions.

Reducing heat generation in machine components is the most fundamental solution to the thermal issues, as it reduces the magnitude of the dominant root cause of the problem. However, energy conversion components can fundamentally never have 100% conversion efficiency, and other machine components such as transmissions, bearings, and the like will only approach 100% efficiency. Therefore, as the accuracy requirements on the machine becomes tighter over each generation, continuous improvement of the thermal errors is required. However, this approach has a fundamental limitation. Also, designing a component with less heat generation is usually a time consuming process.

Isolation of heat source works fine when the location of dominant heat sources is or can be positioned far enough or in isolation from a heat sensitive part of the machine. However, this is not always the case, especially when process heat is a dominant heat source.

Thermal shielding is a solution when an external heat source is the dominant heat source. This is often the case for a high precision measurement system. However, this is not suitable for production machines that have heat generating components inside the machines.

Thermal design is a solution to passively reduce the magnitude of thermal errors by design. However, this does not remove the fundamental cause of the problems, but only reduces its magnitude. Therefore, it is not possible to remove the thermal errors completely. Thermal design is usually only possible at the early stage of its design and therefore is hard to be applied at a later stage or to an existing machine.

Forced cooling is one of the most commonly utilized techniques in thermal error reduction, because it effectively extracts heat from a machine and perhaps because of its ease to get installed in a new or already existing machine. However, the performance of forced cooling is limited mainly by its cooling capability, response speed of the cooling medium to changing heat load intensity, and space availability for the cooling apparatus. Forced cooling is not suitable for cases such as when the heat load intensity changes over time, or the heat load intensity is concentrated in a small space where cooling apparatus cannot reach, or the heat load is moving over space. Therefore, although forced cooling is a versatile solution to many thermal issues, not only for displacement but other thermal issues caused by temperature change, it does not always provide the best performance in precision machines.

Room temperature control is a solution to reduce thermal errors caused by external heat loads. Therefore, it basically possesses the same limitations as thermal shielding method.

Thermal displacement errors can be compensated by thermal error compensation to the predicting accuracy of the mathematical model used in the compensation. Stage control performance is usually good enough to compensate thermal errors in terms of accuracy and speed. Therefore, the prediction accuracy of a compensation model is the main limiting factor of this method. The prediction accuracy is mainly limited by model accuracy

and sensor placement limitations. Model accuracy is mainly limited by uncertainty in distributed, non-stationary, non-uniform boundary conditions and material property uncertainties. Sensor placement limitation is determined by the limitations of the number of sensors and effectiveness of sensor locations to predict the temperature distribution within the machine and the thermal error prediction from a finite number of sensor measurements.

2.5 Thermal error compensation

Among the existing solutions described in the previous section, thermal error compensation is a promising solution for precision machines because of the following reasons: (1) the performance of thermal error reduction can be as good as the prediction accuracy of a model, and (2) thermal error compensation is a versatile solution for various kinds of thermal error issues where heat load is internal or external, heat load amplitude is static or dynamic, heat load is localized or distributed in a machine, and so on. Especially the first reason is important for precision machines such as industrial inkjet printers or optical lithography machines where accuracy and throughput requirements become tighter over each product generation.

However, as already described in the previous section, the accuracy of thermal models is limited by model accuracy limitation, especially boundary conditions and sensor placement limitation. Therefore, in this section, different kinds of thermal error compensation techniques are examined to show their capacity to overcome the limiting factors.

Thermal error compensation aims to reduce thermal errors by adjusting the relative position of the point of interest based on the prediction of thermal errors. Often, thermal errors are predicted using an empirical model that connects sensor measurements such as temperature measurement or heat generation to the thermal displacement at the point of interest. Other types of thermal error prediction use a numerical or analytical model of the machine structure. Then these predicted thermal errors are compensated by controlling the location of the point of interest. For example, when the cutting tool of a machine tool heats up and expands, the height of the cutting tool or the position of the workpiece is adjusted to compensate for the relative displacement of the cutting tool with respect to the workpiece.

2.5.1 Empirical approach

Many thermal error models used in existing systems are empirical models. These models basically connect sensor measurements such as temperature values of several different locations within and around the machine structure to the thermal displacement errors at the point of interest, which are measured off-line using a statistical method. Therefore, pure empirical approaches are inevitably black box type of solutions and do not give much insight into the cause or mechanism of thermal errors. Moreover, the performance of an empirical approach is mainly limited by the capability of the mathematical model used to correlate sensor data to thermal error and quality of sensor data.

Least squares method

Least squares method is one of the most standard methods to correlate an experimentally measured thermal displacement at a point of interest to a set of temperature measurements at several locations within the machine [19], [20], [31], [90], [82], [55], [22], [52]. There is also a modification in which the experimentally measured thermal displacement is correlated with the control signal or the estimated heat load for the same moment [14]. Typical mathematical method used is least squares fitting, which minimizes the sum of the square of the differences between the prediction and each test sample point. This method is generally static, which means that at each moment of time, the temperature data measured at several locations within the machine is correlated to the thermal displacement at the point of interest at the same instance of the time. Therefore, it cannot fully capture the dynamics of the temperature and corresponding thermal displacement behaviours. Nevertheless, there are some advantages of the method: (1) it does not require a complex model of the machine, and (2) the correlation is based on the actual measurement, and thus expected to reflect actual machine parameters. And the disadvantages of the method are: (1) the accuracy of the estimation outside the range of learning data is generally not guaranteed, and (2) the performance depends on the locations of the sensors, and especially whether sensors can be placed near the most dominant heat sources. Also, as this category of method is inherently black box type, it does not explain how machine design parameters or a heat load influence the thermal displacement error. Hence, it does not help to improve the machine design to reduce thermal errors from the design stage.

Artificial intelligence

To further improve the fitting performance even outside the learning data, techniques from artificial intelligence may be used. Methods used in this area of research are Artificial Neural Networks (ANN) [20], [31], [80], [32] with slightly different topologies and configuration, Bayesian Network with Support Vector Machine [68], Genetic Algorithm with ANN [30], Fuzzy Logic, and so on. Similar to utilization of artificial intelligence techniques, modelling techniques from control theory can also be utilized such as dynamic modelling using Kalman filter [86] and predictive control [28]. There are many different ways to fit the experimental temperature data to the displacement error. Some are static models, while some use data history to make the model dynamic. However, the fundamental advantages and disadvantages of the methods are the same as least squares fitting.

Transfer function

Similar to the motion control field, it is possible to measure or calculate transfer functions of a thermal system and analyse the behaviour in the frequency domain. In motion control, it is a common practice to use transfer functions for controlling dynamic systems. The reasons are: (1) the behaviour of a target system at a frequency is dominated by a few number of modes due to the resonance phenomenon, and (2) resonance of a mode can cause instability of the system and controlling a system using transfer function is suitable to make it stable. However, temperature fields expressed in the frequency domain do not have these properties. As it will be described in the next chapter, temperature field can be expressed as a linear combination of thermal modes. However, unlike vibration modes, thermal modes do not exhibit resonance and hence, (1) the behaviour of a thermal system at a frequency is generally not dominated by a few number of modes, and (2) the thermal system does not become unstable. Moreover, another demerit of using a transfer function

is that it is basically a point to point function. Therefore, when a heat load is moving or point of interest is moving, such as in inkjet printers or optical lithography, it requires an enormous number of transfer functions measured or calculated for vast combinations of input/output possibilities and interpolations at an intermediate location [15], [65], [35], [56].

2.5.2 Sensor location optimization based on thermal mode shapes

As described in the least squares method, the performance of correlating thermal displacement error to temperature measurement depends on the selection of sensor locations. Therefore, techniques have been developed to obtain the optimal selection of sensor locations [74], [8]. This approach mainly first tries to reconstruct temperature distribution from the measured data at several locations and then tries to estimate the thermal error for the estimated temperature distribution. Therefore, the accuracy of temperature distribution estimation is quite important.

In this estimation, orthogonal decomposition methods are often used. A reduced order model of the temperature distribution in the machine is made up of a set of mutually orthogonal shapes. The sensor locations are optimally selected to best identify the amplitudes of these orthogonal shapes. Using thermal modes as a means to form a reduced order temperature model is one possible method [87], [90], [57], [49]. However, when information on the disturbance is available, it is possible to take the advantage of this information to create more suitable orthogonal shapes that have better reconstruction accuracy for a reduced order model and finite number of sensors. One way to realize this is Proper Orthogonal Decomposition (POD) [8], [47], [48], [1]. Derived shapes based on the POD are dependent on the load pattern. Therefore, it has a better prediction capability for a case like heat loads with fixed location such as motor or bearing heat generation. However, it is not clear how effective this approach can be for the case of moving heat loads. It might be possible to make POD shapes at each location of the possible heat load to have the best accuracy possible.

Another interesting approach in this area is the use of temperature distribution estimation at each location from the sensor measurements by the least squares method [83]. Mathematically this gives the best estimation capability to estimate the temperature distribution from finite sensors in terms of L_2. Although the technique is developed for mechanical deformation estimation in mind, it can be applied to the temperature domain as well. This technique uses a correlation for a given set of sensor locations and therefore it can have better prediction performance in case that the machine space available for sensor placement is limited.

2.5.3 Summary of empirical approaches

In the empirical approach, thermal displacement errors are predicted using the correlation between the errors and the measurement data such as temperature values without deep understanding of the underlying mechanisms of thermal errors. Therefore, the improvement of the performance mainly relies on either improving the correlation model, increasing the number of sensors, or identifying the best locations of sensors. Improvement of the correlation model can be obtained using a more sophisticated mathematical model which has a more powerful expression capability for complex relation between the

sensor measurement and the output. Increasing the number of sensors reduces the degradation of the prediction capability due to the limited amount of input. Identifying the best locations of sensors improves the prediction of the temperature distribution within the machine structure using a given finite number of sensor information.

2.5.4 Analytical and numerical approach

As opposed to the empirical approach, an analytical or numerical approach explicitly uses a model of the machine structure. Heat transfer within the machine and between the machine and the environment are calculated numerically or analytically. Furthermore, sometimes a model of the amount of heat generation by each heat generating component in the machine is also added to the model.

Analytical approaches calculate the thermal behaviour of a target machine from the first principle. Thermal behaviour of a machine structure is modelled analytically and the analytical solution is derived [73], [45]. The influence of design parameters of the machine on the thermal behaviour are described using equations. The relationships between each design parameter and the thermal errors are described in complete detail [62]. Therefore, analytical approaches are useful when modifying and improving machine designs. However, analytical approaches are limited to a rather simple geometry due to the difficulty to derive an analytical solution. In practice, precision machines do not consist only of such simple geometries. Therefore, analytical approaches are useful at an early design stage where only limited information on the machine design is available.

Numerical approaches can deal with a complex geometry, while at the same time they lose some clear connection between each design parameter and the thermal errors. However, these approaches can be still used to modify the design through parameter studies. The disadvantage of numerical approaches is often that the numerical model is generally time consuming and also requires detailed information of the machine, which is sometimes difficult to obtain [11]. This model can also be used for feedforward control of thermal deformation with heat load input identified experimentally or analytically [76].

2.6 Proposed thermal error reduction techniques

One of the common characteristics of the empirical, analytical, and numerical approaches is that they all predict an output from inputs, and hence, thermal displacement error from heat loads or temperature values. As a result, these approaches cannot reduce the thermal displacement itself, but can only reduce the error caused by the displacement by adjusting the position of a part of the machine.

Considering this fundamental limitation of the existing compensation techniques, a new approach to reduce thermal errors is proposed in this thesis. The approach controls the temperature distribution in such a way that the thermal displacement at the point of interest caused by the temperature distribution is reduced. In this way, it is aimed to control thermal displacement in such a way that it results in minimal thermal displacement error. For this, first Thermal Modal Analysis is introduced in the next chapter as it is used as an analytical basis to analyse the thermal displacements. In Chapter 4 and 5, novel solutions are proposed based on the understanding of the thermal displacement error problem.

2.7 Summary and conclusions

Among a plurality of existing solutions for thermal issues, thermal error compensation is one of the promising solutions for precision machines, considering their increasing requirements on both accuracy and productivity. Among different kinds of thermal error compensation approaches, experimental approaches have a drawback; they are heavily dependent on test data and also do not give insight on the thermal behaviour to further improve the machines thermal design. Their advantage includes not requiring any models and also their accuracy for known conditions. Analytical or numerical approaches, on the other hand, require a lot of effort to first make a model of the machine and also need parameter modifications to fit to the experimental data. However, since they provide insight into the thermal behaviour of the system, they can help designers to improve the design or make design decision based on these results. A somewhat intermediate approach is the optimal sensor location approach. This approach identifies orthogonal shapes from the experiment and constructs a reduced order model. It then makes a prediction of the temperature and the thermal displacement of interest based on the finite number of sensor measurements.

Considering the limitations of the current thermal error compensation techniques, novel thermal error reduction techniques were developed, which have been described in the following chapters.

Chapter 3

Thermal modeling methods

3.1 Overview of this chapter

This chapter introduces Thermal Modal Analysis as a novel technique to analyze the heat conduction and the thermal deformation in precision machines for a wide class of thermal problems, especially for moving heat load/moving point of interest problems. This is achieved by constructing a reduced order model of the temperature distribution and the thermal displacement of the target system and analyzing its behavior in terms of modes. First its base idea and mathematics are introduced in section 3.2. Then its characteristics, its advantages and limitations are described in section 3.3. After that some example analyses of the temperature distribution and the thermal displacement using Thermal Modal Analysis are presented in section 3.4. And finally, the method is compared with other thermal analysis techniques such as Finite Element Method, Lumped Heat Capacity Model, Thermal Transfer Function, Proper Orthogonal Decomposition in section 3.5.

3.2 Thermal Modal Analysis

3.2.1 Modal analysis

Thermal Modal Analysis is a kind of modal analysis technique [23] applied in the temperature and the thermal displacement domains. Structural modal analysis is a widely adapted technique to obtain dynamic properties of structures and their dynamic response under dynamic loads through experimental modal testing and the following data processing. The basic idea of modal analysis is that any vibration in a machine structure can be decomposed into a set of discrete modes. These modes have specific eigen-frequencies and specific spatial vibration patterns. These spatial vibration patterns are mutually orthogonal to each other with respect to the mass matrix and the stiffness matrix. Because of this orthogonality, and assuming linearity of the structure's behavior, the dynamic response of the structure for any input pattern can be described as a sum of the modal responses. Modal analysis can also be used to obtain the dynamic properties of the structure such as the natural frequencies of the structure and the transfer functions between a load position to a measurement point.

For the rest of the thesis, this standard modal analysis dealing with structural vibration is

referred to as "structural modal analysis" to distinguish it from Thermal Modal Analysis[1].

3.2.2 Thermal Modal Analysis overview

Thermal Modal Analysis is a modal analysis technique which is applied to the thermal domain [3], [71], [33], [63]. Instead of analyzing mechanical vibrations in a structure, Thermal Modal Analysis analyzes the temperature distribution within a structure and its change over time through heat conduction. Other means of heat transfers such as convection and radiation are modeled as either boundary conditions or as external heat loads which strength and distribution change with the temperature distribution in the structure and environment. A temperature distribution can be decomposed into thermal modes in the same way as vibration modes in structural modal analysis. Each thermal mode has a thermal mode shape which represents the spatial temperature distribution pattern of the structure together with its time constant. Each thermal mode shows a first order time response, so if no external loads are present, the amplitude of each mode decays exponentially in time with the time constant of the mode.

In the next section, the derivation of the thermal mode shapes, time constants, decomposition of temperature distribution into thermal modes, and reconstruction of temperature distribution from thermal modes are described. Also it is shown that the thermal displacement of the structure corresponding to the temperature distribution can also be reconstructed by the thermal mode's amplitudes and the thermal displacement fields corresponding to the thermal mode shapes.

3.2.3 Introduction to thermal modes

In order to study thermal modes, it is useful to discretize the structure into many small elements. Each element has heat capacity c_{i} and is connected to its neighbors by heat conductances $k_{\mathrm{i,j}}$.
According to Fourier's law of heat conduction, the discretized equation of heat conduction in a structure can be described as follows:

$$\boldsymbol{C}\,\dot{\boldsymbol{T}}(t) + \boldsymbol{K}\,\boldsymbol{T}(t) = \boldsymbol{q}(t) \tag{3.1}$$

$\boldsymbol{C}$ is the diagonal capacity matrix of size $N * N$ where N is the number of elements. $\boldsymbol{K}$ is the symmetric conductivity matrix of size $N * N$. $\boldsymbol{T}(t)$ is a vector of size N consisting of the temperature values at each node in the discretized model at time t. $\boldsymbol{q}(t)$ is a vector of size N comprised of all heat loads applied to each node of the target structure at time t.

To derive the thermal mode shapes, consider the following homogeneous equation of the discretized heat conduction equation.

$$\boldsymbol{C}\,\dot{\boldsymbol{T}}(t) + \boldsymbol{K}\,\boldsymbol{T}(t) = \boldsymbol{0} \tag{3.2}$$

In order to solve this equation, the form of the temperature vector $\boldsymbol{T}(t)$ is assumed to be

[1]Strictly speaking, Thermal Modal Analysis is also a modal analysis of structural behavior. Therefore referring to the modal analysis dealing with vibration as "structural modal analysis" is not very precise wording. Nevertheless, this thesis refers to the modal analysis dealing with vibration as "structural modal analysis" to follow the conventional wording.

$\boldsymbol{T}(t) = \bar{\boldsymbol{T}} e^{-\frac{t}{\tau}}$ and is substituted into equation (3.2).

$$\left(-\frac{1}{\tau}\boldsymbol{C} + \boldsymbol{K}\right)\bar{\boldsymbol{T}} e^{-\frac{t}{\tau}} = \boldsymbol{0} \tag{3.3}$$

For the above equation to have non-trivial solution, the following equation needs to hold.

$$\det\left|-\frac{1}{\tau}\boldsymbol{C} + \boldsymbol{K}\right| = 0 \tag{3.4}$$

This equation has N solutions, τ_i (for i=1...N), which are the eigenvalues of the matrix $\left(\frac{-1}{\tau}\boldsymbol{C} + \boldsymbol{K}\right)$. By substituting eigenvalue τ_i into equation (3.3), the corresponding mode shape $\boldsymbol{\phi}_\mathrm{i}$ of the structure, which represents a temperature distribution of the structure, can be derived. The eigenvalue τ_i (for i=1...N) is the time constant of i-th mode.

In this thesis, the theory of modal analysis and newly developed thermal error compensation techniques are described using a simple example structure shown in Figure 3.1. A 2D aluminum plate of 76 mm*44.5 mm is used as an example structure in analyses throughout this thesis. The plate is thermally insulated on all edges. The plate is assumed to be clamped at its left edge and the thermal deformation of the plate is constrained by this mechanical boundary condition.

In this thesis, thermal mode shapes $\boldsymbol{\phi}_\mathrm{i}$ are scaled in such a way that the minimum and the maximum amplitudes of each mode shape are -1 and +1, respectively. In this way, the amplitude of each mode $\theta_\mathrm{i}(t)$, which will be introduced shortly later in this chapter, represents the magnitude of the contribution of the mode in the temperature distribution $\boldsymbol{T}(t)$.

Also thermal mode shapes $\boldsymbol{\phi}_\mathrm{i}$ and thermal displacement fields $\boldsymbol{\psi}_\mathrm{i}$ of any 2D structure are described using two indices such as $\boldsymbol{\phi}_{\mathrm{i,j}}$ and $\boldsymbol{\psi}_{\mathrm{i,j}}$. In this notation, i represents x directional spatial variation of thermal modes and j represents y directional spatial variation of thermal modes. When talking about 1D thermal modes or discussing about thermal modes of any dimensions in general, the single index notation ($\theta_\mathrm{i}, \tau_\mathrm{i}, \phi_\mathrm{i}, \psi_\mathrm{i}$) is used. When 2D thermal modes are specifically discussed, the 2D indices notation ($\theta_{\mathrm{i,j}}, \tau_{\mathrm{i,j}}, \phi_{\mathrm{i,j}}, \psi_{\mathrm{i,j}}$) is used.

The first 5*5 thermal mode shapes of the 2D rectangle aluminum plate are displayed in Figure 3.2. $\boldsymbol{\phi}_{\mathrm{i,j}}$ can generally be calculated by solving the eigen value problem either manually or by using an FEM software. But it can also be calculated analytically for some simple geometry cases like 2D rectangle (Appendix C). Here, "the first 5*5 thermal mode shapes" means mode shapes $\boldsymbol{\phi}_{\mathrm{i,j}}$ in which i and j take a value between 1...5 (therefore (i, j)=(1,1)...(5,5). Figure 3.3 displays the corresponding total thermal displacement fields of the 2D aluminum plate, meaning that each element in the total thermal displacement field $\boldsymbol{\psi}_{\mathrm{i,j}}$ at location $\boldsymbol{x}$ is defined as $\psi_{\mathrm{i,j}}(\boldsymbol{x}) = \sqrt{\psi_{\mathrm{u,i,j}}(\boldsymbol{x})^2 + \psi_{\mathrm{v,i,j}}(\boldsymbol{x})^2}$ where $\boldsymbol{\psi}_{\mathrm{u,i,j}}$ is the thermal displacement field in x direction and $\boldsymbol{\psi}_{\mathrm{v,i,j}}$ is the thermal displacement field in y direction corresponding to mode (i,j) of the plate where the temperature distribution is identical to the thermal mode shape $\boldsymbol{\phi}_{\mathrm{i,j}}$.

Table 3.2 displays the time constants of the first 10*10 thermal mode shapes $\boldsymbol{\phi}_{\mathrm{i,j}}$ of the aluminum plate. These thermal mode shapes, the time constants and the thermal displacement fields of the 2D aluminum plate are calculated using the eigen solution solver of the commercial Finite Element Method software COMSOL [21]. The thermal mode shapes and the time constants for this simple example can also be derived analytically

Table 3.1: Conversion from two indices (i,j) into a single index i for the first 10*10 modes

mode (1,1) → mode 1		⋮
mode (2,1) → mode 2		mode (10,6) → mode 92
mode (1,2) → mode 3		mode (6,10) → mode 93
mode (2,2) → mode 4		mode (10,7) → mode 94
mode (3,1) → mode 5		mode (7,10) → mode 95
mode (1,3) → mode 6		mode (10,8) → mode 96
mode (3,2) → mode 7		mode (8,10) → mode 97
mode (2,3) → mode 8		mode (10,9) → mode 98
mode (3,3) → mode 9		mode (9,10) → mode 99
⋮		mode(10,10) → mode 100

[63]. Also analytically derived thermal mode shapes and time constants for a finite dimension 2D plate is described in Appendix C. In this thesis, thermal modes (and the corresponding thermal mode shapes and time constants) having smaller index values (i, j) are referred to as "lower modes", while thermal modes having larger index values (i, j) are referred to as "higher modes".

However, sometimes, it is beneficial to describe two dimensional modes, which are usually described using two indices like $\phi_{i,j}$, using a single index. For example, in Figure 3.6, convergence of temperature and thermal displacement values at a point with respect to a different number of modes used in reconstruction are compared. In such a case, it is simpler and easier if the two dimensional modes are described using a single index. Therefore, in this thesis, two dimensional modes are sometimes described using a single index when that is suitable. In Table 3.1, the conversion from two dimensional modes described in two indices to a single index used in this thesis is exhibited.[2]

As in structural modal analysis, the time dependent temperature distribution of a struc-

[2]The ordering of the modes in this thesis is made according to ascending indices of the mode shapes rather than descending time constants of the modes. This is different from the convention in Structural Modal Analysis where modes are ordered according to ascending eigen frequency of the modes. When thermal modes are ordered according to the indices, then the modes are ordered in the ascending spatial frequency of the mode shapes. When thermal modes are ordered according to descending time constants, then the spatial frequency of thermal mode shapes is not ordered from low frequency to high frequency. For analyzing the temperature distribution and the thermal displacement field using a reduced order model which contains a limited number of modes, ordering modes and selecting modes in the order of indices is more suitable. However, ordering thermal modes using the time constants seems to be the more practical approach for general cases as time constants can be obtained together with the mode shapes but the spatial frequency components of modes are not obvious in general cases. In that sense, the ordering of modes according to the mode indices chosen in this thesis is convenient for analytical purpose of understanding thermal modal analysis for a simple geometry where you can calculate the thermal mode shapes analytically. But in general case where analytical solution is not available, ordering thermal modes according to time constants is more suitable.

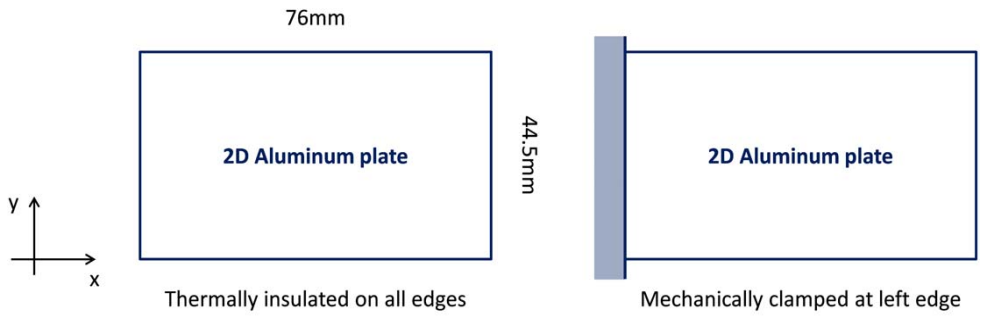

Material property	Value
Thermal conductivity k	201 [W/(K•m)]
Material density ρ	2700 [kg/m^3]
Specific heat capacity c	900 [J/(K•kg)]
Thermal expansion coefficient α_{EXP}	17*10^{-6} [1/K]

Figure 3.1: Dimensions, material properties, and thermal and mechanical boundary conditions of a 2D aluminum plate viewed from above used as an example structure whole through this thesis. Thermal mode shapes of this structure are shown in Figure 3.2 and thermal displacement fields in Figure 3.3 to Figure 3.5. Analyses on thermal modes and thermal mode control in chapter 3 to 5 are conducted for this structure.

ture can be expressed by the sum of these mode shapes times their amplitudes[3] $\theta_{\mathrm{i}}(t)$.

$$\boldsymbol{T}(t) = \sum_{\mathrm{i}=1}^{\mathrm{N}} \boldsymbol{\phi}_{\mathrm{i}} \theta_{\mathrm{i}}(t) = \boldsymbol{\Phi\theta}(t) \tag{3.5}$$

where $\boldsymbol{\Phi}$ is a matrix in which each column consists of mode shape $\boldsymbol{\phi}_{\mathrm{i}}$ and $\boldsymbol{\theta}(t)$ is a vector with modal amplitudes of the corresponding modes. Substitute equation (3.5) into the lumped capacitance heat conduction equation (3.1),

$$\boldsymbol{C\,\Phi\dot{\theta}}(t) + \boldsymbol{K\,\Phi\theta}(t) = \boldsymbol{q}(t) \tag{3.6}$$

Pre-multiply with $\boldsymbol{\Phi}^{\mathrm{T}}$ on both sides of the equation,

$$\boldsymbol{\Phi}^{\mathrm{T}}\boldsymbol{C\,\Phi\dot{\theta}}(t) + \boldsymbol{\Phi}^{\mathrm{T}}\boldsymbol{K\,\Phi\theta}(t) = \boldsymbol{\Phi}^{\mathrm{T}}\boldsymbol{q}(t) \tag{3.7}$$

Due to the orthogonality of the mode shapes with respect to the capacity matrix and the

[3]The units of thermal modal amplitudes $\theta_{\mathrm{i}}(t)$ and thermal mode shapes $\boldsymbol{\phi}_{\mathrm{i}}$ are set as [-] and [K] respectively throughout this thesis. This is because the modal amplitudes $\theta_{\mathrm{i}}(t)$ are also used for reconstructing the thermal displacement field as shown in equation 3.13. Therefore, the unit of the modal amplitudes $\theta_{\mathrm{i}}(t)$ is set to dimensionless ([-]) and the units of the thermal mode shapes $\boldsymbol{\phi}_{\mathrm{i}}$ and the thermal displacement fields $\boldsymbol{\psi}_{\mathrm{u,i}}$ and $\boldsymbol{\psi}_{\mathrm{v,i}}$ are set to [K] and [m]. This is different from a convention that in structural modal analysis, the unit of modal amplitudes are set as [m] and the unit of mode shapes as dimensionless ([-])

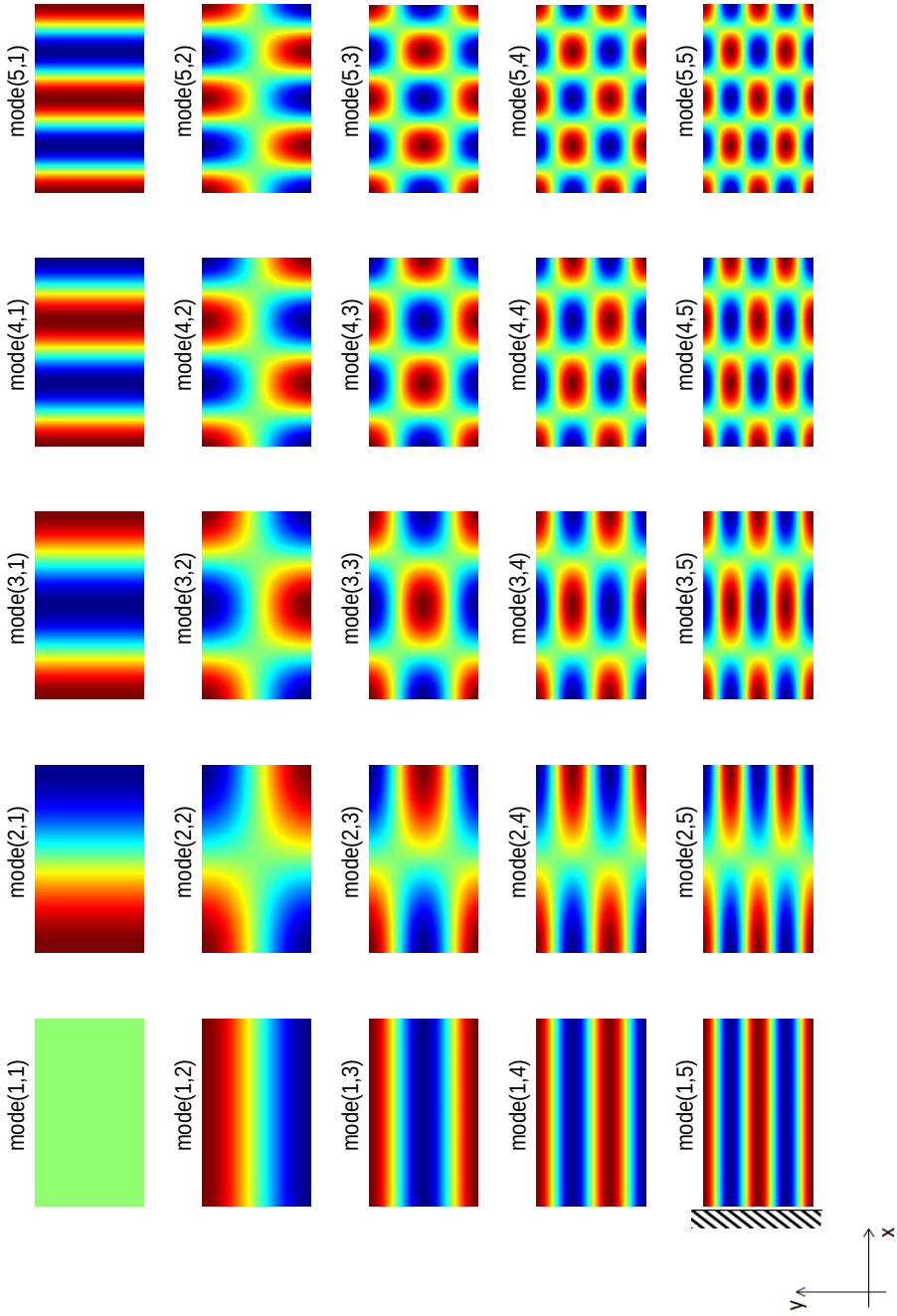

Figure 3.2: Simulated first 5*5 thermal mode shapes of an aluminum plate with thermally insulated boundary conditions using an FEM software COMSOL[21]. The model of the plate used in this calculation is shown in Figure 3.1. The images of the mode shapes are all rotated by 90 degree in this figure. So the clamped left edge of the plate in Fig. 3.1 is now down side of the images. This is the same for Fig. 3.3... Fig. 3.5.

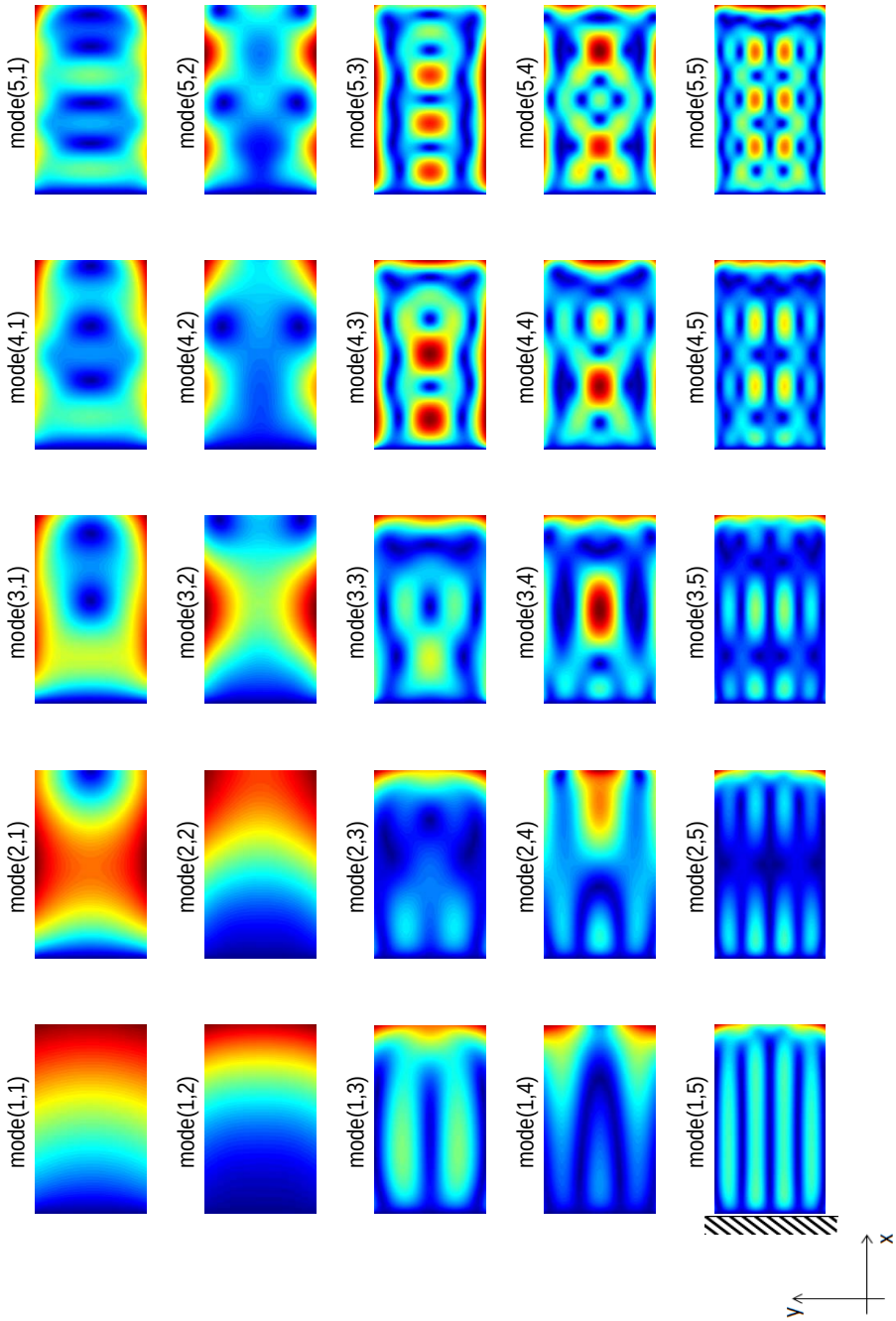

Figure 3.3: Simulated first 5*5 total thermal displacement fields $\sqrt{\psi_{\mathrm{u,i}}^2 + \psi_{\mathrm{v,i}}^2}$ of an aluminum plate. The model of the plate and the software used for this calculation are the same as the ones used for Figure 3.2. The color scales of the displacement fields are different from each other.

conductivity matrix.

$$\boldsymbol{\Phi}^{\mathrm{T}}\boldsymbol{C}\,\boldsymbol{\Phi} = [C_{\mathrm{r}}] \tag{3.8}$$

$$\boldsymbol{\Phi}^{\mathrm{T}}\boldsymbol{K}\,\boldsymbol{\Phi} = [K_{\mathrm{r}}] \tag{3.9}$$

where $[C_{\mathrm{r}}]$ and $[K_{\mathrm{r}}]$ are the diagonal modal capacitance matrix and the diagonal conductivity matrix [4] and the following relation holds:

$$\left[\frac{1}{\tau_{\mathrm{r}}}\right] = [C_{\mathrm{r}}]^{-1}[K_{\mathrm{r}}] \tag{3.10}$$

where $[1/\tau_{\mathrm{r}}]$ is a diagonal matrix of which the diagonal elements are the inverse of the time constant of each mode ($1/\tau_{\mathrm{i}}$ for $\mathrm{i} = 1 \ldots \mathrm{N}$).

From equation (3.8)...(3.10), equation (3.7) becomes:

$$[C_{\mathrm{r}}]\dot{\boldsymbol{\theta}}(t) + [K_{\mathrm{r}}]\boldsymbol{\theta}(t) = \boldsymbol{\Phi}^{\mathrm{T}}\boldsymbol{q}(t) \tag{3.11}$$

$$\dot{\boldsymbol{\theta}}(t) + [1/\tau_{\mathrm{r}}]\boldsymbol{\theta}(t) = [C_{\mathrm{r}}]^{-1}\boldsymbol{\Phi}^{\mathrm{T}}\boldsymbol{q}(t) \tag{3.12}$$

This equation determines the change of the modal amplitudes over time.

Assuming a quasi-static linear thermo-mechanical relation between the temperature distribution and the thermal deformation, the thermal displacement field in the structure can be decomposed into the thermal displacement fields corresponding to the thermal mode shapes.

$$\boldsymbol{U}(t) = \begin{bmatrix} \boldsymbol{u}(t) \\ \boldsymbol{v}(t) \end{bmatrix} = \begin{bmatrix} \sum_{\mathrm{i}=1}^{\mathrm{N}} \boldsymbol{\psi}_{\mathrm{u,i}}\theta_{\mathrm{i}}(t) \\ \sum_{\mathrm{i}=1}^{\mathrm{N}} \boldsymbol{\psi}_{\mathrm{v,i}}\theta_{\mathrm{i}}(t) \end{bmatrix} = \begin{bmatrix} \boldsymbol{\psi}_{\mathrm{u}} \\ \boldsymbol{\psi}_{\mathrm{v}} \end{bmatrix} \boldsymbol{\theta}(t) \tag{3.13}$$

where $\boldsymbol{\psi}_{\mathrm{u,i}}$ and $\boldsymbol{\psi}_{\mathrm{v,i}}$ are the thermal displacement fields of the structure in x and y directions respectively. $\boldsymbol{\psi}_{\mathrm{u}}$ and $\boldsymbol{\psi}_{\mathrm{v}}$ are the matrices with $\boldsymbol{\psi}_{\mathrm{u,i}}$ and $\boldsymbol{\psi}_{\mathrm{v,i}}$ in each column. Each thermal deformation shape $\boldsymbol{\psi}_{\mathrm{u,i}}$ and $\boldsymbol{\psi}_{\mathrm{v,i}}$ can be determined using ,for example, any multi-physics finite element software.

The thermal displacement fields in x and y directions of the example plate shown in Figure 3.1 are shown in Figure 3.4 and 3.5 respectively. These displacement fields are calculated using COMSOL. However these thermal displacement fields are not modes because they are not orthogonal with respect to the capacitance matrix and thermal conductivity matrix in general. Therefore, the thermal displacement field in a machine structure can not directly be decomposed into the thermal displacement fields corresponding to thermal modes but first the temperature distribution needs to be decomposed into thermal modes.

3.2.4 Reduced order thermal model based on thermal modes

As shown in the previous sections, the temperature distribution and the corresponding thermal displacement field in a structure can be reconstructed from the weighted linear

[4] As a result of setting the unit of thermal mode shapes to [K], the units of modal capacitance and modal conductivity are different from the units of thermal capacitance and thermal conductivity themselves which is different from the case of structural modal analysis that modal mass and spring have mass and spring dimensions. However this difference does not pose any problems in calculating the following thermal modal analysis calculations.

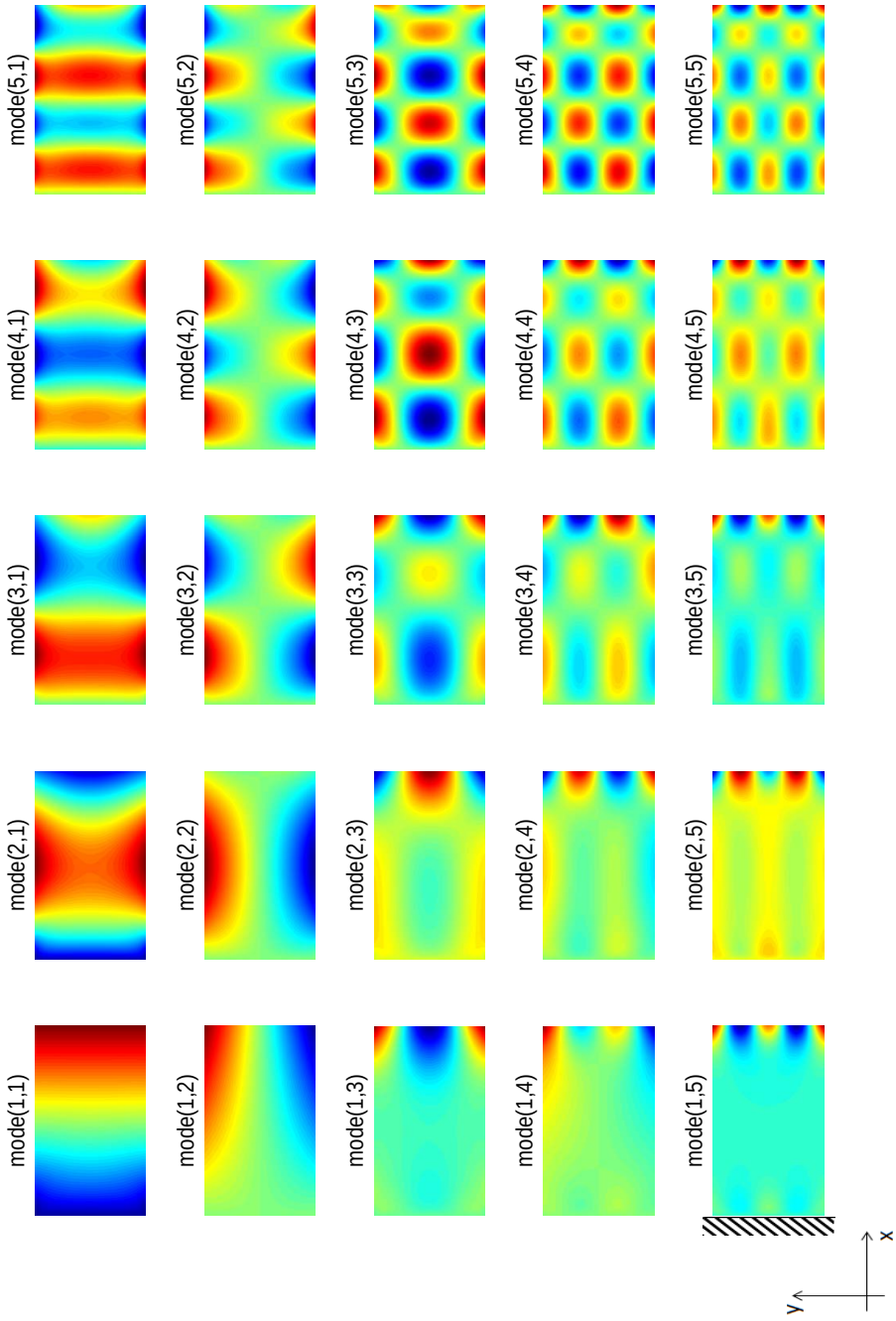

Figure 3.4: Simulated first 5*5 thermal displacement fields of an aluminum plate in x direction. Together with the thermal displacement fields in y-direction displayed in Figure 3.5, it constructs the total thermal displacement fields in Figure 3.3. The color scales of the displacement fields are different from each other.

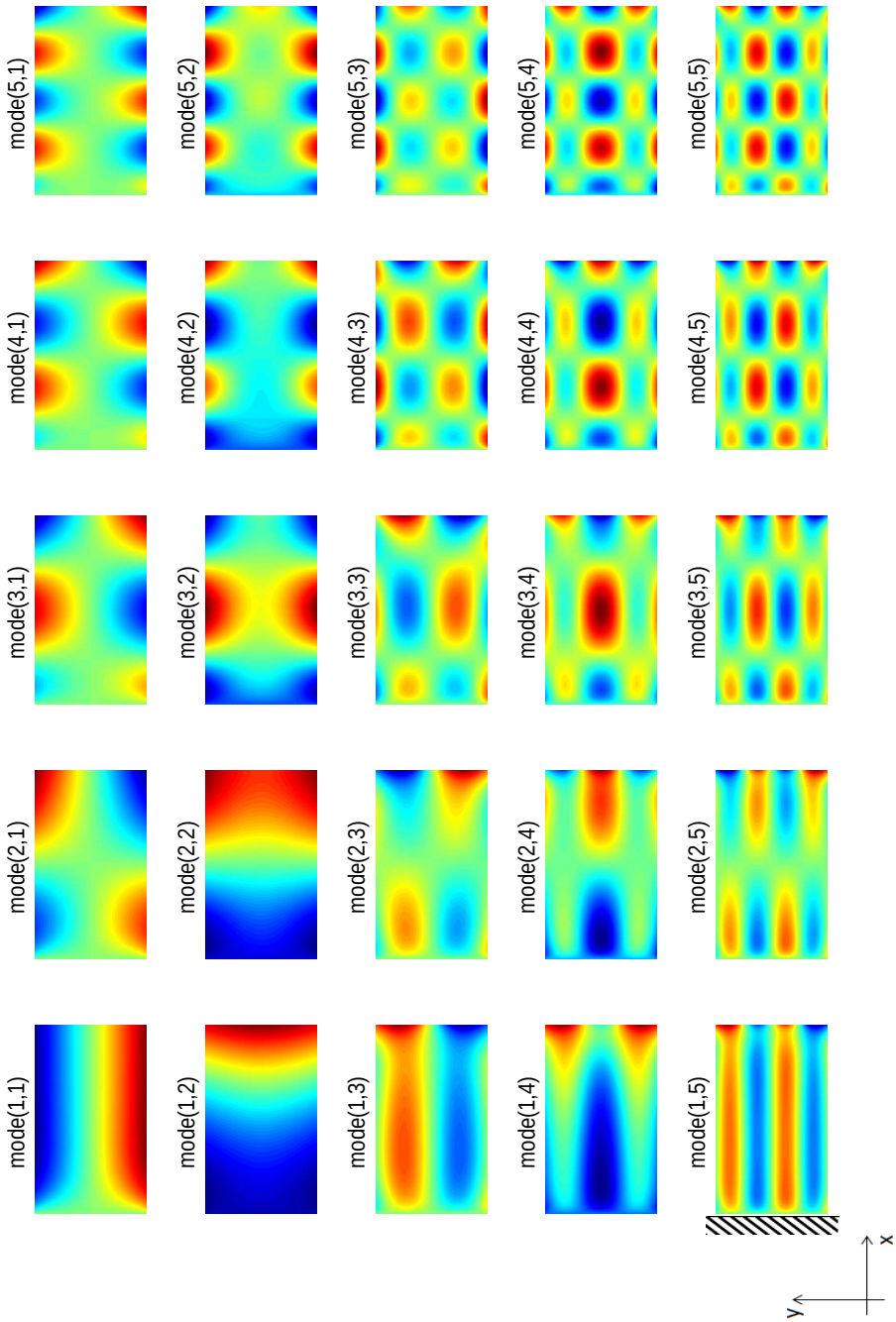

Figure 3.5: Simulated first 5*5 thermal displacement fields of an aluminum plate in y direction. Together with the thermal displacement fields in x-direction displayed in Figure 3.4, it constructs the total thermal displacement fields in Figure 3.3. The color scales of the displacement fields are different from each other.

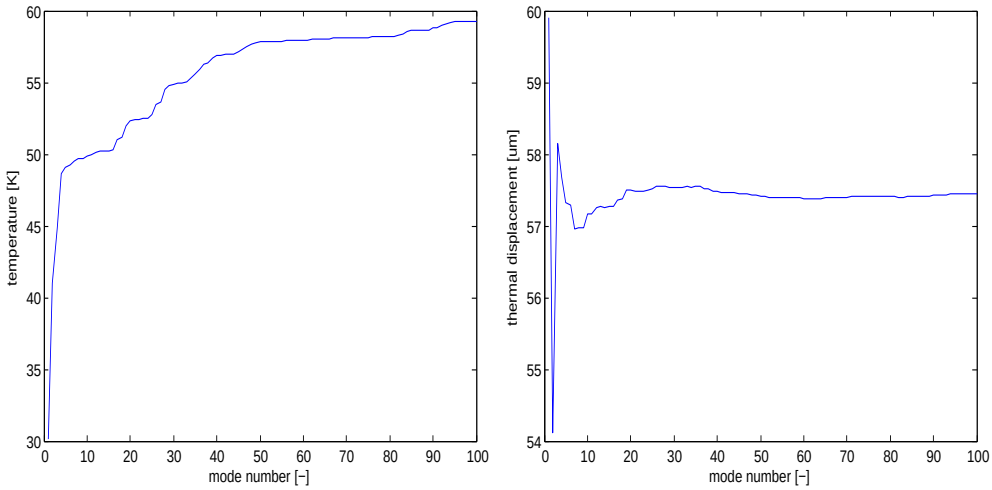

Figure 3.6: Convergence of a temperature value (left) and a total thermal displacement value (right) with respect to the number of modes. The temperature value converges slowly as the number of modes used to reconstruct the temperature field increases. The total thermal displacement value converges quickly with the first 10 modes in the reconstruction.

combination of the thermal modes and the thermal displacement fields. Since each mode shows first order system behavior, its response in time is solely influenced by its time constant τ_i. This τ_i is decreasing for larger values of i which means that modes with higher indices have a faster response speed to inputs but smaller final amplitudes while modes with lower indices have slower response with larger final amplitudes. Figure 3.6 shows the convergence of a reconstructed temperature value at the location of a white arrow shown in Figure 3.7 and the corresponding thermal displacement value at the same location over different number of modes included in the reconstruction. The temperature value requires a large number of modes to obtain an accurate reconstruction. This is due to the sharp temperature peak under the heat load which contains high spatial frequency components. However the thermal displacement at the same location requires a substantially smaller number of corresponding displacement fields. Therefore in the next chapter, a novel technique to control thermal displacement error is introduced. This novel thermal error reduction technique aims at controlling only a small number of modes. This method reduces the magnitude of the low order modes which have large influence to the thermal error. Hence the error at a point of interest is reduced significantly.

3.3 Characteristics and potential use of Thermal Modal Analysis

3.3.1 Characteristics of Thermal Modal Analysis

One of the most important characteristics of Thermal Modal Analysis is that, as in the structural modal analysis, the behavior of the target structure can be predicted by summation of the behavior of all participating modes. The response of each mode can be

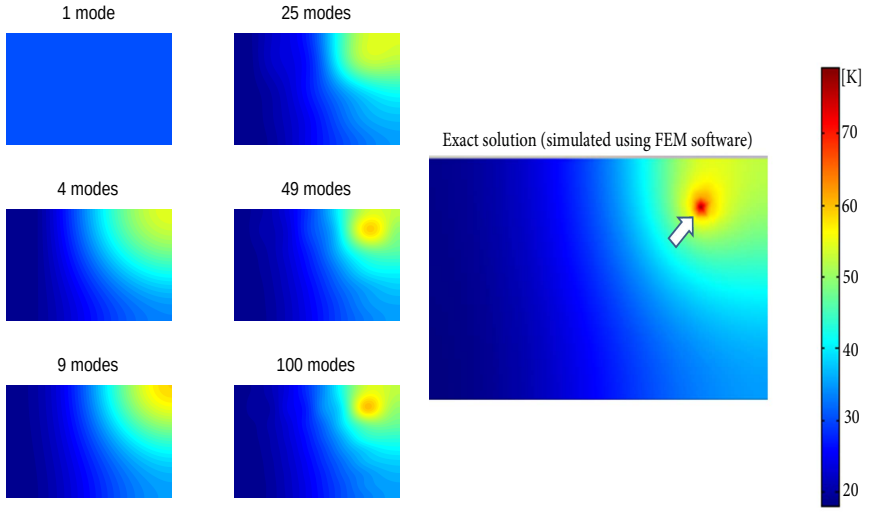

Figure 3.7: A temperature distribution of a rectangular plate as shown in Figure 3.1 is reconstructed using different number of modes (from only the first 1 mode up to the first 10*10 modes) (left). White arrow represents the point where the temperature and thermal displacement values are evaluated in Figure 3.6

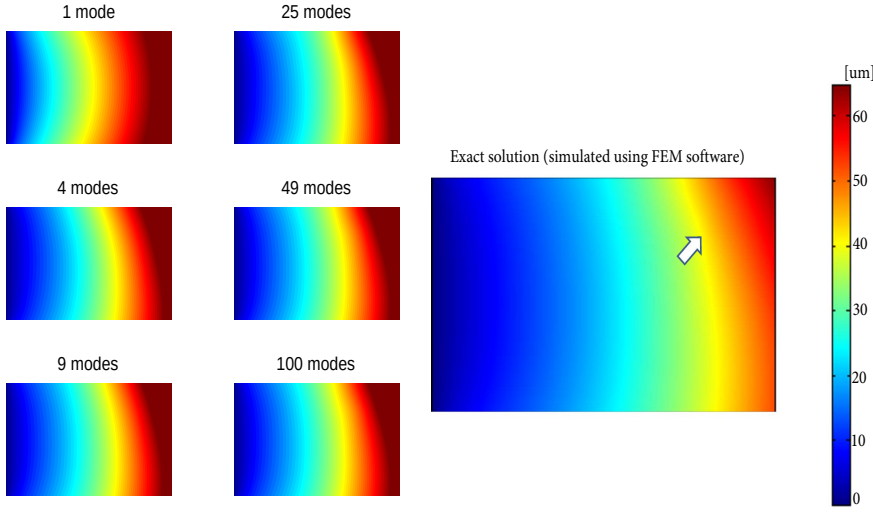

Figure 3.8: The total thermal displacement field (right) corresponding to the temperature distribution in Figure 3.7 is reconstructed using different number of modes (from only the first 1 mode up to the first 10*10 modes) (left). White arrow represents the point where the temperature and thermal displacement values are evaluated in Figure 3.6

Table 3.2: Time constant, first 10*10 modes: Aluminum 76*44.5*0.1 mm: Unit [s]

7.36	3.61	1.43	0.710	0.417	0.273	0.191	0.142	0.109	0.0863
1.82	1.45	0.898	0.549	0.356	0.245	0.177	0.134	0.104	0.0834
0.560	0.519	0.425	0.327	0.247	0.188	0.145	0.115	0.0923	0.0756
0.260	0.251	0.227	0.195	0.164	0.136	0.112	0.0928	0.0776	0.0654
0.149	0.145	0.137	0.125	0.111	0.0974	0.0846	0.0732	0.0634	0.0550
0.0958	0.0945	0.0908	0.0854	0.0787	0.0716	0.0644	0.0576	0.0513	0.0457
0.0668	0.0661	0.0643	0.0615	0.0580	0.0540	0.0498	0.0457	0.0416	0.0378
0.0492	0.0488	0.0478	0.0463	0.0443	0.0419	0.0393	0.0367	0.0340	0.0315
0.0377	0.0375	0.0369	0.0360	0.0347	0.0333	0.0316	0.0299	0.0281	0.0263
0.0298	0.0297	0.0293	0.0287	0.0279	0.0270	0.0259	0.0247	0.0235	0.02223

calculated independently to each other. This allows us to make a reduced order model of the structure which is computationally far less expensive than a full FEM model, for example, while keeping the accuracy high. Some examples will be shown in the next section.

As described in Appendix C, the time constants of a finite dimension 2D plate with uniform material properties are equal to:

$$\tau_{\mathrm{i,j}} = \frac{1}{\frac{k}{\rho c}\left(\left(\frac{(\mathrm{i}-1)\pi}{L_{\mathrm{x}}}\right)^2 + \left(\frac{(\mathrm{j}-1)\pi}{L_{\mathrm{y}}}\right)^2\right) + \frac{2h}{\rho c w}} \tag{3.14}$$

where k is thermal conductivity, ρ is material density, c is heat capacity, L_x and L_y are the length of the plate in x and y directions, h is convection coefficient and w is the width of the plate. The time constants of the thermal modes become shorter as the indices of modes increase (See Figure (3.9)).

The time constants of the modes also influence the amplitudes of thermal modes. For example, when there is a stationary point heat load at $\boldsymbol{x}_0$ with constant amplitude of q_0, then from equation(3.12), the amplitude of mode i is calculated as follows:

$$\dot{\theta}_{\mathrm{i}}(t) + \frac{1}{\tau_{\mathrm{i}}}\theta_{\mathrm{i}}(t) = \frac{1}{c_{\mathrm{i}}}\boldsymbol{\phi}_{\mathrm{i}}(\boldsymbol{x}_0)q_0 \tag{3.15}$$

c_{i} is the modal capacitance of mode i. The solution of the modal amplitude $\theta_i(t)$ becomes:

$$\theta_{\mathrm{i}}(t) = \tau_{\mathrm{i}}\frac{1}{c_{\mathrm{i}}}\boldsymbol{\phi}_{\mathrm{i}}(\boldsymbol{x}_0)q_0\left(1 - e^{-\frac{1}{\tau_{\mathrm{i}}}t}\right) \tag{3.16}$$

So the steady state value of each mode for this heat load becomes as follows:

$$\theta_{\mathrm{i}}(t)|_{t\to\infty} = \tau_{\mathrm{i}}\frac{1}{c_{\mathrm{i}}}\boldsymbol{\phi}_{\mathrm{i}}(\boldsymbol{x}_0)q_0 \tag{3.17}$$

This means that there is a global trend that the modes with large indices have smaller amplitudes because of their fast decay speed within each mode.

Since the time constants become shorter for larger mode indices, the amplitudes of the modes also become smaller as the indices become large (equation (3.17)). On the other

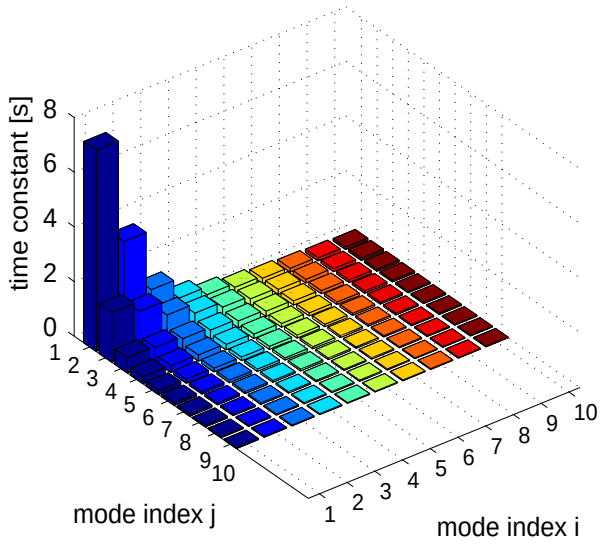

Figure 3.9: Time constants of the first 10*10 modes $\phi_{i,j}$ of the aluminum plate shown in Figure 3.1. Time constants decreases rapidly as the order (indices) of modes increases.

hand, due to the small time constants of modes with larger indices, higher modes react more quickly than lower modes.

Also, as in structural modal analysis, the spatial distribution pattern of each mode never changes over time but only the amplitude of the mode does. Therefore, for example, when there is a temperature distribution which consists of only one mode, then without any external heat loads, the change of the temperature distribution over time occurs such that the overall shape of the temperature distribution remains identical to the initial temperature field shape (e.g. the only mode shape in the temperature distribution at the beginning) while the amplitude of the shape decays exponentially with the time constant of the mode.

This characteristic will be utilized when thermal mode shapes are experimentally obtained from a real structure in a real environment in Chapter 7. Experimental measurement of thermal mode shapes is useful to obtain accurate thermal mode shapes of a real structure by reflecting the influence of boundary conditions in the situation into the mode shapes, which is otherwise difficult to predict by analytical or numerical means. This experimental identification of mode shapes has been studied in [77] and summarized in Chapter 7.

3.3.2 Advantages of using Thermal Modal Analysis

The advantages of Thermal Modal Analysis compared to other thermal modeling methods are summarized in this section:

- Provide a concise thermal model of the thermal displacement field of the structure

- Provide insight into the thermal behavior of the structure

Concise model
Thermal Modal Analysis decomposes the temperature distribution into thermal modes. Temperature distribution usually requires a large number of modes to represent a sharp peak in the temperature field. This sharp local peak in temperature usually occurs if there is a fixed location of the heat source like motor and bearing [3]. However, the corresponding thermal deformation of the structure is mainly dominated by a relatively small number of modes with slower time constants (Figure(3.6)). Therefore a model of the thermal displacement field requires relatively small number of modes, such as 10 modes or 20 modes. Then the model size is small enough to enable a wide range of applications such as real time compensation of thermal error while keeping the accuracy reasonably high.

Insight into the behavior
Thermal mode shapes provide insight into the thermal behavior of the structure by the same mathematics as as those applied for structural vibration [23]. The sensitivity of a mode to a load at each location in the structure is proportional to the value of the mode shape at the same location. For example, the nodes and anti-nodes of a mode shape have the minimum and maximum sensitivity for a heat load applied to the structure, respectively. Excitation of each mode by a heat load can be determined, independent from the other modes, only from the mode shape, the modal amplitude and the heat loads applied to the structure. Also locations of the sensors to measure dominant modes effectively can be rationally selected based on the information of the mode shapes [47].

3.3.3 Limitations of Thermal Modal Analysis

However Thermal Modal Analysis also has some limitations. Major limiting factors of application of Thermal Modal Analysis to thermal modeling are as follows:

- Changing boundary conditions
- Non-linear behavior

First, changing boundary conditions are difficult to take into account in Thermal Modal Analysis. Unlike vibration problems where boundary conditions usually do not change over time and are limited in number by the physical contact points of the machine to the floor, boundary conditions in thermal problems are distributed around the structure and usually changing over time. Heat conduction occurs through the base of the structure to the floor of the factory. Convection occurs from the outer surface of the structure to the environment. The ambient temperature is dynamically changing over time due to the heat exchange with the structure and other influences such as air flow by air conditioners, sun light through the glasses, or heat produced by other adjacent machines. Heat conduction through the structure's bases heats up the floor, changing this boundary condition over time unless the floor is also included in the model. A more practical issue is the changing temperature of the ambient air. The air surrounding the structure heats up by the convection from the machine structure. Air flow occurs around the structure as a result of the air temperature non-uniformity and changing temperature. If the machine has a moving part, the air flow around the part is also disturbed by the movement of the part. For these kinds of changing boundary conditions, one way is to model them as external heat loads at the boundaries. The thermal model in this case can be modeled for thermal

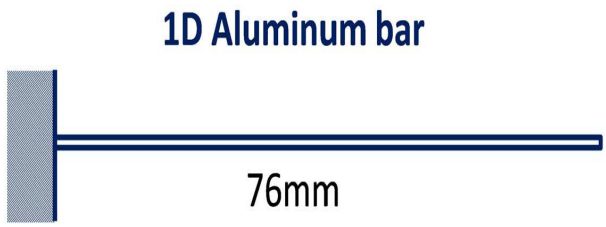

Figure 3.10: 1D beam model used in the analyses shown in chapter 3.4. Temperature variation in the thickness direction and the width direction are ignored and only the variation in the length direction is considered in this 1D model.

insulated boundary conditions. Another way is to assume the boundary conditions to be constant over time. However this of course introduce some errors in the estimation of each modal amplitude and hence prediction accuracy. Therefore how to include the influence of this changing thermal boundary condition is one of the major issues in applying Thermal Modal Analysis into real applications.

Second, the non-linearity of the target structure cannot be reflected in the modal model because the method is based on the assumption that the thermal behavior of the target structure is linear. This will be a problem when the target structure actually shows non-linear behaviors. Examples of non-linear behaviors are non-linear material property within the temperature range of interest or changing contact pressure between mating parts which in turn changes the heat conduction coefficient through the mating parts [78].

3.4 Examples of Thermal Modal Analysis

3.4.1 Temperature field and thermal displacement field calculation using Thermal Modal Analysis

Example 1

The temperature distribution and the corresponding thermal displacement field in an example 1D beam shown in Figure 3.10 are calculated for some example cases using Thermal Modal Analysis. The first 10 thermal mode shapes and thermal displacement fields of the 1D beam are shown in Figure 3.12 and 3.13, respectively.

First, the temperature distribution and the corresponding thermal displacement field under a stationary heat load located in the center of the beam is calculated using Thermal Modal Analysis. The results are compared with the exact solutions in Figure 3.11. The heat load input energy is 1 W/m^2 and the comparisons are made for the temperature distribution and the thermal displacement field at t=2 s.
From Fig 3.11, following things can be observed:

1. The results from Thermal Modal Analysis are closer to the exact solution both in the temperature distribution and the thermal displacement field as the number of modes used in the calculation increases,

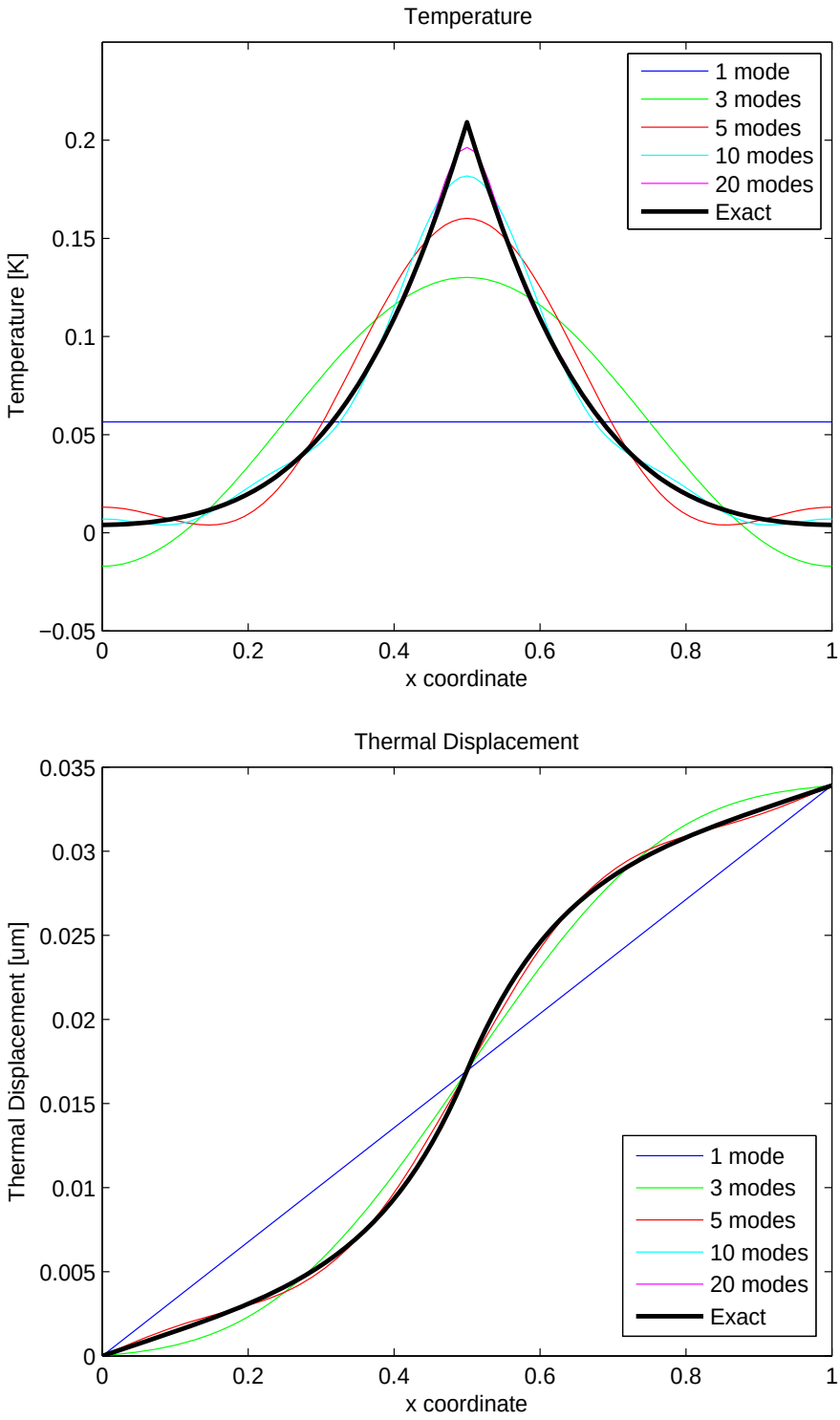

Figure 3.11: (**Example 1: stationary heat load**) Reconstruction of T and U using TMA. Reconstruction using different number of modes are compared with exact solution.

2. The temperature calculation using Thermal Modal Analysis has slower convergence than the thermal displacement field with respect to the number of modes,

3. The error in the temperature distribution using Thermal Modal Analysis is largest at the center location under the stationary heat load.

The second observation indicates that the thermal displacement fields corresponding to higher order thermal modes (the temperature distribution with higher spatial resolution patterns such as modes in the right top in Fig 3.2) do not have a large global contribution. Rather it has a local contribution to the thermal displacement field because of the alternating temperature values in the higher (temperature) mode shapes (see Fig 3.13). As a result, thermal displacement field reconstruction requires a smaller number of modes to provide an accurate reconstruction than required for the temperature reconstruction in general.

The third observation indicates that under a stationary heat load, such as heating up of a machine element like a motor or a bearing where a sharp temperature field occurs around the heat load, the temperature calculation has the largest error. This is because the sharp temperature peak has high spatial frequency components and requires higher order modes to produce an accurate reconstruction of the sharp peak. This is very similar to Fourier series expansion of a pattern with sharp edges where the edges become sharper as higher order components are included into the series. Because of this characteristic of Thermal Modal Analysis, Thermal Modal Analysis has been considered to be an inefficient method to model the temperature distribution [3]. However as described in the second observation, the thermal displacement field reconstruction using Thermal Modal Analysis does not require as many modes as the temperature distribution reconstruction. As described in the previous section, this is one of the advantages using Thermal Modal Analysis in thermal displacement error modeling.

Fig 3.14 shows the amplitudes of the first 12 modes in example 1 above. From the graph, following behaviors of first order systems can be observed:

1. The steady state values are proportional to the input load and the time constant,

2. The slope of the curve depends on the time constants (shorter time constant has sharper slope).

Qualitatively speaking these two behaviors of thermal modes mean that the lower modes can have larger amplitudes compared to higher modes while the speed of the change in the amplitudes are faster in higher modes than lower modes. This can also be observed from the analytical solution of each modal amplitude (Equation 3.16).

Example 2

Another example of Thermal Modal Analysis is shown in Figure 3.15. In this case, a moving heat load is applied over the 1D beam. The heat load moves from the left-end to the right-end at a constant speed over 10 s. The temperature distribution at t=2 s and the corresponding thermal displacement field are calculated using Thermal Modal Analysis and compared with exact solutions.

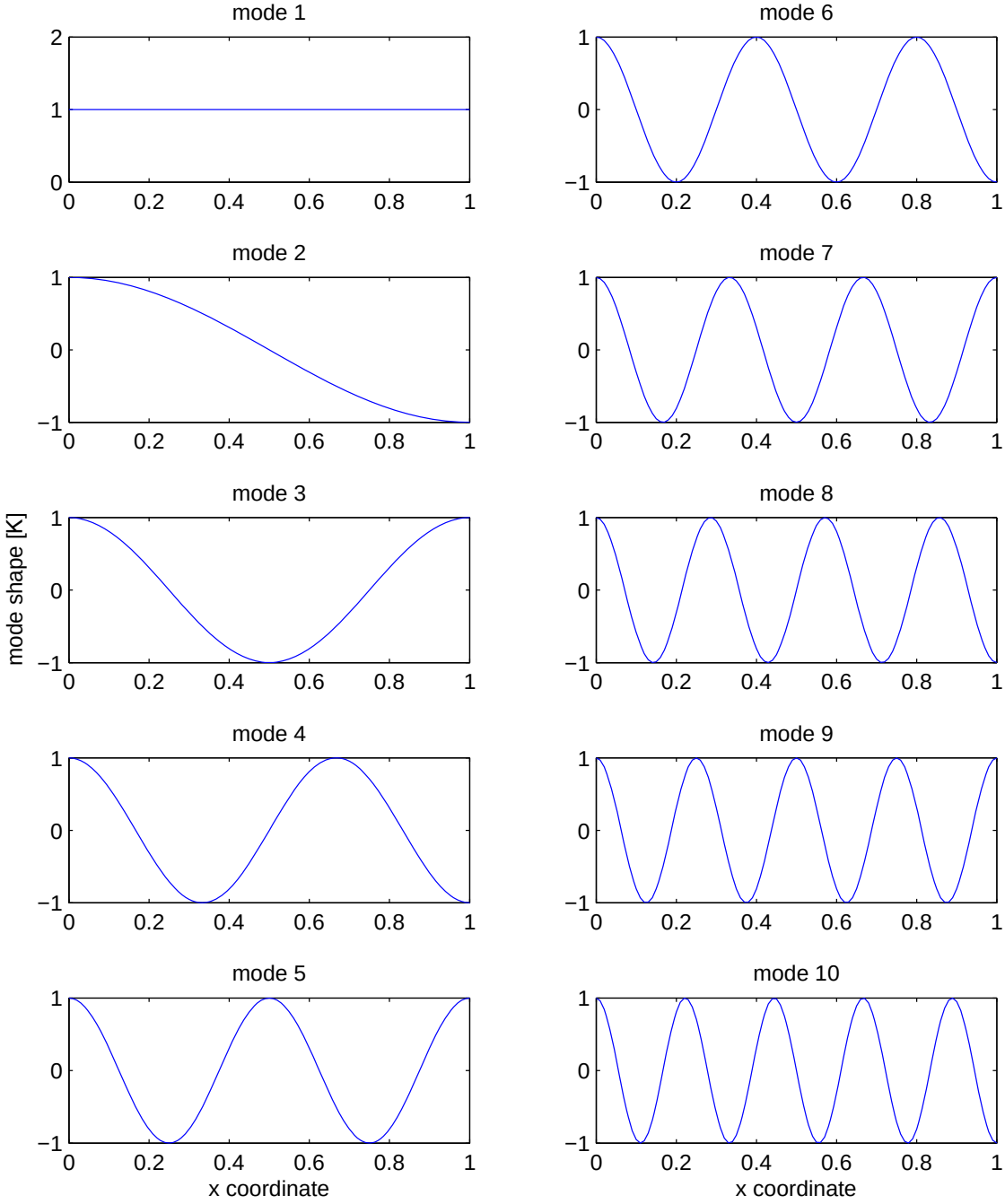

Figure 3.12: First 10 thermal mode shapes of 1D beam. (x coordinate in the graphs are normalized, so the units are dimensionless.)

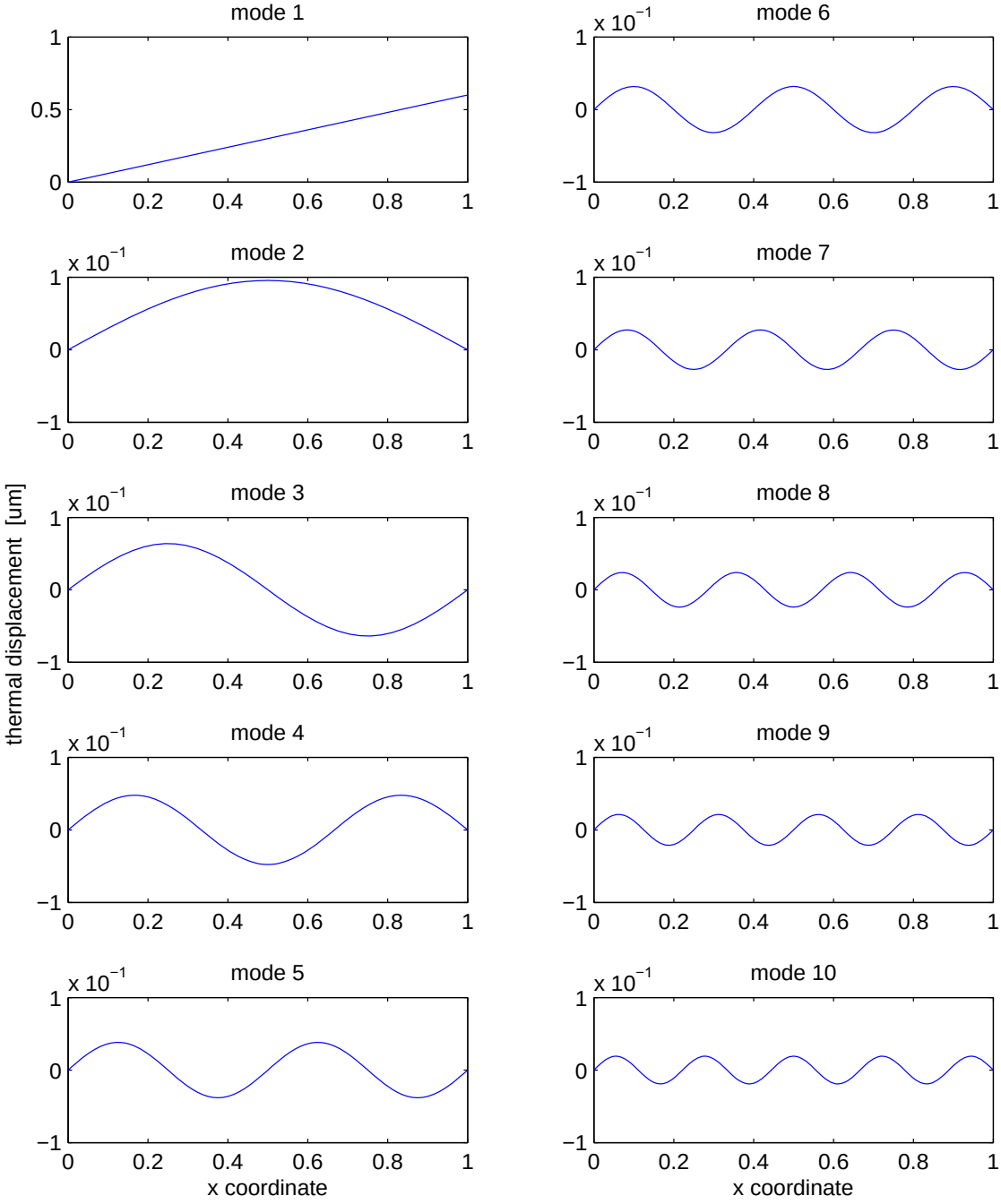

Figure 3.13: First 10 thermal displacement fields corresponding to the thermal modes shown in Fig 3.12. (x coordinate also normalized.)

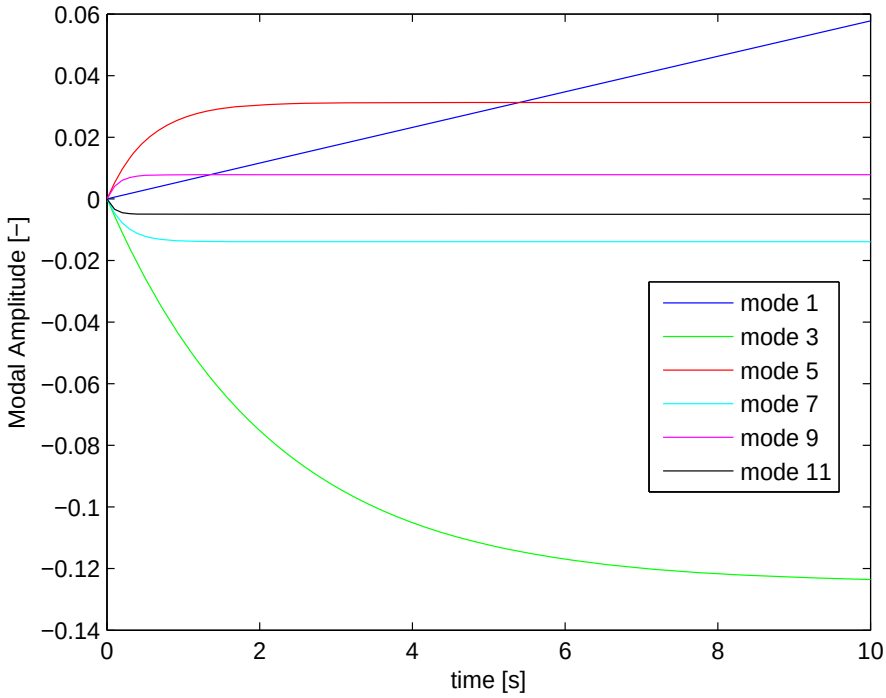

Figure 3.14: The amplitudes of the first 12 thermal modes in example 1. Even order modes are not excited in this example as the heat load is located at the center of the 1D bar and even order modes have zero sensitivity at the center of the 1D beam (Figure 3.12).

As can be seen from the temperature distribution reconstruction using Thermal Modal Analysis, the error in the reconstructed temperature distribution is less prominent compared to the previous case where a sharp peak existed. This is because the moving heat load heats up the whole beam over time and as a result there is no sharp peak in the temperature distribution.

3.5 Comparison with other thermal modeling methods

In this section, comparisons of Thermal Modal Analysis with other existing methods of modeling and solving thermal problems (heat conduction, and temperature distribution calculation and thermal deformation calculation) are provided. These methods are described to describe the advantages and disadvantages of Thermal Modal Analysis. They clarify the benefit of using Thermal Modal Analysis for certain classes of thermal problem over well established methods listed in this section.

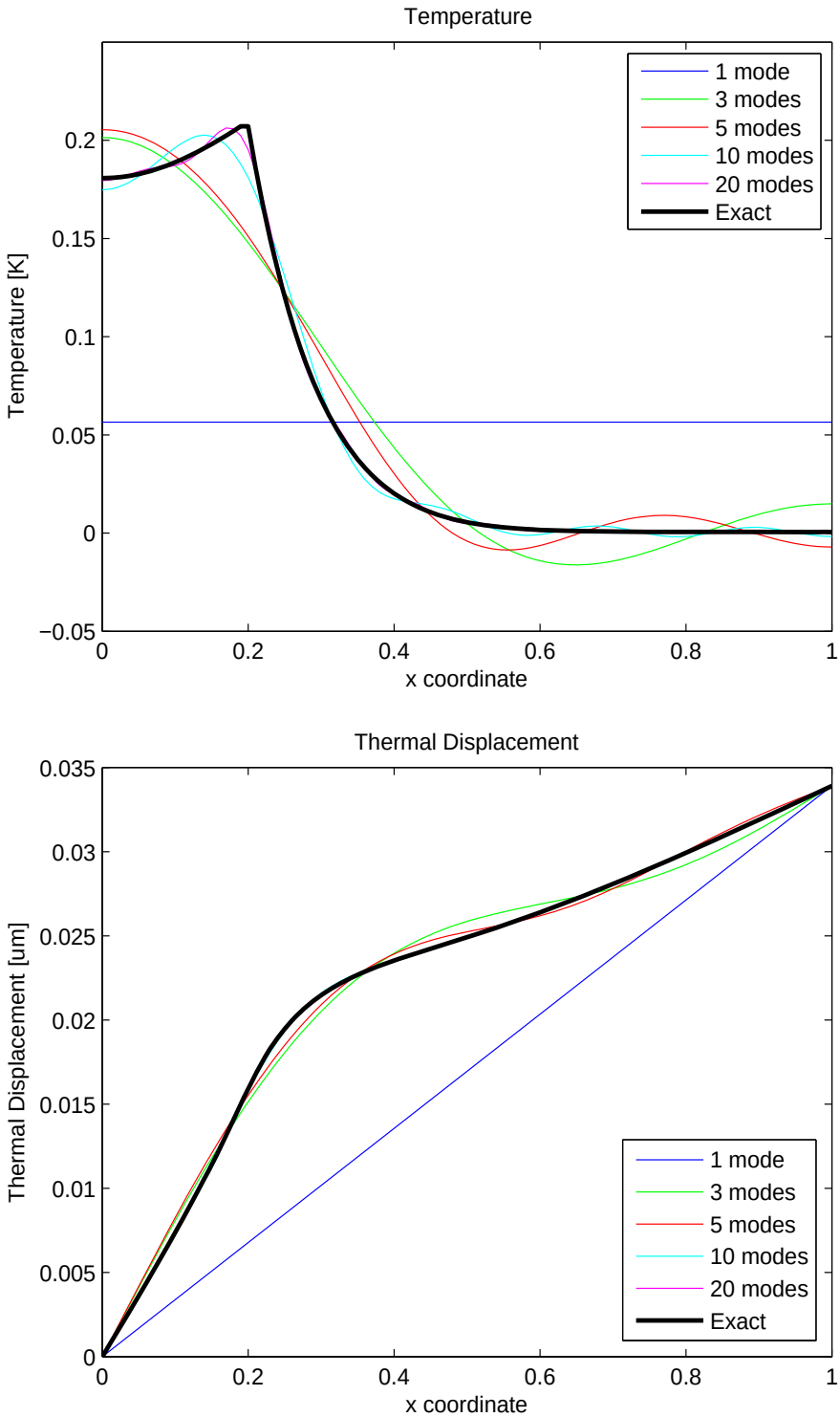

Figure 3.15: (**Example 2: moving heat load**) Reconstruction of T and U using TMA. Reconstruction using different number of modes are compared with exact solution.

3.5.1 Analytical solution for Fourier's equation of heat conduction

Fourier analysis can solve heat conduction problems of simple geometries such as 1D beam, 2D plane, 2D circle, and 3D rectangular cuboid. In these special cases, Fourier analysis gives analytical solutions and these solutions are most accurate and concise for the given problems. However in general, it is not obvious or even not possible to derive the analytical solutions for complex geometries. Even if it is possible to obtain the analytical solution, it does not give a direct answer of how to synthesize a solution to thermal problems of interest in practice. How to create a certain temperature distribution (e.g. what cooling or heating input should be added to the system) or what kind of temperature distribution is desirable to reduce the thermal displacement error at a point of interest cannot be answered directly from the analytical solution. This corresponds to the fact that answering this kind of question is actually the same as solving a dynamic optimization problem and hence is computationally very expensive [40]. Therefore even for a simple geometry case, having the analytical solution is not the only solution to provide a better understanding of the system for further improvement of the thermal design and the thermal control of a target system.

The proposed novel thermal error reduction techniques described later in this thesis (Chapter 4 and 5) utilize Thermal Modal Analysis. These techniques solve the question of what kind of temperature distribution is desirable and how to achieve such a desirable temperature distribution to reduce the thermal displacement error of interest. This can be done because of the characteristics of Thermal Modal Analysis. Different modes have different magnitude of influence to the thermal displacement field of the structure. Therefore an accurate reduced order model can be created by a limited number of modes. And the behavior of each mode in the reduced order model can be obtained independent from the other modes in the reduced order model. In this way, the originally mathematically difficult dynamic optimization problem of how to achieve a certain temperature distribution can be simplified to a less mathematically challenging problem without losing much accuracy in the result.

3.5.2 Transfer function

A transfer function from heat input at a point to the temperature value or thermal displacement at another point can be derived analytically for a simple geometry, or calculated numerically, or measured experimentally in case of complex geometry [65], [15], [35], [56]. Especially an experimentally obtained thermal transfer function gives a realistic model of the system by including the actual conditions of the thermal boundary conditions which is difficult to obtain by analytical modeling alone. It is expected that with sufficient numbers of experiments, it is possible to identify the major thermal modes of a machine structure and to predict transfer functions which are not directly measured experimentally as in structural modal analysis.

Difference from Thermal Modal Analysis is that it is restricted to point-to-point function. Therefore it does not fit to a moving load/moving point of interest problem such as inkjet printing with hot ink or optical lithography process as they require many transfer functions to describe this kind of problems.

3.5.3 Finite Element Method

Finite Element Method (FEM) can obtain detailed computational simulation of the thermal behavior of the system. However this requires detailed information of the machine's geometry, material properties, and the boundary conditions. The method is time consuming to develop and conduct an accurate simulation. Also it is not always clear which part of the model causes the largest error compared to reality and therefore requires further modifications. And this does not directly give insight into the thermal behavior of the system and hence cannot give much insight to how to improve the machine design. Because of these characteristics of FEM, FEM is usually used at the later stage of the design process when the detailed information of geometry and material properties become available.

Finite Difference Element Method (FDEM) is a combination of Finite Difference Method for the temperature field calculation and Finite Element Method for the corresponding thermal displacement field calculation [39], [85], [61], [58]. By doing so the computation time can be reduced. But the basic characteristics and limitations of the method are still the same as Finite Element Method.

Compared to Thermal Modal Analysis, FEM and FDEM are still way computationally expensive methods. Therefore their applications are mainly for the design stage and their use is limited in control or optimization in thermal error compensation.

3.5.4 Thermal network method

The thermal network method models a structure as a network of lumped capacitance elements in which each element has a uniform temperature and is connected to adjacent elements by thermal resistances. Thermal network method is usually applied with large elements, each of which represents a machine part as whole, separated by convection surfaces or contact resistance surfaces. This modeling method, when applied to such large elements, gives an acceptable accuracy under the conditions that the heat conduction within each element is much faster than between the elements so most of the temperature gradient occurs in the connection points. Thermal network model enables a quick, rough estimation of the temperature distribution change in a structure over time without the detailed geometry or material properties information. Therefore it is suitable for evaluating conceptual design at the early stage of design process. However again similar to Finite Element Method, it does not give much insight into what part or aspect of the design most influences the resultant temperature distribution and how to modify the design.

3.5.5 Proper Orthogonal Decomposition

Proper Orthogonal Decomposition (POD) is one of the techniques to make a reduced order model of a system especially when the loads applied to the system are known [18], [41], [47], [1], [81]. POD first calculates POD shapes, which are mutually orthogonal to each other, from sample data which reflects the characteristics of the actual loads expected during the operation. Then these calculated shapes capture the typical temperature distribution caused by the heat loads and the reduced order model constructed from these shapes gives the best reduced order model for a given order of complexity. Then sensor measurements are used to calculate the amplitudes of these shapes in the reduced order model and hence predict the total temperature distribution within the machine from the

sensor measurement during the operation.

Taking advantage of the known load information embedded in the orthogonal shapes, POD is guaranteed to have the most accurate estimation of the temperature distribution for any given number of order reconstructed model in terms of L_2 norm. Therefore POD is a better method compared to the Thermal Modal Analysis in temperature distribution estimation when the heat load pattern is known and does not change at all or not frequently in the application. However the estimation of the amplitudes of these shapes depends on the distribution of the sensors. The accuracy of prediction after all depends on the selection of the sensor locations, which is determined either heuristically or using certain optimal sensor placement algorithm. In [83] the proper orthogonal shapes and the sensor placement are formulated simultaneously to minimize the estimation error rather than first having the set of proper orthogonal shapes and then identify the optimal sensor locations.

As will be introduced and described in the later chapters of this thesis, the proposed thermal error reduction techniques apply external control heat loads to control the temperature distribution of the machine to control and reduce the thermal displacement error. This breaks down the optimality of the calculated POD shapes for the moving disturbance load and these POD shapes are no longer guaranteed to be the optimal set of orthogonal basis. Therefore POD does not fit into the thermal error compensation method proposed in this thesis, at least as it is. Possible extension of the proposed thermal error reduction techniques into POD can be envisioned. However it is not a fundamental issue for the proposed methods whether to use Thermal Modal Analysis or POD as the modeling method. This will be discussed in chapter 6 as recommendation for future research and not further studied in this thesis.

3.6 Conclusions

This chapter provided a mathematical formulation of Thermal Modal Analysis and described its characteristics and some examples. A short evaluation of other known analysis methods has been presented to compare the pros and cons of the existing methods with respect to Thermal Modal Analysis. The Thermal Modal Analysis is an useful tool for obtaining insights into the system behavior and developing ideas for design improvement. Additionally, for a moving load/moving point of interest problem, using Thermal Modal Analysis is a more effective method than deriving a transfer function as it is not based on point-to-point function.

Proper Orthogonal Decomposition is also an interesting reduced order modeling method, but it does not directly fit into the proposed thermal error reduction techniques in this thesis, therefore it has not been further studied in this research. However the future research possibility is discussed in chapter 6 and 9.

Chapter 4

Thermal error compensation

4.1 Overview of this chapter

In this chapter and the next chapter, three novel thermal error compensation techniques based on Thermal Modal Analysis are introduced. These are Mode Cancellation, Modal Control with Linear Quadratic Regulator, and Modal Control adapted to moving external heat load control.

In chapter 2, several types of existing solutions have been introduced. Cooling is an effective means to reduce the temperature increase in the system. Thermal design reduces the thermal displacement errors by design. And thermal error compensation compensates thermal displacement errors mostly by mechanical position adjustment such as stage position adjustment or tool position adjustment. The novel thermal displacement error compensation techniques proposed in this chapter and the next chapter do not fall into any of these categories. They reduce thermal displacement errors by controlling the temperature field in a non-obvious way such as applying and controlling the external control heat loads together with cooling.

The common idea for these methods is that the thermal displacement error at a point of interest is compensated in the temperature domain by controlling the temperature field by applying external control heat loads and cooling to a target structure to be controlled. The control signals for these external heat loads are calculated to minimize either the sum of a finite number of modal amplitudes or the contribution of these modes to the thermal displacement error at the point of interest.

4.2 Mode Cancellation

This chapter introduces the first novel idea of reducing a thermal displacement error by applying and controlling additional heat loads, which we call as "Mode Cancellation". In this method, the temperature distribution and the thermal displacement error of the target machine is expressed in terms of thermal modes using a thermal model based on Thermal Modal Analysis. Mode Cancellation then controls the dominant thermal modes, minimizes their amplitudes. Then the influence of these modes in the temperature distribution and the thermal displacement error are minimized. To control the dominant

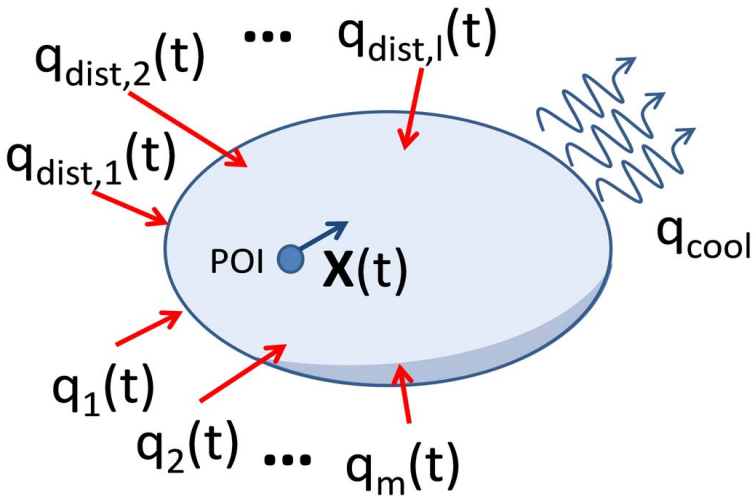

Figure 4.1: Mode Cancellation general problem description.

modes in the temperature field, external control heat loads $q_1(t), \ldots, q_m(t)$ are applied. In addition to the control heat loads, a separate static (= constant strength) cooling $\boldsymbol{q}_{\text{cool}}(t)$ is applied to extract the heat appleid to the system by both the disturbance load and the external control loads. In this way, the amplitude of the first thermal mode, which usually represents the average temperature distribution of the system and has the largest contribution to thermal deformation of the system, can be controlled. Then a selected number of modes ($i = 1 \cdots n$) are canceled out by applying m external control heat loads (with $m \geq n$).

Mode Cancellation can be applied to any 3D structures under disturbance heat loads $q_{\text{dist},1}(t), q_{\text{dist},2}(t), \ldots, q_{\text{dist,l}}(t)$ to control the position $\boldsymbol{x}(t)$ of a point of interest (POI) by applying external control heat loads $q_1(t), q_2(t), \ldots, q_{\text{m}}(t)$ and cooling q_{cool} as summarized in Figure 4.1. The disturbance and control heat loads, and the cooling can be either internal or external. The intensity of the disturbance loads can be a static strength or can change over time. The locations of the disturbance loads can also be stationary or moving over time within the target structure.

Let $\bar{\boldsymbol{\theta}}(t)$ be a vector of amplitudes of only the selected modes which you would like to control and eliminate. From this point on, other matrices such as $\left[\frac{1}{\tau_{\text{r}}}\right]$, $[C_{\text{r}}]$, $[\boldsymbol{\Phi}]$ are also reduced matrices which include only the elements corresponding to the selected modes. When a moving disturbance heat load $\boldsymbol{q}_{\text{mov}}(t)$ is applied to the target system together with the cooling $\boldsymbol{q}_{\text{cool}}(t)$ and the external control heat loads $\boldsymbol{q}_{\text{ext}}(t) = [q_1(t) \ldots q_m(t)]$, equation 3.12 becomes

$$\begin{aligned} &\dot{\bar{\boldsymbol{\theta}}}(t) + \left[\frac{1}{\tau_{\text{r}}}\right] \bar{\boldsymbol{\theta}}(t) \\ &= [C_{\text{r}}]^{-1} \left\{ [\boldsymbol{\Phi}_{\text{mov}}(t)]^{\text{T}} \, \boldsymbol{q}_{\text{mov}}(t) + [\boldsymbol{\Phi}_{\text{cool}}]^{\text{T}} \, \boldsymbol{q}_{\text{cool}}(t) + [\boldsymbol{\Phi}_{\text{nm}}]^{\text{T}} \, \boldsymbol{q}_{\text{ext}}(t) \right\} \end{aligned} \tag{4.1}$$

where $[\boldsymbol{\Phi}_{\mathrm{mov}}(t)]^{\mathrm{T}}$ is a time-dependent extract from the mode shape matrix $\boldsymbol{\Phi}$ for the selected numbers of modes at the location of the moving load $\boldsymbol{q}_{\mathrm{mov}}(t)$, and $[\boldsymbol{\Phi}_{\mathrm{cool}}]^{\mathrm{T}}$ and $[\boldsymbol{\Phi}_{\mathrm{nm}}]^{\mathrm{T}}$ are also similarly extracted matrix for $\boldsymbol{q}_{\mathrm{cool}}(t)$ and $\boldsymbol{q}_{\mathrm{ext}}(t)$.

Let

$$\Delta e_{\mathrm{i}}(t) = \left\{ [\boldsymbol{\Phi}_{\mathrm{mov}}(t)]^{\mathrm{T}} \boldsymbol{q}_{\mathrm{mov}}(t) + [\boldsymbol{\Phi}_{\mathrm{cool}}]^{\mathrm{T}} \boldsymbol{q}_{\mathrm{cool}}(t) \right\}_{\mathrm{i}} \tag{4.2}$$

which describes the excitation of mode i due to the moving disturbance load and the cooling. So equation (4.2) can be rewritten as follows:

$$\dot{\bar{\boldsymbol{\theta}}}(t) + \left[\frac{1}{\tau_{\mathrm{r}}}\right] \bar{\boldsymbol{\theta}}(t) = [C_{\mathrm{r}}]^{-1} \left(\Delta \boldsymbol{e}(t) + [\boldsymbol{\Phi}_{\mathrm{nm}}]^{\mathrm{T}} \begin{bmatrix} q_1(t) \\ \vdots \\ q_m(t) \end{bmatrix} \right) \tag{4.3}$$

where $\Delta \boldsymbol{e}(t)$ is a vector with $\Delta e_{\mathrm{i}}(t)$ in each element.

To avoid a set of target modes to be excited, the external control loads need to excite those same modes by $-\Delta \boldsymbol{e}(t)$. Therefore the time dependent amplitudes of the external heat loads to cancel out the excitation of the target four modes are given by the following equation.

$$\boldsymbol{q}_{\mathrm{ext}}(t) = \begin{bmatrix} q_1(t) \\ \vdots \\ q_m(t) \end{bmatrix} = -([\boldsymbol{\Phi}_{\mathrm{nm}}]^{\mathrm{T}})^{-1} \Delta \boldsymbol{e}(t) \tag{4.4}$$

Selection of the external heat load locations should be made so that the inverse matrix $([\boldsymbol{\Phi}_{\mathrm{nm}}]^{\mathrm{T}})^{-1}$ has only small values and does not amplify the required external heat loads' amplitudes. Also techniques used to determine the optimal sensor placement [47] can be applied to the selection of the external heat load positions.

4.2.1 Simulation and Result

A simulation study is conducted to validate the control of the selected set of modes and the reduction of thermal displacement error.

Simulation model used in this simulation and all the following simulation studies in this thesis is a thermal model of the 2D plate presented in Figure 3.1 using the thermal mode shapes $\boldsymbol{\phi}_{\mathbf{i,j}}$, and the corresponding thermal displacement fields $\boldsymbol{\psi}_{\mathrm{u,i,j}}$ and $\boldsymbol{\psi}_{\mathrm{v,i,j}}$ (for i = 1 ... 10, j = 1 ... 10).

$$\boldsymbol{T}_{\mathrm{sim}}(t) = \sum_{\mathrm{i}=1}^{10} \sum_{\mathrm{j}=1}^{10} \boldsymbol{\phi}_{\mathrm{i,j}} \theta_{\mathrm{i,j}}(t) \tag{4.5}$$

$$\boldsymbol{U}_{\mathrm{sim}}(t) = \begin{bmatrix} \boldsymbol{u}_{\mathrm{sim}}(t) \\ \boldsymbol{v}_{\mathrm{sim}}(t) \end{bmatrix} = \begin{bmatrix} \sum_{\mathrm{i}=1}^{10} \sum_{\mathrm{j}=1}^{10} \boldsymbol{\psi}_{\mathrm{u,i,j}} \theta_{\mathrm{i,j}}(t) \\ \sum_{\mathrm{i}=1}^{10} \sum_{\mathrm{j}=1}^{10} \boldsymbol{\psi}_{\mathrm{v,i,j}} \theta_{\mathrm{i,j}}(t) \end{bmatrix} \tag{4.6}$$

The example simulation problem used for this simulation study is presented in Figure 4.2. It consists of a 2D aluminum plate (76mm*44.5mm*0.1mm) with thermally insulated boundary conditions with mechanical clamped boundary condition at its left edge. Two

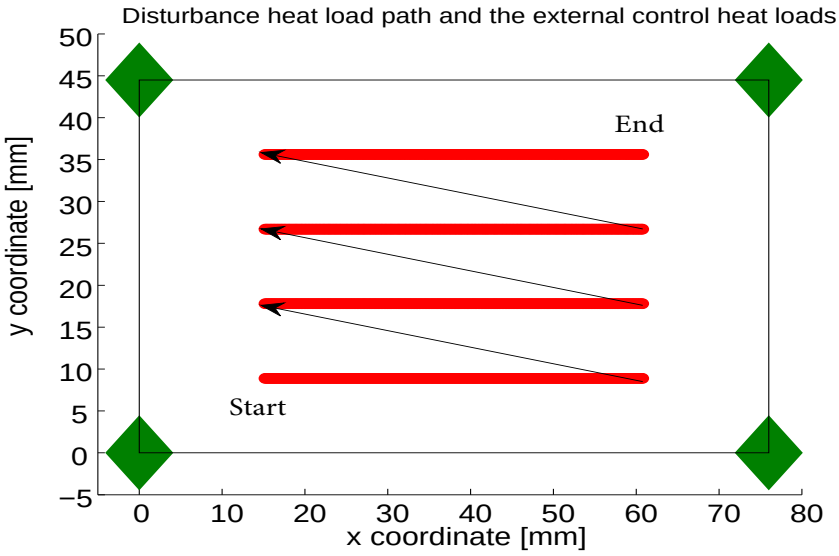

Figure 4.2: Positions of external control heat loads (depicted by green diamonds) and moving heat load path (red lines; black arrows indicate jumps of the moving heat load)

different paths of a moving disturbance heat load (shown in Figure 4.3) of 1 W are applied over 25 s. The moving heat load replicates the load from applications like an inkjet printhead with hot ink or optical lithography exposure process over a wafer. A uniform convective cooling $\boldsymbol{q}_{\text{cool}}(t)$ with a natural convection coefficient of $h = 16.5$ W/(m$^2 \cdot$ K) and various reference temperatures for the cooling T_{ref} are applied to the plate so that the calculated amplitudes of the external heat loads only take positive value.

$$\boldsymbol{q}_{\text{cool}}(t) = -h(\boldsymbol{T}(t) - T_{\text{ref}}) \tag{4.7}$$

In Figure 4.7, the amplitudes of the external control heat loads calculated for the discontinuous path example (above picture Figure 4.3) with the reference temperature equal to the ambient temperature ($\text{T}_{\text{ref}} = \text{T}_{\text{amb}}$) are presented. In this case, the calculated amplitudes of the external loads are all negative for entire simulation period. However, as the reference temperature value is decreased relative to the ambient temperature, the amplitudes of the external heat loads to cancel the target modes become more positive. Then in the end, a reference temperature which make the amplitudes of the external heat loads only positive but still closest to the ambient temperature is selected as the reference temperature for the cooling. The total thermal displacement $\sqrt{\boldsymbol{u}_{\text{sim}}(t)^2 + \boldsymbol{v}_{\text{sim}}(t)^2}$ at the location of the moving heat load is evaluated over the simulation time, thus this becomes a moving load/ moving point of interest problem. Four modes are controlled in the simulation using four external control heat loads. The controlled modes are mode(1,1), mode(2,1), mode(1,2) and mode(2,2). The four external control heat loads are placed at the corners of the plate as depicted in Figure 4.2. Each element in $\boldsymbol{\Phi}_{44}^{-1}$ in equation (4.4) is small and this thus results in a smaller control power $\boldsymbol{q}_{\text{ext}}(t)$. These four external loads' amplitudes are controlled using equation (4.4) and the thermal displacement error at the moving point of interest is simulated over the simulation time.

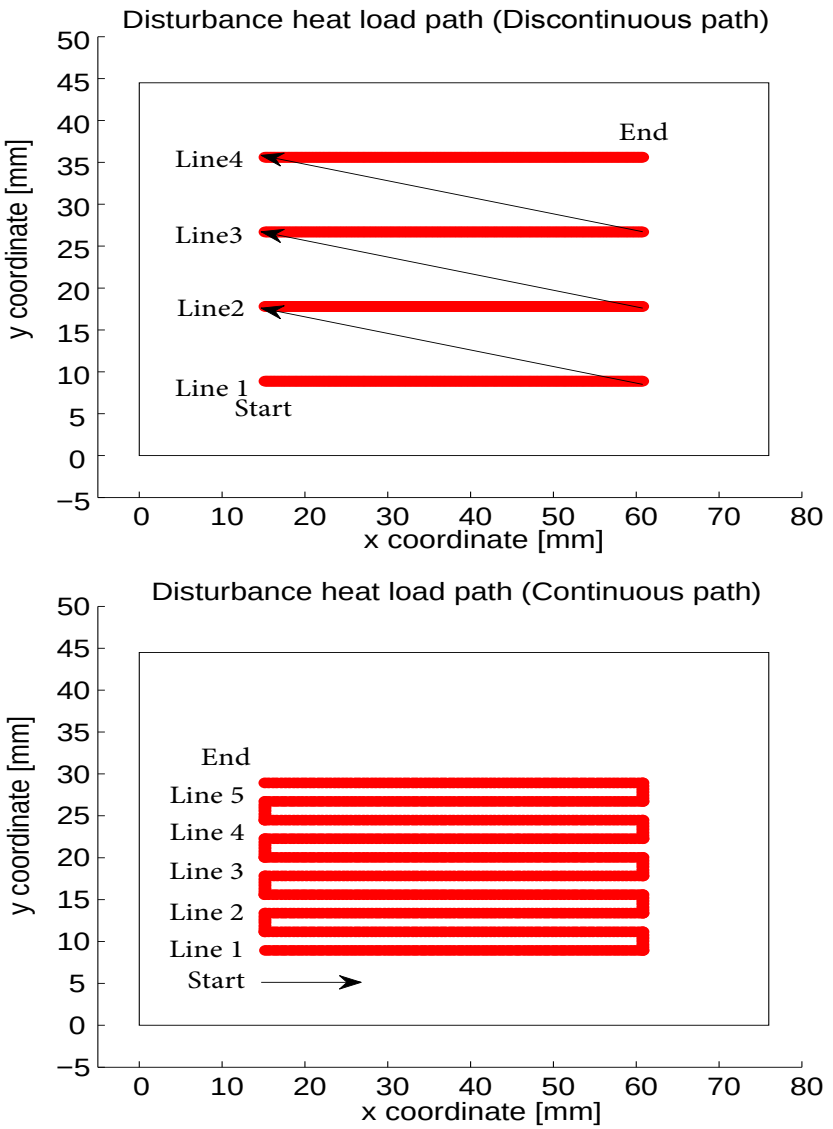

Figure 4.3: Two printing paths. Discontinuous path (top: black arrows indicate jumps of the moving load) and continuous path (bottom: black arrow indicates the start point and direction of the moving load.)

The simulation result of Mode Cancellation in this example is summarized below. Figure 4.4 and Figure 4.5 show the amplitudes of the four target modes (mode(1,1), mode(1,2), mode(2,1) and mode(2,2)) with and without mode cancellation for the two different moving disturbance load paths. The graph above shows the amplitudes of the target modes without any control, that is, the modal amplitudes by the moving disturbance load only. The graph below show the amplitudes of the same modes with Mode Cancellation. The result shows that the mode cancellation eliminates the target modes over the entire simulation time. The calculated amplitudes of the four external control heat loads are shown in Figure 4.6. These calculated amplitudes are of the same order of magnitude as the disturbance heat load of 1 W. The resultant thermal displacement at the point under the moving heat load is shown in Figure 4.8 together with two other results for comparison. Blue line (with legend "Moving disturbance load only") is the error caused by the moving disturbance load plus a convection cooling ($h = 16.5$ W/m$^2 \cdot$ K, $T_{ref} = T_{\text{room}}$ [K]). The green line (with legend "Best cooling") is the error in case uniform and constant strength cooling is applied together with the moving disturbance load. The convection coefficient in this simulation is kept constant ($h = 16.5$ W/m$^2 \cdot$ K) and the reference temperature T_{ref} is chosen to the value which is below the ambient temperature and minimizes the average error over the simulation ($T_{\text{ref}} = T_{\text{room}} - 10$ K). The red line (with legend "Mode Cancellation") is the remaining thermal displacement error after Mode Cancellation (with $h = 16.5$ W/m$^2 \cdot$ K, $T_{\text{ref}} = T_{\text{room}} - 29$ K). Figure 4.9 shows the average contribution of the first 9 modes to the thermal displacement error in the simulation.

The resultant thermal displacement error under the moving heat load after applying our novel technique, Mode Cancellation, is significantly smaller than that obtained with "Best cooling". One thing to note is that this technique reduces the contribution from the target four modes in the temperature field and the corresponding thermal displacement error while the contributions from the remaining modes actually increase (Figure 4.9). However as already stated in section 2.2, higher order modes have a smaller contribution in the thermal displacement field. Therefore it is possible to reduce the thermal displacement error by controlling the four lower modes even considering the increasing contribution of the non-controlled modes.

4.2.2 Control mode selection and control location selection

Mode Cancellation can control a number of modes up to the number of external control heat loads. Therefore the selection of modes to be controlled determines the performance of thermal error reduction. Selection of modes includes both the number of modes to be controlled and the actual selection of modes to be controlled. In the previous section, the first four lower modes (1,1), (1,2), (2,1), (2,2) are chosen for control based on the understanding that lower modes have larger influences both to the temperature field and to the corresponding displacement field in general.

When considering the improvement obtained using Mode Cancellation, there are several questions which naturally arose from the mathematical derivation of the Mode Cancellation technique. The first question is: what happens to the thermal error when the number of external control heat loads is increased and correspondingly the number of modes to be controlled is increased? Second question is: given a certain number of control loads, therefore the number of modes to be controlled, what is the best selection of modes to be controlled to minimize the thermal displacement error? And the third question is: given the number of control loads and the selection of modes to be controlled, what are the

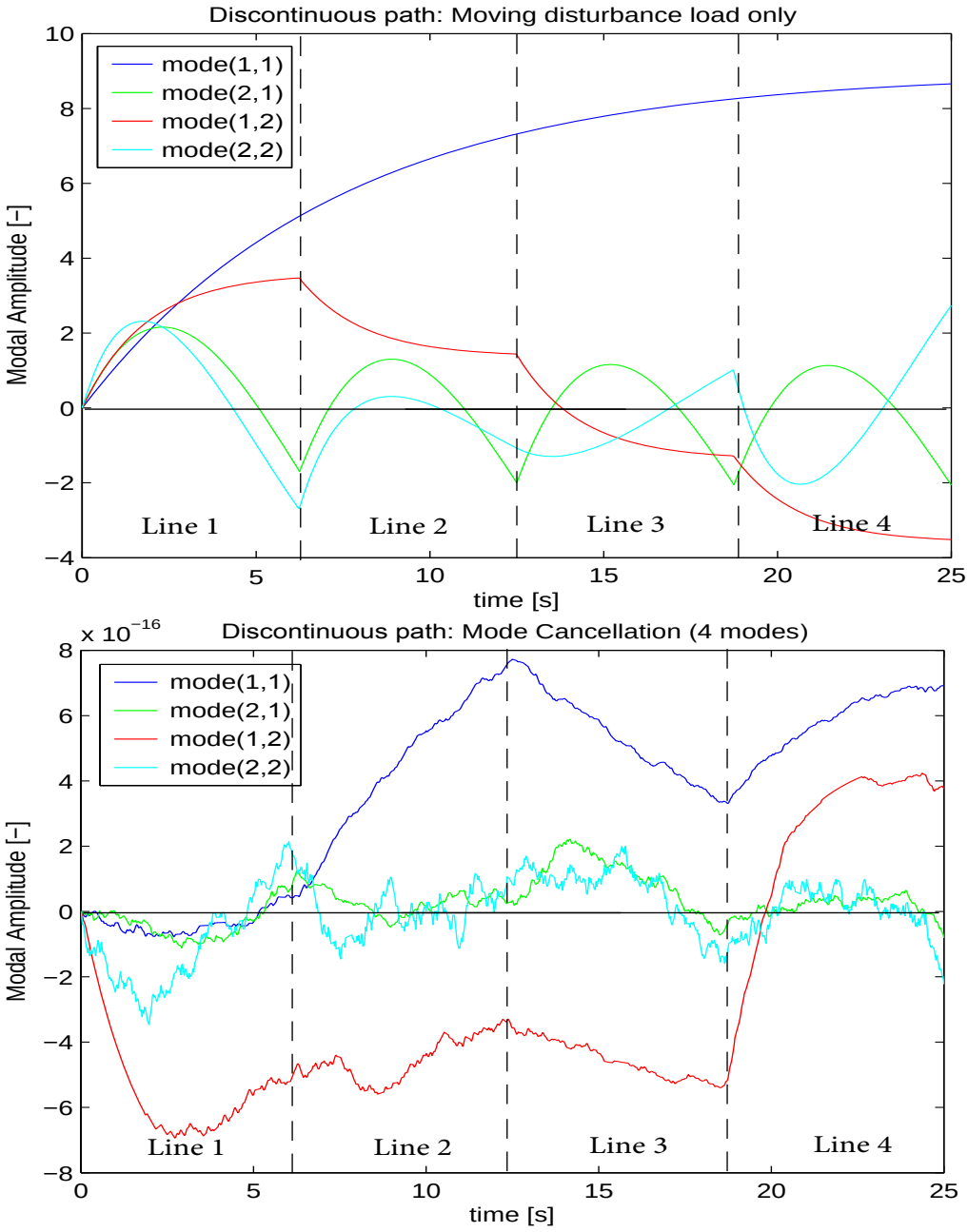

Figure 4.4: Amplitudes of the first 4 modes without control (top) and with control (bottom) for discontinuous path case. The amplitudes of the first 4 modes are controlled to the level of computational error ($\sim 10^{-16}$).

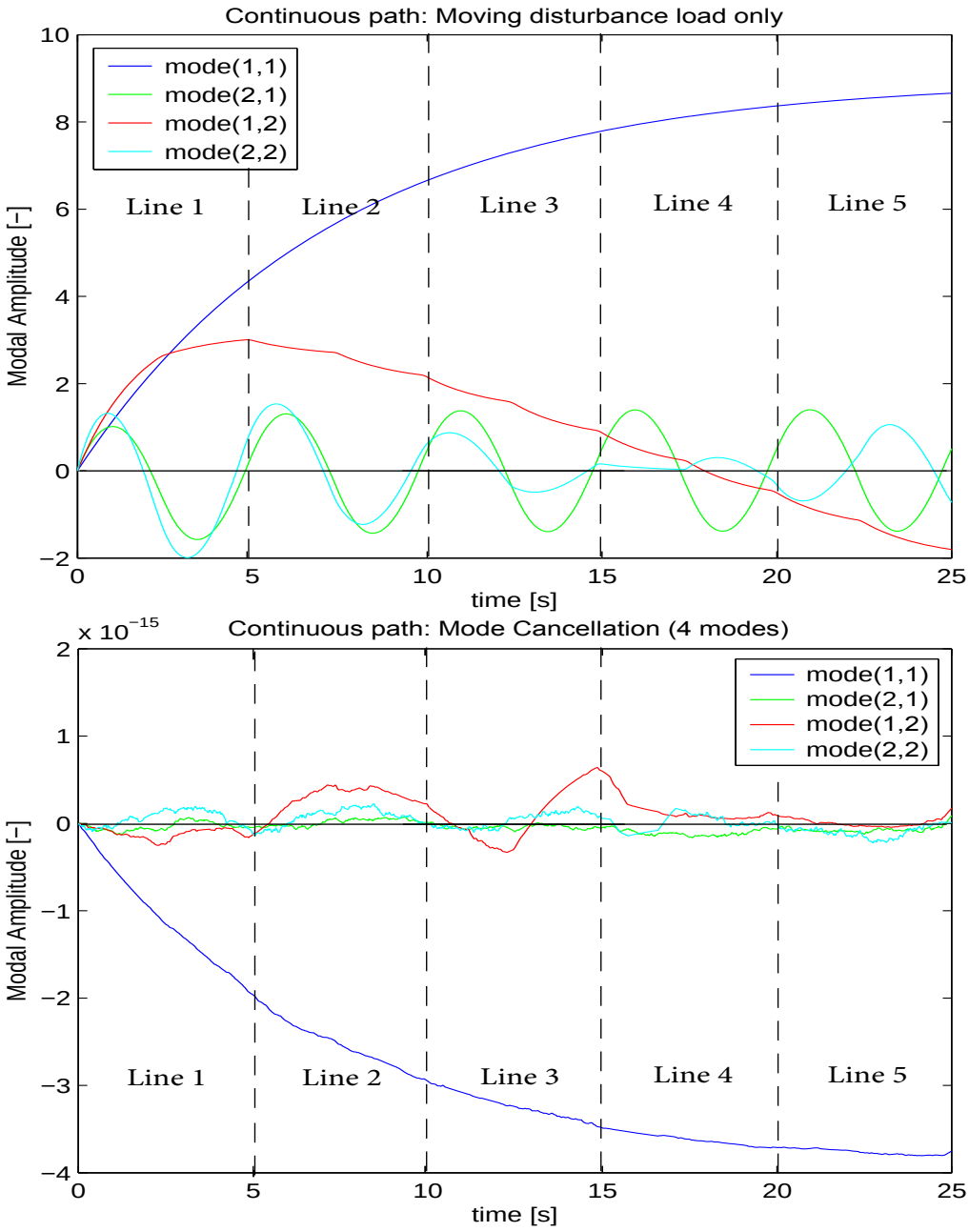

Figure 4.5: Amplitudes of the first 4 modes without control (top) and with control (bottom) for continuous path case. The amplitudes of the first 4 modes are controlled to the level of computational error ($\sim 10^{-15}$).

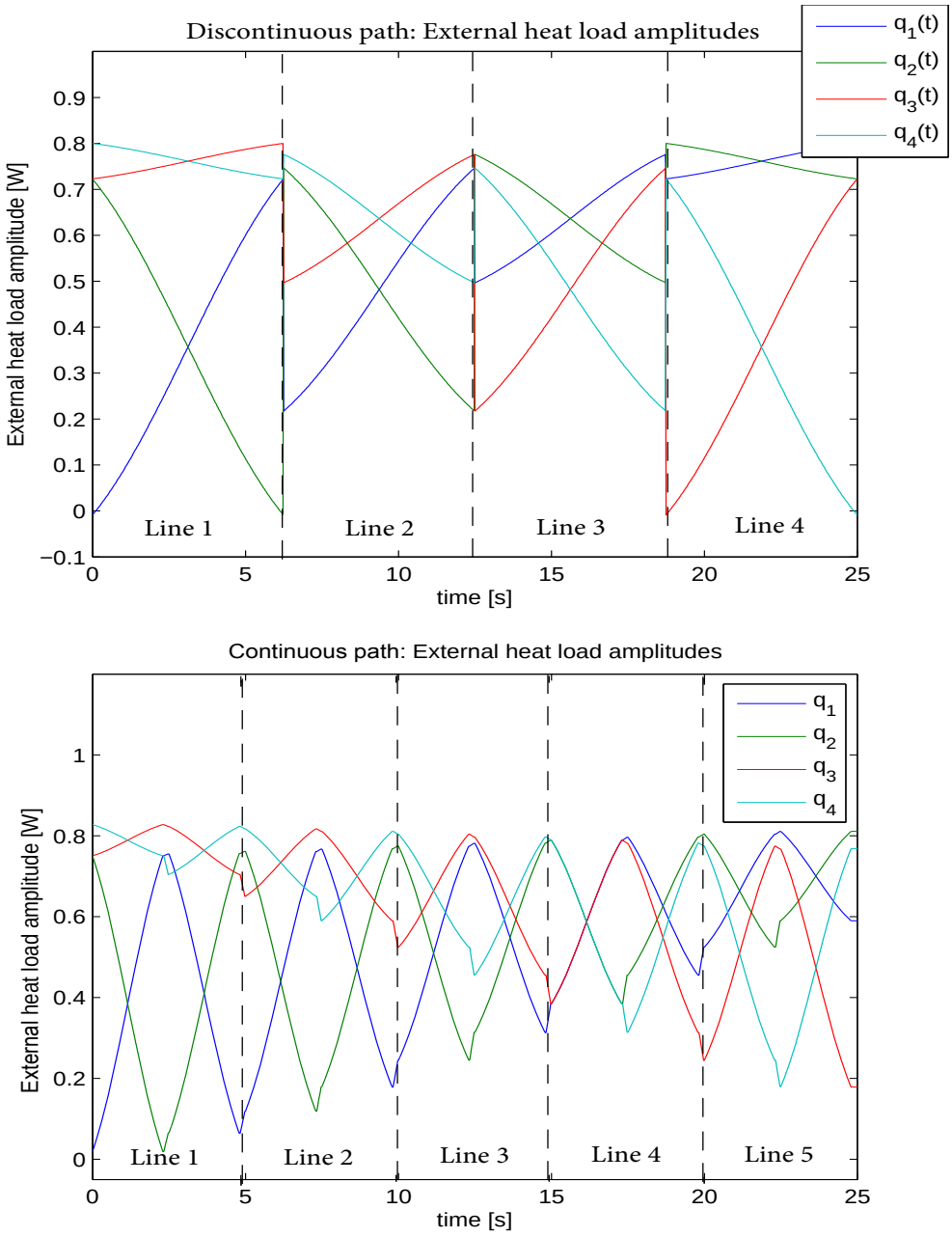

Figure 4.6: The amplitudes of four external heat loads. Top: discontinuous path case. Bottom: continuous path case.

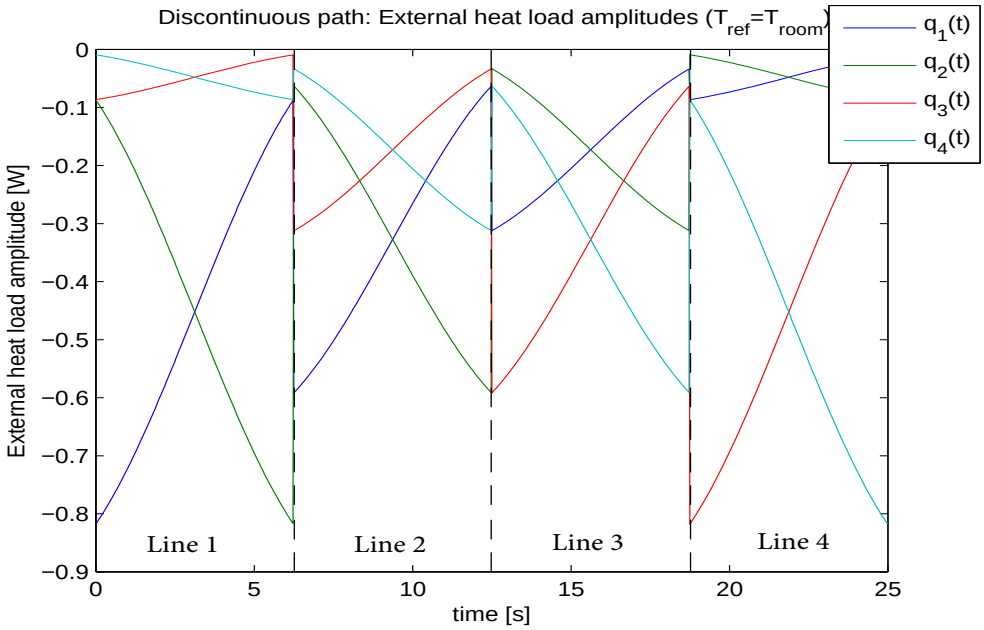

Figure 4.7: The amplitudes of four external heat loads for discontinuous path case with $T_{ref} = T_{room}$

best locations for the control loads?

For the fist question, increasing the number of external control loads has both upside and downside. The upside is that Mode Cancellation can control a larger number of modes and therefore, intuitively speaking, improves thermal error reduction performance. The downside is that it requires more control power as there are more control loads applied to the system. Mode Cancellation also requires cooling to extract the same amount of energy inserted to the system by the external control loads so that the first mode which , in general, has a large contribution to the thermal displacement field of the structure is kept equal to zero. Therefore the increased control energy also means increased cooling energy. Also as a result of the increased control energy to the system, it is expected that the amplitudes of all other modes, modes other than the controlled modes, increase due to the larger total input energy from the external control loads. Therefore it is not clear whether simply increasing the number of external control heat loads actually results in reduction of the thermal displacement error or not.

For the second question, selection of modes to be controlled needs to be made such that the sensitivity matrix $[\boldsymbol{\Phi}_{nm}]^T$ in equation (4.4) is non-singular. This becomes more difficult as the number of modes to be controlled increases. The sensitivity matrix $[\boldsymbol{\Phi}_{nm}]^T$ becomes singular when the sensitivities of multiple modes in the matrix to the external control loads have linearly dependent values. Besides that, the selection of modes needs to be done considering the following aspects: (1) How big is the contribution of a mode, (2) How much does control of a mode influence the non-controlled modes.

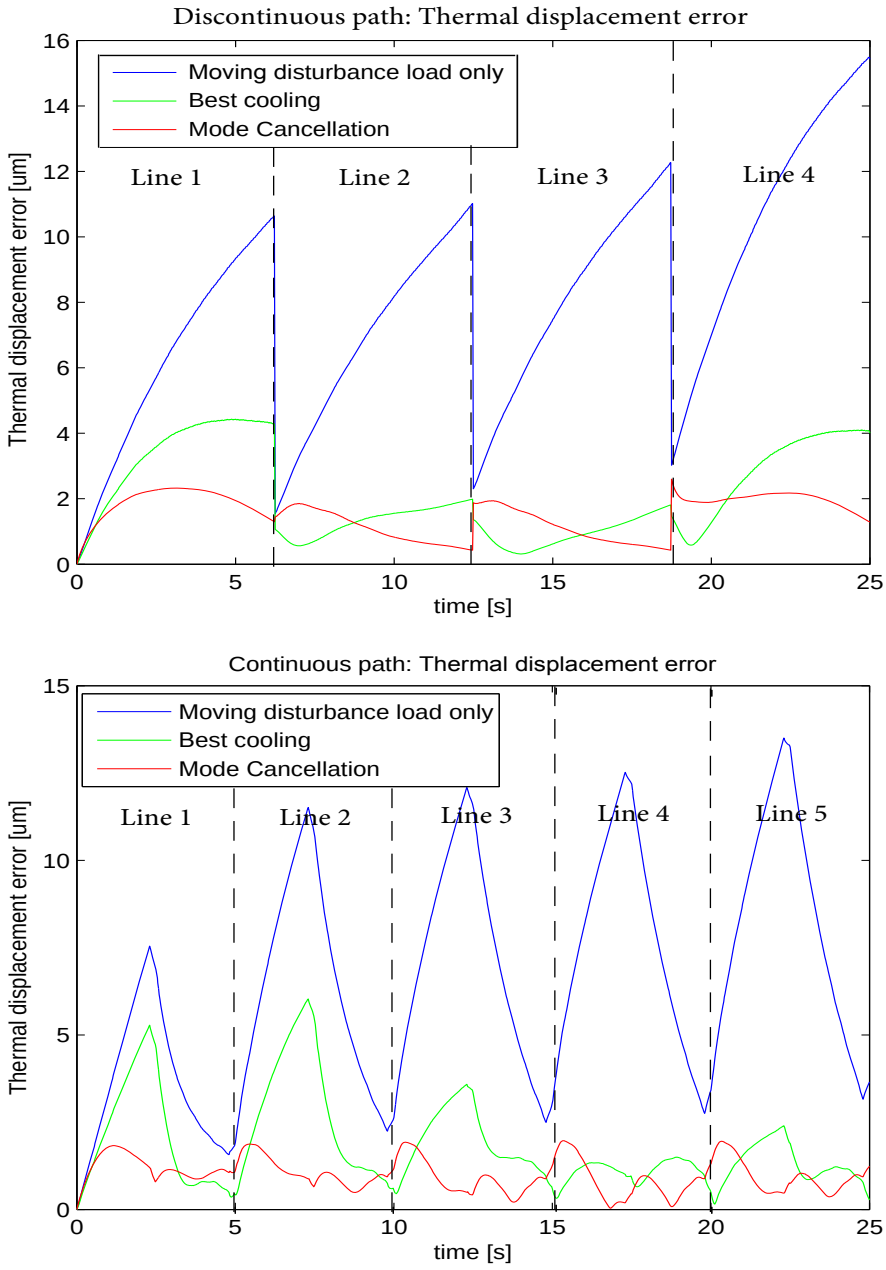

Figure 4.8: Thermal displacement error at the moving point of interest (the same location as the moving disturbance load). Top: discontinuous path case. Bottom: continuous path case.

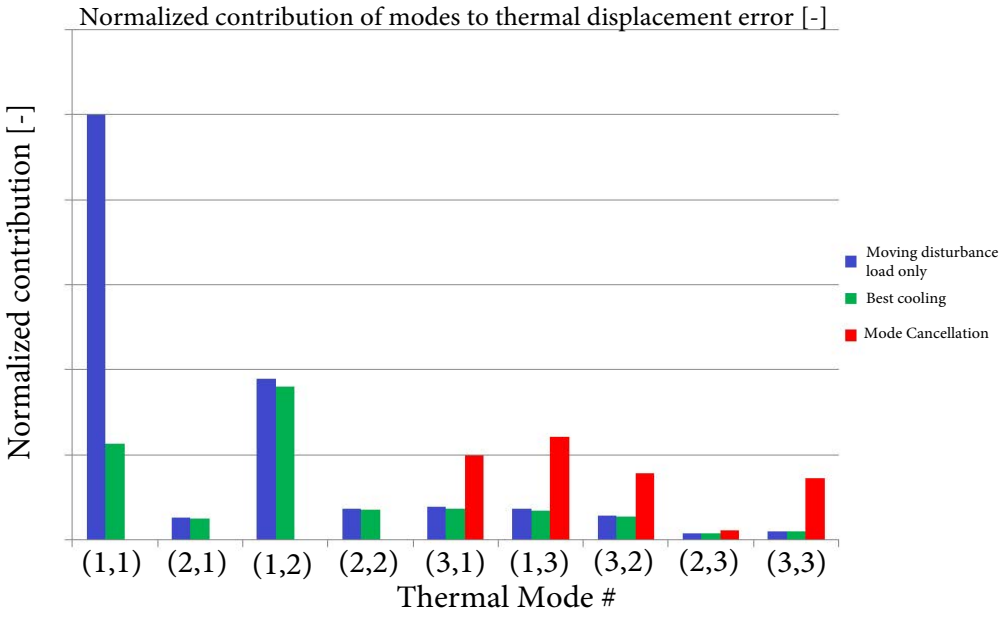

Figure 4.9: Normalized contribution of the first 9 modes after Mode Cancellation to the thermal displacement error at the location of the moving disturbance load for the discontinuous path case.

For the third question, selection of the control load locations needs to be done at least considering the following aspects: (1) Is the sensitivity matrix non-singular or far enough from singularity, (2) Is the set of control loads the most efficient set of control loads to control and eliminate a given set of target modes for control, and (3) How much does the the influence of the control loads influence the non-controlled modes.

To achieve the best performance or close to the best performance of Mode Cancellation, these questions needs to be answered either manually for every different problem or automatically by developing a scheme for calculating the best selection of modes and control loads. To overcome some of these problems, especially the first and second problem, we propose another technique, which we named it as Modal Control, in the next chapter.

4.3 Material properties

In this section, the influence of material properties of a structure to the thermal mode shapes and time constant of the structure is studied using the analytically derived thermal mode shapes and time constants of the structure (the derivation is in Appendix C). In this section, the material properties considered here are: density ρ, heat capacity c, and thermal conductivity k of the plate in the example problems. Here these material properties are assumed to be uniform over space and constant independent from the temperature value. The analytical mode shapes $\phi_{i,j}$ of the plate can be expressed as:

$$\phi_{\mathrm{i,j}}(x,y) = \cos\left(\frac{(i-1)\pi}{L_{\mathrm{x}}}x\right)\cos\left(\frac{(j-1)\pi}{L_{\mathrm{y}}}y\right) \tag{4.8}$$

From the equation, it is clear that the mode shapes in these example cases are material property independent. Therefore the material property has no influences to the mode shapes.

The equation of modal amplitudes becomes as follows:

$$\dot{\theta}_{\mathrm{i,j}}(t) + \frac{1}{\tau_{\mathrm{i,j}}}\theta_{\mathrm{i,j}}(t) = \frac{\int \phi_{\mathrm{i,j}}(\boldsymbol{x})q(\boldsymbol{x},t)\mathrm{d}\boldsymbol{x}}{\rho c w \int\int \phi_{\mathrm{i,j}}(\boldsymbol{x})^2 \mathrm{d}\boldsymbol{x}} \tag{4.9}$$

The left side of the equation 4.9 is governed by the time constant of the mode. The right side is inversely proportional to the product of density ρ and heat capacity c . The time constants of these modes are

$$\tau_{\mathrm{i,j}} = \frac{1}{\frac{k}{\rho c}\left(\left(\frac{(i-1)\pi}{L_{\mathrm{x}}}\right)^2 + \left(\frac{(j-1)\pi}{L_{\mathrm{y}}}\right)^2\right) + \frac{2h}{\rho c w}} \tag{4.10}$$

The time constant of a mode is determined by two contributions. One part is the conduction part which corresponds to

$$\frac{k}{\rho c}\left(\left(\frac{(i-1)\pi}{L_{\mathrm{x}}}\right)^2 + \left(\frac{(j-1)\pi}{L_{\mathrm{y}}}\right)^2\right) \tag{4.11}$$

and the other part corresponds to cooling by air convection

$$\frac{2h}{\rho c w} \tag{4.12}$$

The time constants determine the response speed of the mode and also its steady state value. For example, when a constant heat load q_{ex} is applied to the mode i,j, then its response becomes as follows:

$$\theta_{\mathrm{i,j}}(t) = \frac{q_{\mathrm{ex}}}{\rho c A L_{\mathrm{x}} L_{\mathrm{y}}}\tau_{\mathrm{i,j}}\left(1 - e^{-t/\tau_{\mathrm{i,j}}}\right) \tag{4.13}$$

As can be seen from the equation, the steady state value of the mode is proportional to the applied heat load amplitude q_{ex} and its time constant $\tau_{\mathrm{i,j}}$. And this time constant also determines the temporal behavior of the mode. Lower modes (modes with smaller indices) decay slowly when no longer excited. Higher modes (modes with larger indices) decay quickly when no longer excited. However, the ramp-up speed of a modal amplitude when excited by a heat load is independent from the time constant (equation (4.17)). But a mode with larger time constant does take longer time until it reaches the steady-state and a mode with smaller time constant takes shorter time (Figure 4.10).

$$\begin{aligned}
\theta_{\mathrm{i,j}}(t) &= \frac{q_{\mathrm{ex}}}{\rho c A L_{\mathrm{x}} L_{\mathrm{y}}}\tau_{\mathrm{i,j}}\left(1 - e^{-t/\tau_{\mathrm{i,j}}}\right) && (4.14)\\
&= \frac{q_{\mathrm{ex}}}{\rho c A L_{\mathrm{x}} L_{\mathrm{y}}}\tau_{\mathrm{i,j}}\left(1 - \left(1 - \frac{t}{\tau_{\mathrm{i,j}}} + \frac{t^2}{2!(\tau_{\mathrm{i,j}})^2} + \dots\right)\right) && (4.15)\\
&= \frac{q_{\mathrm{ex}}}{\rho c A L_{\mathrm{x}} L_{\mathrm{y}}}\left(t - \frac{t^2}{2\tau_{\mathrm{i,j}}} + \dots\right) && (4.16)\\
&\simeq \frac{q_{\mathrm{ex}}}{\rho c A L_{\mathrm{x}} L_{\mathrm{y}}} t \quad (\text{for } t << 1) && (4.17)
\end{aligned}$$

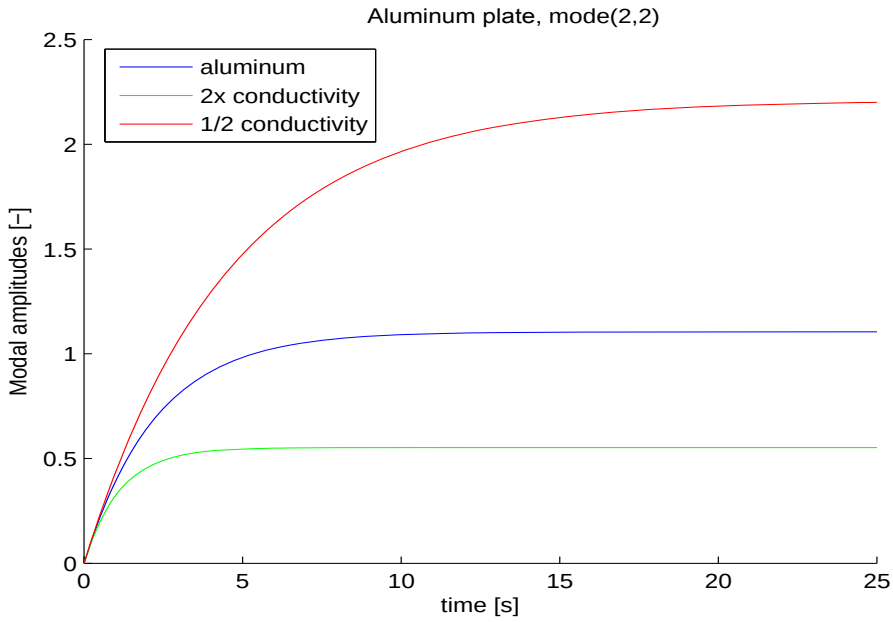

Figure 4.10: Responses of mode(2,2) of aluminum plates with different thermal conductivity. The ramp-ups of the modal amplitudes are at the same speed but different time constants result in different convergence time. The final values are proportional to the time constants.

Figure 4.10 shows the responses of modes with different time constants to a step heat load. In this graph, the step response of mode (2,2) of the aluminum plate are simulated with different conduction speeds. The blue curve has thermal conductivity of $k = 160$ $\mathrm{W}/(\mathrm{m} \cdot \mathrm{K})$. The other two cases are the response of the same mode if the thermal conductivity has double (red) of half (green) of the original value. From equation (4.10), the larger conductivity results in shorter time constants and smaller conductivity results in longer time constants. The graph shows that the difference in the time constants affects both the speed of the amplitudes change and their final amplitudes.

The time constants become shorter when the thermal conductivity of the material is high or the cooling is stronger, or when it has smaller heat capacity (ρc). Heat capacity ρc also appears on the right side of the equation of modal amplitude in equation (4.9). Therefore, heat capacity influences the behavior of each mode in two ways. One is that small heat capacity results in shorter time constants and vice versa. The other way is that small heat capacity makes the sensitivity of each mode to a heat load larger and vice versa.

As the two heat capacity terms ρc in equation 4.18 $\sim$ 4.19 cancel out to each other, the steady state value of a modal amplitude is independent from the heat capacity but only its response speed to a heat load and the decay speed of the mode are influenced by the heat capacity (Figure 4.11).

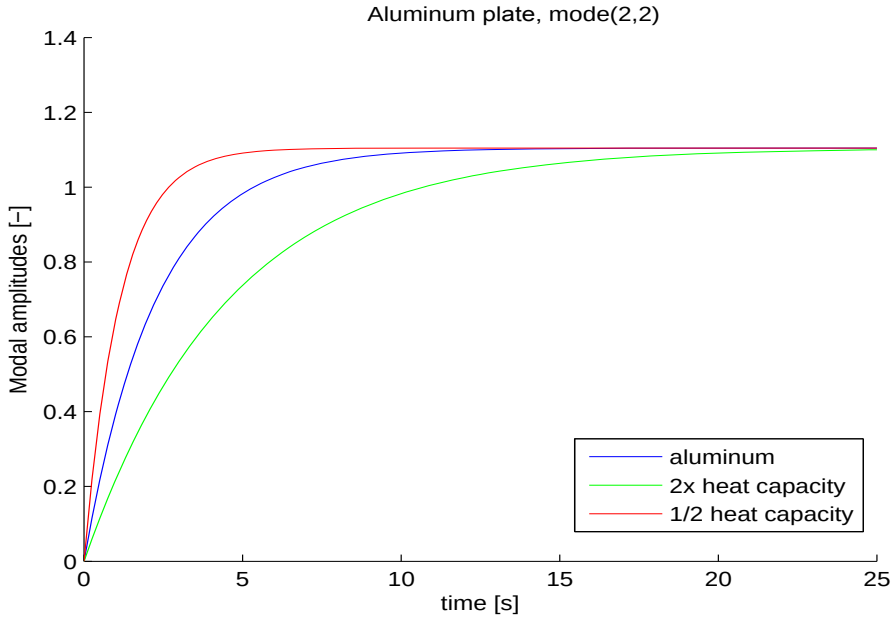

Figure 4.11: Responses of mode(2,2) of aluminum plates with different heat capacity. The ramp-ups of the modal amplitudes are at different speed but the final values are the same.

$$\theta_{\mathrm{i,j}} = \frac{q_{\mathrm{ex}}}{\rho c A L_{\mathrm{x}} L_{\mathrm{y}}} \tau_{\mathrm{i,j}} \left(1 - e^{-t/\tau_{\mathrm{i,j}}}\right) \tag{4.18}$$

$$= \frac{q_{\mathrm{ex}}}{\rho c A L_{\mathrm{x}} L_{\mathrm{y}}} \frac{1}{\frac{k}{\rho c}\left(\left(\frac{(i-1)\pi}{L_{\mathrm{x}}}\right)^2 + \left(\frac{(j-1)\pi}{L_{\mathrm{y}}}\right)^2\right) + \frac{2h}{\rho c w}} \left(1 - e^{-t/\tau_{\mathrm{i,j}}}\right) \tag{4.19}$$

$$= \frac{q_{\mathrm{ex}}}{A L_{\mathrm{x}} L_{\mathrm{y}}} \frac{1}{k\left(\left(\frac{(i-1)\pi}{L_{\mathrm{x}}}\right)^2 + \left(\frac{(j-1)\pi}{L_{\mathrm{y}}}\right)^2\right) + \frac{2h}{w}} \left(1 - e^{-t/\tau_{\mathrm{i,j}}}\right) \tag{4.20}$$

When cooling is much stronger than the heat conduction within the material, then the second term in the equation (4.10) becomes dominant for lower modes. Then the time constants for the lower modes become almost identical.

$$\tau_{\mathrm{i,j}} = \frac{1}{\frac{k}{\rho c}\left(\left(\frac{(i-1)\pi}{L_{\mathrm{x}}}\right)^2 + \left(\frac{(j-1)\pi}{L_{\mathrm{y}}}\right)^2\right) + \frac{2h}{\rho c w}} \tag{4.21}$$

$$\simeq \frac{\rho c w}{2h} \tag{4.22}$$

This means that the contributions of the lower modes all have similar amplitudes due to the fact that the contribution of modes are proportional to the time constants. In this case, Mode Cancellation is expected to have reduced performance since the method depends on the relative importance of the lower modes. This is also the same for Modal

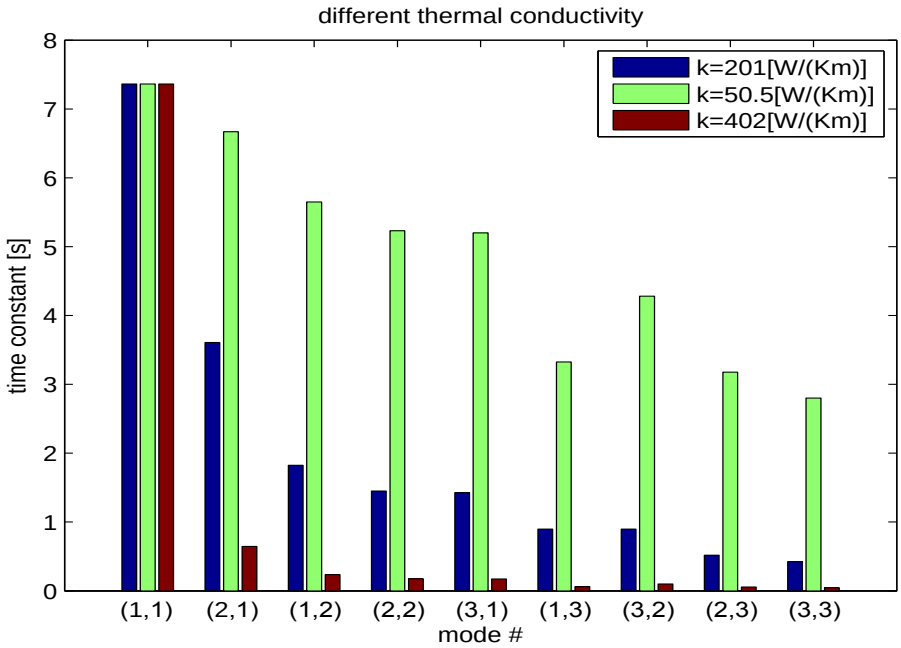

Figure 4.12: First 9 time constants with different heat conduction materials. Heat conduction influences the time constants of the second and higher order modes. Higher heat conduction results in shorter time constants.

Control which will be introduced in the next Chapter. Therefore it is expected that these methods are expected to perform well for highly conductive material such as copper and aluminum but not for low conductivity materials such as plastic or glass (Figure 4.13). First 9 time constants of the 2D plate with different heat conduction is shown in Figure 4.12.

4.4 Geometry

As can be seen from the equation (4.10), width and height of the 2D plate also influence the time constants. When the plate is large, the time constants become large as well for the same thermal conductivity since it takes longer time to convey heat within the larger plate. First 9 time constants of the 2D plate with different substrate size is shown in Figure 4.14. Also the convection cooling becomes relatively more dominant in the time constants since the conduction part in the equation (4.10) becomes smaller for larger plate size. This is the same behavior as found in low conductivity material. Figure 4.14 shows the time constants of the larger plate.

Thickness of the plate influences the relative strength of convection cooling with respect to conduction within the plate. The convection strength is proportional to the surface area while the capacity is proportional to the volume. Therefore the convection term in equation (4.10) of the time constant is inversely proportional to the thickness. Therefore the thicker the plate, the slower the time constants become. This means that a thinner substrate is more influenced by the convection. Also the thickness of the plate affects the

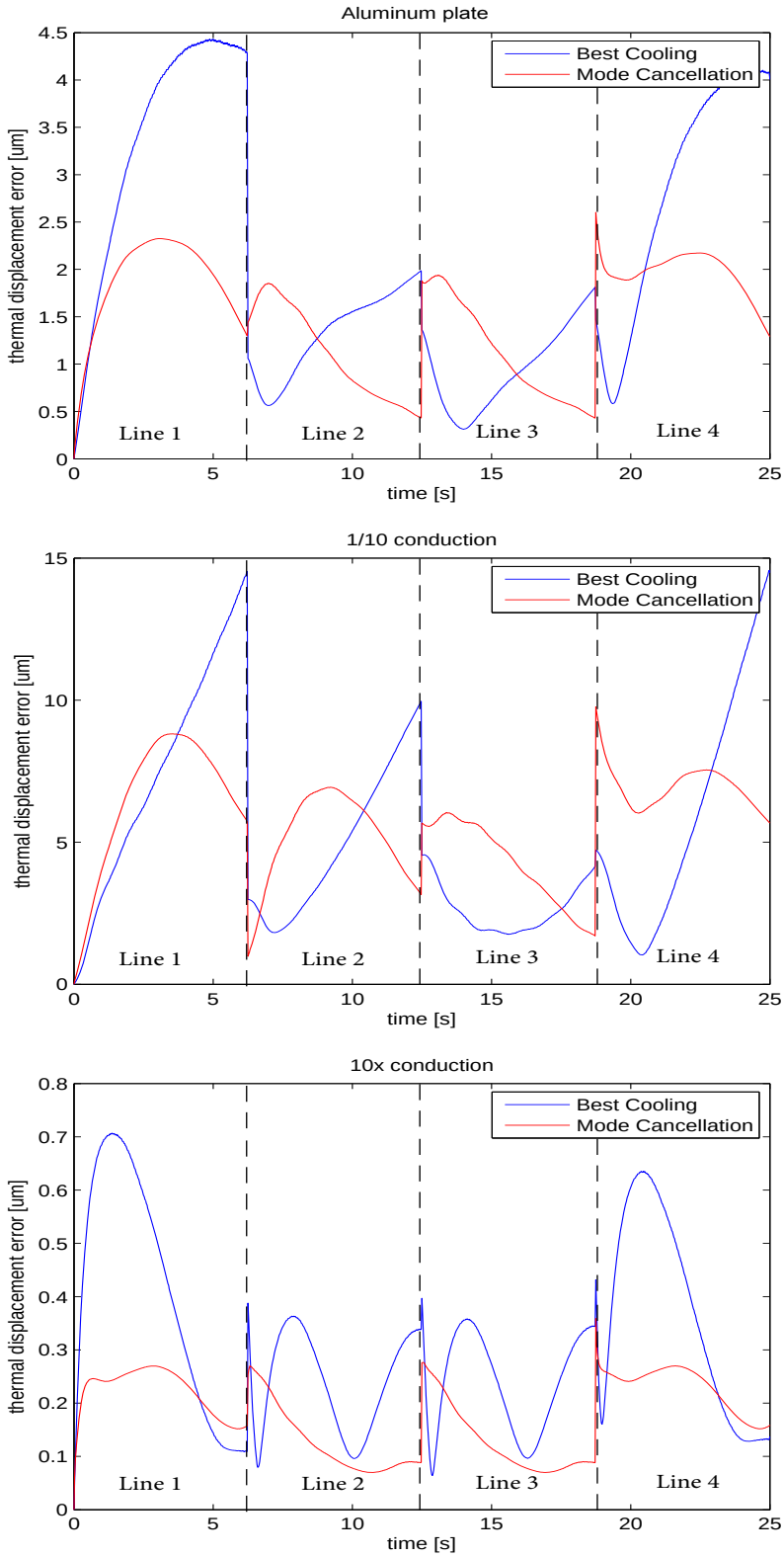

Figure 4.13: Mode cancellation results for different heat conduction materials.

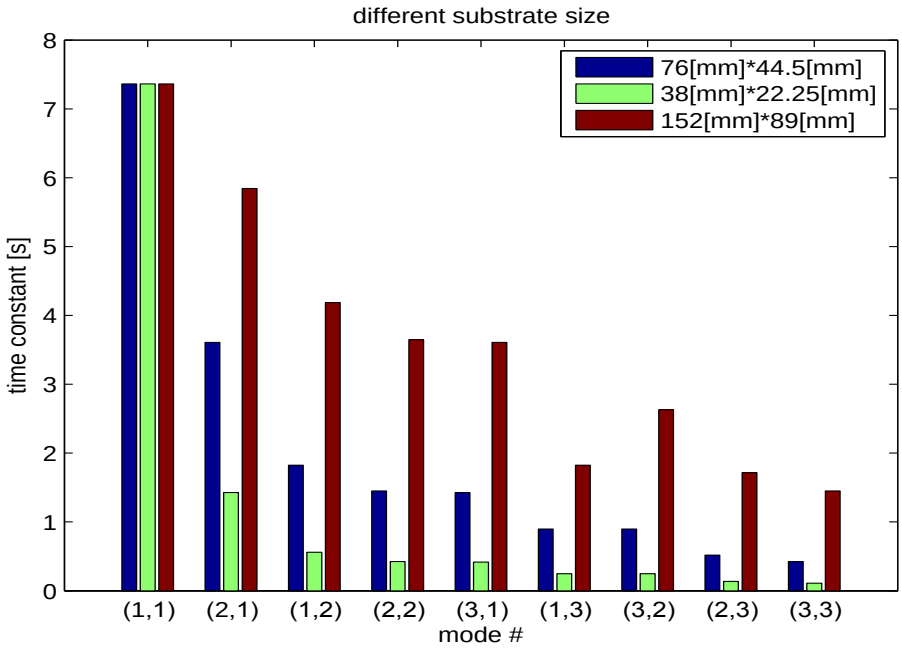

Figure 4.14: First 9 time constants with different substrate size. Smaller substrate has shorter time constants as the distance between the peaks and valleys in mode shapes becomes shorter.

right hand side of equation (4.9). A thinner plate has smaller heat capacity and hence increases the temperature more easily. Figure 4.15 shows the time constants of different thickness plates. Figure 4.16 shows the performance of Mode Cancellation with different thickness.

4.5 Printing path

When a printing area is small relative to the size of the substrate (e.g. path in the bottom figure of Figure 4.17), the resultant temperature change is expected to happen in a smaller area than is the case for a larger printing area as shown in the upper figure in Figure 4.17.[1] Thermal modal analysis becomes less efficient in representing the temperature distribution and the corresponding thermal displacement fields using a small number of modes in such a case. To make this point clear, hypothetical temperature reconstruction in 1D example cases are shown in Figure 4.18. In the above example where the temperature distribution has a wide peak (Left-top of Figure 4.18), most of the contributions from the thermal modes are concentrated in the lower modes (Right-top in Figure 4.18) while an example case bottom-left in the same figure, the number of modes contributing to such a narrow temperature field extends to a large number of modes as shown in the bottom-left in the same figure. This is due to the fact that thermal mode shapes are related to the spatial frequencies of the temperature fields. Lower modes have lower spatial frequencies

[1]Of course, after long enough time with respect to the thermal diffusivity of the substrate, the temperature change due to such a local heat load will spread over the entire substrate unless the cooling is strong enough to extract all the energy by the local heat load before it spread over the entire substrate.

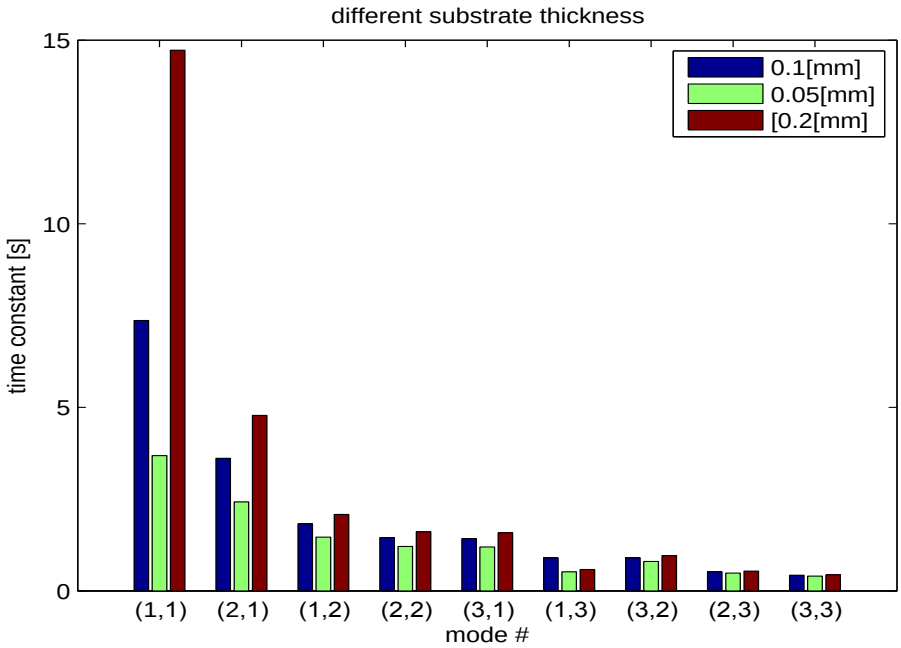

Figure 4.15: First 9 time constants with different substrate thickness. Substrate thickness mostly influences the first mode as the thickness influences the heat capacity of the aluminum plate while convection cooling which determines the time constant of the first mode do not change with the thickness.

of the temperature field while higher modes have higher spatial frequencies components of the temperature field. Therefore a narrow (spatially high frequency) temperature peak requires many modes to have an accurate representation of the temperature field. It is expected that Mode Cancellation results in slightly lower performances in cases where heat loads are not widely spread over the machine but concentrated in a small part of the system. When analyzing a temperature distribution with such a local heat loads, temperature distribution can also be modeled for only a small region of the system such as the region circled by red rectangle in Figure 4.18. Then the temperature distribution of the small area can be combined with the rest of the temperature field which is expected to have a less dynamic change of its temperature field due to the lack of heat loads in the region.

4.6 Cooling

As already discussed in the first section, the cooling affects the time constants of the modes. Time constants of the 2D plate for different cooling strength are shown in Figure 4.19. The important thing is the relative strength of the cooling term with respect to the conduction term in the equation of the time constant. If the cooling term is weaker than conduction term, conduction dominates the thermal behavior and the dominance of lower modes is prominent. But when the cooling term is stronger, or the thickness of the

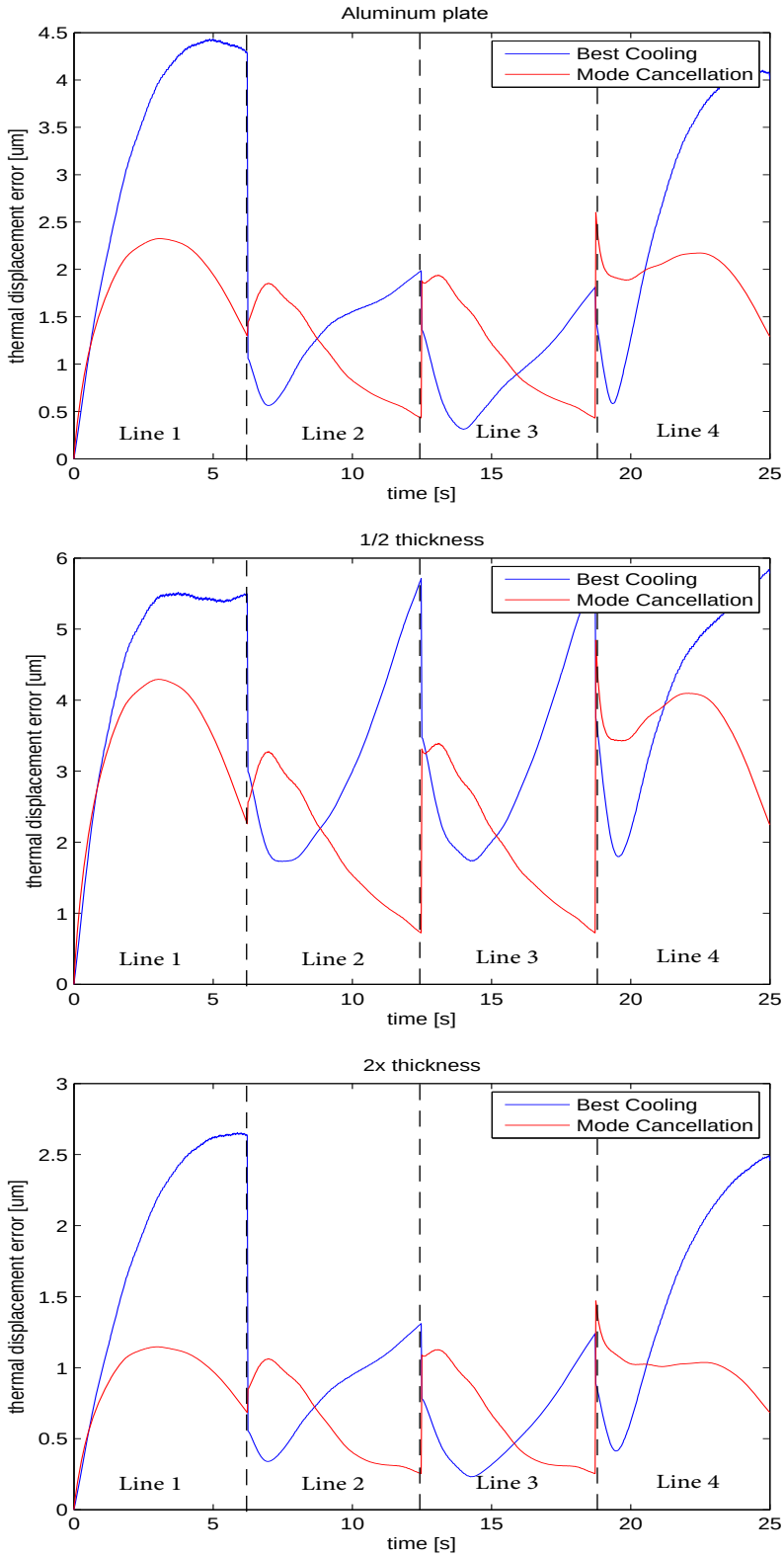

Figure 4.16: Mode cancellation results for different substrate thickness.

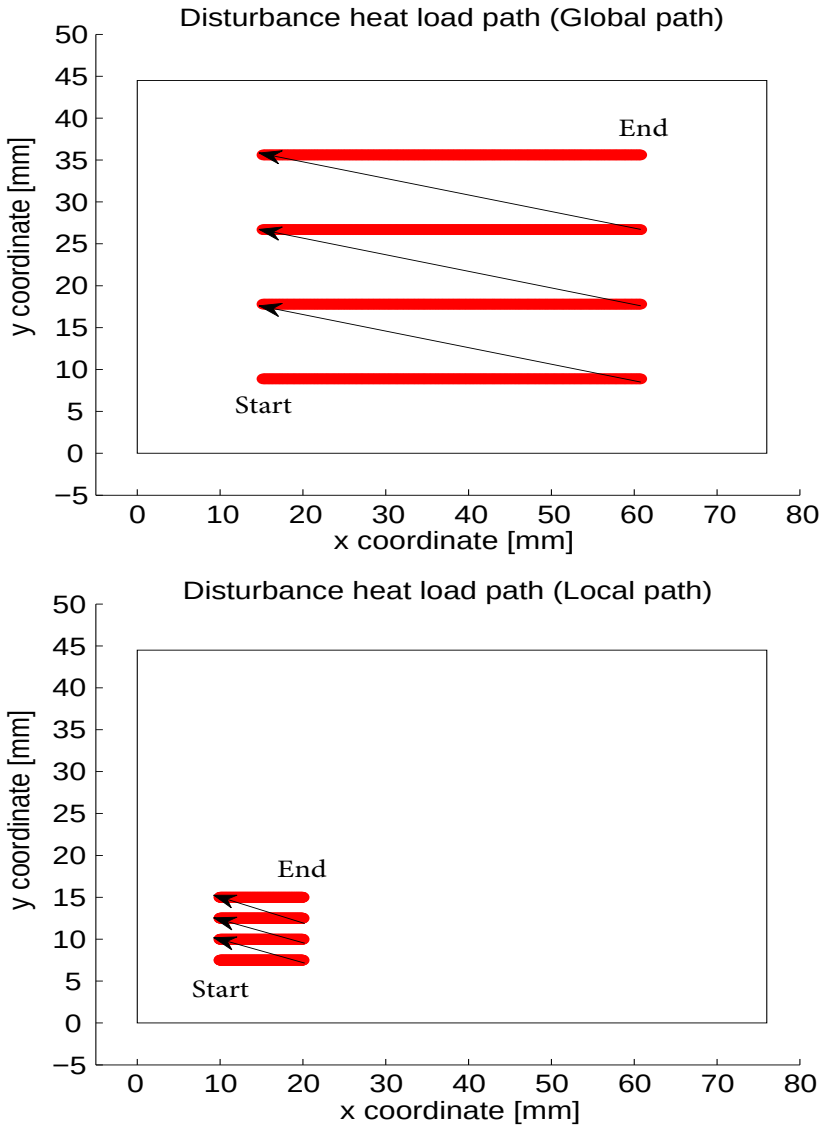

Figure 4.17: Example of global printing path (top) and local printing path(bottom). Black arrows indicate jumps of the moving load.

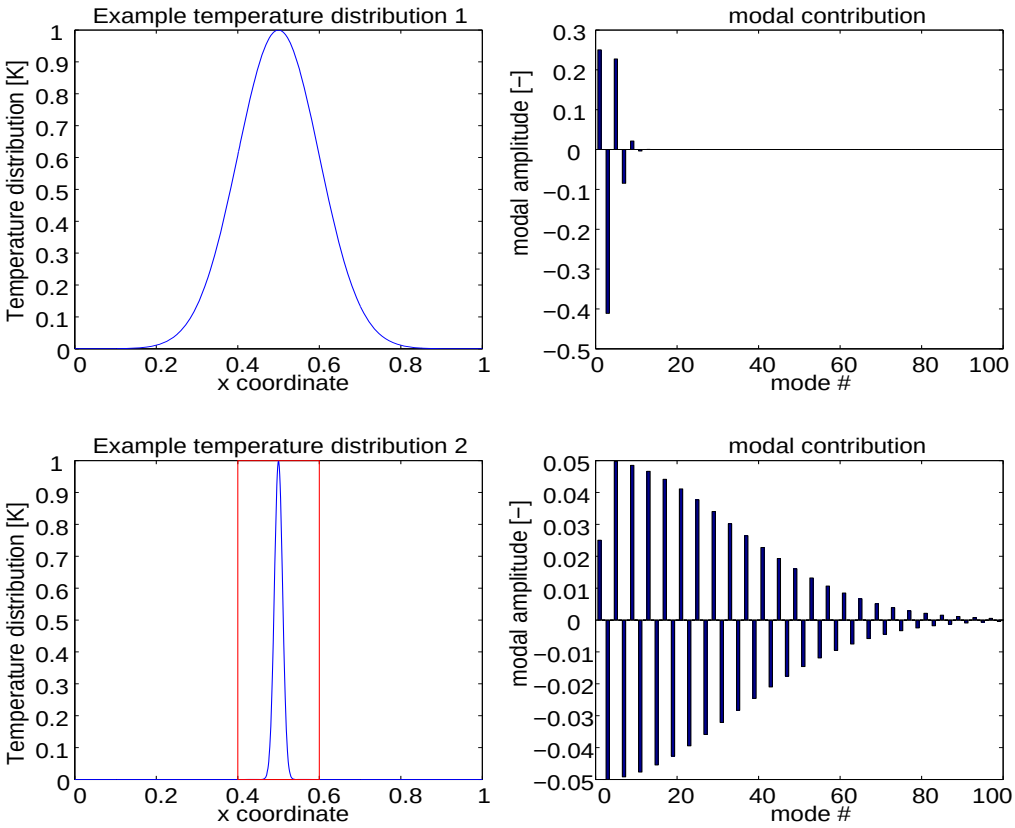

Figure 4.18: Efficiency of thermal modal analysis of wide and narrow temperature fields. The wide temperature field can be reconstructed accurately using only small number of modes while the narrow temperature field requires large number of modes due to its high spatial frequency.

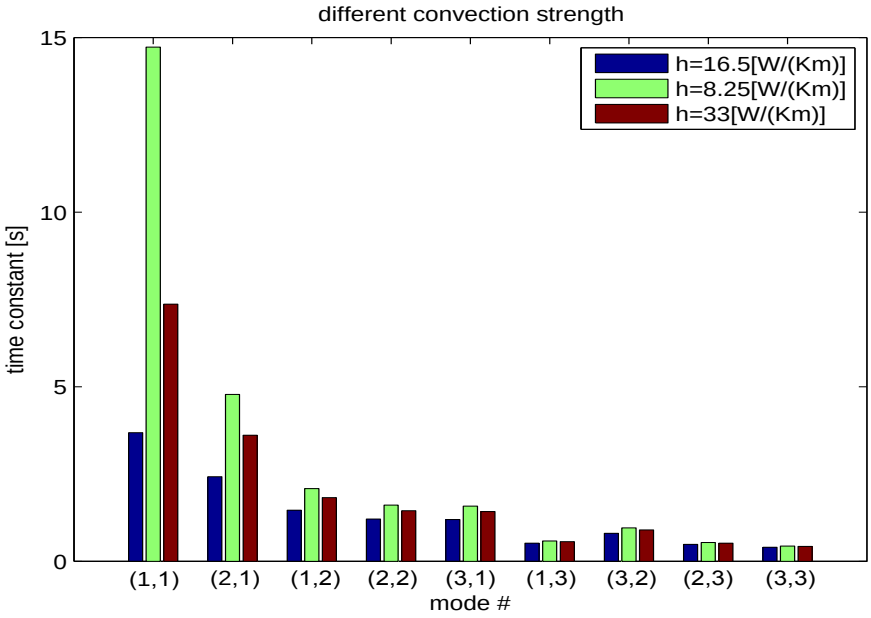

Figure 4.19: First 9 time constants with different convection cooling strength. Convection cooling strength affects all modes but most largely influences the first mode.

plate is thinner so the cooling term becomes relatively stronger, then all the modes behave in similar way and in this case the performance of Mode Cancellation is expected to degrade (Figure 4.20). Therefore, Mode Cancellation is especially suitable when thermal conductivity of the structure material is high and the cooling is not strong enough. On the other hand, Mode Cancellation is expected to perform less for material with small conductivity such as plastic under strong cooling .

4.7 Conclusions

In this chapter Mode Cancellation has been introduced as a novel technique of thermal displacement error compensation. Mode Cancellation is developed based on the understanding of thermal displacement error using Thermal Modal Analysis. Mode Cancellation controls and eliminates a number of modes from a thermal displacement field by applying and controlling external heat loads. As a result, a set of selected modes which have large influence to thermal displacement errors are eliminated and the thermal displacement error are reduced. These external control loads also excite the amplitudes of the remainder of the modes. Therefore, the performance of Mode Cancellation in several configurations was analyzed to understand the conditions in which Mode Cancellation performs well.

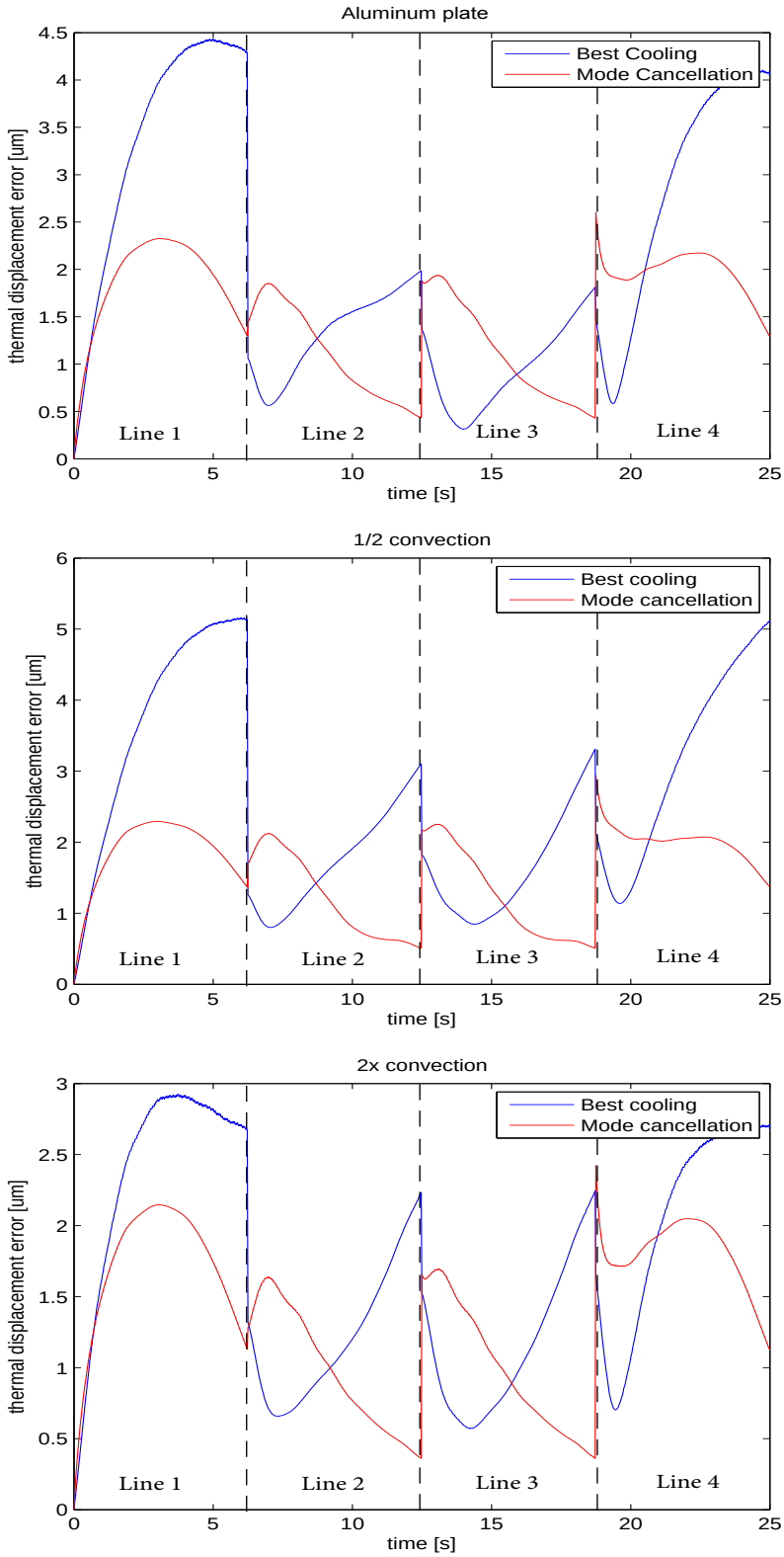

Figure 4.20: Mode cancellation results for different convection cooling strength.

Chapter 5

Modal Control using Linear Quadratic Regulator

5.1 Limitations and extension of Mode Cancellation

In the previous chapter, the idea of reducing thermal displacement error by controlling a selected number of modes, Mode Cancellation, was introduced and proved to be effective for an example case. However a fundamental limitation of Mode Cancellation is that it can only control up to the same number of modes as the number of external control heat loads. So the possibility of performance improvement is restricted by the number of individually controlled external heat loads applied to the target system. Also even if the numbers of external loads are sufficient, some combinations of modes cannot be fully controlled for a given set of external heat load locations. Mathematically, this is due to the singularity of the sensitivity matrix[1] of the target modes to the external loads ($[\boldsymbol{\Phi}_{\mathrm{nm}}]^{\mathrm{T}}$ in equation 4.4). When this matrix is singular or close to singular, then there is no exact solutions or there is only a solution which results in extremely large control power for the external loads.

One obvious solution for this limitation of Mode Cancellation is trying to control more modes than the number of external control heat loads. But obviously it is in that case no longer possible to control all the target modes of interest independently and eliminate them completely from the temperature field and the corresponding thermal displacement field. Instead it is required to balance the contribution from each mode to the thermal displacement error at the point of interest according to some objective function. In the next section, control of multiple modes (a higher number of modes than the number of independently controllable external control heat loads) using Linear Quadratic Regulator (LQR) is introduced. Mathematical formulations and simulation result of thermal displacement error reduction are described.

[1] The sensitivity matrix also becomes singular when a mode to be controlled is not controllable by the external control heat loads. In this case, the only way to control the mode is to change at least one location of the external control heat loads in such a way that the at least one external control heat load can excite the mode and make the mode controllable by the heat loads.

5.2 Modal Control using LQR

To apply LQR control to thermal error problems described using thermal modes, the model needs to be described in state space representation.

Assuming that the control heat loads are stationary point loads, then from equation (3.12), each differential equation describing the behavior of a thermal mode can be rewritten into the following equation:

$$\frac{\mathrm{d}\theta_{\mathrm{i}}(t)}{\mathrm{d}t} = -\frac{\theta_{\mathrm{i}}(t)}{\tau_{\mathrm{i}}} + \frac{\int \phi_{\mathrm{i}}(\boldsymbol{x}) q(\boldsymbol{x}, t) \mathrm{d}\boldsymbol{x}}{\rho c h \int \phi_{\mathrm{i}}(\boldsymbol{x})^2 \mathrm{d}\boldsymbol{x}} \tag{5.1}$$

$$= -\frac{\theta_{\mathrm{i}}(t)}{\tau_{\mathrm{i}}} + C_{\mathrm{i}} \sum_{\mathrm{j}=1}^{\mathrm{N}} \phi_{\mathrm{i}}(\boldsymbol{x}_{\mathrm{j}}) q_{\mathrm{j}}(t) \tag{5.2}$$

where $C_{\mathrm{i}} = \frac{1}{\rho c h \int \phi_{\mathrm{i}}(\boldsymbol{x})^2 \mathrm{d}\boldsymbol{x}}$ and N is the number of external control heat loads.

Then, the thermal model based on thermal modes can be summarized as follows in matrix form.

$$\frac{\mathrm{d}}{\mathrm{d}t} \begin{bmatrix} \theta_1(t) \\ \theta_2(t) \\ \theta_3(t) \\ \vdots \end{bmatrix} = \begin{bmatrix} -\frac{1}{\tau_1} & 0 & 0 & \cdots \\ 0 & -\frac{1}{\tau_2} & 0 & \cdots \\ 0 & 0 & -\frac{1}{\tau_3} & \cdots \\ \vdots & \vdots & \vdots & \ddots \end{bmatrix} \begin{bmatrix} \theta_1(t) \\ \theta_2(t) \\ \theta_3(t) \\ \vdots \end{bmatrix} \tag{5.3}$$

$$+ \begin{bmatrix} C_1 & 0 & 0 & \cdots \\ 0 & C_2 & 0 & \cdots \\ 0 & 0 & C_3 & \cdots \\ \vdots & \vdots & \vdots & \ddots \end{bmatrix} \begin{bmatrix} \phi_1(\boldsymbol{x}_1) & \phi_1(\boldsymbol{x}_2) & \phi_1(\boldsymbol{x}_3) & \cdots \\ \phi_2(\boldsymbol{x}_1) & \phi_2(\boldsymbol{x}_2) & \phi_2(\boldsymbol{x}_3) & \cdots \\ \phi_3(\boldsymbol{x}_1) & \phi_3(\boldsymbol{x}_2) & \phi_3(\boldsymbol{x}_3) & \cdots \\ \vdots & \vdots & \vdots & \ddots \end{bmatrix} \begin{bmatrix} q_1(t) \\ q_2(t) \\ q_3(t) \\ \vdots \end{bmatrix} \tag{5.4}$$

Summarizing this equation into the state space form:

$$\frac{\mathrm{d}}{\mathrm{d}t} \boldsymbol{x}_{\mathrm{s}}(t) = \boldsymbol{A} \boldsymbol{x}_{\mathrm{s}}(t) + \boldsymbol{B} \boldsymbol{u}_{\mathrm{s}}(t) \tag{5.5}$$

where $\boldsymbol{x}_\mathrm{s}$ is the state vector of the system, $\boldsymbol{u}_\mathrm{s}$ is the control input vector[2] and

$$\boldsymbol{x}_\mathrm{s} = \begin{bmatrix} \theta_1(t) \\ \theta_2(t) \\ \theta_3(t) \\ \vdots \end{bmatrix} \tag{5.6}$$

$$\boldsymbol{A} = \begin{bmatrix} -\frac{1}{\tau_1} & 0 & 0 & \cdots \\ 0 & -\frac{1}{\tau_2} & 0 & \cdots \\ 0 & 0 & -\frac{1}{\tau_3} & \cdots \\ \vdots & \vdots & \vdots & \ddots \end{bmatrix} \tag{5.7}$$

$$\boldsymbol{B} = \begin{bmatrix} C_1 & 0 & 0 & \cdots \\ 0 & C_2 & 0 & \cdots \\ 0 & 0 & C_3 & \cdots \\ \vdots & \vdots & \vdots & \ddots \end{bmatrix} \begin{bmatrix} \phi_1(\boldsymbol{x}_1) & \phi_1(\boldsymbol{x}_2) & \phi_1(\boldsymbol{x}_3) & \cdots \\ \phi_2(\boldsymbol{x}_1) & \phi_2(\boldsymbol{x}_2) & \phi_2(\boldsymbol{x}_3) & \cdots \\ \phi_3(\boldsymbol{x}_1) & \phi_3(\boldsymbol{x}_2) & \phi_3(\boldsymbol{x}_3) & \cdots \\ \vdots & \vdots & \vdots & \ddots \end{bmatrix} \tag{5.8}$$

LQR is a well known control technique [40] to minimize the weighted sum of state values plus the weighted sum of input power as described below as an objective function J for a time span from $t = 0$ to $t = \mathrm{T_{end}}$.

$$J = \int_0^{\mathrm{T_{end}}} (\boldsymbol{x}_\mathrm{s}^\mathrm{T} \boldsymbol{Q} \boldsymbol{x}_\mathrm{s} + \boldsymbol{u}_\mathrm{s}^\mathrm{T} \boldsymbol{R} \boldsymbol{u}_\mathrm{s}) \mathrm{d}t \tag{5.9}$$

$\boldsymbol{Q}$ and $\boldsymbol{R}$ are the weighting matrices for the state vector $\boldsymbol{x}_\mathrm{s}$ and the control inputs $\boldsymbol{u}_\mathrm{s}$, respectively. For a thermal model constructed using thermal modes, the state vector $\boldsymbol{x}$ can be chosen as the amplitudes of the modes that have a dominant influence in the thermal displacement error. $\boldsymbol{u}_\mathrm{s}$ is the control input vector which represents the amplitudes of external control heat loads to the system. $\boldsymbol{Q}$ and $\boldsymbol{R}$ are chosen according to the specific needs of the problem. Some examples will be given later in this chapter.

The following equation gives the optimal control proportional gain to minimize the objective function (5.9).

$$\boldsymbol{u}_\mathrm{s} = -\boldsymbol{K} \boldsymbol{x}_\mathrm{s} \tag{5.10}$$

$$\boldsymbol{K} = \boldsymbol{R}^{-1} \boldsymbol{B}^\mathrm{T} \boldsymbol{P} \tag{5.11}$$

where $\boldsymbol{P}$ satisfies the following Riccati equation.

$$\boldsymbol{A}^\mathrm{T} \boldsymbol{P} + \boldsymbol{P} \boldsymbol{A} - \boldsymbol{P} \boldsymbol{B} \boldsymbol{R}^{-1} \boldsymbol{B}^\mathrm{T} \boldsymbol{P} + \boldsymbol{Q} = \boldsymbol{0} \tag{5.12}$$

Using LQR with this thermal mode model, the number of modes to be controlled by the external control loads can exceed the number of the external control loads. Therefore, in principle, it can control all the modes simultaneously, and find out the mathematical optimal solution for the given objective function. Though in this way, the selected modes

[2] In the state space representation, $\boldsymbol{x}$, $\boldsymbol{y}$ and $\boldsymbol{u}$ are the standard notations for the state vector, output vector and input vector, respectively. However these symbols are already used in this thesis for coordinate vectors in equation and thermal displacement vector. Therefore, the state vector, output vector and input vector are denoted as $\boldsymbol{x}_\mathrm{s}$, $\boldsymbol{y}_\mathrm{s}$ and $\boldsymbol{u}_\mathrm{s}$ in this thesis.

to be controlled by this method are not longer controlled independently to each other as was the case of Mode Cancellation. In that sense, it can be stated that Modal Control using LQR makes the best balancing among the modes to be controlled to achieve the optimal value of the objective function.

Example of Modal Control using LQR

To see the performance of this method, thermal displacement error reduction for the same two path cases as presented in the previous Chapter is conducted by controlling 4 modes. The weighting functions $\boldsymbol{Q}$ and $\boldsymbol{R}$ are set as follows:

$$\boldsymbol{Q} = \boldsymbol{I} = \begin{bmatrix} 1 & 0 & 0 & \cdots \\ 0 & 1 & 0 & \cdots \\ 0 & 0 & 1 & \cdots \\ \vdots & \vdots & \vdots & \ddots \end{bmatrix}, \qquad \boldsymbol{R} = r\boldsymbol{I} = \begin{bmatrix} r & 0 & 0 & \cdots \\ 0 & r & 0 & \cdots \\ 0 & 0 & r & \cdots \\ \vdots & \vdots & \vdots & \ddots \end{bmatrix} \tag{5.13}$$

where $\boldsymbol{Q}$ weights all the selected modes equally and $\boldsymbol{R}$ weighs all the external control equally with a small constant value $r \ll 1$ so that practically in this example the control effort can be ignored.

Modal Control of 4 modes
Figure 5.1 shows the calculated amplitudes of the external heat loads which are almost identical[3] to the external loads amplitudes in the case of Mode Cancellation with 4 modes (Figure 4.6). Figure 5.2 shows the calculated amplitudes of the target 4 modes over time. The results show that the amplitudes of the target 4 modes are maintained at close to zero values. The resultant thermal displacement errors are also similar to the results of Mode Cancellation (Figure 5.3). When the number of modes to be controlled and the number of external heat loads are identical, the result from LQR control is practically identical to the results from Mode Cancellation ($\boldsymbol{Q}$ matrix has only diagonal elements and they are all equal to 1, and $\boldsymbol{R}$ matrix has only small values so that the control energy is not considered in the objective function).

5.2.1 Linear Quadratic Regulator with time varying weights [4]

In the previous section, LQR with thermal modes was described and its performance was compared with the performance of Mode Cancellation. One of the largest limitation of the idea is that it cannot cope with the time varying weighing factors as it is. If a time varying weighting factor can be used in this method, then thermal displacement error at a moving point of interest can be described as the objective function expressed by equation (5.9). Then, Modal Control with such a time varying weights $\boldsymbol{Q}(t)$ can minimize the thermal displacement error of the example problem discussed in the previous

[3] Intuitively speaking, the result of Modal Control of 4 modes is "identical" with the result of Mode Cancellation of 4 modes in the previous chapter other than the small difference due to $\boldsymbol{R}$ with very small diagonal weighting factors r in equation 5.13. Strictly speaking, it has not been proven yet if they result in the identical solution or not. For example, when the optimal solution is not unique, then it is not obvious if the Modal Control and Mode Cancellation would result in an identical optimal solution among the optimal "solutions". That is why it is written as "almost identical" in the text.

[4] There actually exists another way to solve LQR problem with time varying cost function $\boldsymbol{Q(t)}$ using Riccati differential equation [44].

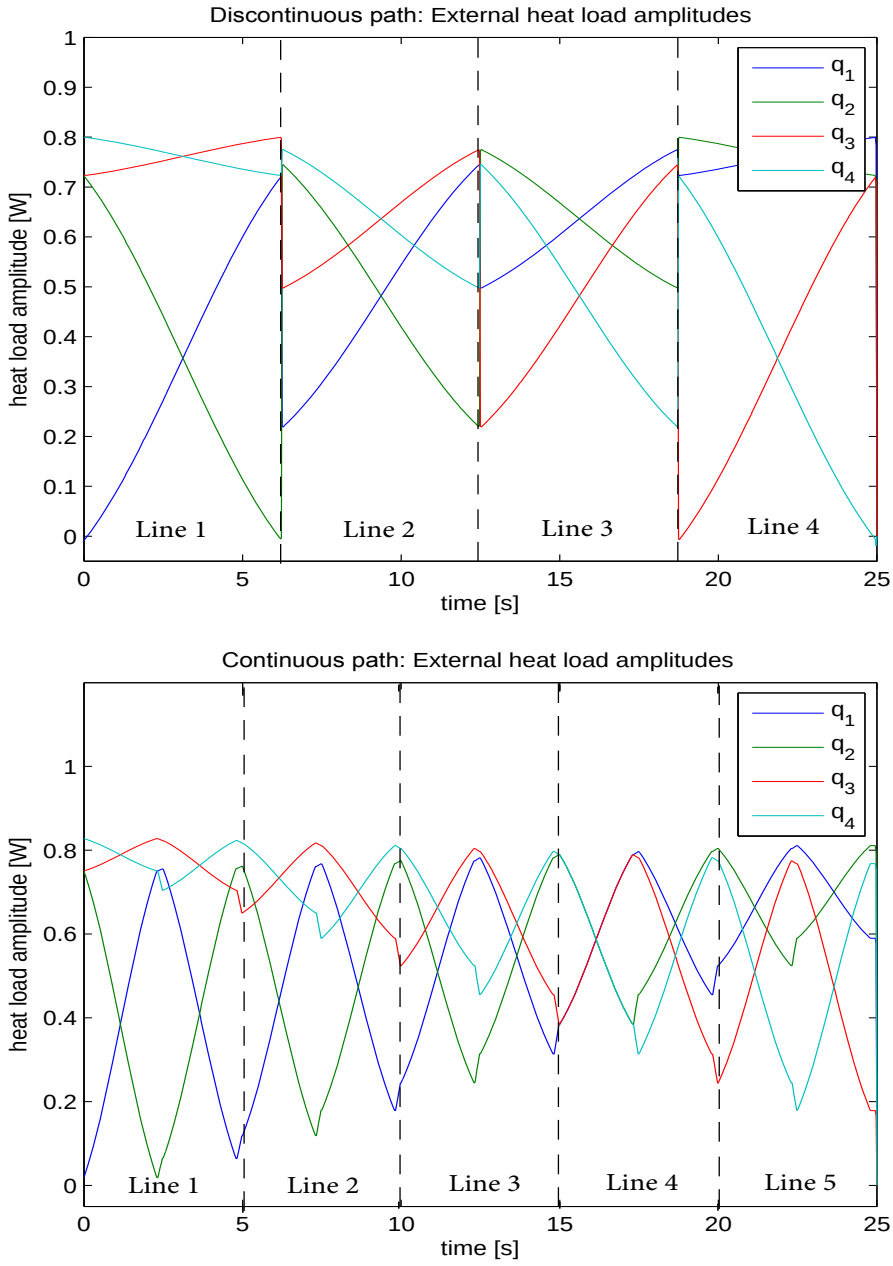

Figure 5.1: The amplitudes of four external heat loads by Modal Control with 4 modes control. Top: discontinuous path case. Bottom: continuous path case.

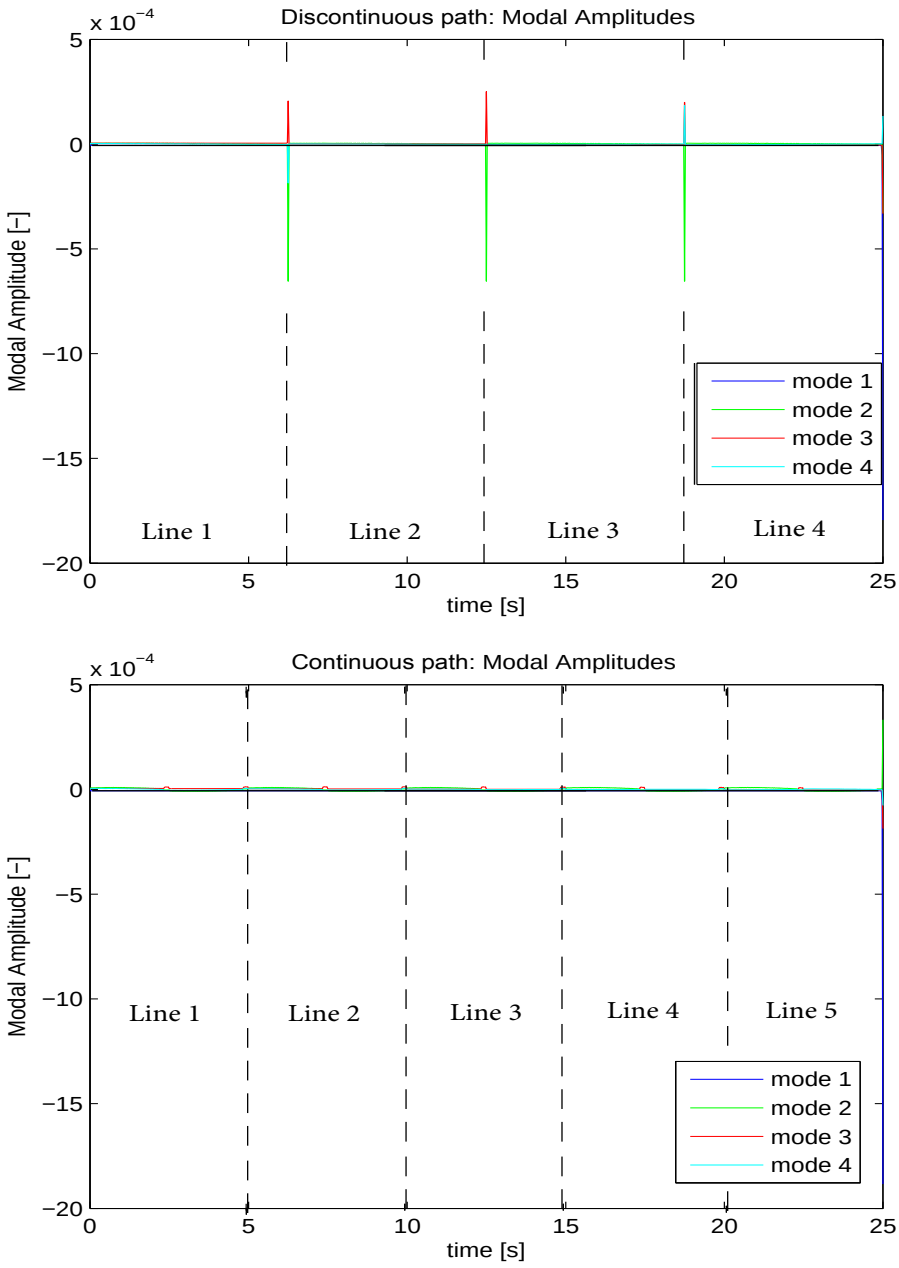

Figure 5.2: The amplitudes of the first 4 modes by Modal Control with 4 modes control. Top: discontinuous path case. Bottom: continuous path case.

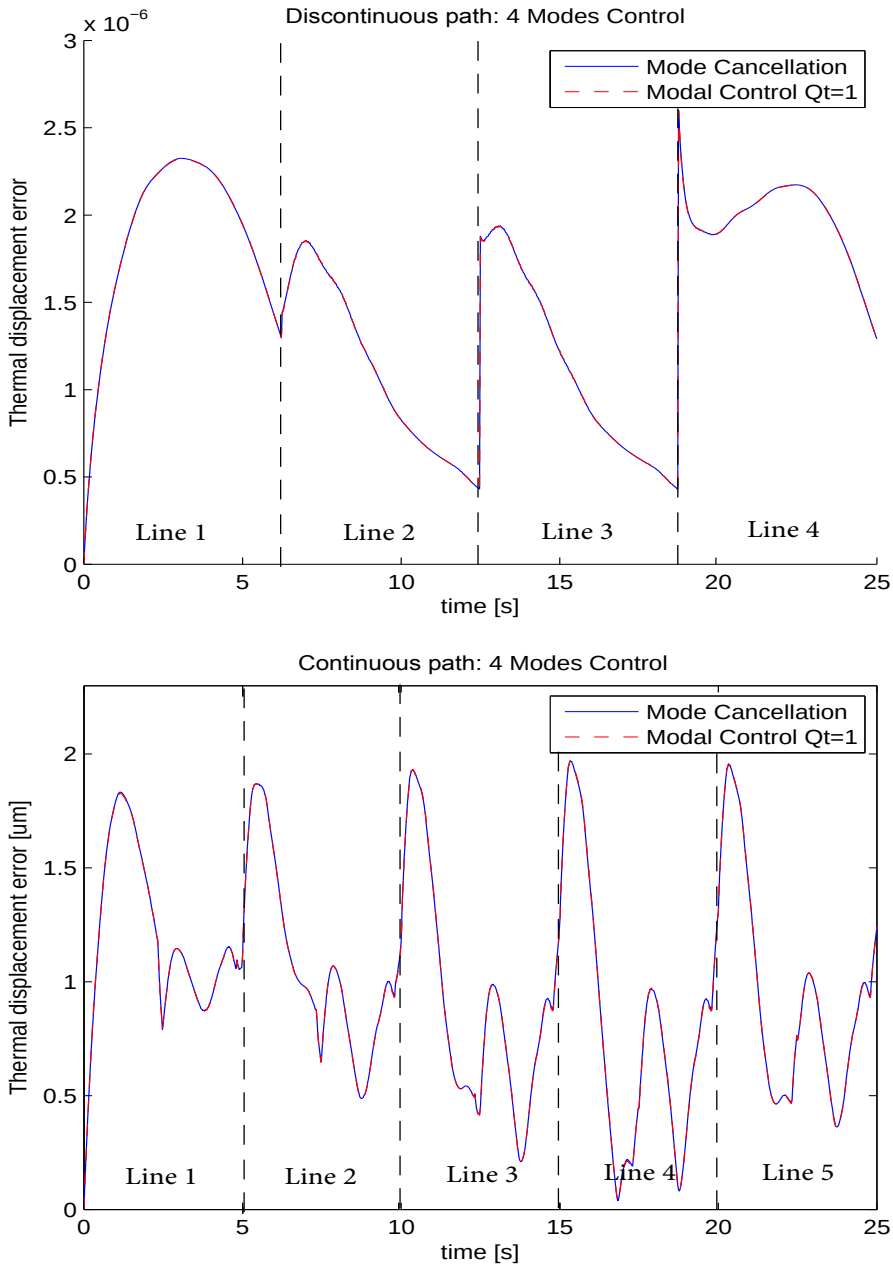

Figure 5.3: Comparison of thermal displacement error by Mode Cancellation with 4 modes (blue) control and Modal Control with 4 modes control (red). Top: discontinuous path case. Bottom: continuous path case.

Chapter. It is also possible to adapt to a situation in which the external loads location are moving over time. The latter will be described in the next section. In this section, how to adapt the time varying weighting factor to Modal Control using LQR is described.

LQR with time varying cost function $\boldsymbol{Q}(t)$ can be implemented by transforming the dynamic equation into a static representation as follows [4]. When the weighting matrix $\boldsymbol{Q}$ is time varying, equation 5.5 and 5.9 become as follows:

$$\frac{\mathrm{d}}{\mathrm{d}t}\boldsymbol{x}_{\mathrm{s}}(t) = \boldsymbol{A}\boldsymbol{x}_{\mathrm{s}}(t) + \boldsymbol{B}\boldsymbol{u}_{\mathrm{s}}(t) \tag{5.14}$$

$$J = \int_0^{\mathrm{T_{end}}} (\boldsymbol{x}_{\mathrm{s}}(t)^{\mathrm{T}}\boldsymbol{Q}(t)\boldsymbol{x}_{\mathrm{s}}(t) + \boldsymbol{u}_{\mathrm{s}}(t)^{\mathrm{T}}\boldsymbol{R}(t)\boldsymbol{u}_{\mathrm{s}}(t))\mathrm{d}t \tag{5.15}$$

To adapt to the time varying weighting factor, the matrix is transformed into a static representation which has all the time changing elements in one single large matrix. In this section, the implementation is described for the 3 states case for simplicity. However this can be extended easily into any number of states.

Let's start with a special case where the weighting matrix $\boldsymbol{Q}(t)$ has only non-zero diagonal elements.

$$\boldsymbol{Q}(t) = \begin{bmatrix} Q_{11}(t) & 0 & 0 \\ 0 & Q_{22}(t) & 0 \\ 0 & 0 & Q_{33}(t) \end{bmatrix} \tag{5.16}$$

Now select a number of points in time $t = t_1, t_2, t_3, \cdots$ to evaluate the matrix $\boldsymbol{Q}$ and then make a static representation $\bar{\boldsymbol{Q}}$:

$$\bar{\boldsymbol{Q}} = \left[\begin{array}{ccc} Q_{11}(t_1) & 0 & 0 \\ 0 & Q_{22}(t_1) & 0 \\ 0 & 0 & Q_{33}(t_1) \\ \hline Q_{11}(t_2) & 0 & 0 \\ 0 & Q_{22}(t_2) & 0 \\ 0 & 0 & Q_{33}(t_2) \\ \hline Q_{11}(t_3) & 0 & 0 \\ 0 & Q_{22}(t_3) & 0 \\ 0 & 0 & Q_{33}(t_3) \\ \hline \vdots & \vdots & \vdots \end{array}\right] \tag{5.17}$$

Every 3*3 matrix in the static representation $\bar{\boldsymbol{Q}}$ corresponds to $\boldsymbol{Q}(t)$ at each time step $t = t_1, t_2, t_3, \cdots$. Similarly, the state vector $\boldsymbol{x}_{\mathrm{s}}(t)$ is also transformed into a static representation $\bar{\boldsymbol{X}}_{\mathrm{s}}$:

$$\bar{\boldsymbol{X}}_{\mathrm{s}} = \begin{bmatrix} x_{\mathrm{s},1}(t_1) \\ x_{\mathrm{s},2}(t_1) \\ x_{\mathrm{s},3}(t_1) \\ \hline x_{\mathrm{s},1}(t_2) \\ x_{\mathrm{s},2}(t_2) \\ x_{\mathrm{s},3}(t_2) \\ \hline x_{\mathrm{s},1}(t_3) \\ x_{\mathrm{s},2}(t_3) \\ x_{\mathrm{s},3}(t_3) \\ \hline \vdots \end{bmatrix} \tag{5.18}$$

Make an artificial output function $\bar{\boldsymbol{Y}}_{\mathrm{s}}$ as follows:

$$\bar{\boldsymbol{Y}}_{\mathrm{s}} = \begin{bmatrix} y_{\mathrm{s},1}(t_1) \\ y_{\mathrm{s},2}(t_1) \\ y_{\mathrm{s},3}(t_1) \\ \hline y_{\mathrm{s},1}(t_2) \\ y_{\mathrm{s},2}(t_2) \\ y_{\mathrm{s},3}(t_2) \\ \hline y_{\mathrm{s},1}(t_3) \\ y_{\mathrm{s},2}(t_3) \\ y_{\mathrm{s},3}(t_3) \\ \hline \vdots \end{bmatrix} = \bar{\boldsymbol{C}}\,\bar{\boldsymbol{X}}_{\mathrm{s}} \tag{5.19}$$

$$\bar{\boldsymbol{C}} = \begin{bmatrix} \sqrt{Q_{11}(t_1)} & 0 & 0 \\ 0 & \sqrt{Q_{22}(t_1)} & 0 \\ 0 & 0 & \sqrt{Q_{33}(t_1)} \\ \hline \sqrt{Q_{11}(t_2)} & 0 & 0 \\ 0 & \sqrt{Q_{22}(t_2)} & 0 \\ 0 & 0 & \sqrt{Q_{33}(t_2)} \\ \hline \sqrt{Q_{11}(t_3)} & 0 & 0 \\ 0 & \sqrt{Q_{22}(t_3)} & 0 \\ 0 & 0 & \sqrt{Q_{33}(t_3)} \\ \hline \vdots & \vdots & \vdots \end{bmatrix} \tag{5.20}$$

Also, transform the control input $\boldsymbol{u}_{\mathrm{s}}(t)$ into a static representation $\bar{\boldsymbol{U}}_{\mathrm{s}}$ as well.

$$\bar{\boldsymbol{U}}_{\mathrm{s}} = \begin{bmatrix} u_{\mathrm{s},1}(t_1) \\ u_{\mathrm{s},2}(t_1) \\ u_{\mathrm{s},3}(t_1) \\ \hline u_{\mathrm{s},1}(t_2) \\ u_{\mathrm{s},2}(t_2) \\ u_{\mathrm{s},3}(t_2) \\ \hline u_{\mathrm{s},1}(t_3) \\ u_{\mathrm{s},2}(t_3) \\ u_{\mathrm{s},3}(t_3) \\ \hline \vdots \end{bmatrix} \tag{5.21}$$

Also same for $\boldsymbol{R}(t)$.

$$\bar{\boldsymbol{R}} = \begin{bmatrix} r_{11}(t_1) & 0 & 0 \\ 0 & r_{22}(t_1) & 0 \\ 0 & 0 & r_{33}(t_1) \\ \hline r_{11}(t_2) & 0 & 0 \\ 0 & r_{22}(t_2) & 0 \\ 0 & 0 & r_{33}(t_2) \\ \hline r_{11}(t_3) & 0 & 0 \\ 0 & r_{22}(t_3) & 0 \\ 0 & 0 & r_{33}(t_3) \\ \hline \vdots & \vdots & \vdots \end{bmatrix} \tag{5.22}$$

So, the objective function J in equation 5.15 can be rewritten into:

$$\bar{J} = \bar{\boldsymbol{Y}}_{\mathrm{s}}{}^{\mathrm{T}} \bar{\boldsymbol{Y}}_{\mathrm{s}} + \bar{\boldsymbol{U}}_{\mathrm{s}}{}^{\mathrm{T}} \bar{\boldsymbol{R}} \bar{\boldsymbol{U}}_{\mathrm{s}} = \bar{\boldsymbol{X}}_{\mathrm{s}}{}^{\mathrm{T}} \bar{\boldsymbol{Q}} \bar{\boldsymbol{X}}_{\mathrm{s}} + \bar{\boldsymbol{U}}_{\mathrm{s}}{}^{\mathrm{T}} \bar{\boldsymbol{R}} \bar{\boldsymbol{U}}_{\mathrm{s}} \tag{5.23}$$

In the discrete form of the state space representation (5.14), $\boldsymbol{y}_{\mathrm{s}}(t)$ can be rewritten into:

$$\boldsymbol{x}_{\mathrm{s}}(\mathrm{k}+1) = \boldsymbol{A}_{\mathrm{d}} \boldsymbol{x}_{\mathrm{s}}(\mathrm{k}) + \boldsymbol{B}_{\mathrm{d}} \boldsymbol{u}_{\mathrm{s}}(\mathrm{k}) \tag{5.24}$$

$$\boldsymbol{y}_{\mathrm{s}}(\mathrm{k}) = \boldsymbol{C}_{\mathrm{d}}(\mathrm{k}) \boldsymbol{x}_{\mathrm{s}}(\mathrm{k}) \tag{5.25}$$

Here, k is the discrete time variable. $\boldsymbol{A}_{\mathrm{d}}$ and $\boldsymbol{B}_{\mathrm{d}}$ are discrete state space representation of matrix $\boldsymbol{A}$ and $\boldsymbol{B}$ in equation (5.14). $\boldsymbol{C}_{\mathrm{d}}(\mathrm{k})$ is discrete time representation of the static representation matrix $\bar{\boldsymbol{C}}$ at k-th time step:

$$\boldsymbol{C}_{\mathrm{d}}(\mathrm{k}) = \begin{bmatrix} \sqrt{Q_{11}(\mathrm{k})} & 0 & 0 \\ 0 & \sqrt{Q_{22}(\mathrm{k})} & 0 \\ 0 & 0 & \sqrt{Q_{33}(\mathrm{k})} \end{bmatrix} \tag{5.26}$$

In the same manner,

$$\begin{aligned} \boldsymbol{y}_{\mathrm{s}}(\mathrm{k}+1) &= \boldsymbol{C}_{\mathrm{d}}(\mathrm{k}+1) \boldsymbol{x}_{\mathrm{s}}(\mathrm{k}+1) && (5.27) \\ &= \boldsymbol{C}_{\mathrm{d}}(\mathrm{k}+1)(\boldsymbol{A}_{\mathrm{d}} \boldsymbol{x}_{\mathrm{s}}(\mathrm{k}) + \boldsymbol{B}_{\mathrm{d}} \boldsymbol{u}_{\mathrm{s}}(\mathrm{k})) && (5.28) \end{aligned}$$

$$\begin{aligned} \boldsymbol{y}_{\mathrm{s}}(\mathrm{k}+2) &= \boldsymbol{C}_{\mathrm{d}}(\mathrm{k}+2) \boldsymbol{x}_{\mathrm{s}}(\mathrm{k}+2) && (5.29) \\ &= \boldsymbol{C}_{\mathrm{d}}(\mathrm{k}+2)(\boldsymbol{A}_{\mathrm{d}} \boldsymbol{x}_{\mathrm{s}}(\mathrm{k}+1) + \boldsymbol{B}_{\mathrm{d}} \boldsymbol{u}_{\mathrm{s}}(\mathrm{k}+1)) && (5.30) \\ &= \boldsymbol{C}_{\mathrm{d}}(\mathrm{k}+2)(\boldsymbol{A}_{\mathrm{d}}^2 \boldsymbol{x}_{\mathrm{s}}(\mathrm{k}) + \boldsymbol{A}_{\mathrm{d}} \boldsymbol{B}_{\mathrm{d}} \boldsymbol{u}_{\mathrm{s}}(\mathrm{k}) + \boldsymbol{B}_{\mathrm{d}} \boldsymbol{u}_{\mathrm{s}}(\mathrm{k}+1)) && (5.31) \\ & && (5.32) \end{aligned}$$

Then the output vector $\bar{\boldsymbol{Y}}_{\mathrm{s}}$ can be summarized as follows:

$$\begin{aligned}
\boldsymbol{Y}_{\mathrm{s}}(t) &= \left[\begin{array}{c} y_{\mathrm{s},1}(t_1) \\ y_{\mathrm{s},2}(t_1) \\ \hline y_{\mathrm{s},3}(t_1) \\ \hline y_{\mathrm{s},1}(t_2) \\ y_{\mathrm{s},2}(t_2) \\ \hline y_{\mathrm{s},3}(t_2) \\ \hline y_{\mathrm{s},1}(t_3) \\ y_{\mathrm{s},2}(t_3) \\ \hline y_{\mathrm{s},3}(t_3) \\ \hline \vdots \end{array}\right] = \left[\begin{array}{c} \boldsymbol{y}_{\mathrm{s}}(t_1) \\ \boldsymbol{y}_{\mathrm{s}}(t_2) \\ \boldsymbol{y}_{\mathrm{s}}(t_3) \\ \vdots \end{array}\right] && (5.33) \\
&= \left[\begin{array}{c} \boldsymbol{c}(t_1) \\ \boldsymbol{c}(t_2)\boldsymbol{A}_{\mathrm{d}} \\ \boldsymbol{c}(t_3)\boldsymbol{A}_{\mathrm{d}}^2 \\ \boldsymbol{c}(t_4)\boldsymbol{A}_{\mathrm{d}}^3 \\ \vdots \end{array}\right] \boldsymbol{x}_{\mathrm{s}}(t_1) \\
&+ \left[\begin{array}{cccc} \boldsymbol{0} & \boldsymbol{0} & \boldsymbol{0} & \cdots \\ \boldsymbol{c}(t_1)\boldsymbol{B}_{\mathrm{d}} & \boldsymbol{0} & \boldsymbol{0} & \cdots \\ \boldsymbol{c}(t_2)\boldsymbol{A}_{\mathrm{d}}\boldsymbol{B}_{\mathrm{d}} & \boldsymbol{c}(t_2)\boldsymbol{B}_{\mathrm{d}} & \boldsymbol{0} & \cdots \\ \boldsymbol{c}(t_3)\boldsymbol{A}_{\mathrm{d}}^2\boldsymbol{B}_{\mathrm{d}} & \boldsymbol{c}(t_3)\boldsymbol{A}_{\mathrm{d}}\boldsymbol{B}_{\mathrm{d}} & \boldsymbol{c}(t_3)\boldsymbol{B}_{\mathrm{d}} & \cdots \\ \vdots & \vdots & \vdots & \ddots \end{array}\right] \left[\begin{array}{c} \boldsymbol{u}_{\mathrm{s}}(t_1) \\ \boldsymbol{u}_{\mathrm{s}}(t_2) \\ \boldsymbol{u}_{\mathrm{s}}(t_3) \\ \boldsymbol{u}_{\mathrm{s}}(t_4) \\ \vdots \end{array}\right] && (5.34) \\
&= \bar{\boldsymbol{O}}\boldsymbol{x}_{\mathrm{s}}(t_1) + \bar{\boldsymbol{H}}_{\mathrm{CT}}\bar{\boldsymbol{U}}_{\mathrm{s}} && (5.35)
\end{aligned}$$

where

$$\bar{\boldsymbol{O}} = \left[\begin{array}{c} \boldsymbol{c}(t_1) \\ \boldsymbol{c}(t_2)\boldsymbol{A}_{\mathrm{d}} \\ \boldsymbol{c}(t_3)\boldsymbol{A}_{\mathrm{d}}^2 \\ \boldsymbol{c}(t_4)\boldsymbol{A}_{\mathrm{d}}^3 \\ \vdots \end{array}\right] \tag{5.36}$$

$$\bar{\boldsymbol{H}}_{\mathrm{CT}} = \left[\begin{array}{cccc} \boldsymbol{0} & \boldsymbol{0} & \boldsymbol{0} & \cdots \\ \boldsymbol{c}(t_1)\boldsymbol{B}_{\mathrm{d}} & \boldsymbol{0} & \boldsymbol{0} & \cdots \\ \boldsymbol{c}(t_2)\boldsymbol{A}_{\mathrm{d}}\boldsymbol{B}_{\mathrm{d}} & \boldsymbol{c}(t_2)\boldsymbol{B}_{\mathrm{d}} & \boldsymbol{0} & \cdots \\ \boldsymbol{c}(t_3)\boldsymbol{A}_{\mathrm{d}}^2\boldsymbol{B}_{\mathrm{d}} & \boldsymbol{c}(3)\boldsymbol{A}_{\mathrm{d}}\boldsymbol{B}_{\mathrm{d}} & \boldsymbol{c}(t_3)\boldsymbol{B}_{\mathrm{d}} & \cdots \\ \vdots & \vdots & \vdots & \ddots \end{array}\right] \tag{5.37}$$

Then

$$\begin{aligned}
\bar{\boldsymbol{Y}}_{\mathrm{s}}{}^{\mathrm{T}}\bar{\boldsymbol{Y}}_{\mathrm{s}} &= \bar{\boldsymbol{O}}\boldsymbol{x}_{\mathrm{s}}(t_1) + \bar{\boldsymbol{H}}_{\mathrm{CT}}\bar{\boldsymbol{U}}_{\mathrm{s}})^{\mathrm{T}}(\bar{\boldsymbol{O}}\boldsymbol{x}_{\mathrm{s}}(t_1) + \bar{\boldsymbol{H}}_{\mathrm{CT}}\bar{\boldsymbol{U}}_{\mathrm{s}}) && (5.38) \\
&= \bar{\boldsymbol{O}}^{\mathrm{T}}\bar{\boldsymbol{O}}\boldsymbol{x}_{\mathrm{s}}(t_1)^2 + \bar{\boldsymbol{O}}^{\mathrm{T}}\bar{\boldsymbol{H}}_{\mathrm{CT}}\bar{\boldsymbol{U}}_{\mathrm{s}}\boldsymbol{x}_{\mathrm{s}}(t_1) \\
&+ \bar{\boldsymbol{U}}_{\mathrm{s}}{}^{\mathrm{T}}\bar{\boldsymbol{H}}_{\mathrm{CT}}^{\mathrm{T}}\bar{\boldsymbol{O}}\boldsymbol{x}_{\mathrm{s}}(t_1) + \bar{\boldsymbol{U}}_{\mathrm{s}}{}^{\mathrm{T}}\bar{\boldsymbol{H}}_{\mathrm{CT}}^{\mathrm{T}}\bar{\boldsymbol{H}}_{\mathrm{CT}}\bar{\boldsymbol{U}}_{\mathrm{s}} && (5.39)
\end{aligned}$$

At the optimal solution, the derivative of the objective function $\bar{J}$ in equation 5.23 with respect to $\bar{\boldsymbol{U}}_{\mathrm{s}}$ should be 0.

$$\frac{\partial \bar{J}}{\partial \bar{\boldsymbol{U}}_{\mathrm{s}}} = \frac{\partial}{\partial \bar{\boldsymbol{U}}_{\mathrm{s}}}(\bar{\boldsymbol{Y}}_{\mathrm{s}}{}^{\mathrm{T}}\bar{\boldsymbol{Y}}_{\mathrm{s}} + \bar{\boldsymbol{U}}_{\mathrm{s}}{}^{\mathrm{T}}\bar{\boldsymbol{R}}\bar{\boldsymbol{U}}_{\mathrm{s}}) \tag{5.40}$$

$$= \frac{\partial}{\partial \bar{\boldsymbol{U}}_{\mathrm{s}}}[\bar{\boldsymbol{O}}^{T}\bar{\boldsymbol{O}}\boldsymbol{x}_{\mathrm{s}}(t_1)^2 + \bar{\boldsymbol{O}}^{\mathrm{T}}\bar{\boldsymbol{H}}_{\mathrm{CT}}\bar{\boldsymbol{U}}_{\mathrm{s}}\boldsymbol{x}_{\mathrm{s}}(t_1) + \bar{\boldsymbol{U}}_{\mathrm{s}}{}^{\mathrm{T}}\bar{\boldsymbol{H}}_{\mathrm{CT}}^{\mathrm{T}}\bar{\boldsymbol{O}}\boldsymbol{x}_{\mathrm{s}}(t_1) \tag{5.41}$$

$$+ \bar{\boldsymbol{U}}_{\mathrm{s}}{}^{\mathrm{T}}\bar{\boldsymbol{H}}_{\mathrm{CT}}^{\mathrm{T}}\bar{\boldsymbol{H}}_{\mathrm{CT}}\bar{\boldsymbol{U}}_{\mathrm{s}} + \bar{\boldsymbol{U}}_{\mathrm{s}}{}^{\mathrm{T}}\bar{\boldsymbol{R}}\bar{\boldsymbol{U}}_{\mathrm{s}}] \tag{5.42}$$

$$= 2\bar{\boldsymbol{H}}_{\mathrm{CT}}^{\mathrm{T}}\bar{\boldsymbol{O}}\boldsymbol{x}_{\mathrm{s}}(t_1) + 2(\bar{\boldsymbol{H}}_{\mathrm{CT}}^{\mathrm{T}}\bar{\boldsymbol{H}}_{\mathrm{CT}} + \bar{\boldsymbol{R}}) \tag{5.43}$$

$$= \boldsymbol{0} \tag{5.44}$$

Therefore,

$$\bar{\boldsymbol{U}}_{\mathrm{s}} = -(\bar{\boldsymbol{H}}_{\mathrm{CT}}^{\mathrm{T}}\bar{\boldsymbol{H}}_{\mathrm{CT}} + \bar{\boldsymbol{R}})^{-1}\bar{\boldsymbol{H}}_{\mathrm{CT}}^{\mathrm{T}}\bar{\boldsymbol{O}}\boldsymbol{x}_{\mathrm{s}}(t_1) \tag{5.45}$$

Example
To demonstrate how LQR with time varying cost function $\boldsymbol{Q}(t)$, a result of LQR control with time varying $\boldsymbol{Q}(t)$ is shown in Figure 5.4. LQR controls first four modes (1,1), (1,2), (2,1), (2,2) with time varying cost function $\boldsymbol{Q}(t)$ which is equal to 1 for $t = 5 \ldots 10$ s and $t = 15 \ldots 20$ s and 0 for the rest of time (red lines in the graphs in Figure 5.4). As can be seen from the modal amplitudes' graphs (blue curves) in Figure 5.4, they are well controlled for the period of $t = 5 \ldots 10$ s and $t = 15 \ldots 20$ s. Figure 5.5 shows the amplitudes of the external loads for the example case. The external loads are not equal to zero during $t = 0 \ldots 5$ s and $t = 10 \ldots 15$ s to to make the target modes' modal amplitudes as small as possible at $t = 5$ s and $t = 15$ s. After $t = 20$ s, the external amplitudes are equal to zero, with zero control to all modes as there is no period after $t = 20$ s to be weighted by the cost function.

Non-diagonal weight matrix $\boldsymbol{Q}(t)$
For the case that weighting matrix $\boldsymbol{Q}(t)$ is not diagonal matrix, it is necessary to calculate the square root of the $\boldsymbol{Q}$ matrix. In general this is not possible unless the matrix has certain properties, for example it needs to be a symmetry matrix. In this research, the objective is to reduce the thermal displacement error for a moving point of interest. This can be implemented into a diagonal weighting matrix $\boldsymbol{Q}(t)$ as shown below. So first, the implementation of such $\boldsymbol{Q}(t)$ is described. And then calculation of square root of a symmetric matrix using modified Cholesky decomposition method is described.

$\boldsymbol{Q}(t)$ matrix for thermal displacement error over a moving point of interest
In the previous section LQR was used to control the amplitude of the lower thermal modes, with the underlying assumption that the resulting thermal displacement would be small as a result. In this section the thermal displacement error Err(t) will be used directly to control the amplitudes of the control heat loads. Thermal displacement error Err(t) along with the path of the original heat load $\boldsymbol{x}_{\mathrm{POI}}$ can be written as follows:

$$\mathrm{Err}(t) = \sqrt{\left(\sum_{i=1}^{\infty}(\psi_{\mathrm{u,i}}(\boldsymbol{x}_{\mathrm{POI}}(t))\theta_{\mathrm{i}}(t))\right)^2 + \left(\sum_{i=1}^{\infty}(\psi_{\mathrm{v,i}}(\boldsymbol{x}_{\mathrm{POI}}(t))\theta_{\mathrm{i}}(t))\right)^2} \tag{5.46}$$

Thermal displacement field in x and y direction $\boldsymbol{\psi}_{\mathrm{u}}$ and $\boldsymbol{\psi}_{\mathrm{v}}$ have only single index "i" here for the sake of simplifying the following equations. But the equation is compatible

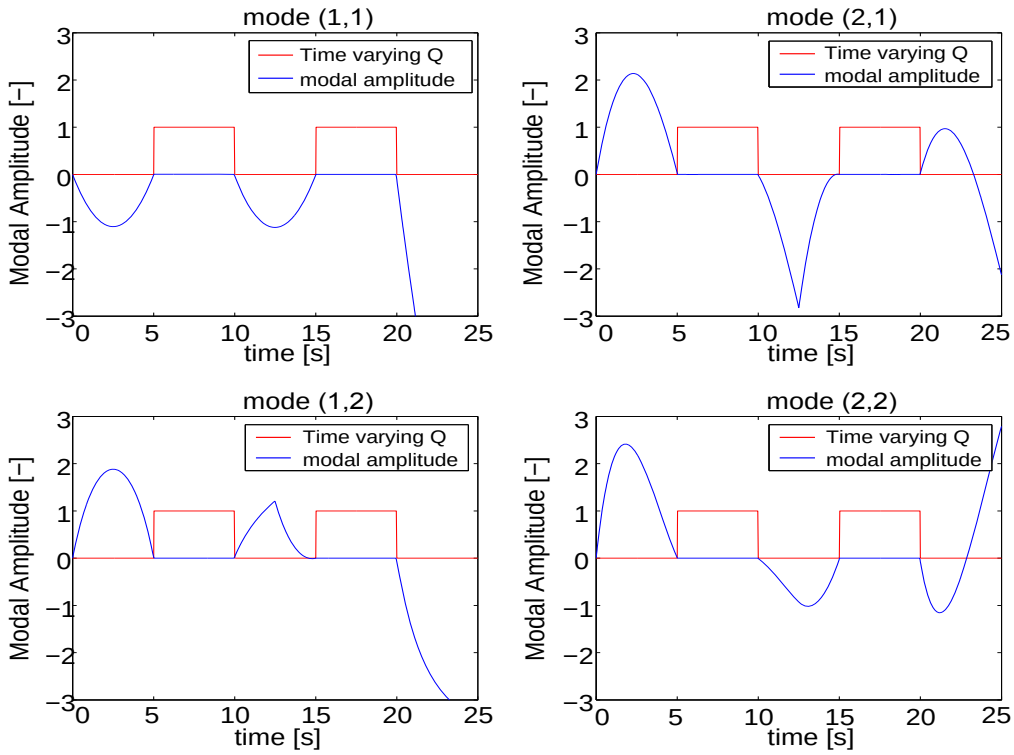

Figure 5.4: Modal control with time varying cost function $\boldsymbol{Q}(\mathrm{t})$. When time varying cost function $\boldsymbol{Q}(\mathrm{t})$ (red) is equal to 1, the amplitude of each mode (blue) are controlled to be equal to 0.

with thermal displacement field with two indices "(i,j)" as well.

From the observation that Err(t) becomes minimum at the same location as $\mathrm{Err(t)}^2$, the weighting factor $\boldsymbol{Q}(t)$ is formulated as follows:

$$\boldsymbol{Q}(t) = \begin{bmatrix} \psi_{\mathrm{u},1}^2 + \psi_{\mathrm{v},1}^2 & \psi_{\mathrm{u},1}\psi_{\mathrm{u},2} + \psi_{\mathrm{v},1}\psi_{\mathrm{v},2} & \psi_{\mathrm{u},1}\psi_{\mathrm{u},3} + \psi_{\mathrm{v},1}\psi_{\mathrm{v},3} & \cdots \\ \psi_{\mathrm{u},2}\psi_{\mathrm{u},1} + \psi_{\mathrm{v},2}\psi_{\mathrm{v},1} & \psi_{\mathrm{u},2}^2 + \psi_{\mathrm{v},2}^2 & \psi_{\mathrm{u},2}\psi_{\mathrm{u},3} + \psi_{\mathrm{v},2}\psi_{\mathrm{v},3} & \cdots \\ \psi_{\mathrm{u},3}\psi_{\mathrm{u},1} + \psi_{\mathrm{v},3}\psi_{\mathrm{v},1} & \psi_{\mathrm{u},3}\psi_{\mathrm{u},2} + \psi_{\mathrm{v},3}\psi_{\mathrm{v},2} & \psi_{\mathrm{u},3}^2 + \psi_{\mathrm{v},3}^2 & \cdots \\ \vdots & \vdots & \vdots & \ddots \end{bmatrix} \tag{5.47}$$

where each $\psi_{\mathrm{x,i}}$ and $\psi_{\mathrm{v,j}}$ (i,j=1… the number of modes in the model) are thew time dependent thermal displacement field value at the the location of the moving point of interest:

$$\psi_{\mathrm{u,i}} = \psi_{\mathrm{u,i}}(\boldsymbol{x}_{\mathrm{POI}}(t)) \tag{5.48}$$
$$\psi_{\mathrm{v,j}} = \psi_{\mathrm{v,j}}(\boldsymbol{y}_{\mathrm{POI}}(t)) \tag{5.49}$$

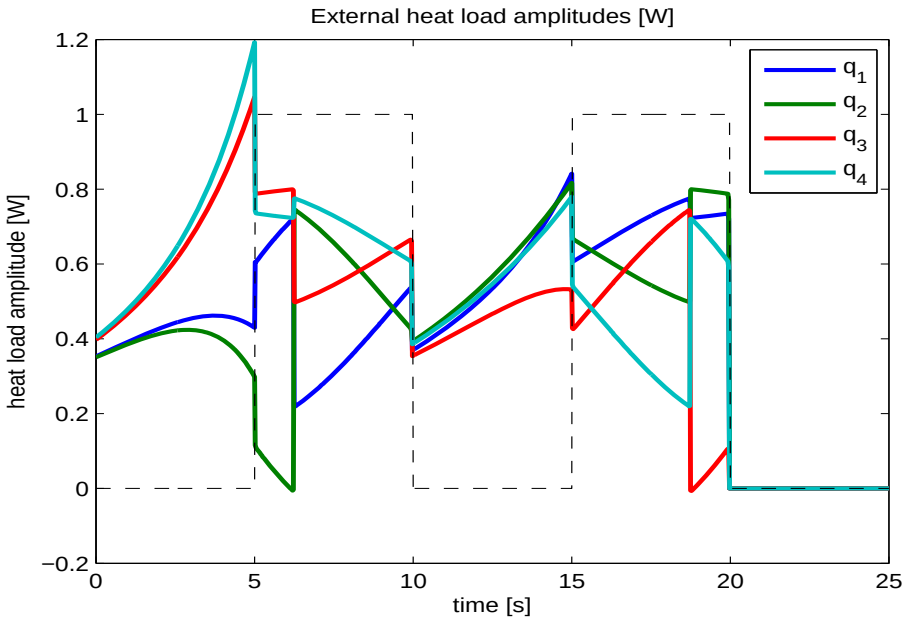

Figure 5.5: External heat load amplitudes calculated by Modal Control with time varying cost function $\boldsymbol{Q}$(t). Dashed line represents time varying cost function $\boldsymbol{Q}(t)$. The external control loads have non zero values even during the periods of $\boldsymbol{Q}(t) = 0$. Even during these periods, the amplitudes of the target modes need to be controlled so that the amplitudes of the modes become 0 at the beginning of the period of $\boldsymbol{Q}(t) = 1$.

Then

$$\mathrm{Err}(t)^2 = \boldsymbol{x}_\mathrm{s}(t)^T \boldsymbol{Q}(t) \boldsymbol{x}_\mathrm{s}(t) \tag{5.50}$$

The optimal solution which minimizes the objective function J using this $\boldsymbol{Q}(t)$ in the equation (5.50) is also minimizes $\mathrm{Err}(t)$.

The matrix $\boldsymbol{Q}(t)$ is symmetric. Then the square root of this matrix can be calculated using a modified Cholesky method. The static representation of the matrix can be calculated in the same way as equation (5.17). Then the square root of $\boldsymbol{Q}(t)$ at each time step is calculated using a modified Cholesky method as described below. Then the following equations (equation (5.18) to equation (5.45)) can be calculated in the same manner as described in this section.

Modified Cholesky decomposition

Modified Cholesky decomposition decomposes a symmetric matrix into a set of triangular matrices and diagonal matrices. The principle of the method can be found in literature [27], [24]. A matlab function for conducting modified Cholesky decomposition is available at [9]. Using modified Cholesky decomposition method, symmetrical matrix $\boldsymbol{Q}(t)$ can be decomposed as follows.

$$\boldsymbol{Q}(t) = \boldsymbol{L}(t)\boldsymbol{D}(t)\boldsymbol{L}(t)^T - \boldsymbol{E}(t) \tag{5.51}$$

$\boldsymbol{L}(t)$ is a triangular matrix and $\boldsymbol{D}(t)$ and $\boldsymbol{E}(t)$ are diagonal matrices. Then the artificial output function $\boldsymbol{y}_{\mathrm{s}}(t)$ can be formulated as follows:

$$\boldsymbol{y}_{\mathrm{s}}(t) = \boldsymbol{L}(t)^{\mathrm{T}} \boldsymbol{x}_{\mathrm{s}}(t) \tag{5.52}$$

And the objective function J can be written as:

$$\bar{J} = \bar{\boldsymbol{Y}}_{\mathrm{s}}{}^{\mathrm{T}} \bar{\boldsymbol{D}} \bar{\boldsymbol{Y}}_{\mathrm{s}} - \bar{\boldsymbol{X}}_{\mathrm{s}}{}^{\mathrm{T}} \bar{\boldsymbol{E}} \bar{\boldsymbol{X}}_{\mathrm{s}} + \bar{\boldsymbol{U}}_{\mathrm{s}}{}^{\mathrm{T}} \bar{\boldsymbol{R}} \bar{\boldsymbol{U}}_{\mathrm{s}} \tag{5.53}$$

Then similar to equations (5.40) to (5.45), the control input $\bar{\boldsymbol{U}}_{\mathrm{s}}$ can be calculated by making the derivative of the objective function J by the control input vector $\bar{\boldsymbol{U}}_{\mathrm{s}}$ equal to 0.

$$\frac{\partial \bar{J}}{\partial \bar{\boldsymbol{U}}_{\mathrm{s}}} = \frac{\partial}{\partial \bar{\boldsymbol{U}}_{\mathrm{s}}} (\bar{\boldsymbol{Y}}_{\mathrm{s}}{}^{\mathrm{T}} \bar{\boldsymbol{D}} \bar{\boldsymbol{Y}}_{\mathrm{s}} - \bar{\boldsymbol{X}}_{\mathrm{s}}{}^{\mathrm{T}} \bar{\boldsymbol{E}} \bar{\boldsymbol{X}}_{\mathrm{s}} + \bar{\boldsymbol{U}}_{\mathrm{s}}{}^{\mathrm{T}} \bar{\boldsymbol{R}} \bar{\boldsymbol{U}}_{\mathrm{s}}) \tag{5.54}$$

$$= \frac{\partial}{\partial \bar{\boldsymbol{U}}_{\mathrm{s}}} (\bar{\boldsymbol{Y}}_{\mathrm{s}}{}^{\mathrm{T}} \bar{\boldsymbol{D}} \bar{\boldsymbol{Y}}_{\mathrm{s}}) + \frac{\partial}{\partial \bar{\boldsymbol{U}}_{\mathrm{s}}} (\bar{\boldsymbol{U}}_{\mathrm{s}}{}^{\mathrm{T}} \bar{\boldsymbol{R}} \bar{\boldsymbol{U}}_{\mathrm{s}}) \tag{5.55}$$

$$= 0 \tag{5.56}$$

$$\bar{\boldsymbol{U}}_{\mathrm{s}} = -(\bar{\boldsymbol{H}}_{\mathrm{CT}}^{\mathrm{T}} \bar{\boldsymbol{D}} \bar{\boldsymbol{H}}_{\mathrm{CT}} + \bar{\boldsymbol{R}})^{-1} \bar{\boldsymbol{H}}_{\mathrm{CT}}^{\mathrm{T}} \bar{\boldsymbol{D}} \bar{\boldsymbol{O}} \boldsymbol{x}_{\mathrm{s}}(t_1) \tag{5.57}$$

The results of Modal Control with LQR are compared with Mode Cancellation control in Figure 5.6. The result of 4 modes modal control (target controlled modes are mode(1,1), mode(1,2), mode(2,1) and mode(2,2), the same 4 modes as the Mode Cancellation example in the previous chapter) with $\boldsymbol{Q}(t)$ in equation (5.47) is the blue curve (referred to as "Modal Control 4, Qt=Err" in Figure 5.6). Compared to the result of Mode Cancellation with 4 modes control (red curve (referred to as 'Mode Cancellation 4')), Modal Control with 4 modes control resulted in lower overall thermal displacement error over the printing path although the maximum value is slightly larger in 4 modes Modal Control than 4 modes Mode Cancellation. The result of Modal Control with 9 modes (green curve, referred to as 'Modal Control 9, Qt=Err', target controlled modes are mode(1,1), mode(1,2), mode(2,1), mode(2,2), mode(1,3), mode(3,1), mode(2,3), mode(3,2) and mode(3,3)) shows even smaller thermal errors over the printing path and better than 4 modes Mode Cancellation at all points.

The results show that Modal Control with the time varying cost weight $\boldsymbol{Q}(t)$ in equation (5.47) gives better control than Mode Cancellation. Strictly speaking, Modal Control with time varying cost weight $\boldsymbol{Q}(t)$ in equation 5.47 does not guarantee to result in the smallest thermal displacement error. Instead, it guarantees that the result gives the smallest thermal displacement errors in L_2 norm for a reduced order thermal model with only the thermal modes that are included in the cost weight $\boldsymbol{Q}(t)$. Therefore, 4 modes Modal Control with $\boldsymbol{Q}(t)$ in equation (5.47) will result in the smallest thermal error for the reduced order model which includes only those first 4 modes (mode(1,1), (2,1), (1,2), and (2,2)). However, the expectation is that, as lower modes are more dominant in the thermal displacement field compared to the higher order modes, aiming for a minimum thermal displacement error for a reduced order model also results in small, although not necessarily minimum, thermal displacement error.

The calculated external control heat load amplitudes are shown in Fig 5.7. The amplitudes of the external loads are around the same magnitude of 1 W of the moving

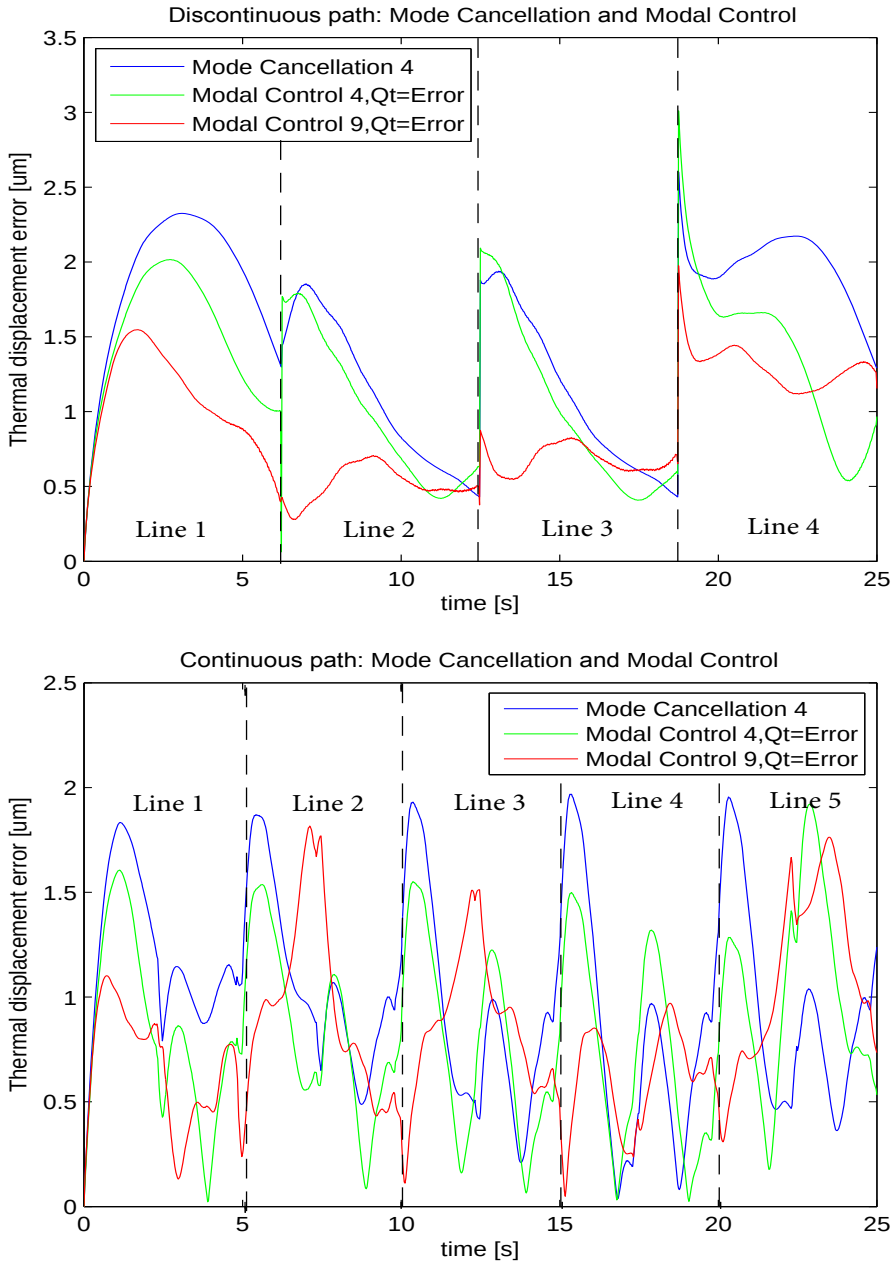

Figure 5.6: Results of Modal Control using LQR compared with Mode Cancellation. Top: discontinuous path case. Bottom: continuous path case. Modal Control with time varying cost function $\boldsymbol{Q}(t)$ gives the minimum thermal displacement error in terms of a reduced order model in L_2 norm. It does not guarantees the minimum thermal displacement error in the full order model. Therefore, when the number of modes controlled by Modal Control increases, the thermal displacement error initially becomes smaller as the number of controlled modes increases but beyond a certain number the error will not become any smaller.

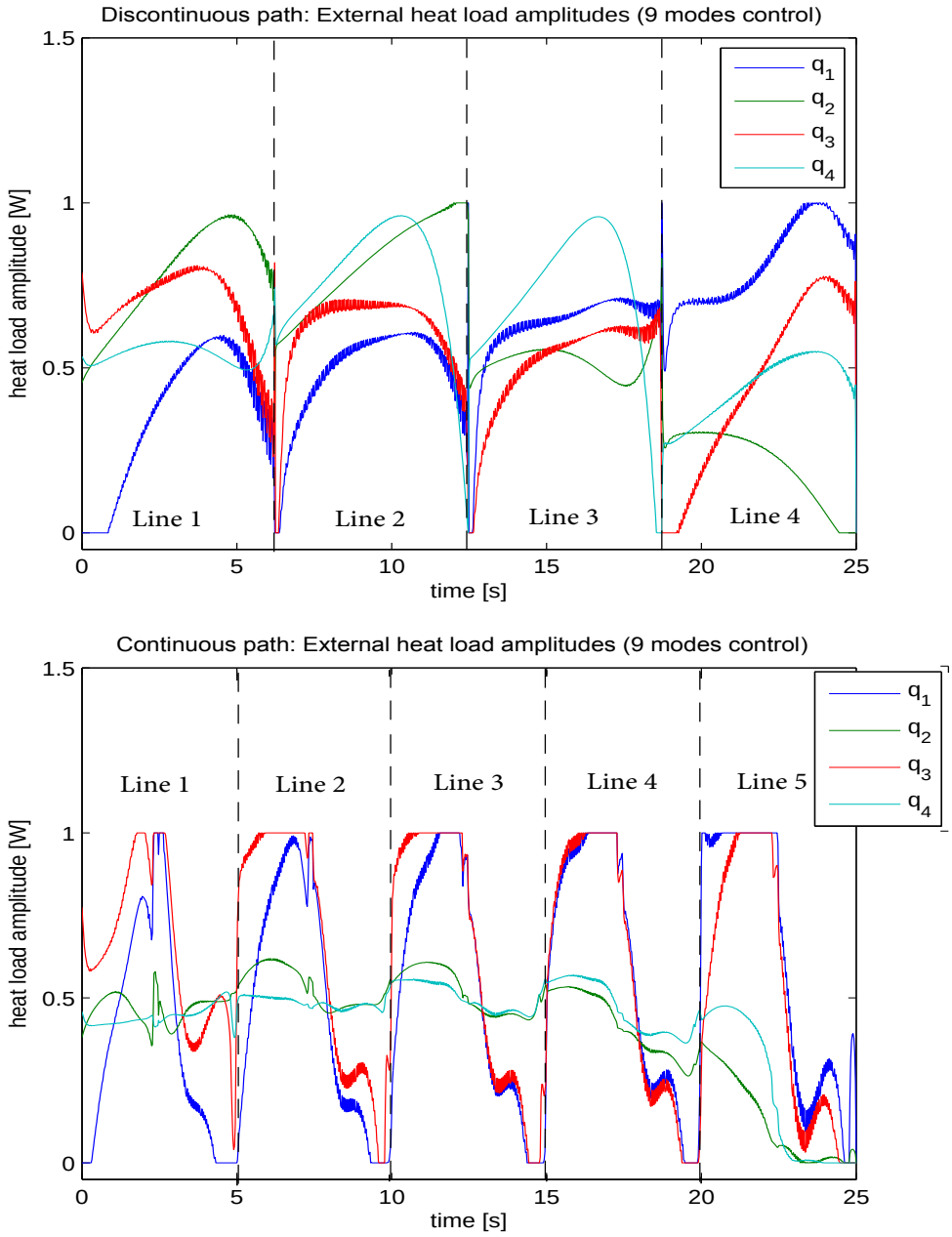

Figure 5.7: Result of Modal Control using LQR with 9 modes control: amplitudes of external control heat loads q_{ext}. Top: discontinuous path case. Bottom: continuous path case. The external load amplitudes are bound between 0 and 1 W to avoid large external load amplitudes. In Modal Control using LQR, when the number of modes controlled increases, the maximum amplitudes of the external loads calculated by LQR tend to become larger. To avoid this, the amplitudes of the external loads are cut off at the amplitude of the moving disturbance load (=1 W).

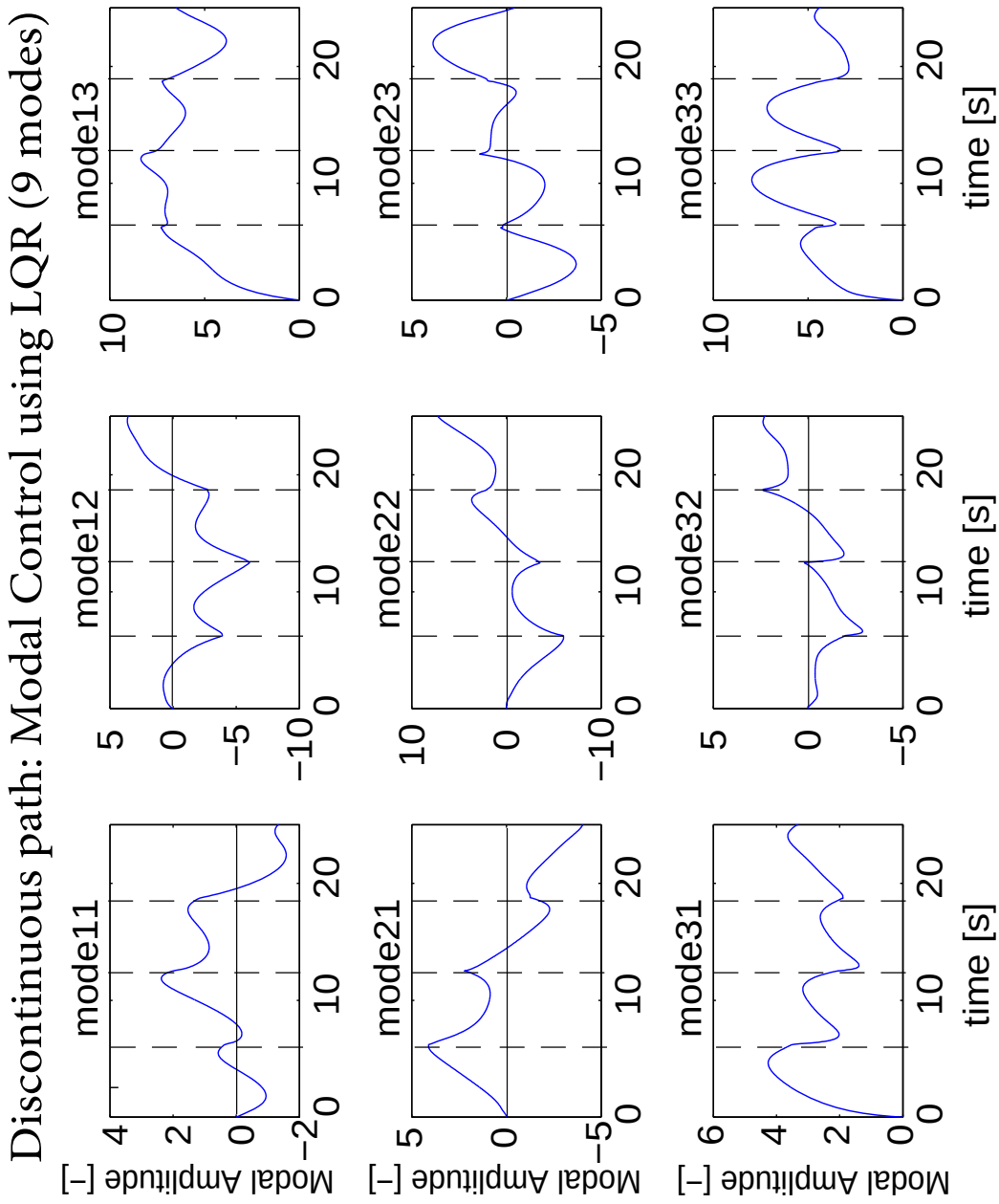

Figure 5.8: Resultant modal amplitudes after Modal Control using LQR and time varying weighting factor $\boldsymbol{Q}(t)$ with 9 modes control (Discontinuous path) (Corresponds to "Modal Control 9, Qt=Err" in Fig 5.6 top). The amplitude of the controlled 9 modes are displayed. As opposed to the case of Mode Cancellation, the target modes are not controlled to be equal to 0 as the amplitudes of the target modes themselves are not the objective of control in the Modal Control.

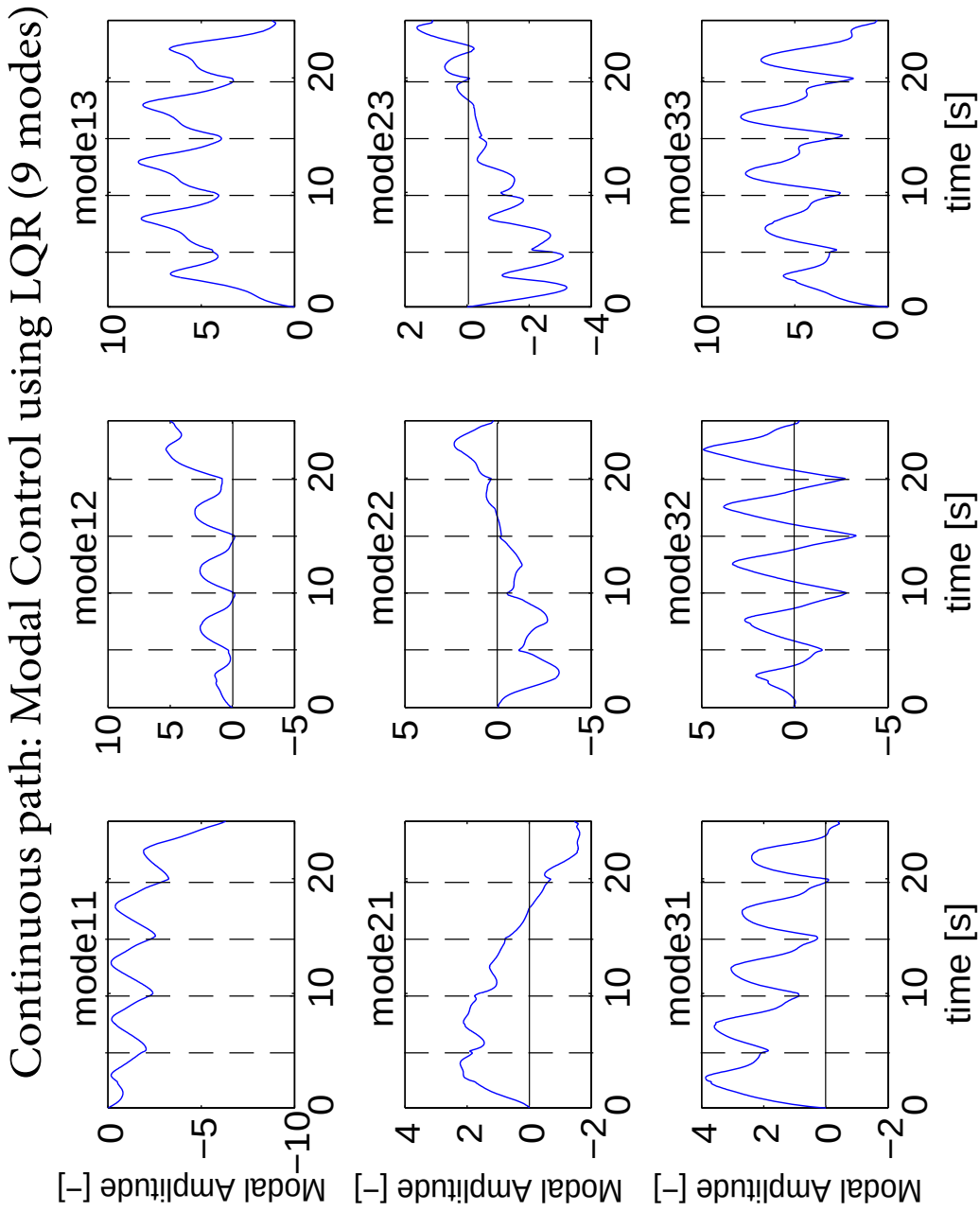

Figure 5.9: Resultant modal amplitudes after Modal Control using LQR and time varying weighting factor $\boldsymbol{Q}(t)$ with 9 modes control (Continuous path) (Corresponds to "Modal Control 9, Qt=Err" in Fig 5.6 bottom). The amplitude of the controlled 9 modes are displayed. As opposed to the case of Mode Cancellation, the target modes are not controlled to be equal to 0 as the amplitudes of the target modes themselves are not the objective of control in the Modal Control.

disturbance load. When the number of modes controlled by the Modal Control increases, the calculated external control heat load amplitudes tend to become larger. To avoid too large external control amplitudes, they are cut off at 1 W. This has two functions (1) to avoid unrealistically large amplitudes for the external control loads even for a short period of time and (2) to avoid large excitation of non-controlled modes which might increases the thermal displacement error in the full-order model. Also calculated amplitudes below 0 W are also cut-off and kept at 0 in the cases of negative amplitudes so that the external control heat loads only take positive values. Because of this cut-off, the thermal displacement error in Figure 5.6 will not be the optimal solution even for the reduced order model. To include constraints on the amplitudes of the external control heat loads, a further advanced control (optimization) scheme such as Quadratic Programming [13] needs to be used.

The modal amplitudes after the Modal Control with 9 modes are shown in Fig 5.8 (Discontinuous path case) and 5.9 (Continuous path case). As opposed to Mode Cancellation, the target modes (in this case mode(1,1), mode(1,2), mode(2,1), mode(2,2), mode(1,3), mode(3,1), mode(2,3), mode(3,2), mode(3,3)) are not controlled to be equal to 0 as the amplitudes of the target modes themselves are not the objective of control in the Modal Control.

5.3 Moving external loads

A possible further extension to Modal Control using LQR can be implemented for cases where the disturbance load is moving over time. That extension would be to allow the external control heat loads to move together with the moving disturbance heat load. Intuitively, one could suspect that the closer these external loads are located to the moving disturbance heat load and/or the point of measurement, the better, the faster, or the more efficient these heat loads can compensate the thermal displacement error. Therefore instead of using stationary heat loads attached to places away from the disturbing load such as corners of the substrate, now moving external loads attached to the moving disturbance heat load are analyzed.

With only a small modification to allow for a time varying $\boldsymbol{B}$ matrix to the previous time varying weight LQR controller with thermal mode states, the moving external control heat loads can be implemented in Modal Control.

$$\frac{\mathrm{d}}{\mathrm{d}t}\boldsymbol{x}_{\mathrm{s}}(t) = \boldsymbol{A}\boldsymbol{x}_{\mathrm{s}}(t) + \boldsymbol{B}(t)\boldsymbol{u}_{\mathrm{s}}(t) \tag{5.58}$$

Similar to the method for the time-dependent matrix $\boldsymbol{Q}(t)$, the control input $\bar{\boldsymbol{U}}_{\mathrm{s}}$ can be calculated by modifying $\bar{\boldsymbol{H}}_{\mathrm{CT}}$ for time varying $\boldsymbol{B}(t)$. The only difference will be in $\bar{\boldsymbol{H}}_{\mathrm{CT}}$ matrix which becomes:

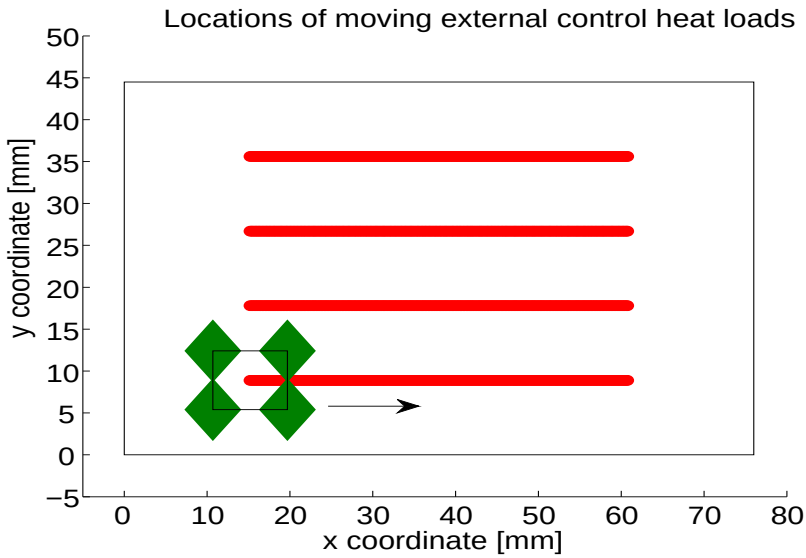

Figure 5.10: Configuration of moving external loads. The moving external control heat loads are separated by ±9 mm in x direction and by ±7 mm in y direction from the moving disturbance load (black arrow indicate the start point and direction of the moving disturbance and external control heat loads.)

$$\bar{\boldsymbol{H}}_{\mathrm{CT}} = \begin{bmatrix} \mathbf{0} & \mathbf{0} & \mathbf{0} & \cdots \\ \boldsymbol{c}(t_1)\boldsymbol{B}_{\mathrm{d}}(t_1) & \mathbf{0} & \mathbf{0} & \cdots \\ \boldsymbol{c}(t_2)\boldsymbol{A}_{\mathrm{d}}\boldsymbol{B}_{\mathrm{d}}(t_1) & \boldsymbol{c}(t_2)\boldsymbol{B}_{\mathrm{d}}(t_2) & \mathbf{0} & \cdots \\ \boldsymbol{c}(t_3)\boldsymbol{A}_{\mathrm{d}}^2\boldsymbol{B}_{\mathrm{d}}(t_1) & \boldsymbol{c}(t_3)\boldsymbol{A}_{\mathrm{d}}\mathbf{B}_{\mathrm{d}}(t_2) & \boldsymbol{c}(t_3)\boldsymbol{B}_{\mathrm{d}}(t_3) & \cdots \\ \vdots & \vdots & \vdots & \ddots \end{bmatrix} \tag{5.59}$$

Then the remainder of the derivation is the same as for the time invariant $\boldsymbol{B}$ matrix case.

Figure 5.11 shows simulation results of Modal Control with moving external loads for the discontinuous printing path (referred to as "Moving Ext. loads 4" or "Moving Ext. loads 9") compared with Modal Control with stationary external heat loads (referred to as "Modal Control 4" or "Modal Control 9"). In this simulation, 4 external control heat loads move together with the moving disturbance load with the offset of 9 mm in x direction and 7 mm in y direction (correspond to 10% of the substrate size) (See Figure 5.10). 4 modes Modal Control with moving external loads using the time varying $\boldsymbol{B}$ matrix (equation (5.58)) results in smaller thermal displacement error along the printing path than Modal Control with stationary external heat loads. The performance of Modal Control with moving external loads improves as the number of modes to be controlled increases. However, the reduction of thermal displacement error by increasing the number of controlled modes is not as pronounced as for the stationary external loads cases.

Modal Control with moving external loads gives better results than Modal Control with stationary external loads at each corner of the substrate. This is due to a better control

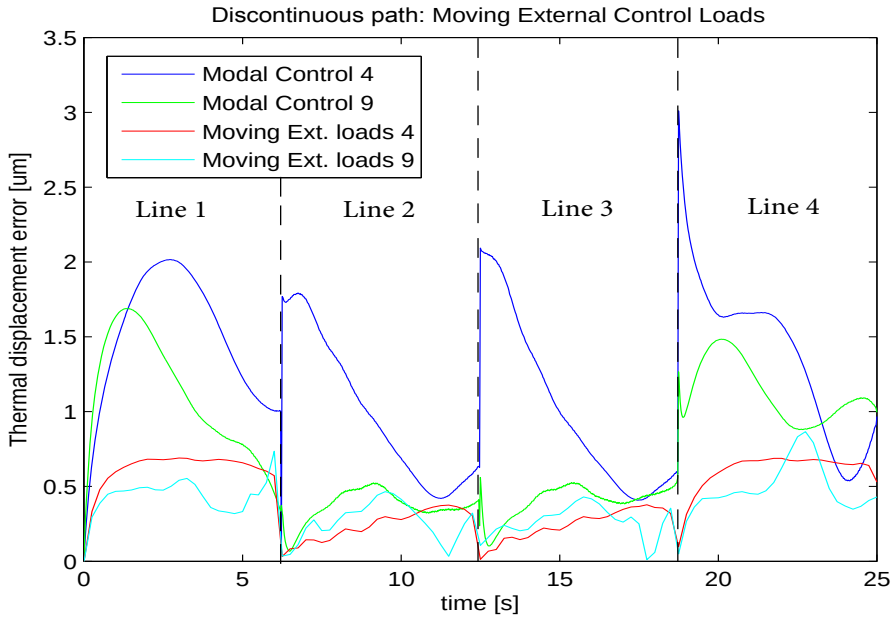

Figure 5.11: Result of Modal Control using LQR with moving external control loads (red and cyan) compared with Modal Control using LQR with stationary external control loads (blue and green) for discontinuous path case. Moving external loads control gives much better thermal error reduction than stationary external loads control.

of modes of interest during the control. When external loads are fixed to each corner of the substrate, the sensitivity of modes to the external loads (the value of the mode shapes at the locations of the external loads) are generally different from the sensitivity of the same modes to the disturbance load. This is especially the case when the disturbance load is moving. When sensitivities of the modes to the external loads are higher than the sensitivities of the same modes to the disturbance load, it is generally easier to compensate by using external loads. However when the sensitivity of the modes of interest to the external control loads are smaller than the sensitivity to the disturbance load, larger heat loads are required to control the modes. As a results, other non-controlled modes are also excited more and result in a smaller thermal error reduction.

When external control loads are moving together with the moving disturbance load with certain offset, sensitivities of a controlled mode to the disturbance load and to the external moving control loads are similar if the controlled mode is a lower order mode with small spatial frequency mode shape. This means that the mode shape values of a mode of interest at these load points are similar to each other. Therefore, regardless of the location of the disturbance load on the substrate, external loads can excite and control each target mode without having any singularity points that would result in any of the target modes to go out of control.

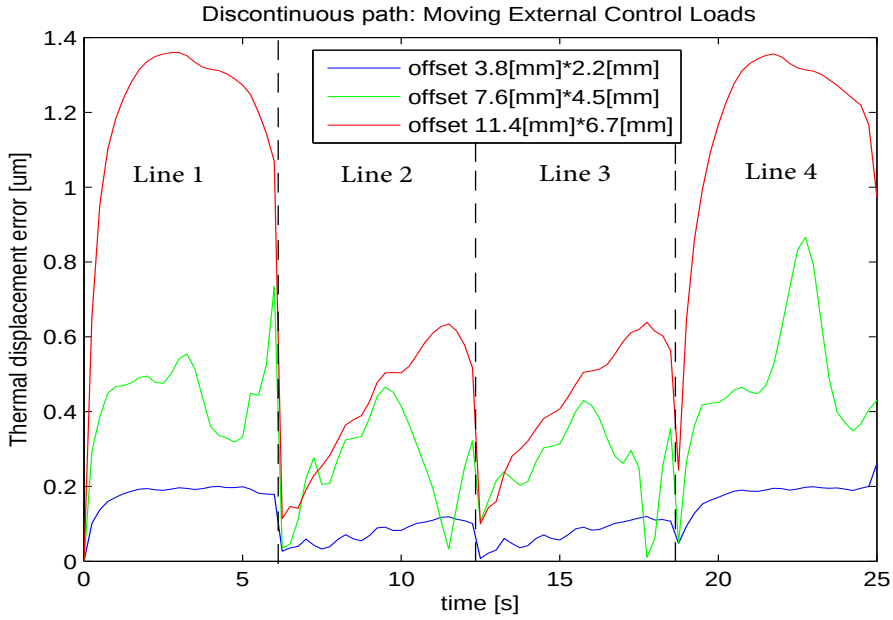

Figure 5.12: Result of Modal Control using LQR with moving external control loads with different offset distance of the moving external loads from the the moving disturbance load position (Discontinuous path). Shorter offset (moving external control loads closer to the moving disturbance load) results in smaller thermal displacement error.

5.4 Optimal offset distance of external moving heat loads from the disturbance load

Figure 5.12 shows the result of a simulation of moving external load Modal Control with three different offsets. The result shows that a shorter offset distance results in a smaller thermal displacement error as expected from the analysis above.

The best offset to minimize the thermal displacement error along a moving disturbance load is to have zero distance offset where the location of the disturbance heat load and all external control heat loads are the same. In this situation, the thermal error is obviously zero if the sum of the external control loads and the disturbance load are equal to zero. Then all the thermal energy brought into the substrate by the disturbance load is extracted by the negative inputs of the external loads. Therefore there is no net input to the substrate and hence no temperature change, no thermal deformation, and no thermal errors. If a negative heat load, which can move together with the disturbance load, is available, this is the obvious solution. However this is not a very interesting solution from practical point of view considering the relative difficulty of using such a negative load in an actual machine. Therefore there should be a larger than zero offset distance for the external control heat loads which reduces the thermal error better than having stationary external loads at each corner of the substrate but will still result in all the external loads to have positive amplitudes.

5.5 Conclusions

This chapter introduced Modal Control to overcome the limitations of Mode Cancellation proposed in the previous chapter. Modal Control controls a larger number of modes than Mode Cancellation for the same number of external control heat loads to minimize an objective function by balancing the amplitudes of selected number modes. Therefore in general Modal Control provides the possibility of better control and reduction of thermal displacement error than Mode Cancellation. Modal Control also avoids the limitation of singularity in the sensitivity matrix in Mode Cancellation in equation (4.4). Modal Control automatically avoids modes which cannot be controlled by the set of available external control heat loads. Therefore no manual selection of controlled modes and/or external controlled location selection is necessary. Modal Control with time varying weight matrix $\boldsymbol{Q}(t)$ minimizes the thermal displacement error in a reduced order model. This gives the smallest thermal displacement error in the reduced order model with these controlled modes. This result also produces a good result for the thermal displacement error in the full order model, although it does not guarantee the smallest error.

Modal Control with time varying $\boldsymbol{B}$ matrix can represent moving external control loads. This produces even better than results than Modal Control with stationary external control loads. The sensitivities of the target modes to moving external loads take similar values with the sensitivities of the same modes to the moving disturbance load. This makes it easy to control the target modes excited by the disturbance loads with the external control loads.

Chapter 6

Comparison of proposed methods

6.1 Comparison of Mode Cancellation and Modal Control

In the previous Chapters, Mode Cancellation and Modal Control were introduced as novel thermal error reduction techniques. These techniques use a thermal model based on Thermal Modal Analysis and control the temperature distribution within the target structure by applying external control heat loads to reduce the thermal displacement error. Mode Cancellation has certain limitations in that (1) the number of controlled modes are less than or equal to the number of external control loads, and (2) the set of controlled modes and the locations of the external control heat loads need to be chosen manually while avoiding singularity of the sensitivity matrix $\boldsymbol{\Phi}_{\mathrm{nm}}$ in equation (4.4). Modal Control extends Mode Cancellation method further by solving these issues. In Modal Control, the thermal model based on Thermal Modal Analysis is expressed in a state space model. Then it uses Linear Quadratic Regulator (LQR) to calculate the external control heat load amplitudes to minimize the thermal displacement error in a reduced order model of the thermal model. Modal Control can control a higher number of modes than the number of external control heat loads. Also the singularity of the sensitivity matrix is no longer a problem. If the sensitivity matrix becomes singular for a set of controlled modes and the set of external control heat load locations, then LQR still calculates the best possible solutions by either excluding some modes from the original set of controlled modes or by controlling all the selected modes but not completely independent to each other. Still, Modal Control has certain limitations.

6.2 Comparison of fixed external loads and moving external loads

Moving external loads can reduce thermal errors better than fixed external control heat loads for the example case of a moving disturbance load and moving point of interest. This is mainly due to the fact that sensitivities of target control modes to the moving external control heat loads will change in a similar way as the sensitivities of the same modes to

the disturbance heat loads. Therefore if the offset distance between the disturbance load and the external loads is smaller, it becomes more efficient in thermal error reduction.

6.3 Influence of spot size

Up to now, in the theoretical development and simulation of Mode Cancellation and Modal Control, point heat loads are assumed for both the disturbance and the external control heat loads. In Chapter 8, experimental validation of Mode Cancellation and Modal Control will be discussed. In the experimental validation, finite spot size heat loads are used instead of infinitely small point loads in order to compensate for a limited power density in the experimental setup. In this section, the influence of such finite spot size heat loads to the results of Mode Cancellation and Modal Control are discussed before proceeding to the experimental validation in Chapter 8.

Figure 6.1 shows results of Mode Cancellation (4 modes control) with three different load sizes for the external control heat loads. The blue curve shows the result of external point loads. The red curve is the result of finite but small radius external loads. The green curve is the result of large radius external loads. When point loads or small size loads compared to the spatial frequency of a mode shape excites that mode, the sensitivity of the mode is close to equal to the value of the mode shape at the same location. When a large spot size compared to the spatial frequency of the mode shape excites the mode, the sensitivity of the mode to the large spot load can be different from the value of the mode shape at the centre location of the spot. When the spot size is larger than the spatial wavelength in the mode shape pattern, then the sensitivity of the mode to the large spot is averaged and becomes smaller than the case of point load or very small spot size load. Therefore Large spot size heat loads (green curves) result in smaller amplitudes for the higher order modes compared to point loads (blue curves) and small spot size loads (red curve) in Figure 6.1. This means that conducting Mode Cancellation or Modal Control with a finite spot size does not have negative influences to the control results as it results in less excitation of the higher modes which are generally outside of the control. Therefore the experimental validation of Mode Cancellation and Modal Control which will be conducted in Chapter 8 with a finite spot size is not influenced by the spot size. Rather it has further reduced the thermal displacement error as it excites higher order modes less than in the case of point loads or small spot size loads.

6.4 List of further possible extensions of the proposed methods

In this section, a list of possible extension or continuation of the study in this research is introduced and each possible study is briefly described.

6.4.1 Model uncertainty

When applying these techniques to real problems, the accuracy of the thermal model is important to obtain an accurate result. However in reality, it is very difficult to obtain accurate simulation parameters. For example, convection by the surrounding air seems to be one of the most difficult influences to accurately model. In reality, the temperature of the surrounding air continuously changes over time by the mutual interaction between the

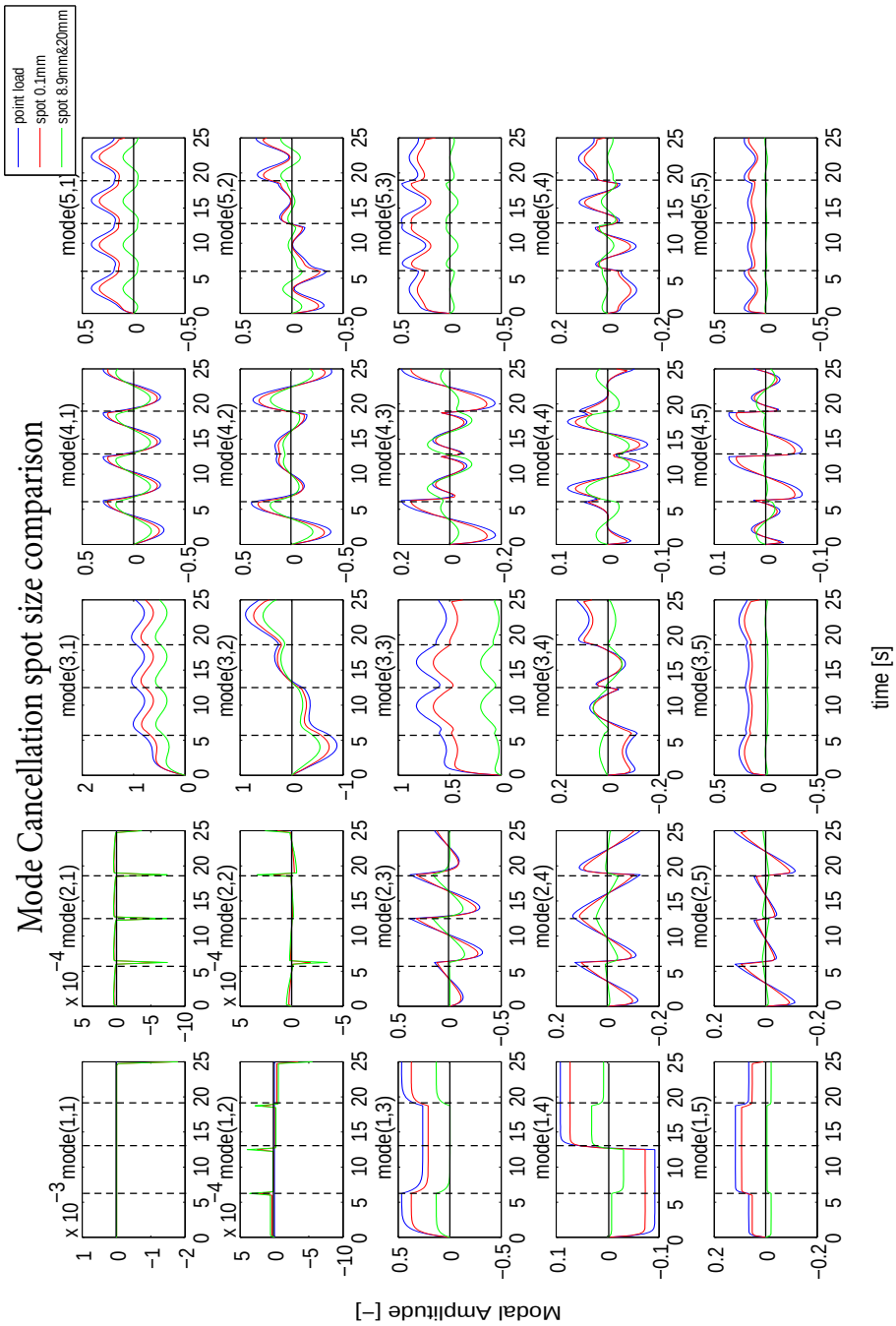

Figure 6.1: The amplitudes of the first 5*5 modes by Mode Cancellation (4 modes control) with different spot size for the external control loads and the moving disturbance loads. The larger the spot size becomes, the smaller the excitation of higher order modes becomes. Higher order modes are excited less by larger spot size as the peaks and valleys of higher order modes are smaller than the spot size.

structure and surroundings. Hence the convection might be not uniform or not constant over time as opposed to the assumption made in this analysis. Also the material properties are not known in detail and possibly not uniform or not constant over the range of temperatures of interest..

However it is still possible to estimate how large these variations can be to some extent based on analysis of experiments. For example, when the coefficient of convection is 10% wrongly estimated from the actual value, its influence mostly appears only on the first mode which time constant is inversely proportional to the convection coefficient. Time constants of the other modes are less influenced by the convection when the conduction within the material is much faster (convey more energy per unit time) than the cooling. And the amplitude of each mode is proportional to the time constant. So the influence of the error of the convection coefficient estimation mostly appears only in the first mode. Another remedy for model uncertainty is to apply feedback control. However generally it is advisable to have an accurate model as possible to improve the performance of the techniques presented in this thesis.

Therefore, the study on either improving thermal model accuracy or reducing the influence of model accuracy to the error reduction performance are important subjects for the application of the proposed thermal error reduction techniques in this thesis.

6.4.2 Quadratic programing

From a practical point of view, it is also desirable not only to weight the amount of power consumption in control heat loads but also to set upper and lower boundaries for them. In the previous Chapters, the amplitudes of the external control heat loads are cut-off after the optimal control amplitudes are calculated if they exceed certain limit. However, this limitation on the external load amplitudes is an artificial modification to the control loads outside of the optimization calculation. Therefore, after the cut-off, the optimality of the solutions are not guaranteed anymore. It is desirable that if limitations on external control heat load amplitude are included within the optimization scheme so that the optimal control load amplitudes calculation includes the limitations on the control load amplitudes. For that purpose, the use of Quadratic Programing [13] in a similar manner as the use of Linear Quadratic Regulator can also address the issue. Quadratic Programing allows to set more fine tuned cost functions such as minimizing the maximum error during the process or change the relative importance of the error depending on the location of point of interest during the process.

6.4.3 Using Proper Orthogonal Decomposition

For all the techniques proposed in chapter 4 and chapter 5, using Proper Orthogonal Decomposition (POD), instead of Thermal Modal Analysis, may improve the performance of the proposed techniques. As described in chapter 3, POD can be a more problem specific alternative to create a better (and actually best, in terms of L_2 norm) reduced order model of the temperature distribution if information of the disturbance heat load is know in advance and the disturbance load is stationary. In the case of moving heat load where the heat load path is known, it is still possible to make a better reduced order model based on POD than based on thermal modal analysis. However in this case, POD shapes and the model using POD shapes needs to be created for every different location of the moving loads and hence it is a question how efficient it can be in modeling a target

system in this manner. But in terms of accuracy, POD seems to be the best choice if the accuracy of the model has top priority.

However, using POD in Mode Cancellation or Modal Control is not straight forward. When external control heat loads are applied to the target structure, then the external loads actually changes the typical temperature distribution of the structure which is already captured in the POD shapes. Therefore, after applying external control heat loads, probably the POD model is not the best reduced order model any more. Or at least there is no guarantee that the POD shapes and any model using the POD shapes offers the best model.

Therefore, some remedies are required for this. One possibility might be to iteratively calculate the POD shapes and external control heat loads until convergence.

6.5 Summary

In this chapter, comparison of the novel thermal error reduction techniques, Mode Cancellation and Modal Control, proposed in this thesis are compared. Also some analyses to extend these techniques further to be implemented in practical applications have been presented.

Chapter 7

Experimental setup

7.1 Overview of this chapter

In the next chapter, experimental validation of the proposed novel thermal error reduction techniques is reported. In this chapter, the experimental setup used for the experimental validation is introduced. The conceptual design, the components used in the setup, the working principle and preliminary experiments conducted for evaluating the setup are described in this chapter.

The experimental setup design is based on the following design considerations.

- Flexibility and agility to apply easily changeable moving disturbance heat load and external control heat loads
- Concentrate on temperature domain measurement

The main objective of the experimental validation using the setup is to validate the temperature control in terms of thermal modes. One reason is that the proposed methods are mainly about how to control the temperature distribution in terms of modes. The other reason is that the connection between the temperature domain and the thermal deformation has been well established in the past. Therefore it is not essential for the purpose of validating the proposed methods to measure the results in the thermal displacement domain. Rather it is important to measure the temperature distribution and analyze them in terms of thermal modes.

Because of these reasons, a setup with a high power video projector, an infrared (IR) camera and a substrate suspended between the projector and the IR camera has been designed and developed. This design enables easy and flexible application of moving heat load and dynamically changing external control heat loads.

7.2 Objectives of test set up

This chapter introduces the design and the construction of the experimental setup for experimental validation of the proposed thermal error reductions techniques. Objectives of the experimental setup are to conduct the following experiments:

1. Measurement of Thermal Modes

2. Temperature control in terms of Thermal Modes

3. Experimental validation of the proposed thermal error reduction techniques

In this chapter, the design and the building up of the setup, a short summary of the preliminary experiments to improve the setup's performance, and the results of the thermal modes measurement are exhibited. The development of the setup is explained in detail in [77].

7.3 Design of the setup

7.3.1 Requirements of the test setup

As already mentioned, the purpose of the setup is to experimentally validate our novel thermal error reduction techniques. Therefore the requirements for the setup are:

1. Ability to apply moving heat loads to represent a moving disturbance load and moving external control loads

2. Ability to modulate the amplitudes of the external control heat loads

3. Ability to measure temperature distribution over space and time to identify the amplitudes of the dominant thermal modes

4. Ability to measure in-plane thermal displacement at a moving point of interest

In the setup described in this chapter, the first three requirements have been realized. The last one, the thermal displacement measurement at a moving point is conducted separately. So the setup we introduce here only operates and measures in the thermal domain. The development of the displacement measurement setup and the experimental validation of the thermal displacement model will be given in the Appendix A.

7.3.2 Conceptual design and component selection

Conceptual Design

To achieve the three requirements listed above for the temperature distribution control and measurement setup, we developed the following conceptual design (Figure 7.1).

The setup consists of a large video projector (1), a lens (2), a mirror (3), a substrate (4), and an infrared (IR) camera (6) (Numbering are in accordance with the right figure in Figure 7.1). The video projector provides a means to easily produce dynamic heat loads which change over time and space. The lens and mirror focus and reflect the image pattern from the projector to the substrate. The substrate is made of a thin aluminum plate in this experiment. The substrate is mounted by strings from the four corners to the supporting structure to reduce thermal conduction through the mechanical supports as much as possible. The substrate is supported horizontally to reduce non-uniform influence from the air convection. The substrate is illuminated by the projector, absorbs the light energy and converts it into heat. As a result, the temperature of the substrate rises and thermal deformation occurs. The temperature rise is measured by the IR camera situated above the substrate.

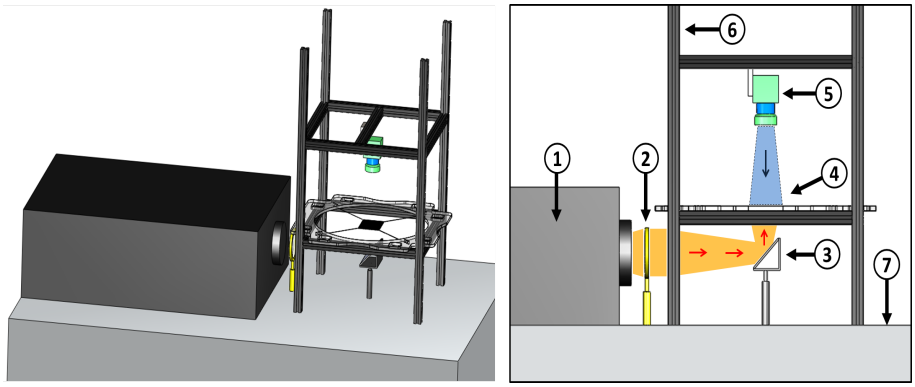

Figure 7.1: Conceptual Design of the thermal experiment setup. A video projector (1) projects an dynamically changeable image pattern onto a substrate made of an aluminum plate (4) through a lens (2) and a mirror (3). The temperature distribution of the substrate is measured by an infrared camera (5) positioned above the substrate.

Figure 7.2: Picture of the developed setup. The setup is surrounded by white paper to block the air flow from an air conditioner in the laboratory.

Based on this conceptual design, the setup was constructed (Figure 7.2). The frame is shielded with sheets of paper as in the bottom pictures of Figure 7.2 in order to prevent uncontrolled air flow from the environment to interfere with the experiment. Using this setup, a moving disturbance heat load is applied over the substrate and also external control heat loads are applied to the corners of the same substrate to control the temperature distribution of the substrate. Then the temperature distribution of the substrate is measured by the IR camera and the amplitudes of the target modes are identified. There are some differences from the simulation. (1) forced cooling is not applied in this setup and hence mode (1,1), which represents the average temperature over the substrate is not controlled in the experiments. Therefore, in the experimental validation of Mode Cancellation, only 3 modes are controlled as opposed to 4 modes control in the simulation. The IR camera measures the temperature of the substrate with 4 Hz frequency. This slow measurement frequency is mainly caused by the large computational time required to calculate modal amplitudes of the modes of interest in real-time for the purpose of feedback control. The computer connected to the projector and IR camera controls the image projected by the projector and records the data from the IR camera.

The projector can, for example, project four printing line as shown in Figure 4.2 over 25 s while amplitudes of the four external control heat loads can be controlled at the same frequency as the measurement frequency of 4 Hz. The amplitudes of the external loads are controlled in feedforward and feedback manner. The feedback control is a proportional (P) control with its gain calculated to minimize the sum of the error over the time of interest using equation (4.4) together with Linear Quadratic Regulator (LQR) control.

7.4 Preliminary experiments

In this section, a brief summary of the preliminary measurements conducted to evaluate and improve the behavior of the setup for the purpose of conducting the validation experiment are summarized. For the details of each procedure, please refer to [77].

1. Projector non-uniformity measurement and its compensation (Figure 7.3)

   A large and powerful video projector is used in the experimental setup to project a video pattern onto the substrate and apply a moving heat load and control heat loads to the substrate. However, the intensity of the projector output is not uniform over the projection area. The top figures of Figure 7.3 shows the light intensity measured at each location of discretized sections on the substrate using a light intensity meter when the projector outputs an uniform white image. If the projector and all intermediate components, such as the lens and mirror, do not have any spatial variations, the light intensities measured at several locations on the substrate should be uniform. However the figure suggests that the projector intensity is weak at the right-top corner. Therefore only a fragment of the whole projection area (the rectangular area enclosed by the thick black line in the left-top figure in Figure 7.3) has been used for further experiment. After that the intensity measurements taken at each location in this selected area are used to compensate the non-uniformity strength within this area. The result of the compensation is shown in the bottom figures in Figure 7.3).

2. Canceling Gamma correction

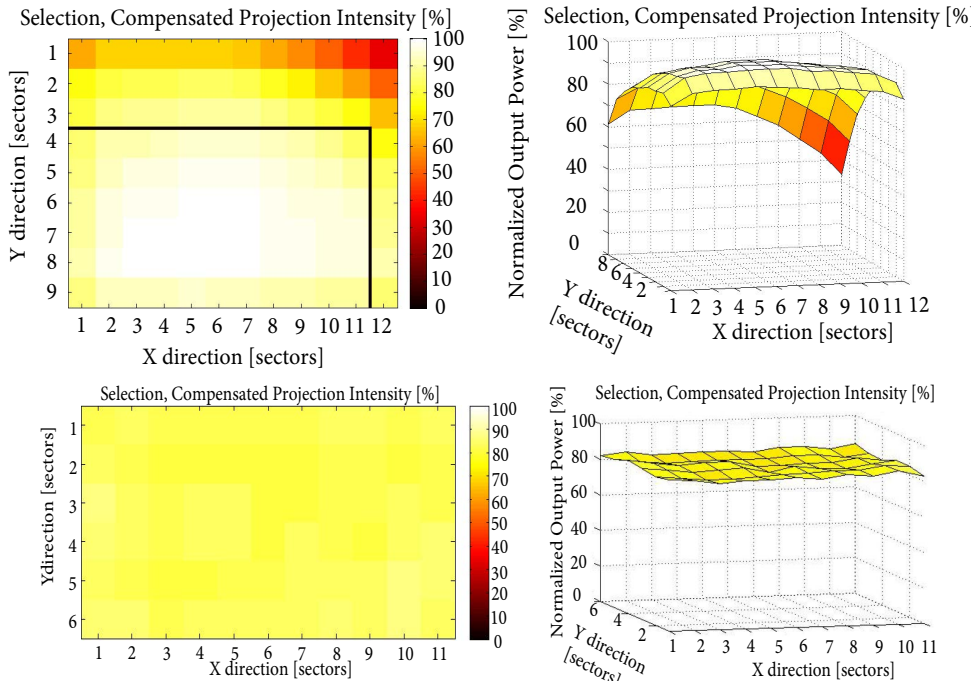

Figure 7.3: Projection non-uniformity compensation. Top figure: Uncompensated light intensity measured at the substrate surface. Bottom figure: Compensated beamer light intensity based on the intensity measurement above.

Gamma correction of the video projector needs to be compensated to have linear output intensity with respect to the video image intensity. Gamma correction is applied to many standard projectors to adjust the non-linearity of human-eye perception. When the brightness of an image changes linearly, the actual projector output light intensity changes non-linearly to compensate for the human eye non-linearity (Top figure, left-middle figure, and left-bottom figure of Figure 7.4). Also the projector output intensity saturates beyond certain intensity (Top figure of Figure 7.4). The top figure of Figure 7.4 shows the output intensity of the projector for different contrast settings. The different contrast curves show different Gamma correction curves and saturation intensities. Since the highest contrast (100) has the least saturation of the output intensity, the highest contrast is used throughout the whole experiments in this thesis. For the highest contrast setting, the gamma curve is highly repeatable as shown in the left-middle figure in Figure 7.4. The intensities of the projected image are corrected so the projector output light intensity linearly changes with the original input image intensity into the projector. The right-middle figure is the linearity compensated output intensity of the projector. The left-down figure shows the result of finer intensity measurement than the left-middle figure case. The right-bottom figure is a closeup of the left-bottom figure. As can be seen from the close-up figure, the gamma curve has some step wise change in its intensity. Therefore, the non-linearity compensation of the projector by the resolution of this step intensity.

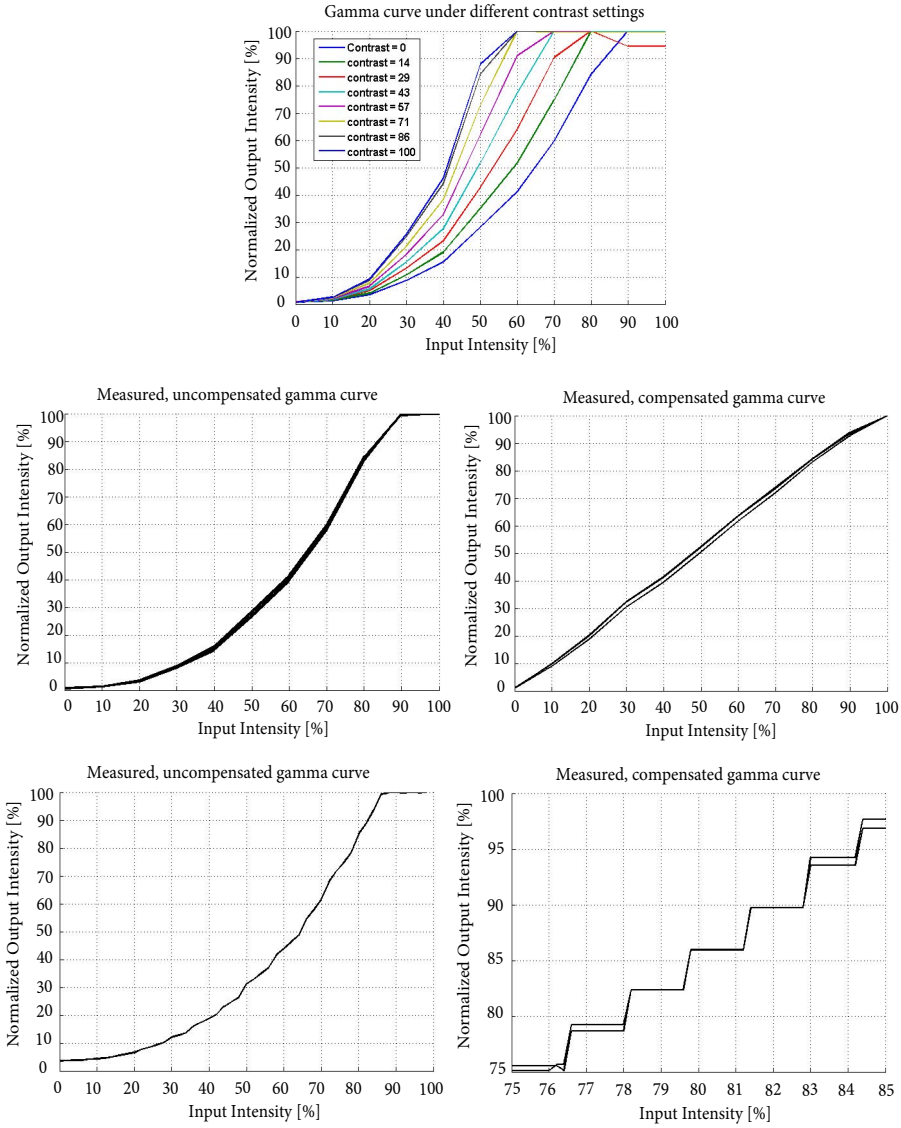

Figure 7.4: Gamma correction of the projector. Top figure: Measured gamma curve with different contrast. Left middle figure: Gamma curve of "contract=100" measured at several locations. Right-middle figure: Compensated Gamma curve. Left bottom figure: Finer measurement of the Gamma curve of "contract=100". Right bottom figure: Zoom in view of the fine Gamma curve.

3. IR Camera reflection subtraction

   When measuring the temperature distribution of the substrate using the IR camera hanged above the substrate, the measured image contains the heat radiation from the IR camera itself reflected by the substrate. Therefore, this reflection needs to be subtracted from the measurement data. The top figures in the Figure 7.5 are the original measurement data taken by the IR camera which includes the reflection of the IR camera heat radiation. This reflection pattern was measured (middle figures in Figure 7.5) and is subtracted from the raw measurement data (top figure). This results in the bottom figure in Figure 7.5. After the subtraction, the IR radiation pattern is mostly removed from the measurement data. As the reflection pattern does not change much over time, the reflection pattern is measured just before each experiment and is subtracted from the measurement data taken during the experiment.

4. Barrel distortion compensation

   Due to a relatively close distance (about 15cm) between the substrate and the IR camera, the obtained temperature data is distorted by barrel distortion (Left picture in Figure 7.6). Therefore this distortion is compensated using a barrel distortion compensation program with the distortion parameter adjusted to make that the compensated picture rectangular (Right picture in Figure 7.6).

5. Environmental temperature

   During the temperature measurement by the IR camera, a change of the room temperature may cause shifting of the measurement results. To identify and compensate for the influence of the room temperature change, the room temperature in the laboratory is measured over 10 hours (Top figure in Figure 7.7). The measurement result shows that the temperature in the laboratory changes about 7 degrees over time. However in a short time span of 30 seconds,the same time scale as single experiment, there hardly appears a drifting of the temperature except one case which is caused by the resetting of the IR camera which occasionally happens. From the result, it can be seen that the absolute temperature values are spread within about 1.5 K range. However, in the following measurements only the relative temperature change is taken into account and not the absolute temperature as mode 1 which represents the average temperature of the substrate is not to be controlled. Therefore, this variation in the absolute temperature value does not influence the experimental validation of the proposed thermal error reduction techniques.

6. IR camera measurement drift

   The temperature measurement of the aluminum substrate using the IR camera drifts over time during measurement. This is caused by mainly two factors. One is the radiation from the IR camera. The other is the fluctuation of the room temperature within the lab.

   The substrate receives radiation from the IR camera. When the IR camera is switched on, the temperature of the IR camera increases over time until it reaches a steady state value. As the temperature of the IR camera increases, the radiation from the IR camera to the substrate also increases.

   The top figure in Figure 7.8 shows that correlation between the increasing IR camera temperature after it has been and the measured temperature of the substrate. The graph also contains the room temperature measured by humidiprobe (blue).

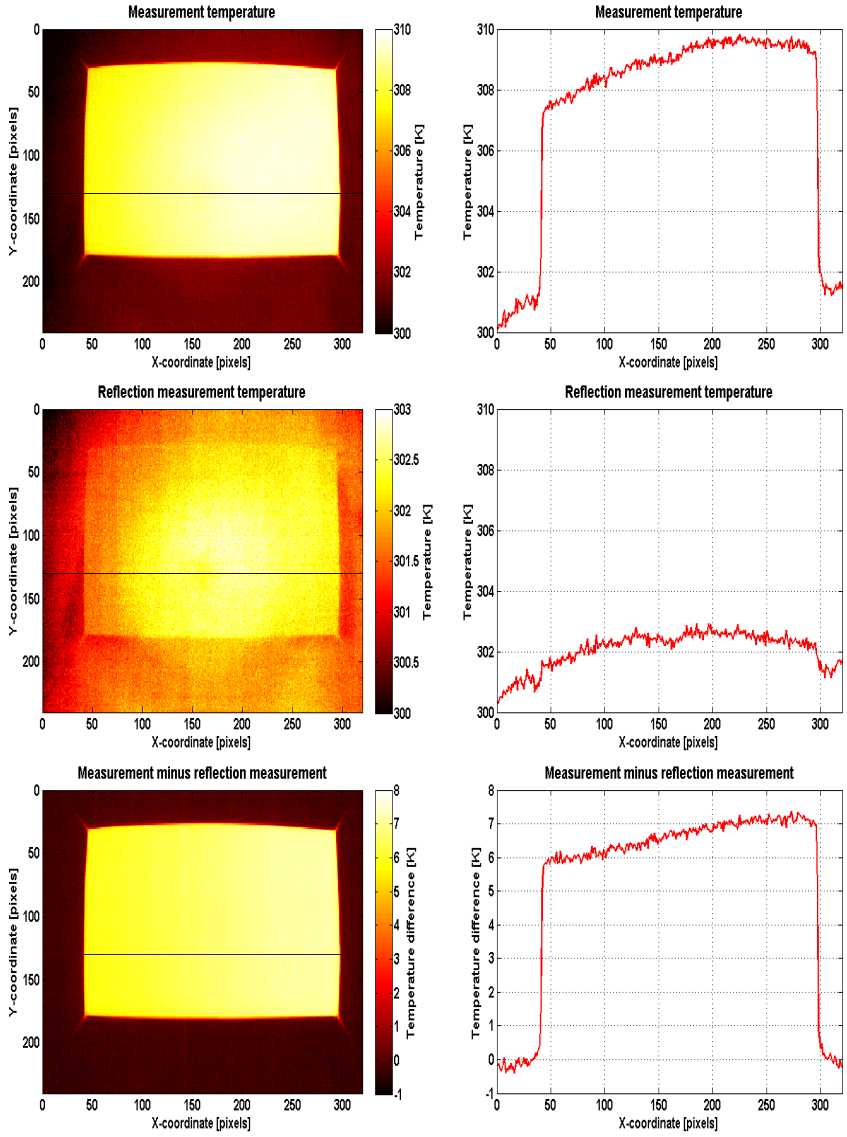

Figure 7.5: IR camera reflection compensation: (Top-left) Original measurement including camera reflection. (Top-right) side view of the original measurement. (Middle-left) Reflection pattern measurement. (Middle-right) Side view of the reflection measurement. (Bottom-left) After subtracting the reflection measurement from the original image. (Bottom-right) Side view of the subtracted image.

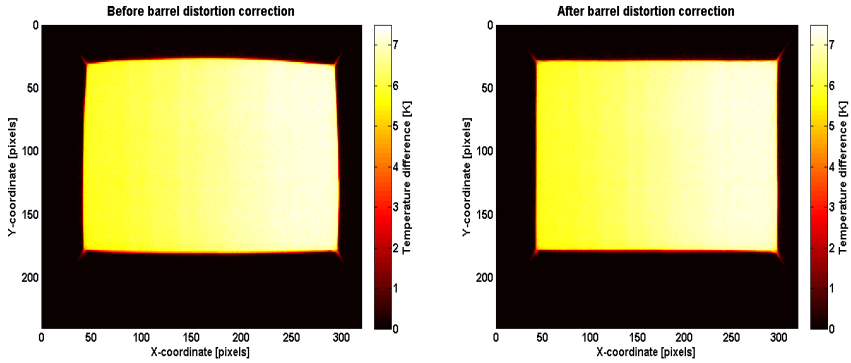

Figure 7.6: Barrel distortion correction: (Left) Original image before compensation. (Right) After barrel distortion compensation.

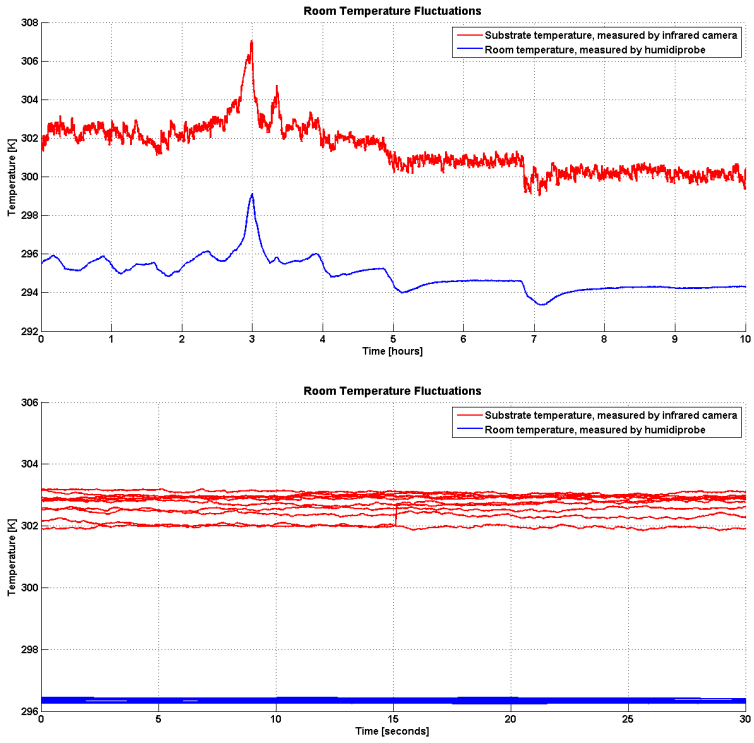

Figure 7.7: Room temperature measurement: (Top) Room temperature measurement over 10 hours. (Bottom) Room temperature measurement over 30 seconds.

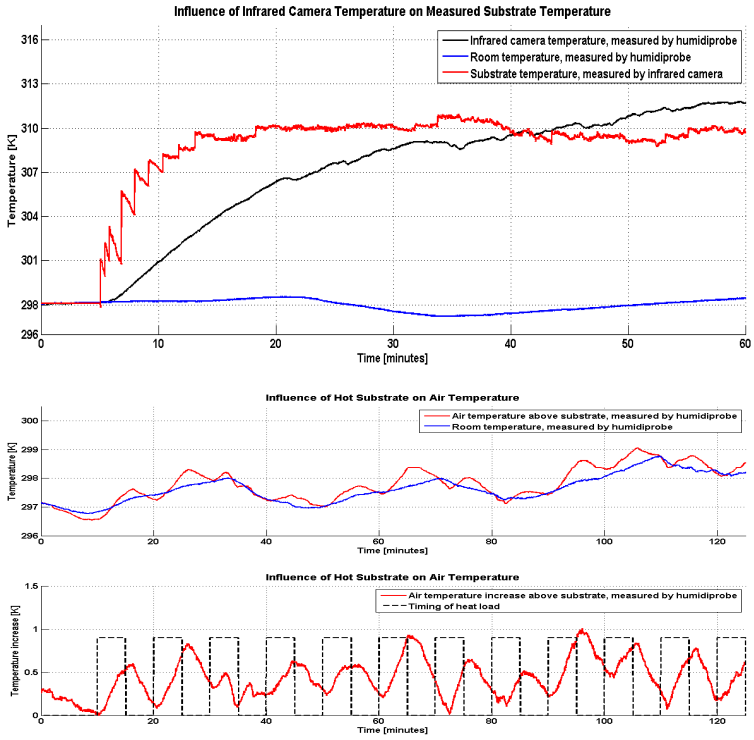

Figure 7.8: IR camera drift compensation: (Top) IR camera temperature and its influence to the measured substrate temperature. (Middle) Measured substrate temperature and the room temperature. (Bottom) Measured substrate temperature minus room temperature (red) shows the clear correlation with the heat load pattern (dotted blue).

The room temperature changes only about 1 K over 1 hour while the substrate temperature measured using the IR camera changes by about 12 K. The curve clearly shows an exponential relationship. This is due to the heat transfer from the IR camera by radiation. To avoid the change of the substrate temperature during experiments, the IR camera is switched on long before the start of any experiments. Then the temperature of the IR camera already reaches a stable value and does not change any more during the experiments. In this way, the change of the substrate temperature due to the changing radiation from the IR camera over time can be avoided.

The pictures in the middle and the bottom of Figure 7.8 show the measurement of the average temperature of the substrate with the projector output switched on and off with 5 minutes interval [1]. The middle picture shows the room temperature (blue) fluctuation and the average temperature of the substrate measured by the IR camera (red). This average temperature minus the room temperature results in the red plot in the bottom picture with blue dotted rectangular patterns which

[1] the IR camera itself is kept switched on all over the experiment to keep the temperature of the IR camera stable. Here "switch off" means that the projector outputs a black image (= Its RGB values are all (0,0,0)).

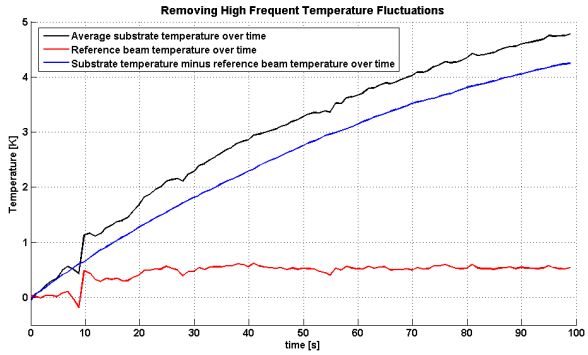

Figure 7.9: IR camera flickering compensation: Reference bar average temperature (red), original measurement (black), flickering subtracted from the original data (blue).

are the heat load pattern from the projector. The bottom figure clearly shows the correlation between the average temperature increase and decrease (red) with the switching on and off of the beamer (blue). The influence of the room temperature fluctuation takes place on a longer time scale than the time scale of the experiments in this research. Therefore the fluctuation of the room temperature is not subtracted from the measurement data. If a single experiment continues for longer period, then the influence of the room temperature may also need to be subtracted from the measurement.

7. IR camera flickering

   The measurement from the IR camera contains high (temporal) frequency components that are uniform over the entire image. To eliminate this flickering, a reference measurement is conducted within the same field of view of the IR camera. Next to the substrate to be measured, a thick aluminum bar that is a part of the setup structure is situated in view of the camera. This aluminum bar has a far larger heat capacity compared to the substrate due to its large mass. As a result, the temperature of the bar is far less sensitive to the change of the room temperature than the substrate. Therefore, assuming that the temperature of this bar does not change during a single experiment, a measured temperature fluctuation over time in this bar area can be assumed to be the flickering of the IR camera. Subtracting this flickering from the substrate temperature measurement gives the substrate temperature distribution without the flickering error. Figure 7.9 shows this reference bar temperature (red) and the average measured temperature of the substrate (blue) and the result after subtraction (black) which is assumed to be the surface temperature of the substrate without the flickering.

7.5 Preliminary experiments before the experimental validation

Before conducting the experimental validation of the proposed thermal error reduction techniques in the next chapter, some preliminary experiments are conducted. The prelim-

inary experiments are conducted to evaluate the setup performance and to adjust model parameters in the simulation model based on the results of the preliminary experiments.

7.5.1 Repeatability measurement

First, the repeatability of the experimental setup is evaluated. In the first experiment, a constant and uniform heat load is applied to the substrate for 240 s and then the heat load is switched off. The temperature change of the substrate is measured by the IR camera and the average temperature of the substrate is plotted in Figure 7.10. The bottom graph of Figure 7.10 shows the standard deviation of the average temperature over 10 experiments. For the first 60 s, there was no input and during this period the standard deviation is about 0.025 K. This can be thought as the variation of the measurement setup. After 60 s, a constant uniform heat load is applied. As the average temperature increases, the variation among the curves also increases. The standard variation during this period is about 0.6% to 1.4% of the average temperature. After the heat input is switched off, the average temperature goes down and becomes close to zero again. However in this period, the variation among the curves is bigger than at the beginning of the experiment. This seems to be caused by an increasing variation of the reference bar temperature during each experiment.

When conducting experimental validation of the proposed techniques, the measurement error in the measurement setup is the largest source of error. Figure 7.11 shows the average temperatures of the substrate without any inputs. These noises are random errors from the measurement setup and therefore averaging of multiple experiment results are conducted to reduce the influence of the variation. The validation experiments in the next chapter are conducted over 30 s for each experiment and 10 experiments are conducted and averaged to reduce the measurement variation.

7.5.2 Time constant and effective cooling coefficient

The convection coefficient used in the thermal error model is estimated from the preliminary experiments. Also the time constants of thermal modes in the model are updated using equation (4.10) and the identified convection coefficient h. The identified convection coefficient and the time constants are used in the thermal error model used in the proposed thermal error reduction techniques. The simulation results using the updated model are compared with the experimental results in the next chapter to validate the proposed thermal error reduction techniques.

7.6 Thermal mode shapes measurement

This section introduces the result of experimental measurements of thermal modes shapes using the setup. The purpose of conducting this experiment is to validate the basis of the theory of Thermal Modal Analysis: the thermal modes. When thermal modes are successfully measured, they are compared with the calculated mode shapes. If there are any significant discrepancies among them, that information should be used to further improve the experimental setup or update the model to reflect the factors in the experimental setup that cause the discrepancies.

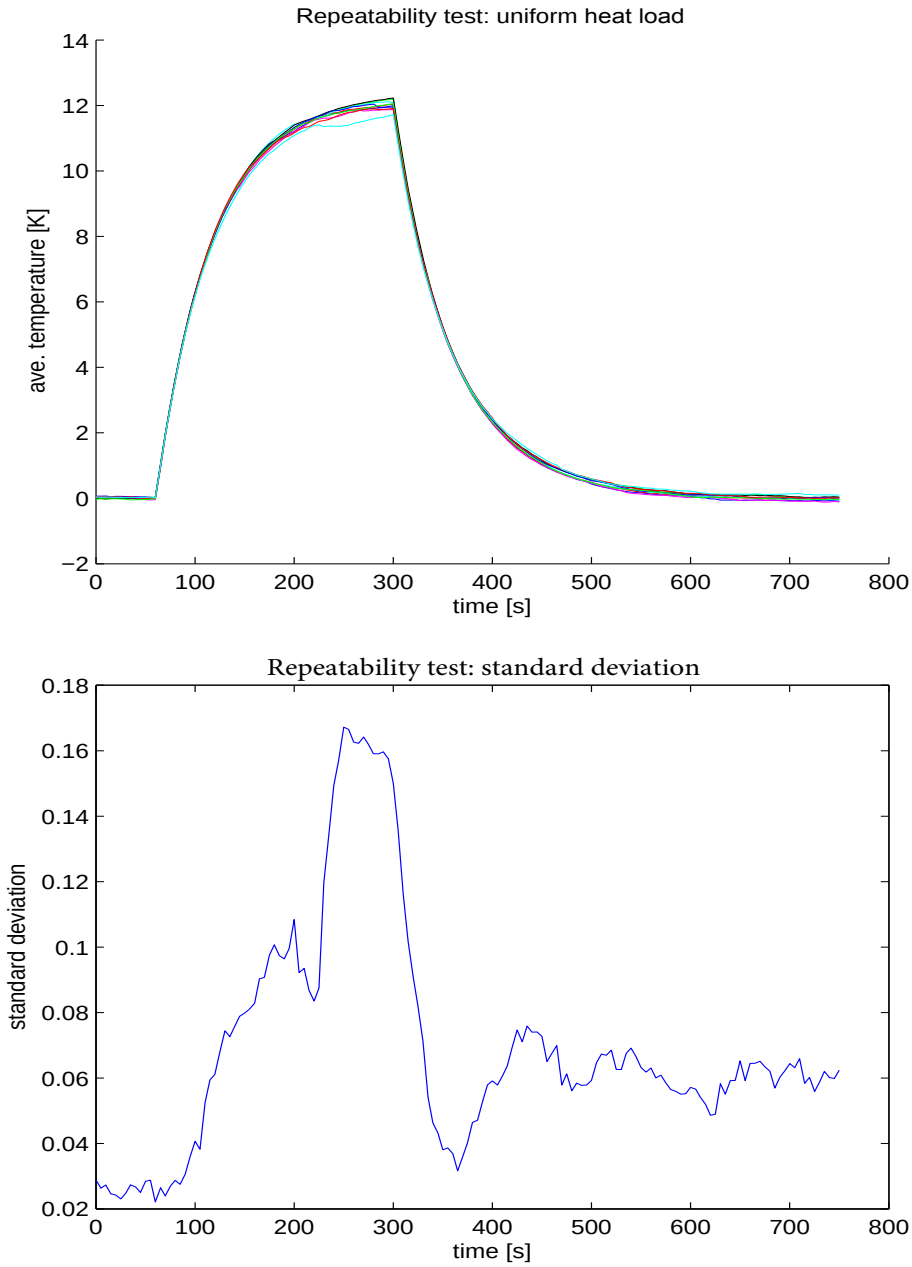

Figure 7.10: Repeatability of the setup when uniform heat load over the substrate is projected and measured by the infrared camera. (Top: Average temperature of the substrate. Bottom: Standard deviation of above lines.)

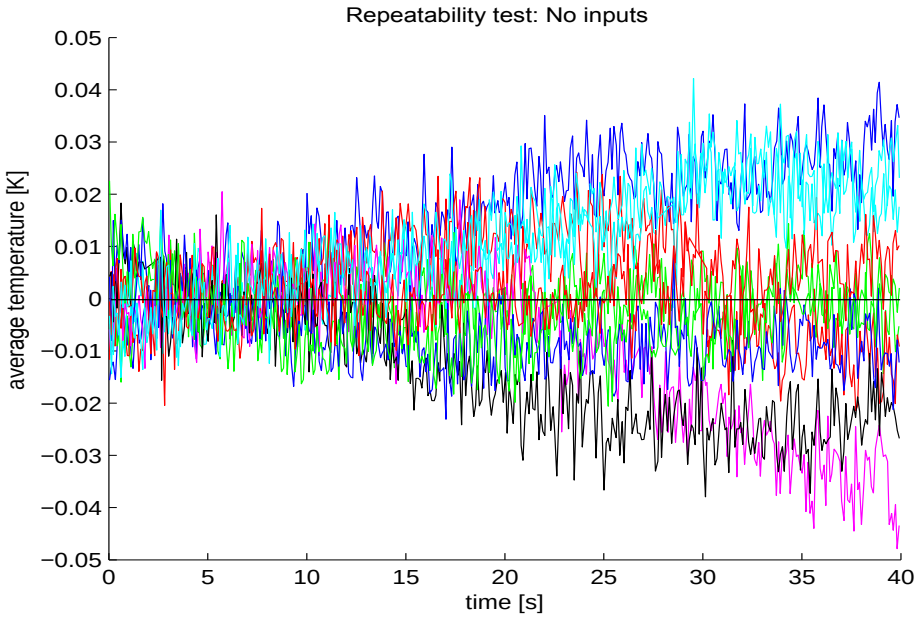

Figure 7.11: Repeatability of the setup when no image is projected, meaning no heat loads applied, to the substrate. The average temperature of the substrate varies about ± 10 mK over short time ($\sim$ 5 s). The average temperature drifts away from zero over long time ($>$ 10 s).

7.6.1 Experimental protocol

The detailed procedure is a bit complex and therefore only the main idea of the protocol is described in this section. For the details, please refer to [77].

The mode shape identification experiment is designed based on the following characteristics of thermal modes.

1. The behaviors of thermal modes are independent to each other.
2. Therefore, when there is only one single mode present in the temperature distribution and no heat loads are applied to the system, then the temperature distribution does not have any other modes and only the amplitude of the present mode changes over time with the decay speed equal to the time constant.
3. The time constants of thermal modes become shorter as the indices of modes increase.
4. Mode shapes are mutually orthogonal to each other with respect to heat capacity and conductivity matrices.

Using these characteristics of thermal modes, the following procedures are developed.

1. Apply a heat load pattern of an analytically calculated lowest mode shape by the projector to the substrate and heat up the substrate by the pattern.

2. Switch off the heat load when the temperature distribution of the substrate does not change any more.
3. Measure the temperature distribution of the substrate over time from the moment of switching off the heat load.
4. If the applied heat load pattern is identical to the actual lowest thermal mode shape of the substrate, then the temperature distribution of the substrate does not change its shape over time and only the amplitude of the mode decreases exponentially over time. If this happens, the temperature distribution at any time gives the mode shape of the lowest mode and the time constant can be obtained from the decay speed of the mode.
5. If the applied heat load pattern is not identical with the actual lowest mode shape, then the temperature distribution of the substrate contains not only the lowest mode but contains one or multiple other modes. Then these modes decay at different speeds according to the time constants. The mode with the smallest indices has the longest time constant among these modes. Therefore, after certain time, there only remains the lowest mode in the temperature distribution. After this time, the temperature distribution does not change its shape any more over time but only the amplitude does. Then the temperature distribution at this moment is the mode shape of the lowest mode.
6. Once the mode shape of the lowest mode is identified, it is possible to subtract the contribution of the lowest mode from the temperature distribution measurement data which also contains other modes. To do so, the amplitude of the lowest mode needs to be identified first. The amplitude of the lowest mode can be obtained by multiplying the lowest mode shape with the temperature distribution at each coordinate and integrate the multiplication. Due to the orthogonality of thermal mode shapes, this gives the amplitude of the lowest mode in the temperature distribution. Then the lowest mode shape multiplied by the amplitude of the lowest mode becomes the contribution of the lowest mode in the temperature distribution and the multiplication result can be subtracted from the original temperature distribution.
7. The obtained contribution of the lowest mode gives the amplitude of the lowest mode in the measurement data over time. Apply a curve fitting algorithm to the identified lowest modal amplitude. Then the time constant of the lowest mode can be obtained.
8. Choose a mode shape which time constant is longest among modes not identified yet. Apply a heat load pattern of this mode shape to the substrate and measure the temperature distribution after the heat load is switched off.
9. Repeat step 6 for each already identified mode shape to subtract the contribution of already identified mode shapes from the measured temperature distribution.
10. Identify the mode shape and time constant of the mode in the same manner.
11. Repeat the process until all mode shapes of interest are identified.

All mode shapes besides the lowest one, which represents the average temperature of the substrate, vary from -1 to 1. However the projector of the experimental setup can only apply positive heat load. Therefore the actual heat load pattern applied to the substrate in the above protocol is a combination of the lowest mode plus the target mode to be identified so that any mode shape to be identified can be excited using only positive input.

7.6.2 Measurement result

Figure 7.12 shows the identified first 25 thermal modes of the substrate. Experimentally identified mode shapes match well with analytically calculated mode shapes (Figure 3.2).

Convection influence to mode shapes and time constants

From the experiment identification of thermal mode shapes, it is also observed that the influence of convection is more prominent in lower modes than higher order modes in terms of time constants. To give this observation some theoretical explanation, following analysis for a simplified situation is conducted to see how the influence of convection affects different modes. Analyzing a situation where the air temperature distribution surrounding the substrate can be regarded as uniform and constant over space and time (so $\boldsymbol{q}_{\mathrm{air}}(t) = -h(\boldsymbol{T}(t) - T_{\mathrm{ambient}})$), then the time constants of the modes becomes as follows as already introduced in equation (3.14).

$$\tau_{\mathrm{i,j}} = \frac{1}{\frac{k}{\rho c}\left(\left(\frac{(\mathrm{i}-1)\pi}{L_{\mathrm{x}}}\right)^2 + \left(\frac{(\mathrm{j}-1)\pi}{L_{\mathrm{y}}}\right)^2\right) + \frac{2h}{\rho c w}} \tag{7.1}$$

As the conduction part in the equation $\frac{k}{\rho c}\left(\left(\frac{(\mathrm{i}-1)\pi}{L_{\mathrm{x}}}\right)^2 + \left(\frac{(\mathrm{j}-1)\pi}{L_{\mathrm{y}}}\right)^2\right)$ becomes larger as the indices of the modes become larger, the influence of convection becomes smaller in the time constants of higher modes. This means that the time constants of lower modes change largely due to the actual convection strength while the time constants of higher modes change less (Figure 7.13).

When looking at the experimentally identified time constants in Figure 7.14, it can be seen that the identified time constants indeed show this trend. Also from this result, it is possible to estimate the approximation of the actual convection coefficient value. Putting this estimated coefficient back into the simulation, a good agreement in the experimental and simulated time constants is observed for lower modes.

7.7 Conclusions

This chapter introduces the design of a thermal experimental setup. We developed the setup and conducted several preliminary experiments to identify the characteristics of the setup, and improved the design of the setup and the subsequent data processing. After that, experimental identification of the thermal mode shapes of the substrate identified the first 25 mode shapes of the rectangular substrate. The identified mode shapes showed good agreement with the calculated mode shapes. Experimental validation of the proposed thermal error reduction techniques were conducted using the setup. This is described in the next Chapter.

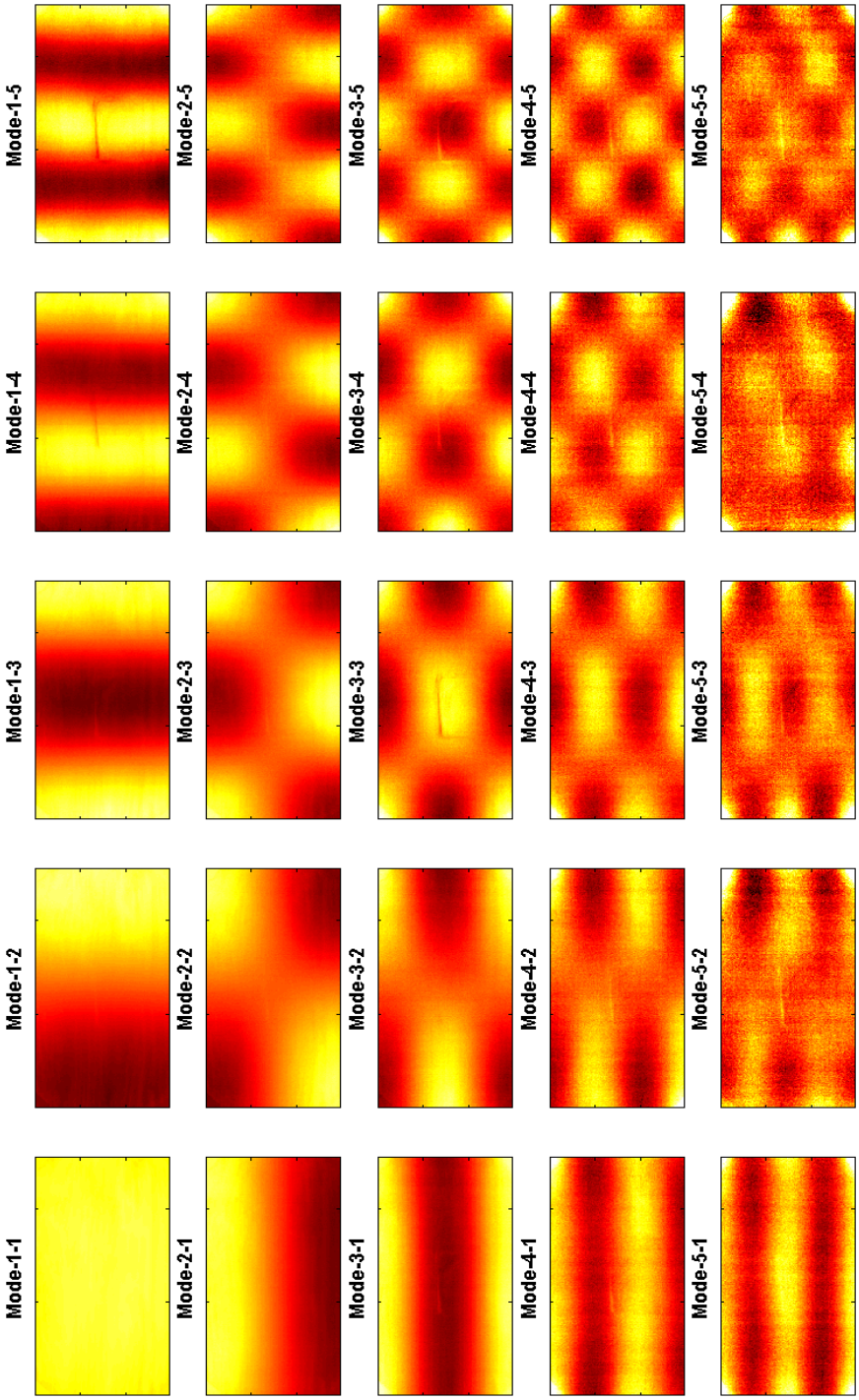

Figure 7.12: First 25 measured thermal modes of a thin aluminum foil.

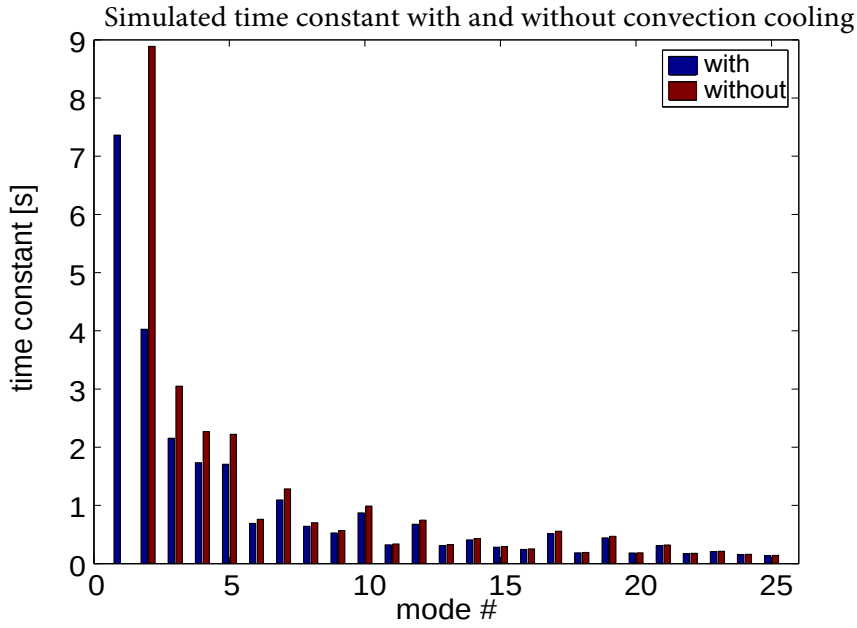

Figure 7.13: Simulated time constants with and without convection. Convection cooling affects mostly the time constants of lower order modes and less higher order modes.

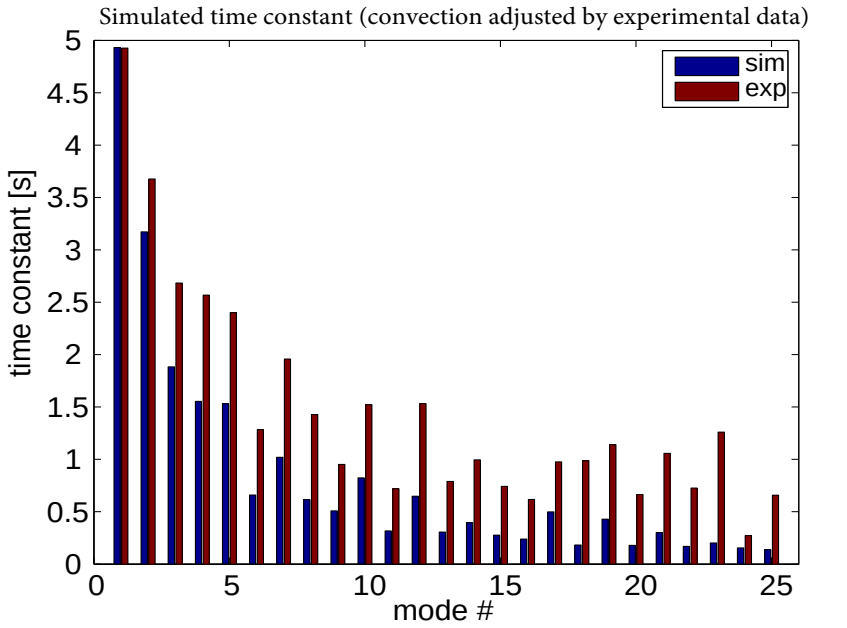

Figure 7.14: Simulated time constants compared with experimentally identified time constants. The simulated time constants are calculated using the identified convection coefficients from the preliminary experiment.

Chapter 8

Experimental validation

8.1 Overview of this chapter

This chapter shows the results of the experimental validation of the proposed thermal error reduction techniques in the temperature domain. First, experimental Mode Cancellation is conducted using the experimental setup described in the previous chapter. Three modes (mode(2,1), mode(1,2) and mode(2,2)) are controlled in this experiment by the external control heat loads the amplitude of which are calculated by Mode Cancellation. Second, experimental Modal Control is conducted. In the experiment, 8 modes are controlled which is comparable to the simulation Modal Control with 9 modes control (mode(1,1) $\sim$ mode(3,3)) except the first mode(1,1) is not controlled due to the lack of forced cooling capability in this setup. In each case, the validation was conducted only in the temperature domain. The thermal displacement error itself was not measured in this experiment.

8.2 Mode Cancellation

8.2.1 Experiment details

In this section, the result of the experimental validation of Mode Cancellation using the setup (Figure 8.1) described in the previous chapter is described. The validation experiment is conducted in the temperature domain to observe the control of the temperature distribution in terms of thermal modes.

The detailed conditions of the experiment in the temperature domain are as follows. The moving disturbance heat load draws four lines (Figure 8.2, the same pattern as "discontinuous path" in the simulation study in Chapters 4 and 5) on a thin aluminum substrate of 76 mm * 44.5 mm * 0.5 mm over 25 s (Figure 8.4). In the simulation in chapter 4 and chapter 5, a point load is assumed, but in the experiment, a rather large radius of heat spot needs to be applied to generate the moving point load. This was necessary as the energy density of the projector is small and therefore to heat up the substrate sufficiently compared to the noise level of the setup, a large spot size is required to achieve the required input energy. The external control heat loads applied at the corners also have a finite spot size for the same reason. The radius of the spots are 8.9 mm for the moving load and 20 mm for the control loads.

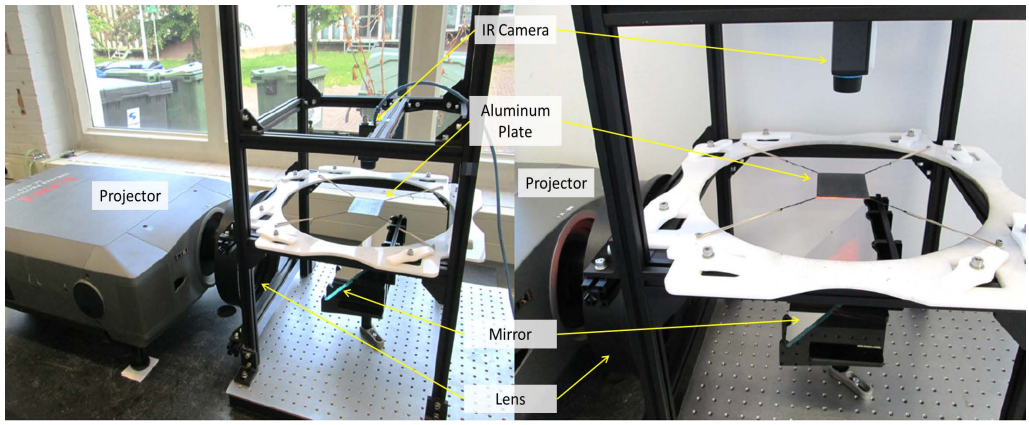

Figure 8.1: Experimental setup.

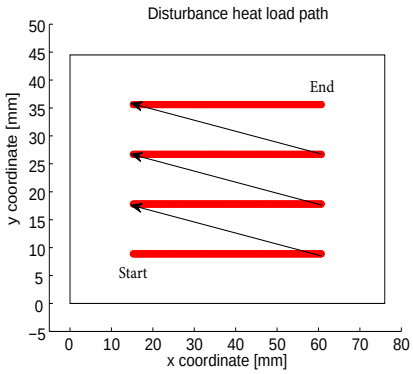

Figure 8.2: Heat load path (point load)

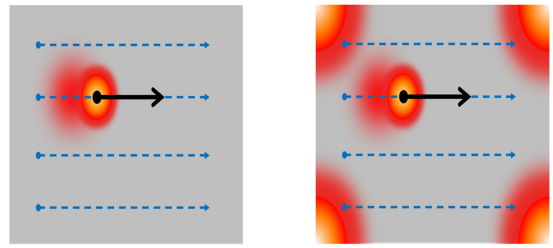

Figure 8.3: Heat load path and external control loads (Finite spot size)

Figure 8.4: Aluminum substrate used in the experimental setup. The aluminum substrate is painted by black paint on both sides to increase heat absorption of the projector light and to reduce the reflection of the radiation from the IR camera which is then measured as measurement error by the IR camera. At each corner, small hole is made and a string hangs the substrate through the hole.

Therefore the actual control loads looks like Figure 8.3. In this experiment only 3 modes are controlled (mode(2,1), mode(1,2) and mode(2,2)) but not mode(1,1) which represents the average temperature of the substrate. This is because the setup does not have a capability to apply strong enough cooling to the substrate to extract the input energy from the substrate. However, for the experiment validation of Mode Cancellation it is sufficient to control the three modes to prove the control of the temperature distribution in terms of modes.

Using equation (4.4), target modes can be controlled in feedforward manner. A remaining error can be further controlled by feedback. In this thesis, a proportional gain feedback control is used. The proportional gain K (Figure 8.5) is calculated using Linear Quadratic Regulator method from the state space model of the system below (equation(8.1)) with the objective function J (equation(8.2)):

$$\begin{aligned} \dot{\bar{\boldsymbol{\theta}}}(t) &= -\left[\frac{1}{\tau_{\mathrm{r}}}\right]\bar{\boldsymbol{\theta}}(t) \\ &+ \quad [C_{\mathrm{r}}]^{-1}\left\{[\boldsymbol{\Phi}_{\mathrm{mov}}(t)]^{\mathrm{T}}\,\boldsymbol{q}_{\mathrm{mov}}(t) + [\boldsymbol{\Phi}_{\mathrm{cool}}]^{\mathrm{T}}\,\boldsymbol{q}_{\mathrm{cool}}(t) + [\boldsymbol{\Phi}_{\mathrm{nm}}]^{\mathrm{T}}\,\boldsymbol{q}_{\mathrm{ext}}(t)\right\} \end{aligned} \tag{8.1}$$

$$J = \sum_{k=1}^{N}\left(\bar{\boldsymbol{\theta}}(t_k)^{\mathrm{T}}\boldsymbol{I}\bar{\boldsymbol{\theta}}(t_k) + \boldsymbol{q}_{\mathrm{ext}}(t_k)^{\mathrm{T}}\boldsymbol{R}\boldsymbol{q}_{\mathrm{ext}}(t_k)\right) \tag{8.2}$$

where $\boldsymbol{I}$ is a unit matrix which weights all the selected modes equally and $\boldsymbol{R}$ is a cost matrix for the control effort. In this thesis, $\boldsymbol{R}$ is chosen to be negligibly small compared to the unit matrix. Then the optimal feedback gain K with respect to the objective function J can be obtained to minimize the sum of the selected modal amplitudes. Figure 8.5 shows the control block diagram of the combination of feedforward and LQR feedback control of target modes.

Four different experiments are conducted and compared after data processing. The first experiment applies the moving disturbance load alone. The second experiment applies feedforward control of the external control loads using equation (4.4). The third experiment applies feedback control of the external control loads using equation (4.4) and a Linear Quadratic Regulator to calculate the proportional gain K. The fourth experiment is the combination of feedforward control and feedback control. The sampling frequency of these experiments is chosen to be 4 Hz and the control signal is also controlled at 4 Hz. This is determined by the speed of the IR camera measurement, data transferring speed from the IR camera to the controlling computer, and the computer's processor speed to calculate the modal amplitudes of control from the temperature images taken by the IR camera. The same experiments are conducted 10 times for each experiment and results are averaged to reduce the influence of random noise in the results and summarized in Figure 8.7.

8.2.2 Result and Analysis

Figure 8.6 shows the experimental results when only the moving disturbance load is applied to the substrate. The amplitudes of mode(2,1), mode(1,2) and mode(2,2) averaged over 10 experiments are compared with the simulation results for the same conditions.

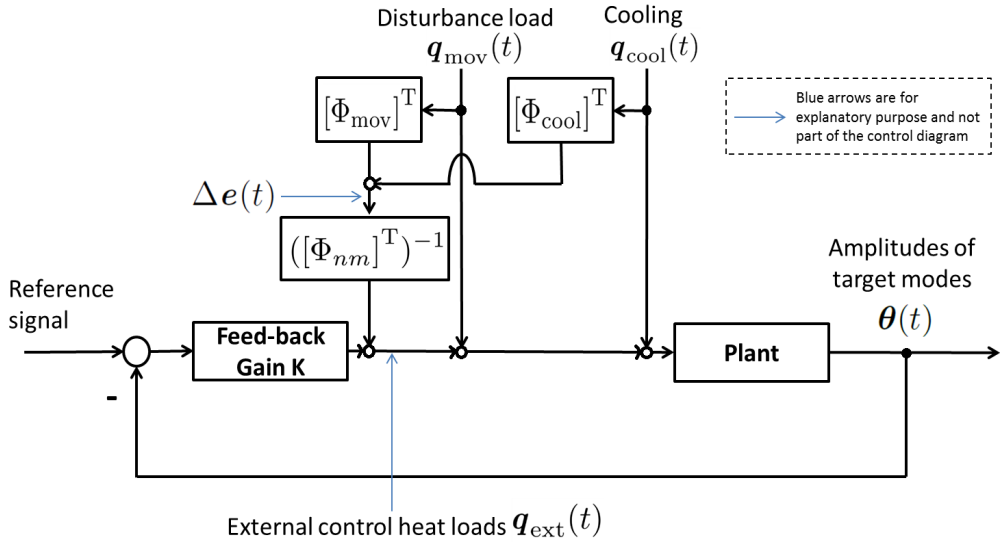

Figure 8.5: Control block diagram. Blue arrows are for explanatory purpose and not part of the control diagram.

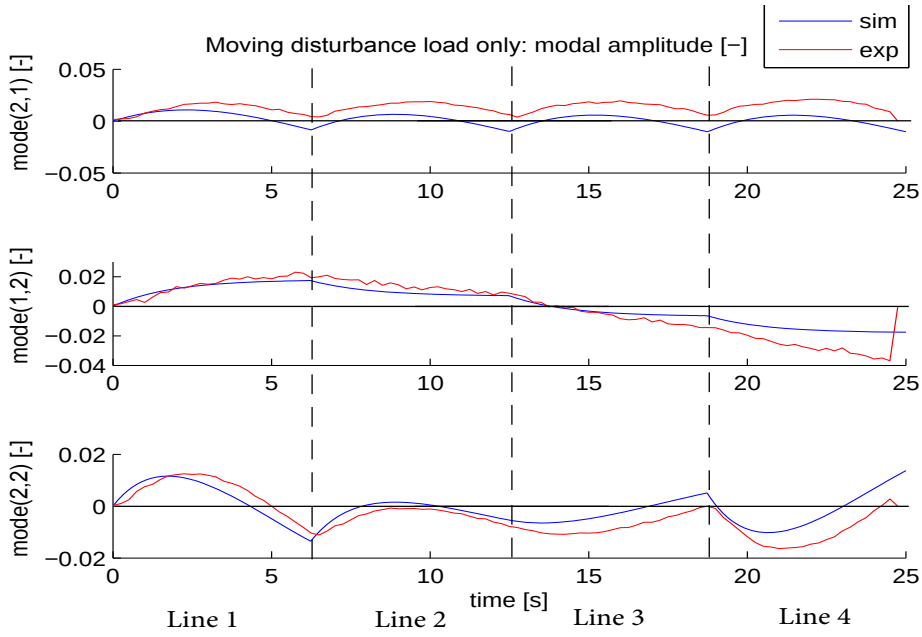

Figure 8.6: Modal amplitudes of mode(2,1), mode(1,2) and mode(2,2) by the moving disturbance load. Simulation (blue) and experimental result (red) are compared. The graphs show good agreement in the overall behavior of these modes between the simulation and experiment.

The experimentally obtained amplitudes of these modes match well to the simulation results.[1] So the simulation model is close to the thermal behavior of the experimental setup.

Figure 8.7 shows the results of experimental Mode Cancellation. The amplitudes of mode(2,1), mode(1,2) and mode(2,2) are averaged over 10 experiments for each case. The blue curves in the graphs show the amplitudes of these modes when only the moving disturbance load is applied to the substrate, that is, before Mode Cancellation control. The red curves are the amplitudes of the modes when the external loads are also applied in feedforward manner. The green curves are the amplitudes of the modes when the external loads are controlled in feedback manner with a proportional gain calculated from the system model equation 5.5 to 5.8 using LQR (the values for $\boldsymbol{Q}$ and $\boldsymbol{R}$ are same as equation (5.13)). The cyan curves are the amplitudes of the modes when the external loads amplitudes are controlled by the combination of feedforward and feedback.

Feedforward control (red curves) show the cancellation of the excitation of modes 2, 3 and 4 due to the moving disturbance load by properly controlling the external control heat load amplitudes. However as time proceeds, the controlled amplitudes of mode 2 (top figure in Figure 8.7) deviates from zero. This is thought to be caused by the difference between the model and the actual setup. Feedback control (green curves) do not have this deviation as this kind of deviation caused by model imperfection can be compensated by feedback control. However due to very low control frequency of 4 Hz, there are large over shoots in the modal amplitudes at the beginning of each printing line (at $t = 0, 6.25, 12.5, 18.75$ s) where a large error occurs due to discontinuous jumps of the point of interest. Therefore the combination of feedforward and feedback is expected to solve these problems specifically associated with feedforward control and feedback control as the feedforward error is compensated by the feedback control and the feedback over shoots are prevented by feedback control. This is actually observed in the cyan curves where both of the aforementioned problems are solved well. Figure 8.8 shows the average remaining amplitudes of the 3 controlled modes. The graph clearly shows that the combination of feedforward and feedback control (cyan) gives the best cancellation of the 3 controlled modal amplitudes.

The performance of feedforward control can be improved by improving the model accuracy and/or improving of the setup. Possible improvements of the setup are the use of finer non-uniformity compensation curve and finer gamma curve compensation. Adding forced cooling by an electric fan is expected to increase the convection uniformity and reduce the difference between the model and the setup. The performance of feedback control can be further improved by simply increasing the control frequency. It is expected that the results of feedback control would improve to some extent as the control frequency increases. However even the current setup performs clearly well enough for the purpose of the experimental validation of Mode Cancellation.

8.2.3 Summary

The results of these experiments show the validity of the temperature control in terms of thermal modes by applying and controlling the amplitudes of the external control heat loads based on the theory of Mode Cancellation described in chapter 4. This result itself shows that modes can be controlled independently up to the number of modes equal

[1] Correlations between the simulation and 10 times average of experiments are 0.6026 for Mode(2,1), 0.9858 for Mode(1,2), and 0.8456 for Mode(2,2).

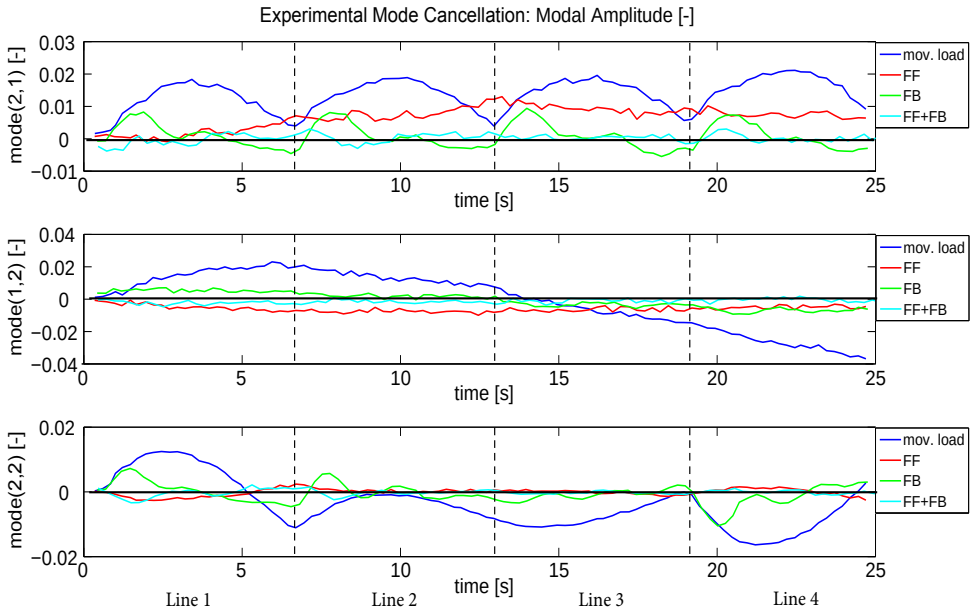

Figure 8.7: Experimentally obtained modal amplitudes of mode(2,1), mode(1,2) and mode(2,2) by Mode Cancellation (3 modes control). The zero control case (blue, "mov. load") is compared with Mode Cancellation by feedforward (red, "FF"), feedback (green, "FB") and combination of both (cyan, "FF+FB"). Feedforward controls all 3 modes well at the beginning but starts to drift away from 0 because of the accumulation of various errors. Feedback shows a good control over time but has some overshoots at the beginning of each line in the discontinuous path. This is due to the nature of feedback control that the feedback control can start correcting errors only after there occur some errors. Combination of feedforward and feedback shows the best control by taking the benefit of both feedforward and feedback controls.

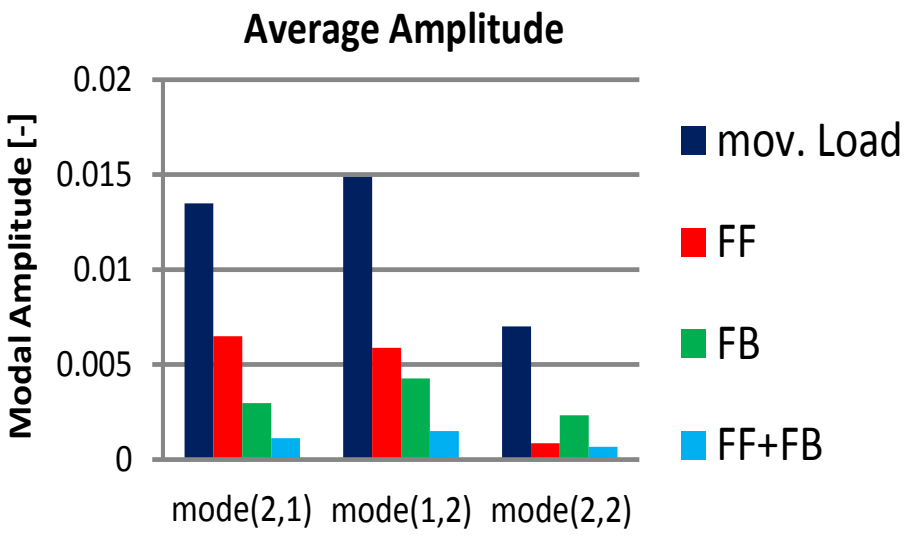

Figure 8.8: Average of the modal amplitudes of mode(2,1), mode(1,2) and mode(2,2) in Figure 8.7. The graph clearly shows that the combination of feedforward and feedback (cyan, legend "FF+FB") shows the best control over feedforward only (red, legend "FF") and feedback only (green, legend "FB').

to the control loads as expected from the theory of Thermal Modal Analysis and Mode Cancellation. However as described already in chapter 4, this is not always true when the sensitivity matrix (equation 4.4) of the target modes at the locations of the external control loads is singular in which case it is not possible to control all the target modes independently. Also when the sensitivity matrix is close to singularity, the amount of energy required from the control heat loads becomes prohibitively high and also the excitation of non-controlled modes is more prominent and diminishes the merit of eliminating the lower modes from the thermal error. Therefore, there is always an inevitable heuristic part which requires clever selection of modes to be controlled and selection of control load locations, probably depending on the specific conditions of each situation. Therefore, Modal Control using Linear Quadratic Regulator (LQR) which allows control of a higher number of modes is a more versatile method and its experimental validation is described in the next section.

8.3 Modal Control using LQR

Modal control by Linear Quadratic Regulator (LQR) solves the issue of singularity of the sensitivity matrix in Mode Cancellation. The method can control a higher number of modes than the number of external control loads. Also it can take the weighted importance of thermal modes depending on the magnitudes of their influences to the thermal error depending on the path. Even when the sensitivity matrix becomes singular, the process automatically ignores some of the modes and gives the best solution for the given path

based on the objective function to be minimized.

8.3.1 Experiment details

Almost the identical experiment is conducted as for the experimental validation for Mode Cancellation. The differences are that the amplitudes of the external heat loads at each corner of the substrate are controlled based on Modal Control and more than 3 modes (excluding the first mode) are controlled in this experiment. In Figure 8.9 in the next section, experimental and simulation results of Modal Control of the first 9 modes with the time variant $\boldsymbol{Q}(t)$ in equation 5.47 are compared (with the exception of the first mode). As the experimental setup does not have a cooling, the first mode is not controlled in the experiment. So in simulation, 9 modes Modal Control is conducted to minimize the thermal displacement error in the discontinuous path example. In the experiment first 9 modes with the exception of the first mode are controlled. Then the comparison is performed for the first 16 modes (mode(1,1) $\sim$ mode(4,4)) to see whether the controlled modes are controlled to the same level in the experiment as predicted in simulation. The control of the external load amplitudes are conducted in feedforward only in this experiment due to the lack of the computational power in the setup to calculate a higher number of modal amplitudes in real time for feedback control.

8.3.2 Result and analysis

Figure 8.9 shows the comparison of the first 16 modal amplitudes (mode(1,1) $\sim$ mode(4,4)) of Feedforward Modal Control with 9 modes in simulation (blue curve) and experiment (red curve). The first 9 modes (mode(1,1) $\sim$ mode(3,3) are the controlled modes and the other modes (mode(4,1), (1,4), (4,2), (2,4), (4,3), (3,4), (4,4)) are not controlled.

Overall, a good agreement between the simulation and the experimental results can be observed although there are a few modes which show bad agreement. First, the difference in mode(1,1) is simply because of the lack of cooling in the experiment whereas the simulation also includes cooling to keep the overall temperature (= the amplitude of mode(1,1)) equal to 0. Significant discrepancies are found between the simulation and the experiment in mode(1,3) and mode(3,1). As most of the amplitudes of the other modes show good agreement, it is reasonable to think that the modal amplitudes are controlled in the experiment as predicted in the simulation. However there are some additional factors which are not included in the simulation which influence the behaviors of the modes showing difference in the experiment from the simulation such as mode (1,3) and (3,1). The cause of the discrepancies might be due to the influence of the convection between the surrounding air and the substrate where the actual spatial distribution and the intensity change over time may depend on the aluminum substrate temperature distribution over time and space. Therefore in this case, it is expected that the influence of convection appears as an additional excitation of mode(1,3) and (3,1) that has resulted in the differences in the amplitudes.

8.3.3 Summary

The comparison between experimental and simulation Modal Control shows a good agreement in the first 4*4 modes with the exception of a few modes. Therefore the concept of Modal Control is experimentally validated in a fundamental sense. Improvement of the experimental setup is still required in order to match all modal amplitudes between

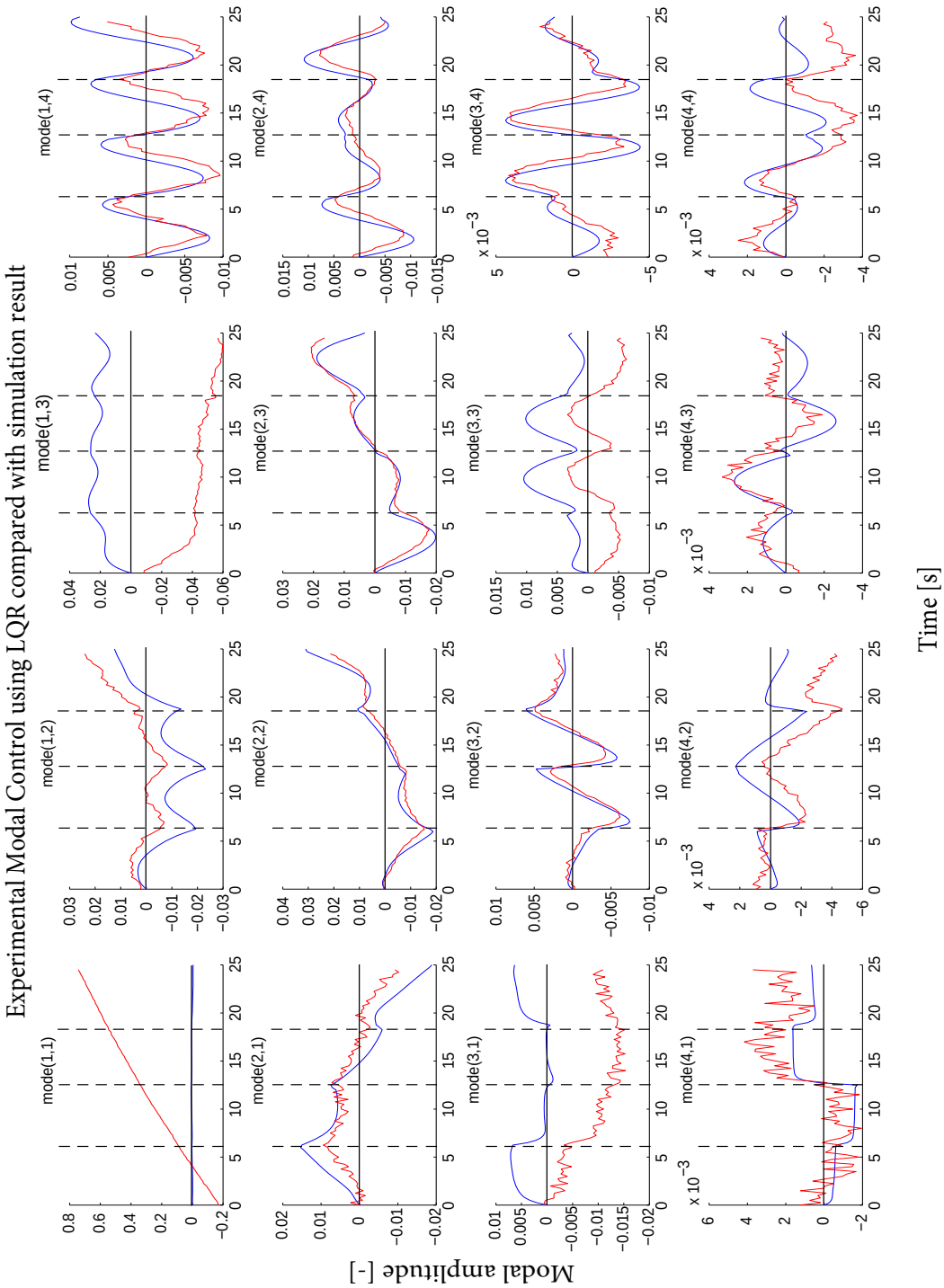

Figure 8.9: The amplitudes of the first 4*4 modes by Modal Control using LQR (9 modes control). The experimental result (red) is compared with simulation result (blue). As mode(1,1) is not controlled in the experiment, this mode shows different behavior between experiment and simulation. Other modes show good agreement in general except mode(1,3) and mode(3,1). This is considered to be caused by the influence of non-uniform convection cooling in the experimental setup.

the experiment and simulation for the real application of the thermal error reduction technique.

8.4 Discussion on experimental results

Experimental validation of Mode Cancellation and Modal Control were conducted and results were summarized in this chapter. It was experimentally proven that modes could be controlled as desired such as keeping a set of modal amplitudes equal to zero or to control a number of modes simultaneously to realize a desired temperature distribution to minimize a thermal displacement error. The modal amplitudes are well controlled in the experiments, although there are certain issues that need to be addressed for practical applications. There are some difficulties encountered in thermal experiments. One of the largest difficulties is the invisible air fluctuation that can easily have a dominant influence on the experimental results. To further improve the performance of the experiments, improvements in the setup are required such as placing the setup in a better temperature controlled room or adding a cooling device which can be modeled accurately into the model.

8.5 Conclusions

This chapter showed the results of the experiments conducted using the setup described in the previous chapter. The results of the experiments showed that temperature distribution can be controlled in terms of modes. Therefore experimental Mode Cancellation and Modal Control have been validated in the temperature domain. Another setup designed for in-plane thermal displacement measurement is described in the appendix A.

Chapter 9

Conclusions

In this thesis, three novel thermal error reduction techniques have been proposed. These techniques are developed based on Thermal Modal Analysis, for example, for a hypothetical printing device. These proposed techniques are suitable to solve thermal issues in precision machine where continuous improvement of thermal error performance is required. The mathematical formulation of each technique is described, and the performance of the proposed techniques is evaluated using numerical simulation. An experimental setup has been designed and developed to conduct experimental validation of the proposed techniques in terms of thermal mode control. Mode Cancellation and Modal Control methods are validated through the experimental validation conducted using the setup. Through the development of the novel thermal error reduction techniques and the experimental validation of the techniques, understanding of characteristics of thermal modelling using Thermal Modal Analysis, including experimentally obtained mode information, have also been developed.

9.1 Proposed novel thermal error reduction techniques

Three novel thermal error reduction techniques have been proposed. In these techniques, the temperature distribution and the corresponding thermal deformation of the machine structure are expressed using or based on thermal modes. In the reconstruction of the resulting thermal deformation and the thermal displacement error, only a small number of lower modes dominate a large part of these. Therefore, controlling only these dominant thermal modes largely influences the thermal deformation of the machine structure and results in the reduction of thermal displacement errors.

Mode Cancellation

Mode Cancellation controls and eliminates a set of selected modes by applying and controlling the amplitudes of external control heat loads. The set of modes is manually selected based on a set of criteria, which are, having large contributions to the thermal error, having high sensitivities with respect to the external loads, and having non-singular sensitivity matrix with respect to the external loads. Mode Cancellation controls up to the same number of modes as the number of the external control loads. These controlled modes are fully controlled to have zero amplitudes. This results in the removal of the selected dominant thermal modes from the thermal error; however, the same external loads

also increase the magnitudes of the other non-controlled modes. As the result of the example case in Chapter 3 showed, even though the contribution from the non-controlled modes increased due to the external loads, the reduction of the thermal error is larger due to the removal of the controlled modes. Therefore, Mode Cancellation exhibits the capability and possibility of a new kind of thermal error reduction solution that actively applies heat loads to control the temperature distribution to reduce thermal displacement error. This method is quite inventive in the sense that it intentionally applies heat loads to reduce thermal error. Most of the current thermal error reduction techniques try to reduce thermal error by reducing the temperature increase or thermal deformation. Therefore, applying cooling or using material properties with smaller thermal expansion coefficients are the standard solutions. There hardly exists a solution which intentionally applies heat. A notable exception is [31]. To the authors knowledge, there is no structured formulation to apply and control heat loads for the purpose of thermal error reduction. In this aspect, Mode Cancellation proposes a fundamentally novel kind of solution to the field of thermal error reduction.

However, Mode Cancellation has certain limitations. This technique cannot control a set of modes which sensitivity matrix with respect to the external control heat loads becomes singular. Practically, even if the sensitivity matrix is not singular but close to singular, meaning that its inverse matrix contains very large entries, the required amplitudes for the external loads become very large. This results in large excitation of non-controlled modes, and therefore the thermal error may not be reduced in that case. Moreover, the selection of controlled modes and selection of the locations of the external control heat loads need to be chosen manually. During the selection, following aspects need to be considered: (1) the contribution of each thermal mode to the thermal error, (2) sensitivities of selected modes with respect to the external loads depending on the locations and (3) availability of space for the control loads in the machine structure.

Modal Control using LQR

To overcome these limitations of Mode Cancellation and to further extend the capability of the thermal error reduction technique using Thermal Modal Analysis, Modal Control using Linear-Quadratic Regulator (LQR) is developed. In Modal Control using LQR, a dynamic cost function $\boldsymbol{Q}(t)$ is utilized so that the cost function, multiplied and pre-multiplied by state vector $\boldsymbol{x}_\mathrm{s}(t)$ $(= \boldsymbol{x}_\mathrm{s}(t)^\mathrm{T}\boldsymbol{Q}(t)\boldsymbol{x}_\mathrm{s}(t))$, represents the thermal error in a reduced order model using a set of selected modes. This requires a transformation of standard LQR with static cost function $\boldsymbol{Q}$ into one adapted for a dynamic cost function. This guarantees obtaining the minimum remaining error in L_2 norm in the reduced order thermal model using only the selected modes. This of course does not guarantee that the thermal error in the full order model will be minimized as well. However, the results for example cases exhibit the thermal error reduction in the full order model as well. Modal Control also automates the process of selecting a proper set of modes to be controlled. If a certain set of modes make up a singular sensitivity matrix with respect to the external control loads, some of the modes are not controlled at all in Modal Control. That is practically the same as excluding some of the modes from the selected set of modes to make the sensitivity matrix non-singular. In this way, Modal Control using LQR extend the two major limitations of Thermal Modal Analysis: (1) the number of controlled modes can be larger than the number of external control loads, and (2) controlled modes are selected automatically to include the modes with a large contribution to the thermal error while having high sensitivities to the control loads and avoid singular sensitivity matrix.

Modal Control using LQR adapted for moving external control loads

Modal Control using LQR is further extended to adapt to a dynamic $\boldsymbol{B}(t)$ matrix. This enables to add moving external control heat loads to the Modal Control scheme. Using the moving external control loads enables to control the target modes more efficiently, as the sensitivity of the target modes with respect to the moving disturbance load and the sensitivities of the same modes with respect to the moving external control heat loads are similar because of spatial proximity of these loads. Because of this similarity in the mode sensitivities with respect to the disturbance and external control loads, Modal Control adapted for moving external control loads exhibits a capability of achieving a better thermal error reduction than stationary external control heat loads. In an extreme case, if the distance between the disturbance load and the control loads is equal to zero, it has the highest efficiency in reducing thermal error. However, in this case, negative control heat loads, that is moving and dynamically controllable cooling, are required. In this extreme case, the obtained solution is simply the application of the same strength of cooling by the control loads as the amount of heat by the disturbance loads. On the other hand, in another extreme case where the external control heat loads are placed at the corners of the substrate, then positive external control heat loads with the help of a cooling can control the thermal displacement of an internal point of interest within the substrate. From these two extreme cases, it is expected that when the moving control loads are spatially separated from the disturbance loads with a certain distance, then the thermal error can be minimized or at least reduced by only applying positive external control heat loads under a uniform constant cooling.

9.2 Thermal model by Thermal Modal Analysis

A thermal model developed using Thermal Modal Analysis has unique characteristics. Using different number of thermal modes, different order of reduced thermal model can be created. The model accuracy increases as the number of modes used in the reduced model increases. However, as shown in this thesis, a large part of thermal displacement, and hence thermal displacement errors, mostly consist of the contribution of a limited number of lower modes. Therefore, even a low order model has a good accuracy in thermal displacement error modelling. The behaviour of each mode can be easily calculated independent of each other by solving a first order differential equation of the mode. Therefore, once the mode shapes are obtained, the behaviour of the reduced order model can be calculated within a short time with small computational power. Different thermal modes have different spatial frequency shapes and time constants. By analysing a reduced order model including modes with different highest spatial frequencies, the thermal behavior at different spatial scales can be analyzed and also decay behavior at different time scales.[1]

9.3 Experimental Thermal Modal Analysis

Experimental Thermal Modal Analysis enables a designer to study the realities of the setup or system that are difficult to be studied using analytical or numerical models. For example, material property differences from the model to the reality can be studied by adjusting the model parameters if it can be expressed in a simple manner, such as

[1] but not the excitation of modes at different time scales as it is independent from the time constants.

uniform values for each parameter like conductivity, density, or capacity. Using thermal mode shapes, non-uniform material properties can also be expressed in terms of mode shapes. Therefore, experimental thermal mode shapes and a thermal model using these experimental modes can better describe a complex machine thermal behaviour. If this is done with numerical model based on a straightforward manner such as finite element method, it is less straightforward to obtain a proper set of data to obtain this information and how to reflect them into the model.

Also, online temperature measurement is helpful to predict the temperature distribution and thermal displacement during the machine operation more accurately. This enables to reduce the influence of uncertainties in the model such as the actual surrounding air temperature distribution or fluctuation of the heat generation within the machine during the actual machine process.

9.4 Design guide line

The proposed techniques exhibit that control of temperature distribution by applying and controlling external heat loads is an alternative method to control and reduce the thermal displacement errors other than by just applying cooling, choosing a material with small thermal expansion coefficient, reducing heat source magnitudes, or compensating for the thermal error. Especially positioning the heat loads close to the point of interest has a better control capability to the thermal displacement at the point. Therefore, the proposed novel thermal error reduction techniques give a new design possibility when a designer thinks about the thermal design. Also, Thermal Modal Analysis enables to analyse the thermal behaviour of a machine at different time scales and spatial frequencies.

9.5 Recommendations for future research

To further extend this research, following subjects are suggested as recommendations for future research.

1. **1. Further development of the proposed thermal error reduction techniques.**
   Three novel thermal error reduction techniques are developed and their performances and characteristics are studied in this research. However, further studies and development of these techniques are required to fully develop the potential of the proposed techniques or other techniques utilizing the unique characteristics of Thermal Modal Analysis. For example, Modal Control using LQR can be extended by using Quadratic Programming to apply more complex conditions such as the limitations of heat load amplitudes within the optimization. In this research, the heat load limitations are applied after the optimization by simply cutting off any heat load amplitudes that exceed a certain range. Therefore, the optimized heat load amplitudes after the cut-off are actually not the optimal solution. However, using Quadratic Programming, such a constraint can be implemented within the optimization scheme, and therefore the obtained control heat load amplitudes are the optimal solution, given the restriction on the heat load amplitudes. Another example is the use of proper orthogonal Decomposition or any other orthogonal decomposition techniques, which use the disturbance load information in obtaining the orthogonal basis. Using such bases using disturbance load information would

give a better reduced order model of the thermal problem of interest and therefore are expected to have a better thermal error reduction capabilities.

2. **2. Accurate and efficient thermal modelling through experiment and numerical modelling.**
   Accuracy of the thermal model is an important aspect of solving thermal issues, especially in thermal error compensation techniques. However, the accuracy of a thermal model can be limited by several factors such as changing and distributed thermal boundary conditions, limitations in accuracy of material properties or thermal properties, or non-linearity in thermal behaviour. Therefore, improving thermal model accuracy is one of the most important subjects for thermal error reduction. Thermal Modal Analysis offers a unique way of modelling these factors into a thermal model by including the effects into the thermal mode shapes. Therefore, it is expected that the thermal modelling accuracy would be improved by further studying the capability of experimental mode shape measurement together with numerical study of the influence of these parameters to the thermal modes.

3. **3. Estimate (quantify) effects of changing thermal boundary conditions from the thermal mode measurement.**
   Modelling distributed and changing boundary conditions is one of the most challenging problems in thermal modelling. This limits the accuracy of thermal modelling, which further limits the performance of many sophisticated solutions using thermal model, especially thermal error compensation techniques which rely on the accuracy of the thermal model. Therefore, applying Thermal Modal Analysis, analysing the behaviour of thermal boundary conditions, and characterizing thermal boundary conditions using Thermal Modal Analysis will provide interesting results and insights.

   For example, the change in the temperature distribution of the environment has large effects on the thermal behaviour of a machine within the environment. Simulating the air flow and the temperature distribution using computational fluid dynamics might be a way to evaluate the impact. However, this is a time consuming and computationally expensive solution. Measuring the environment temperature at multiple locations might be an alternative. But then the question is to determine the number of sensors and their locations. However, what is actually most relevant for the machines thermal behaviour is how the environment affects the machines behaviour, but not to estimate the temperature distribution of the environment itself. Thermal Modal Analysis can evaluate the dominant part of the influence from the environment by measuring the modal amplitudes of the lower order modes. The locations of the sensor placement can be determined by analysing the machine structure rather than the dynamic temperature distribution of the environment. Therefore, in this way, it is expected that the influence of the environment to the machine behaviour can be well identified using Thermal Modal Analysis in a much simpler manner.

4. **4. Parameter estimation such as material properties of a target system using thermal modes measurement.**
   Identification of material properties of a machine or a part is also an interesting application of Thermal Modal Analysis. Practically, it is not known exactly what are the material property values of the target machine, how they relate to the thermal issue of interest, or how large the influence is. It is difficult to evaluate these material

properties precisely rather than obtaining average values. However, Thermal Modal Analysis can analyse thermal issues at different spatial frequencies and time scales. Therefore, when the thermal modes and time constants for a structure with non-uniform material properties are studied, this would give interesting insights on how to evaluate or what to evaluate regarding the material properties of real machines.

5. **5. Apply the developed thermal error reduction techniques to an actual problem with a real machine.**
   When solving thermal issues, many different kinds of solutions can be used to solve similar problems. The factors that make one particular solution more suitable than the others are the many practical requirements specific to each issue. For example, when heat generated inside a machine causes a thermal issue in the machine, attaching a cooling device might be the best solution. Changing the material property of a part of the machine structure might even be a better solution than applying cooling. Any other kinds of solutions might also work better for that particular issue. The actual choice of a solution (or even combination of different solutions) depends on the requirements, working conditions, machine space availability, project boundary conditions, and so on. In view of this, it would be helpful to have a concrete problem with a real machine to study the applicability of the proposed thermal error reduction techniques or the applicability of Thermal Modal Analysis for thermal modelling or analysing thermal issues. Developing thermal design guideline would also be more practical.

6. **6. Apply and extend the developed technique to optimal cooling design and control.**
   The proposed thermal error reduction techniques in this thesis automatically calculate the best heat inputs together with a uniform and constant cooling to minimize thermal errors. These techniques exhibit an interesting insight that it can be beneficial to add heat rather than just applying cooling to minimize thermal errors. However, in practice, the technique would more easily be accepted if it is to be used for optimizing cooling design or control. Using the proposed technique, spatial and/or temporal variation of the cooling can be optimized or even dynamically programmed depending on the conditions of the machine. This already is a unique capability for designing cooling for machines.

7. **Develop further thermal design guideline.**
   Thermal Modal Analysis can analyse the thermal behaviour of a machine structure at different spatial frequencies and time scales. Analysing the thermal behaviour of a machine structure using Thermal Modal Analysis gives an opportunity to view the thermal behaviour from different perspectives than existing thermal analysis techniques. Therefore, continuing the study on the development of thermal design guideline based on the understanding on thermal behaviours in machine structures using Thermal Modal Analysis is a recommended research topic.

Appendix A

Thermal displacement model validation

A.1 Development of experimental setup

A.1.1 The objective

A setup is developed to measure in-plane thermal displacement within a plate [67]. Using this setup, the thermal displacement model used in this research to evaluate the thermal displacement error at the moving point of interest is validated.

A.1.2 Design

The setup is shown in Figure A.1.

The setup consists of a plate of which displacement is being measured, a block resistor which produces a heat input to the plate, an adapter which restricts the heat conduction path in a well defined shape (circular) and an optical microscope to measure the in-plane displacement.

The in-plane thermal displacement is measured by keeping track of a mark on the plate by optical microscope and post-processed by an image correlation based displacement identification algorithm Ncorr [66]. Two images taken at the same location at different time are compared and the program calculates a shift between the two images which maximizes the correlation between these two images. The distance and direction of the shift calculated by the program gives the best estimate of the displacement between these two images.

A support bar is put on the other side of the setup to support the plate to avoid the bending of the plate due to the gravity since this gravity bending cause the out of focus direction motion of the plate and image, and result in the displacement evaluation error.

Also, an electric circuit is build to switch on and off the current running through the resistor in a predetermined manner and also triggers image capturing by the microscope at predetermined intervals.

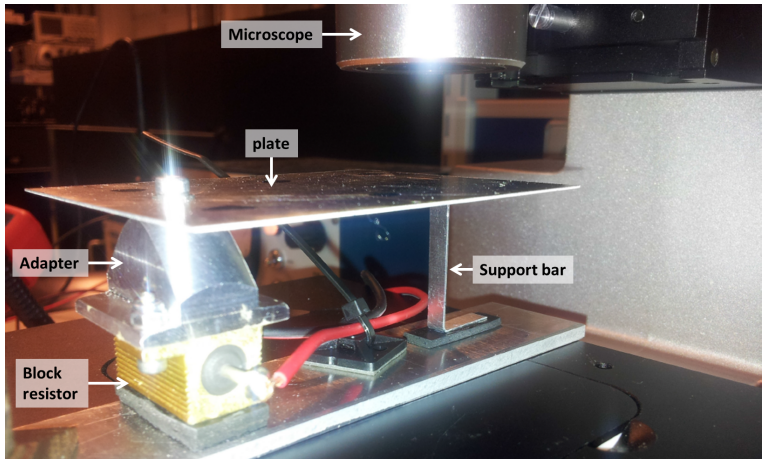

Figure A.1: Developed setup for in-plane thermal displacement measurement. Electric current running through the block resistor heats up the resistor and the heat is conducted through the adapter to the plate. The displacement of the position of a point within the plate is observed and recorded by the microscope above the plate. The recorded images are processed using image correlation algorithm to identify the in-plane displacement of the point of interest.

A.1.3 Measurement

Figure A.2 is an image of the plate in the setup pictured by an infrared camera. The figure shows a typical temperature distribution in the plate during measurements conducted by the setup. The black small dot on the left center is added into the original figure to exaggerate the point of measurement. The displacement of the point is measured using the setup. Figure A.3 shows the result of measurement for some different settings. The figure shows that higher voltage setting results in better repeatability in the measurement due to better stability of the power supplier at higher voltage.

A.2 Experimental validation of thermal displacement model

The thermal displacement model used throughout this research consists of the thermal displacement fields corresponding to the thermal modes of a structure. As in the reconstruction of the temperature distribution in the target structure, the thermal displacement field corresponding to the same temperature distribution can be reconstructed from the sum of a thermal displacement field times the amplitude of the corresponding thermal mode. Therefore:

$$\boldsymbol{T}(t) = \sum_{i=1}^{N} \boldsymbol{\phi}_{\mathrm{i}} \theta_{\mathrm{i}}(t) = \boldsymbol{\Phi\theta}(t) \tag{A.1}$$

$$\boldsymbol{U}(t) = \sum_{i=1}^{N} \boldsymbol{\psi}_{\mathrm{i}} \theta_{\mathrm{i}}(t) = \boldsymbol{\Psi\theta}(t) \tag{A.2}$$

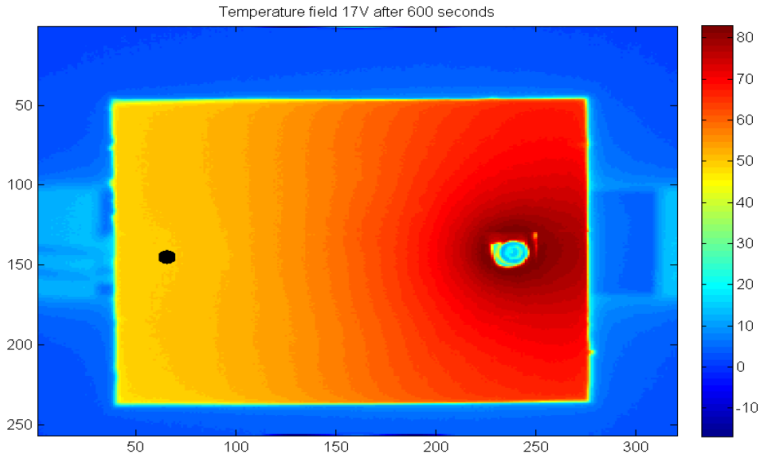

Figure A.2: Temperature distribution of the plate in the setup measured by an infrared camera. The resistor (heat source) and the adapter are located on the right side of the plate (location of the cyan circle) and the point to measure the in-plane displacement is on the left side of the plate marked by a black dot.

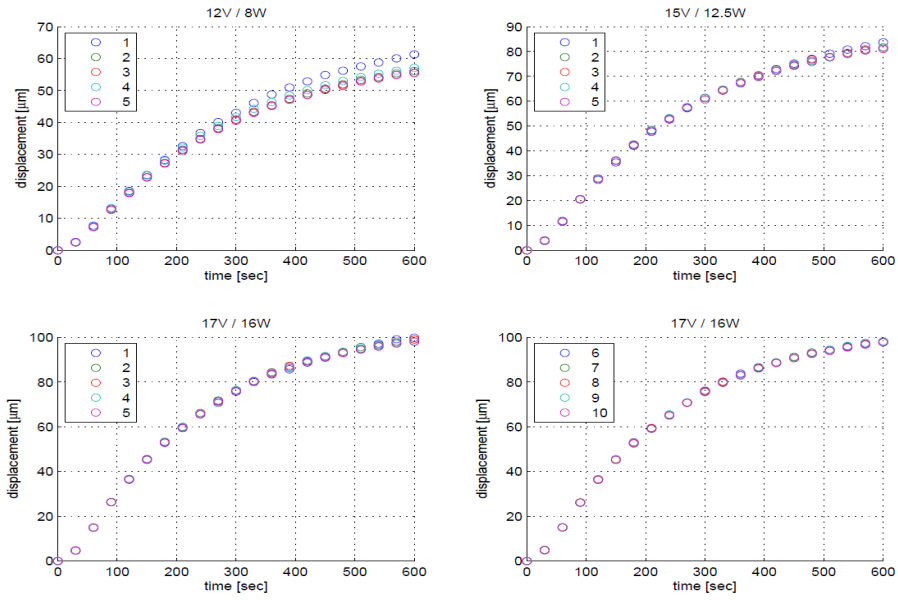

Figure A.3: The results of in-plane thermal displacement measurement using the setup. The results show reduced repeatability in the low voltage setting to control the current in the resistor due to the instability of the power amplifier in the low voltage region.

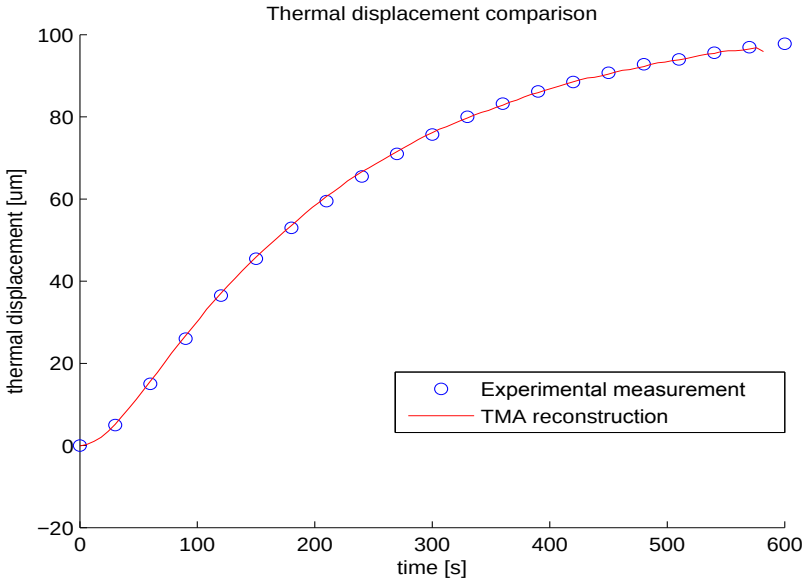

Figure A.4: Comparison of the experimentally measured in-plane thermal displacement using the setup and thermal displacement predicted using a simulation model. The simulation used experimentally obtained temperature measurement data in the calculation. Also the thermal expansion coefficient of the plate in the simulation model was adjusted to match the simulation and experimental measurement of the in-plane displacement measurement. The result shows a good agreement between the simulation model and the experimental measurement over the measurement period of 600 s.

Each thermal displacement field of the target structure can be calculated using any standard FEM software such as COMSOL [21] or ANSYS [5].

Figure A.4 shows the averaged thermal displacement measurement results from 17 V/16 W measurements in Figure A.3 (blue circles) and a result of thermal displacement prediction based on equation A.2 (red curve) with a thermal expansion coefficient adjusted to fit to the experimental data. The result shows a good agreement between the experimentally measured in-plane thermal displacement and the prediction using a simulation model based on Thermal Modal Analysis.

Appendix B

Thermal mode shapes and thermal displacement fields

In this appendix, the first 10*10 thermal mode shapes and thermal displacement fields are presented for thermally-insulated boundary condition (=free-free boundary condition) and mechanically supported boundary condition at one (left) end (=fix-free boundary condition) as shown in Figure 3.1.

Figure B.1 shows the thermal mode shapes $\boldsymbol{\phi}_{\mathrm{i,j}}$. Figure B.2 shows the corresponding thermal displacement fields in x-direction $\boldsymbol{\psi}_{\mathrm{u,i,j}}$ where the color of every displacement field is scaled individually to show the field in best detail. Figure B.3 is the corresponding thermal displacement fields in y-direction $\boldsymbol{\psi}_{\mathrm{v,i,j}}$, again the color is scaled individually. Figure B.4 is the total thermal displacement fields $\boldsymbol{\psi}_{\mathrm{i,j}} = \sqrt{\boldsymbol{\psi}^2_{\mathrm{u,i,j}} + \boldsymbol{\psi}^2_{\mathrm{v,i,j}}}$ where the color is scaled individually. Figure B.5 is the corresponding thermal displacement fields in x-direction $\boldsymbol{\psi}_{\mathrm{u,i,j}}$ where the color of all fields is scaled with the same amount to better illustrate their ratio. Figure B.6 is the corresponding thermal displacement fields in y-direction $\boldsymbol{\psi}_{\mathrm{v,i,j}}$ where the color is scaled by the same scaling. Figure B.7 is the total thermal displacement fields $\boldsymbol{\psi}_{\mathrm{i,j}} = \sqrt{\boldsymbol{\psi}^2_{\mathrm{u,i,j}} + \boldsymbol{\psi}^2_{\mathrm{v,i,j}}}$ where the color is scaled by the same scaling.

Figure B.1 to Figure B.4 show the spatial patterns of the thermal mode shapes and the corresponding thermal displacement fields. Figure B.5 to Figure B.7 show relative magnitudes of the thermal displacement fields. From these figures, it is clear that the lower order modes have larger magnitudes and thus have larger influence on thermal displacement fields and thermal displacement errors.

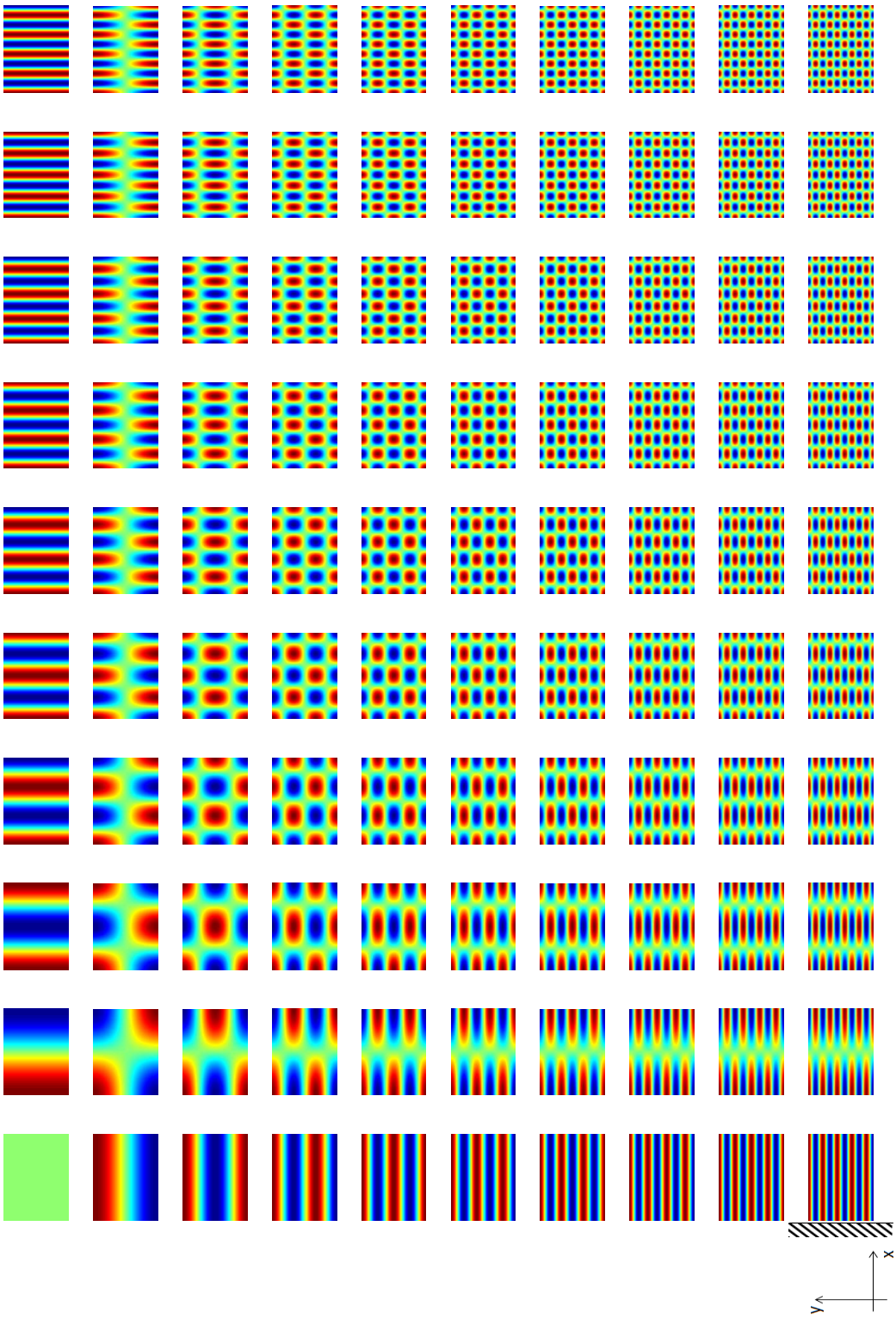

Figure B.1: First 10*10 thermal modes $\phi_{i,j}$ for thermally insulated thermal boundary condition. Mode indices are (1,1) from the left bottom to (10,10) to the top right. The images of the mode shapes are all rotated by 90 degree in this figure. So the clamped left edge of the plate in Figure 3.1 is now down side of the images. This is the same for Figure B.2... Figure B.7.

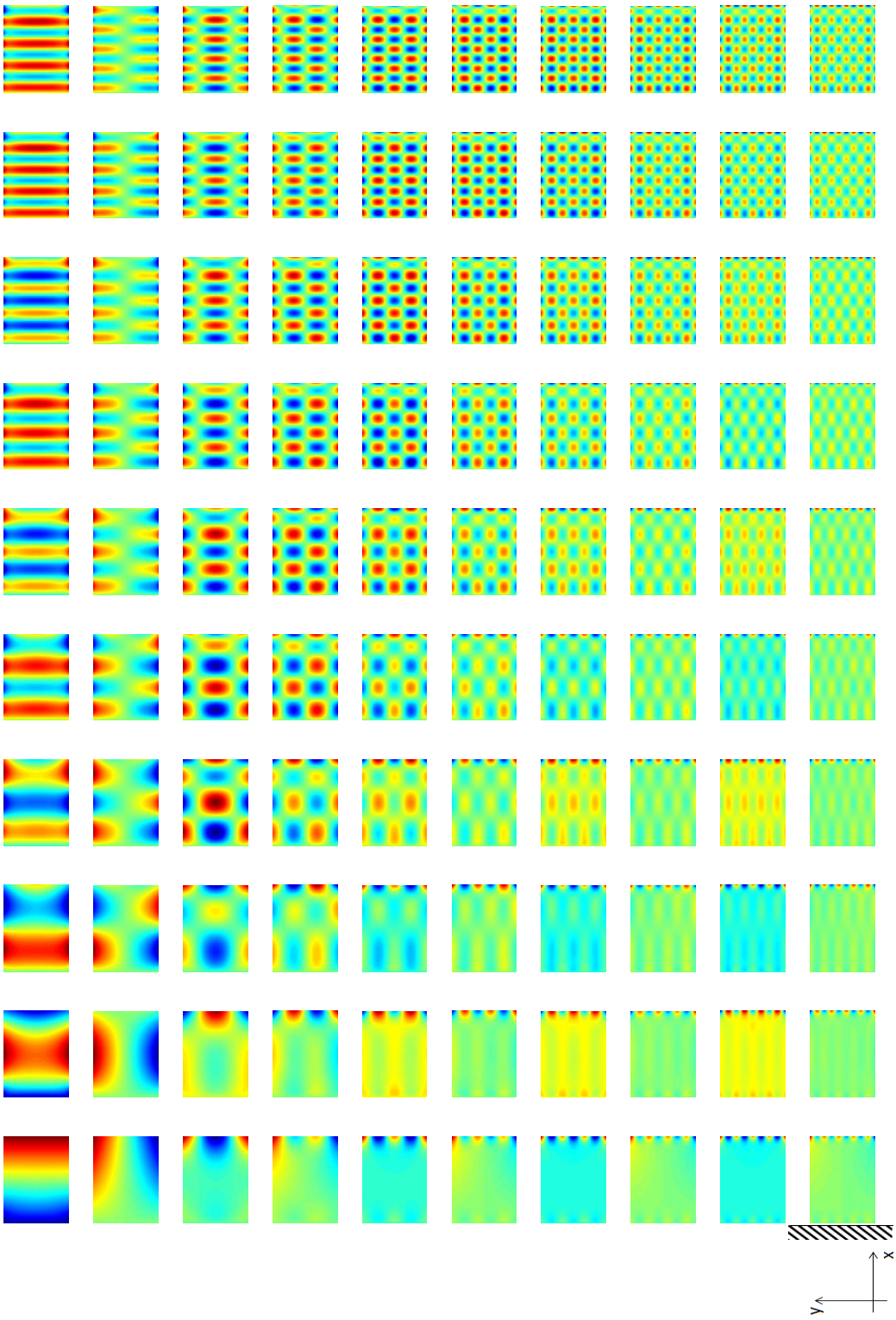

Figure B.2: First 10*10 thermal displacement fields in x direction $\psi_{u,i,j}$ for fixed-free mechanical boundaries with thermally insulated boundary conditions. Mode indices are (1,1) from the left bottom to (10,10) to the top right.

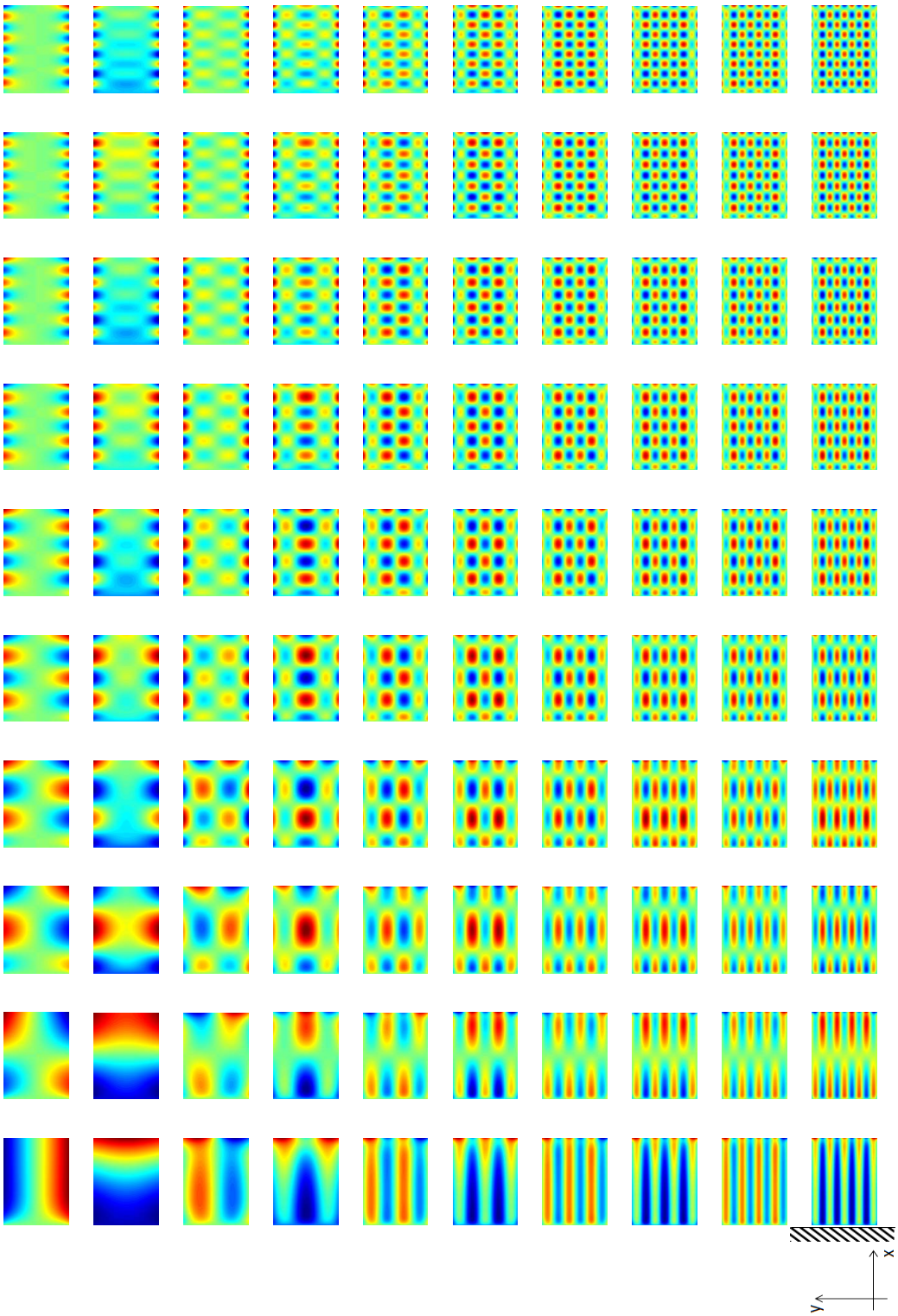

Figure B.3: First 10*10 thermal displacement fields in y direction $\psi_{v,i,j}$ for fixed-free mechanical boundaries with thermally insulated boundary conditions. Mode indices are (1,1) from the left bottom to (10,10) to the top right.

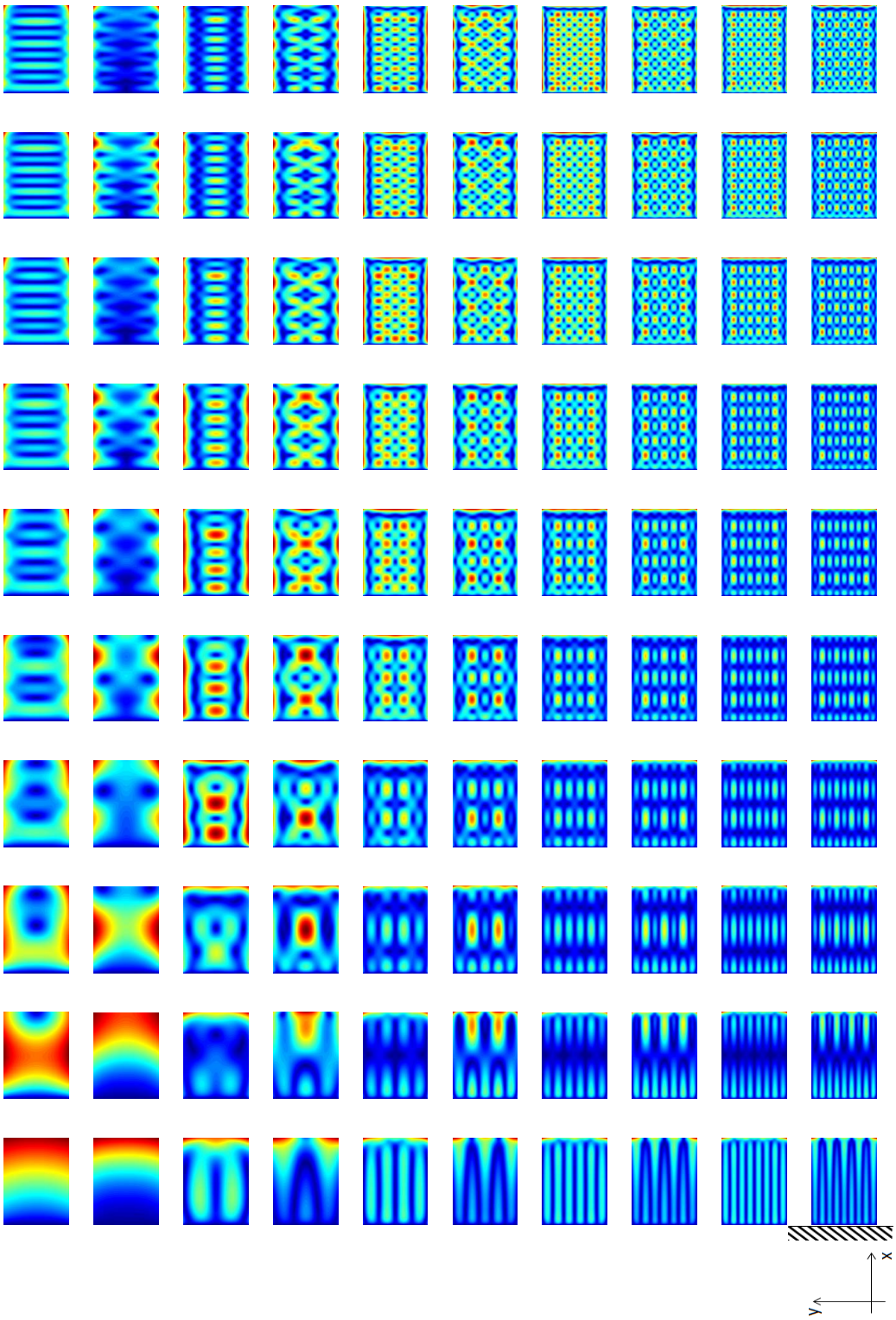

Figure B.4: First 10*10 total thermal displacement fields $\boldsymbol{\psi}_{\mathrm{i,j}} = \sqrt{\boldsymbol{\psi}^2_{\mathrm{u,i,j}} + \boldsymbol{\psi}^2_{\mathrm{v,i,j}}}$ for fixed-free mechanical boundaries. Mode indices are (1,1) from the left bottom to (10,10) to the top right.

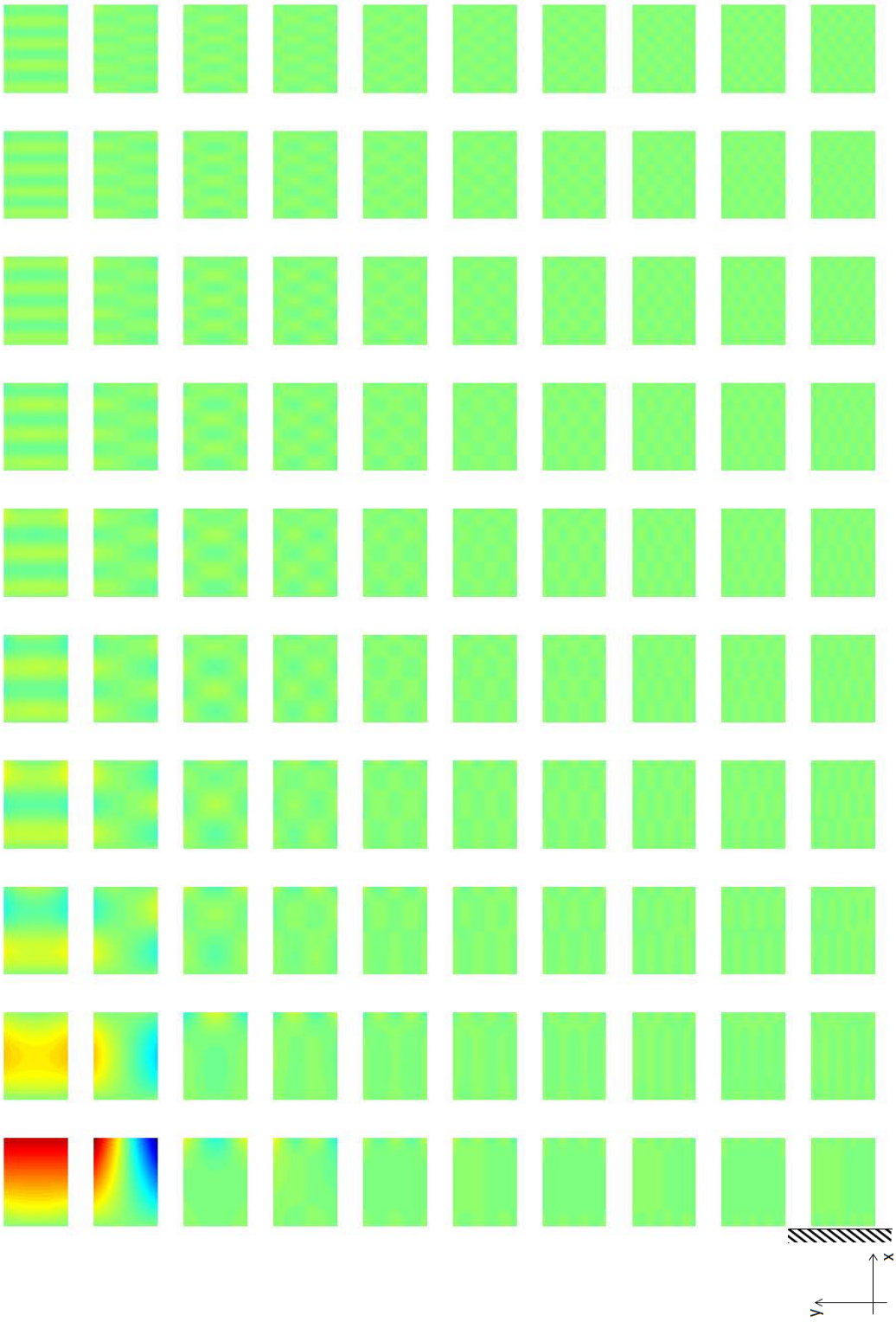

Figure B.5: First 10*10 thermal displacement fields in x direction $\psi_{u,i,j}$ for fixed-free mechanical boundaries with thermally insulated boundary conditions (same scaling for all pictures). Mode indices are (1,1) from the left bottom to (10,10) to the top right.

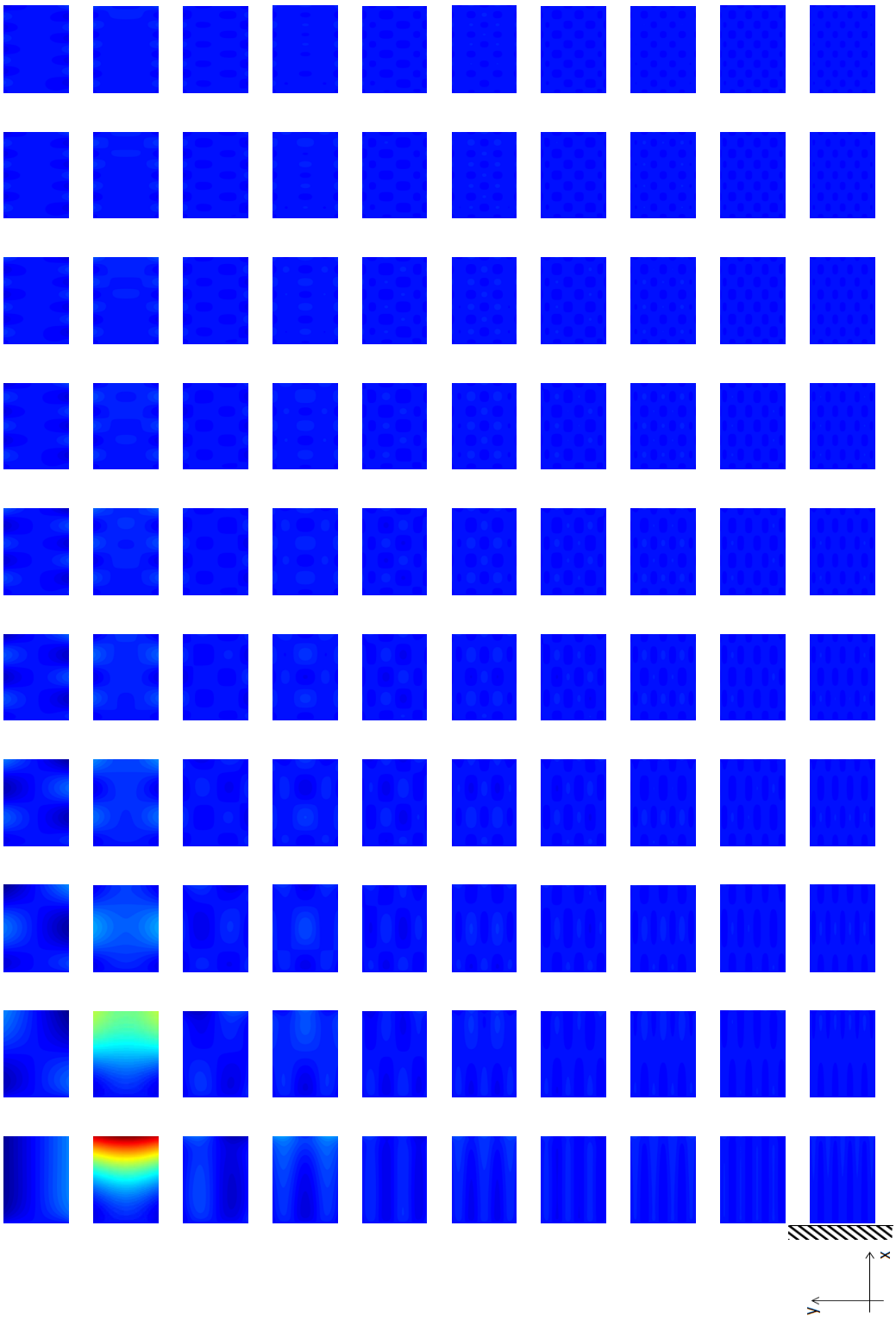

Figure B.6: First 10*10 thermal displacement fields in y direction $\psi_{v,i,j}$ for fixed-free mechanical boundaries with thermally insulated boundary conditions (same scaling for all pictures). Mode indices are (1,1) from the left bottom to (10,10) to the top right.

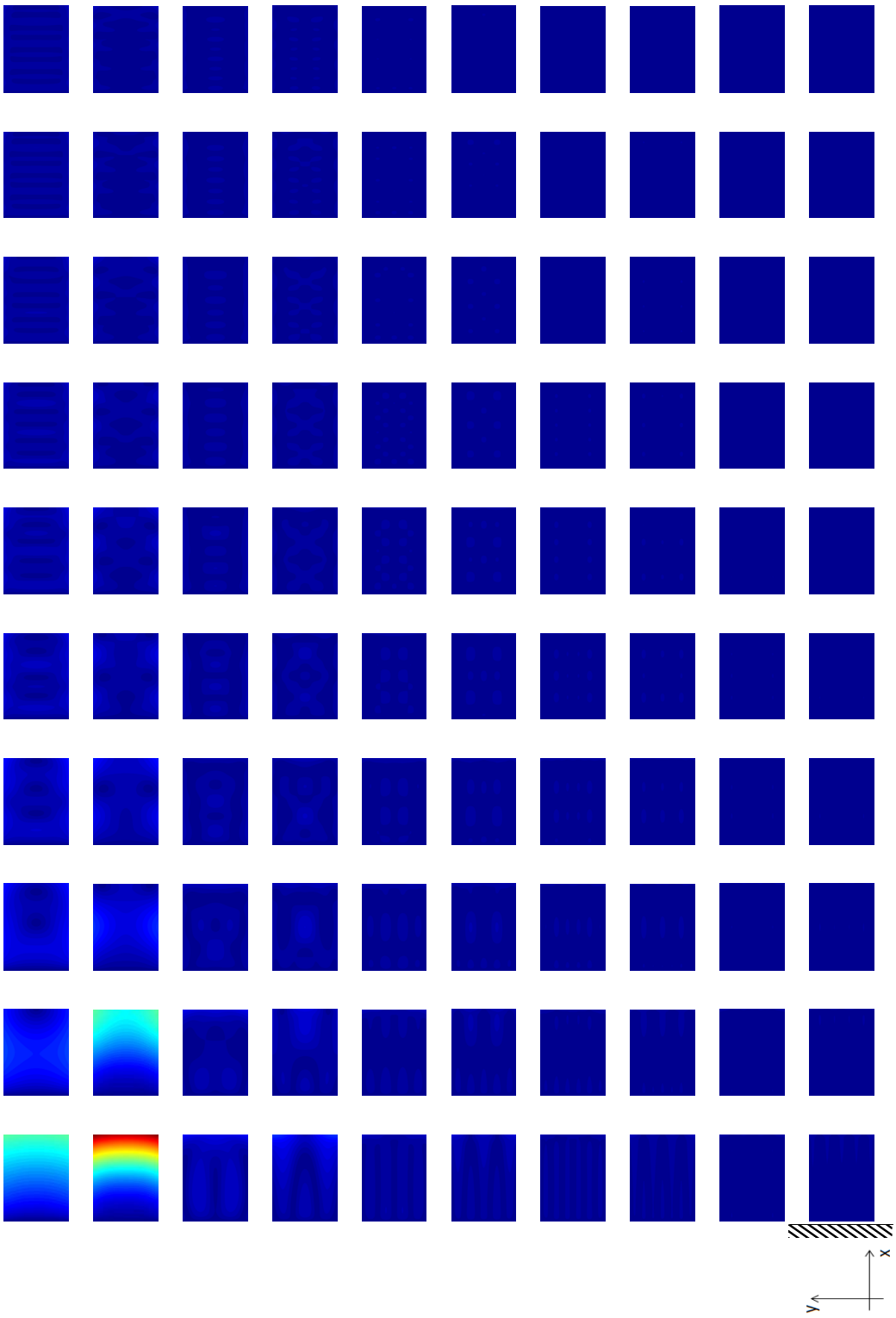

Figure B.7: First 10*10 total thermal displacement fields $\boldsymbol{\psi}_{\mathrm{i,j}} = \sqrt{\boldsymbol{\psi}^2_{\mathrm{u,i,j}} + \boldsymbol{\psi}^2_{\mathrm{v,i,j}}}$ for fixed-free mechanical boundaries with thermally insulated boundary conditions (same scaling for all pictures). Mode indices are (1,1) from the left bottom to (10,10) to the top right.

Appendix C

Analytically derived thermal modes

In this appendix, an analytical derivation of the thermal model based on Thermal Modal Analysis and the thermal mode shapes and time constants of a 2D rectangular plate are described. [1]

According to the Fourier's law of heat conduction, the equation of heat transfer in a structure with uniform material properties is described by the following equation:

$$\rho c \frac{\partial T(\boldsymbol{x},t)}{\partial t} = k\nabla^2 T(\boldsymbol{x},t) + q(\boldsymbol{x},t) \tag{C.1}$$

where ρ is the density of the material, c is the specific heat capacity, k is the heat conductivity, $T(\boldsymbol{x},t)$ is the temperature distribution, and $q(\boldsymbol{x},t)$ is the heat load to the system. A general solution for this equation can be found using the method of separation of variables [79]:

$$T(\boldsymbol{x},t) = \sum_{i=1}^{\infty} \phi_{\mathrm{i}}(\boldsymbol{x})\theta_{\mathrm{i}}(t) \tag{C.2}$$

where $\boldsymbol{\phi}_{\mathrm{i}}(\boldsymbol{x})$ is the i-th thermal mode shape and $\theta_{\mathrm{i}}(t)$ is the amplitude of the mode. As in structural modal analysis, the temperature distribution can thus be decomposed into thermal modes which are only spatially depend on the geometry of the structure and its boundary conditions, multiplied with the time dependent amplitudes of these modes.

⟨ **EXAMPLE** ⟩
As an example, the thermal mode shapes of a 2D rectangular plate model supported along

[1] Strictly speaking, the derived thermal model, and the thermal mode shapes and time constants in this appendix are just the analytical solution of a Fourier's equation of heat conduction for a finite dimension 2D rectangular plate. They are not based on Thermal Modal Analysis in the strict sense. However the thermal model, and the thermal modes and the time constants of the 2D model derived using the matrix equations in Chapter 3 converge to these analytical solutions of the Fourier's equation when the dimensions of the matrix approach towards infinity. Therefore we will designate the analytical solutions of Fourier's equation of heat conduction as "analytically derived thermal model based on Thermal Modal Analysis" and "analytically derived thermal mode shapes and time constants of a 2D rectangular plate". Then these analytical solutions can be used to analyze the characteristics of the thermal model based on Thermal Modal Analysis, and the thermal modes and time constants.

one thermally insulated edge shown in Figure 3.1 are presented.

$$T(x,t) = \sum_{i=1}^{\infty}\sum_{j=1}^{\infty}\left(\cos\left(\frac{\lambda_{\mathrm{i}}x}{\sqrt{\alpha}}\right)\cos\left(\frac{\chi_{\mathrm{j}}y}{\sqrt{\alpha}}\right)\theta_{\mathrm{ij}}(t)\right) \tag{C.3}$$

where the thermal mode shapes $\boldsymbol{\phi}_{\mathrm{ij}}(\boldsymbol{x})$ for $i,j = 1,2,3,\cdots$ are:

$$\phi_{\mathrm{ij}}(\boldsymbol{x}) = \cos\left(\frac{\lambda_{\mathrm{i}}x}{\sqrt{\alpha}}\right)\cos\left(\frac{\chi_{\mathrm{j}}y}{\sqrt{\alpha}}\right) \tag{C.4}$$

and λ_{i} and χ_{j} are

$$\lambda_{\mathrm{i}} = (\mathrm{i}-1)\pi\frac{\sqrt{\alpha}}{L_x} \qquad (\text{for } i = 1,2,3,\cdots) \tag{C.5}$$

$$\chi_{\mathrm{j}} = (\mathrm{j}-1)\pi\frac{\sqrt{\alpha}}{L_y} \qquad (\text{for } j = 1,2,3,\cdots) \tag{C.6}$$

L_x and L_y are length of the plate and α is the thermal diffusivity $\alpha = k/\rho c$. Each mode changes its amplitude in time with its time constant τ_{ij}:

$$\tau_{\mathrm{i,j}} = \frac{1}{\frac{k}{\rho c}\left(\left(\frac{(i-1)\pi}{L_{\mathrm{x}}}\right)^2 + \left(\frac{(j-1)\pi}{L_y}\right)^2\right) + \frac{2h}{\rho c w}} \tag{C.7}$$

The derived thermal mode shapes for the finite dimension 2D plate correspond well with the thermal mode shapes shown in Figure 3.2 or Figure B.1 and the time constants in Table. 3.2

⟨ **End of EXAMPLE** ⟩

The general equation to calculate the amplitude of each mode $\theta_{\mathrm{i}}(t)$ is derived in the following way. Substitute equation C.2 into equation C.1.

$$\rho c\sum_{i=1}^{\infty}\phi_{\mathrm{i}}(\boldsymbol{x})\frac{\mathrm{d}\theta_{\mathrm{i}}(t)}{\mathrm{d}t} = k\sum_{i=1}^{\infty}\theta_{\mathrm{i}}(t)\nabla^2\phi_{\mathrm{i}}(\boldsymbol{x}) + q(\boldsymbol{x},t) \tag{C.8}$$

Each thermal mode $\phi(\boldsymbol{x})_{\mathrm{i}}$ times the amplitude of the mode $\theta_{\mathrm{i}}(t)$ satisfies the homogeneous equation of equation C.1:

$$\phi_{\mathrm{i}}(\boldsymbol{x})\frac{\mathrm{d}\theta_{\mathrm{i}}(t)}{\mathrm{d}t} = \alpha\theta_{\mathrm{i}}(t)\nabla^2\phi_{\mathrm{i}}(\boldsymbol{x}) \tag{C.9}$$

Divide the above equation by $\phi_{\mathrm{i}}(\boldsymbol{x})\theta_{\mathrm{i}}(t)$, then:

$$\frac{1}{\theta_{\mathrm{i}}(t)}\frac{\mathrm{d}\theta_{\mathrm{i}}(t)}{\mathrm{d}t} = \alpha\frac{1}{\phi_{\mathrm{i}}(\boldsymbol{x})}\nabla^2\phi_{\mathrm{i}}(\boldsymbol{x}) = -\frac{1}{\tau_{\mathrm{i}}} \tag{C.10}$$

Since the left hand side of the above equation only depends on time and the right hand side depends on space variable, the equation is equal to a constant value $-\frac{1}{\tau_{\mathrm{i}}}$. Transform equation C.10 and obtain the following equation:

$$\nabla^2\phi_{\mathrm{i}}(\boldsymbol{x}) = -\frac{\phi_{\mathrm{i}}(\boldsymbol{x})}{\alpha\tau_{\mathrm{i}}} \tag{C.11}$$

Substitute equation C.11 into equation C.8 to eliminate $\nabla^2\phi_{\mathrm{i}}(\boldsymbol{x})$:

$$\rho c\sum_{i=0}^{\infty}\phi_{\mathrm{i}}(\boldsymbol{x})\frac{\mathrm{d}\theta_{\mathrm{i}}(t)}{\mathrm{d}t} = k\sum_{i=1}^{\infty}\theta_{\mathrm{i}}(t)\frac{-1}{\alpha\tau_{\mathrm{i}}}\phi_{\mathrm{i}}(\boldsymbol{x}) + q(\boldsymbol{x},t) \tag{C.12}$$

$$\rho c\sum_{i=1}^{\infty}\phi_{\mathrm{i}}(\boldsymbol{x})\left(\frac{\mathrm{d}\theta_{\mathrm{i}}(t)}{\mathrm{d}t} + \frac{1}{\tau_{\mathrm{i}}}\theta_{\mathrm{i}}(t)\right) = q(\boldsymbol{x},t) \tag{C.13}$$

Multiplying both sides of the equation with $\phi_{\mathrm{i}}(\boldsymbol{x})$ and taking the integral over the geometry, this equation can be decoupled into a set of independent equations as follows:

$$\frac{\mathrm{d}\theta_{\mathrm{i}}(t)}{\mathrm{d}t} + \frac{1}{\tau_{\mathrm{i}}}\theta_{\mathrm{i}}(t) = \frac{\iint_A \phi_{\mathrm{i}}(\boldsymbol{x}) q(\boldsymbol{x},t) dA}{\rho c \iint_A \phi_{\mathrm{i}}(\boldsymbol{x})^2 dA} \qquad (\text{for } i = 1, 2, 3, \cdots) \tag{C.14}$$

By solving these 1st order differential equations, the amplitude of each mode over time can be calculated. The general solution for equation C.1 can be calculated from equation C.2 with $\theta_{\mathrm{i}}(t)$ obtained by solving equation C.14.
Assuming quasi-static thermo-mechanical behavior, the thermal displacement field of the structure can be decomposed into a weighted summation of thermal displacement fields corresponding to the thermal mode shapes.

$$u(\boldsymbol{x},t) = \sum_{i=0}^{\infty} \psi_{\mathrm{i}}(\boldsymbol{x})\theta_{\mathrm{i}}(t) \tag{C.15}$$

where $\psi_{\mathrm{i}}(\boldsymbol{x})$ is the thermal deformation of the structure when only i-th thermal mode exists in the temperature field and $\theta_{\mathrm{i}}(t)$ again is the amplitude of the mode. Since especially the lower order modes dominate the thermal deformation, an accurate reduced order thermal displacement model can be constructed using only a limited number of modes.

Bibliography

[1]

[2] Joong-Yong Ahn, Tae-Hoon Kim, and Sung-Chong Chung. Real time estimation of temperature distribution in a ball screw system using observer and adaptive algorithm. *Transaction of the KSME, A.*, 25/1:pp.145–152, 2001.

[3] J. Anderes. Application of the modal analysis approach to transient thermal problems. *NASA report*, nr. NASA-CR-182959, 1981.

[4] Brian D. O. Anderson and John B. Moore. Optimal control: Linear quadratic methods. *Dover Publications, New York, USA*, 2014.

[5] ANSYS. http://www.ansys.com/.

[6] A. Balsamo, D. Marques, and S. Sartori. A method for thermal-deformation corrections of cmms. *Anals of CIRP*, vol.39/1:pp.557–560, 1990.

[7] P. Bárta, O. Horejs, and J. Vyroubal. Thermal transfer function based control method of a machine tool cooling system. *Proc. of the topical meeting: thermal effects in precision systems, Maastricht*, 2007.

[8] Can Bikcora, Siep Weiland, and Wim M.J. Coene. Thermal deformation prediction in reticles for extreme ultraviolet lithography based on a measurement-dependent low-order model. *IEEE transactions on semiconductor manufacturing*, 27/1:pp.104–117, 2014.

[9] Brian Borchers. Matlab modified cholsky decomposition package, http://www.mathworks.com/matlabcentral/fileexchange/47-ldlt.

[10] Bernd Bossmanns and Jay. F. Tu. A thermal model for high speed motorized spindles. *Int. J. of machine tools & manufact.*, vol.39:pp.1345–1366, 1999.

[11] Sjef Box. Towards thermo-mechanical system modelling. *Proc. of the topical meeting, Thermal Effects in precision systems, Maastricht*, 2007.

[12] Sjef Box. Design and temperature control for nanometre precision. *Mikroniek*, 3:12–16, 2008.

[13] Stephan Boyd and Lieven Vandenberghe. Convex optimization. *ISBN 978-0-521-83378-3, Cambridge university press, Cambrdige*, 2004.

[14] C. Brecher and P Hirsch. Compensation of thermo-elastic machine tool deformation based on control internal data. *CIRP Annals of Manuf. Tech.*, 53/1:pp.299–304, 2004.

[15] C. Brecher and A. Wissmann. Compensation of thermo-dependent machine tool deformations due to spindle load: investigation of the optimal transfer function in consideration of rough machining. *Prod. Eng. Res. Devel.*, vol.5:pp.565–574, 2011.

[16] J. Bryan. International status of thermal error research(1990). *Annals of the CIRP*, vol.39/2:pp.645–656, 1990.

[17] Jaehyuk Chang, Carl J. Martin, Roxann L. Engelstad, and Edward G. Lovell.

[18] Aindya Chatterjee. An introduction to the proper orthogonal decomposition. *Current science*, vol.78/7/10:pp.808–817, 2000.

[19] Jenq-Shyong Chen. A study of thermally induced machine tool errors in real cutting conditions. *Int. J. Mach. Tools Manufact.*, vol.36/12:pp.1401–1411, 1996.

[20] J.S. Chen and J. Yuan, J.and Ni. Thermal error modelling for real-time error compensation. *Int. J. Adv. Manuf. Technol.*

[21] COMSOL. http://www.comsol.com/.

[22] M. A. Donmez, D. S. Blomquist, R. J. Hocken, C. R. Liu, and M. M. Barash. A general methodology for machine tool accuracy enhancement by error compensation. *Precision engineering*, vol.8/4, 1986.

[23] D. J. Ewins. Modal testing 2nd. edition, theory, practice, and application. *Research Studies Press, Baldock, Hertfordshire, England*, 2000.

[24] Hawren Fang and Dianne P. O'Leary. Modified cholesky algorithms: A catalog with new approaches. *Mathematical Programming A*, pages DOI:10.1007/s10107–007–0177–6, 2007.

[25] Adolf Frank and Fritz Ruech. Thermal errors in cnc machine tools. focus on ballscrew expansion. *Technical University Graz, Austria.*

[26] Peter Giesen and Erick Folgering. Design guidelines for thermal stability in opto-mechanical instruments. *Proc. SPIE 5176, Optomechanics 2003*, 126:doi:10.1117/12.510285, 2003.

[27] P. E. Gill, W. Murray, and M. H. Wright. Practical optimization. *Academic Press*, vol.:pp., 1981.

[28] A. Haber, A. Polo, I. Maj, S.F. Pereira, H.P. Urbach, and M. Verhaegen. Predictive control of thermally induced wavefront aberrations. *Optics Letters*, 21/18:pp.21530–21541, 2013.

[29] Zhao Haitao, Yang Jianuo, and Shen Jinhua. Simulation of thermal behavior of a cnc machine tool spindle. *Int. J. of machine tools & manufact.*, vol.47:pp.1003–1010, 2007.

[30] Wu Hao, Zhang Hongtao, Guo Qianjian, Wang Xiushan, and Yang Jianguo. Thermal error optimization modeling and real-time compensation on a cnc turning center. *Journal of Materials processing Technology*, vol.207:pp.172–179, 2007.

[31] Y. Hatamura, T. Nagao, M. Mitsuishi, K. Kato, S. Taguchi, and T. Okumura. "development of an intelligent machining center incorporating active compensation for thermal distortion. *Annals of the CIRP*, vol.42/1:pp.549–552, 1993.

[32] M. Hattori and S. adn Suto T. andInoue H. Noguchi, H. andIto. Estimation of thermal-deformation in machine tools using neural network technique. *Journal of Materials Processing Technology*, vol.56:pp.765–772, 1996.

[33] E.C. Hooijkamp, R. Saathof, F. van Keulen, and J. van Eijk. Measured thermal modes for design optimization. *Proceedings of the 12th international conference of the european society for precision engineering and nanotechnology (euspen)*, pages pp.416–419, 2012.

[34] Otakar Horejš. Thermo-mechanical model of ball screw with non-steady heat sources. *Thermal issues in Emerging Technologies,ThETA 1, Cairo, Egypt*, 2007.

[35] O. Hores, M. Mares, P. Kohut, P. Barta, and J. Hornych. Compensation of machine tool thermal errors based on transfer function. *MM Science Journal*, pages pp.162–165, 2010.

[36] Ying Huang and Tetsutaro Hoshi. Optimization of fixture design with consideration of thermal deformation in face milling. *J. of Manufac. Sys.*, vol.19/5:pp., 2000.

[37] Yoshimi Ito. Thermal deformation in machine tools. *ISBN 0071635173/9780071635172, McGraw-Hill, US*, 2010.

[38] Jerzy Jędrzejewski, Jan Kaczmarek, Zbigniew Kowal, and Zdzisław Winiarski. Numerical optimization of thermal behaviour of machine tools. *Annals of the CIRP*, vol.39/1, 1990.

[39] Z. Jędrzejewski, J. andKowal, W. Kwaśny, and W. Modrzycki. Hybrid model of high speed machining centre headstock. *Annals of the CIRP Manuf. Tech.*, vol.53/1:pp285–288., 2004.

[40] Morton I. Kamien and Nancy L. Schwartz. Dynamic optimization: The calculus of variations and optimal control in economics and management. *Elsevier Science; 2nd edition*, pages ISBN:978–0444016096, 1991.

[41] Gaetan Kerschen, Jean-Claude Golinval, Alexander Vakakis, and Lawrence A. Bergman. The method of proper orthogonal decomposition for dynamical characterization and order reduction of mechanical systems: an overview. *Nonlinear Dynamics*, vol.41:pp.147–169, 2005.

[42] Jong-Jin Kim, Young Hun Jeong, and Dong-Woo Cho. Thermal behavior of a machine tool equipped with linear motor. *Int. J. of Machine tools & manufact.*, vol.44:pp.749–758, 2004.

[43] S. K. Kim and D. W. Cho. Real-time estimation of temperature distribution in a ball-screw system. *Int. J. Mach. Tools Manufact.*, vol.37/4:pp.451–464, 1997.

[44] A. Morris Kirsten. Introduction to feedback control. *Academic Press, San Diego, California, USA*, 2001.

[45] Tae Jo Ko, Tae-weon Gim, and Jae-yong Ha. Particular behavior of spindle thermal deformation by thermal bending. *Int. J. of machine tools & manufact.*, vol.43:pp.17–23, 2003.

[46] Takehiko Kodera, Kazuhiro Yokoyama, Kazuo Miyaguchi, Yutaka Nagai, Takamasa Suzuki, Masami Masuda, and Takanori Yazawa. Real-time estimation of ball-screw thermal elongation based upon temperature distribution of ball-screw. *JSME Int. J., Series C*, vol.47/4, 2004.

[47] A.H. Koevoets, H.J. Eggink, J. van der Sanden, J. Dekkers, and T.A.M. Ruijl. Optimal sensor configuration techniques for the compensation of thermo-elastic deformations in high-precision systems. *THERMINIC 2007, Budapest, Hungary*, 2007.

[48] Marco Koevoets, Jack van der Sanden, and Theo Ruijl. Thermal-elastic compensation models for position control. *Proceedings of the ASPE Annual Meeting*, 2009.

[49] L Köster, H. Gerth, and H. Haase. Thermal modes and their application to turbogenerator rotors. *Electrical Eng.*, vol.82:pp.135–144, 2000.

[50] Hue P. Le. Progress and trends in ink-jet printing technology. *Journal of Imaging Science and Technology*, 42:49–62, 1998.

[51] J.W. Li, W.J. Zhang, G.S. Yang, S.D. Tu, and X.B. Chen. Thermal-error modeling for complex physical systems: the-state-of-arts review. *Int. J. Adv. Manuf. Technol.*, vol.42:pp.168–179, 2009.

[52] Shuhe Li, Yiqun Zhang, and Guoxiong Zhang. A study of pre-compensation for thermal errors of nc machine tools. *Int. J. Mach. Tools Manufact.*, vol.37/12:pp.1715–1719, 1997.

[53] P. S. Lingard, M. E. Purss, C. M. Sona, E. G. Thwaite, and G. H. Mariasson. Temperature perturbation effects in a high precision cmm. *Precision engineering*, 0141-6359/91/010041-11, 1991.

[54] Z. Q. Liu and P. K. Venuvinod. Error compensation in cnc turning solely from dimensional measurement of previously machined parts. *Annlas of the CIRP*, vol.48/1, 1999.

[55] Chih-Hao Lo, Jingxia Yuan, and Jun Ni. Optimal temperature variable selection by grouping approach for thermal error modeling and compensation. *Int. J. of Machine tools & manufact.*, vol.39:pp.1383–1396, 1999.

[56] Martin Mares, Otakar Horejš, Jan Hornych, and Peter Kohut. Compensation of machine tool angular thermal errors using controlled internal heat sources. *J. of Machine Eng.*, vol.11/4, 2011.

[57] M. Matsuo, T. Yasui, T. Inamura, and M. Matsumura. High-speed test of thermal effects for a machine-tool structure based on modal analysis. *Precision engineering*, vol.8/2, 1986.

[58] Josef Mayr, Markus Ess, Sascha Weikert, and Konrad Wegener. Compensation of thermal effects on machine tools using fdem simulation approach. *Proc. Lamdamap*, vol.9:ISBN1861941188, 2009.

[59] Josef Mayr, Markus Ess, Sascha Weikert, and Konrad Wegener. Simulation and prediction of the thermally induced deformations on machine tools caused by moving linear axis using the fdem simulation approach. *Proceedings ASPE Annual Meeting*, 2009.

[60] Josef Mayr, Jerzy Jędrzejewski, Eckart Uhlmann, M. Alkan Domez, Wolfgang Knapp, Frank Härtig, Klaus Wendt, Toshimichi Moriwaki, Paul Shore, Robert Schmitt, Christian Brecher, Timo Wurz, and Konrad Wegener. Thermal issues in machine tools. *Annals of the CIRP Manuf. Tech.*, vol. 61/2:pp.771–791, 2012.

[61] Josef Mayr, Sascha Weikert, and Konrad Wegener. Comparing the thermo-mechanical-behavior of machine tool frame designs using a fdm-fea simulation approach. *ASPE, Proceedings of: the twenty-second annual meeting*, pages pp.17–20, 2007.

[62] Xu Min, Jiang Shuyun, and Cai Ying. An improved thermal model for machine tool bearings. *Int. J/ of Machine tools & manufact.*, vol.47:pp.53–62, 2007.

[63] Takeshi Morishima, Ron van Ostayen, Jan van Eijk, and Rob Munnig Schmidt. Development of transient thermal deformation control techniques using thermal modal analysis based design methods. *Int. Conf. of Precision Eng., Awaji, Japan*, 2012.

[64] Toshimichi Moriwaki. Thermal deformation and its on-line compensation of hydrostatically supported precision spindle. *Annals of the CIRP*, vol.37/1, 1988.

[65] Toshimichi Moriwaki and Eiji Shamoto. Analysis of thermal deformation of an ultraprecision air spindle system. *Annals. of the CIRP*, vol.47/1, 1998.

[66] Ncorr. http://www.ncorr.com/.

[67] P. Ouwehand. Improving repeatability of a thermal expansion measurement setup. *Course Report - Mechatronic system design 2*, 2013.

[68] R. Ramesh and A. N. andKeerthi S. S. Mannan, M.A. andPoo. Thermal error measurement and modelling in machine tools. part ii, hybrid bayesian network-support vector machine model. *Int. J. of machine tools & manufact.*, vol.43:pp.405–419, 2003.

[69] T. A. M. Ruijl. Ultra precision coordinate measuring machine; design, calibration and error compensation. *Ph.D. Thesis, Delft university of technology*, pages ISBN 90–6464–287–7, 2001.

[70] T.A.M. Ruijl. Thermal effects in precision systems: Design considerations, modeling, compensation and validation techniques. *Diamond Light Source Proceedings*, vol.1, 360:MEDSI–6, 2011.

[71] T.a.m. Ruijl, A.H. Koevoets, J. Dekkers, H.J. Eggink, and J.C.G. van der Sanden. "compensation model based on thermal mode shape. *Euspen SIG seminar, Eindhoven.*, 2006.

[72] T. Sata, Y. Takeuchi, M. Sakamoto, and M. Weck. Improvement of working accuracy on nc lathe by compensation for the thermal expansion of tool. *Annals of the CIRP*, vol.30/1, 1981.

[73] G. Spur, Z. Hoffmann, E. andPaluncic, K. Benziger, and H. Nymoen. Thermal behavior optimization of machine tools. *Annals of the CIRP*, vol.37/1, 1988.

[74] Cyrille Stephan. Sensor placement for modal identification. *Mechanical systems and Signal processing*, vol.27:pp.461–470, 2012.

[75] Satoshji Takahashi, Yuichiro Miki, Kazuo Maeno, Noriyuki Hirayanagi, Kazuhiro Maeda, and Motoharu Tateishi. Finite element analysis on global and local estimation for thermo-mechanical response of epl wafer heating. *Precision Engineering*, vol.29:pp.347–353, 2005.

[76] Y. Takeuchi, M. Sakamoto, and K. Imura. Development of integrated turning system with predictive compensatory function for machining errors. *Annals of CIRP*, vol.34/1, 1985.

[77] C. Teunissen. Experimental identification of thermal modes. *master thesis, Delft University of Technology, the Netherlands*, 2013.

[78] Toshio Tomimura, Toshihiro Kurozumi, Xing Zhang, and Motoo Fujii. Estimating the thermal contact conductance of metals by ultrasonic waves. *Heat transfer-Japanese Research*, vol.27/2, 1998.

[79] Donald W. Trim. Applied partial differential equations. *PWS Publishing Company, USA*, 1990.

[80] S. C. Veldhuis and M .A. Elbestawi. A strategy for the compensation of errors in five-axis machining. *Annals of the CIRP*, vol.44/1, 1995.

[81] Ravon Venters, Brian T. Helenbrook, Kun Zhang, and Minc-C. Cheng. Proper-orthogonal decomposition based thermal modeling of semiconductor structures. *IEEE trans. on electronics devices*, vol.59/11, 2012.

[82] Raghunath Venugopal and Moshe Barash. Thermal effects on the accuracy of numerically controlled machine tools. *Annals of the CIRP*, vol.35/1, 1986.

[83] J. G. Vogel, A. Tejada, J. W. Spronck, and R. H. Munnig Schmidt. Estimation of the deformation of a plate using a limited number of sensors. *In Proc. ASPE 2013 Spring Topical Meeting, Boston, MA*, 2013.

[84] M. Weck, P. McKeown, R. Bonse, and U. Herbst. Reduction and compensation of thermal errors in machine tools. *Annals of the CIRP*, vol.44/2:pp.589–598, 1995.

[85] Xiang XUE, Jing TIAN, and Guom XIU. Numerical simulation of thermal stress in castings using fdm/fem integrated method. *Material Science Forum*, vol.490-491:pp.85–90, 2005.

[86] Hong Yang and Jun Ni. Dynamic neural network modeling for nonlinear, non stationary machine tool thermally induced error. *Int. Journal of Machine Tools & Manufacture*, vol.45:pp.455–465, 2004.

[87] Jianguo Yang, Jingxia Yuan, and Jun Ni. Thermal error mode analysis and robust modeling for error compensation on a cnc turning center. *Int. J. of Machine Tools & Manufacturer*, vol.39:pp.1367–1381, 1998.

[88] Hayato Yoshioka, Shimpei Matsumura, Hitoshi Hashizume, and Hidenori Shinno. Minimizing thermal deformation of aerostatic spindle system by temperature control of supply air. *JSME Int. J., Series C*, vol.49/2, 2006.

[89] Jingxia Yuan and Jun Ni. The real-time error compensation technique for cnc machining systems. *Mechatronics*, vol.8:pp.359–380, 1998.

[90] Jie Zhu, Jun Ni, and Albert J. Shih. Robust machine tool thermal error modeling through thermal mode concept. *J. of manufact. science and eng.*, vol.130/061006, 2008.

Samenvatting

Het relatieve belang van thermische fouten in precisiemachines is in de afgelopen jaren gestegen. De vereisten voor precisiemachines, zoals grotere precisie en hogere productiviteit, worden voor iedere productgeneratie strikter. De verhoogde precisie van precisiemachines heeft het belang van thermische fouten in precisiemachines vergroot. Om de productiviteit van precisiemachines te verhogen, moet in het algemeen meer energie verbruikt, hetgeen resulteert in verhoogde warmteontwikkeling en thermische fouten, en verminderde prestaties met betrekking tot de precisie. Om de precisie van precisiemachines verder te verbeteren en tegelijkertijd een hogere productiviteit te bereiken, dienen thermische fouten in precisiemachines te worden onderzocht en verder te worden gereduceerd.

Dit proefschrift bestudeert technieken voor het reduceren van thermische fouten aan de hand van een industrile inkjetprinter met hete, gesmolten inkt als voorbeeldprobleem. In het bijzonder zijn de fouten ten gevolge van de thermische verplaatsing van het printsubstraat gedurende het printproces bestudeerd. In dit voorbeeldprobleem is een zich verplaatsende verstorende warmtebron ten gevolge van het deponeren van de hete, smeltende inkt en de hete printerkop aangebracht aan het substraat en is de thermische verplaatsing van de ondergrond bij de verplaatsende positie van de printerkop geminimaliseerd om thermische fouten gedurende het printproces te verminderen. Dit probleem onderscheidt zich van andere, meer conventionele onderzoeken naar thermische fouten doordat nu zowel de verstorende warmtebron als het referentiepunt waarin de thermische fout bestudeerd wordt tijdens het gebruik van de machine verplaatsen.

Dit proefschrift maakt gebruik van thermische modale analyse om thermische fouten te bestuderen, een gereduceerd model te maken voor de beschrijving van de thermische fouten en nieuwe technieken te ontwikkelen om thermische fouten te verminderen. Thermische modale analyse is een veel voorkomende analysetechniek die wordt toegepast in het temperatuurdomein en het thermische verplaatsingsdomein. Bij het gebruik van thermische modale analyse wordt de verdeling van de temperatuur van een mechanisme verdeeld over een beperkt aantal thermische modi. Iedere thermische modus beschrijft een bepaalde verdeling van de temperatuur in het systeem met een zekere spatile frequentie en een tijdafhankelijke amplitude. Het thermische foutenmodel is opgesteld met behulp van de thermische verplaatsingsvelden behorende bij de geselecteerde thermische modi.

Gebaseerd op het inzicht in thermische fouten, verkregen door het gebruik van thermische modale analyse, stellen wij in dit proefschrift twee nieuwe technieken voor om thermische fouten te verminderen. De voorgestelde technieken verminderen de thermische fouten van een systeem door het regelen van de temperatuurverdeling in het systeem. De temperatuurverdeling wordt bij deze technieken geregeld door het toepassen van geregelde externe

warmtebronnen in combinatie met een uniforme en sterke, constante koeling.

De eerste techniek die in dit proefschrift is ontwikkeld, wordt aangeduid met de term Mode Cancellation. Bij Mode Cancellation wordt een gelijk aantal thermische modi in het temperatuurdomein geregeld als het aantal extern gecontroleerde warmtebronnen. Mode Cancellation elimineert een aantal thermische modi uit de temperatuurverdeling in het systeem en elimineert de thermische verplaatsingsvelden gerelateerd aan de geregelde thermische modi in het thermische verplaatsingsdomein van het systeem. De selectie van de thermische modi die worden geregeld, is zodanig gekozen dat deze in het thermische verplaatsingsdomein de grootst mogelijke bijdrage leveren aan de thermische fout. Door het op deze manier beheersen van de temperatuurverdeling van het systeem worden de dominante thermische verplaatsingsvelden gelimineerd en wordt de thermische fout gereduceerd.

De tweede techniek die in dit proefschrift wordt gentroduceerd, wordt aangeduid met de term Modal Control. Modal Control berekent de amplitudes van externe gecontroleerde warmtebronnen door het gebruik van de Linear Quadratic Regulator. Deze methode is ontwikkeld om de belangrijkste beperkingen van Mode Cancellation te overwinnen. Het aantal gecontroleerde thermische modi is bij het gebruik van deze methode niet beperkt tot het aantal externe gecontroleerde warmtebronnen. Dit leidt tot een beter vermogen om thermische fouten te reduceren in vergelijking met Mode Cancellation. Vermijding van matrixsingulariteit in de gevoeligheidsmatrix van de regelaar is bij Modal Control niet vereist, in tegenstelling tot wat het geval is bij Mode Cancellation. Deze eigenschap van Modal Control elimineert de noodzaak van handmatige selectie van de geregelde modi bij Mode Cancellation.

Het is ook aangetoond dat het mogelijk is om de Modal Control-methode uit te breiden en bewegende externe gecontroleerde warmtebronnen te implementeren. In het geval van bewegende externe geregelde warmtebronnen worden de geregelde warmtebronnen dichter bij de bewegende verstorende warmtebron geplaatst en bewegen samen met de verstorende warmtebron over het substraat. Dit resulteert in een verbeterd vermogen tot het reduceren van thermische fouten in vergelijking met de situatie waarbij de externe gecontroleerde warmtebronnen een vaste positie hebben ten opzichte van het substraat, zoals bijvoorbeeld aan elke hoek van het printoppervlak.

Een proefopstelling is daarna ontwikkeld voor experimentele thermische modale analyse en experimentele toetsing van de voorgestelde nieuwe technieken ter reductie van de thermische fouten. Eerst is een proefopstelling voor temperatuurregeling en -meting gebaseerd op thermische modi ontwikkeld en zijn diens eigenschappen gevalueerd en gecorrigeerd. Daarna zijn experimentele metingen van de thermische modes in een vlak substraat uitegvoerd om de thermisch modale analysemethode te toesten.

Na de evaluatie van de proefopstelling is experimentele toetsing van Mode Cancellation en Modal Control uitgevoerd. In beide experimenten is alleen de temperatuurverdeling van het substraat gemeten, mede omdat de relatie tussen temperatuurverdeling en thermische vervorming al goed beschreven is en niet behoort tot het eigenlijke doel van dit proefschrift. De resultaten van de proefopstelling zijn in goede overeenstemming met de gesimuleerde resultaten, zodat de voorgestelde technieken voor het reduceren van thermische fouten succesvol zijn getoetst.

About the Author

Takeshi Morishima was born on 31st May 1980 in Hamakita, Shizuoka, Japan. He studied Precision Engineering and Nuclear Engineering, and received his bachelor degree from the University of Tokyo, Japan, in 2004. His bachelor thesis title was "Effect of laser pulse propagation on ultrafast electronic spin manipulation". He then studied Mechanical Engineering and received his MSc degree from Delft University of Technology, the Netherlands, in 2007. His MSc thesis title was "Design of a non-contact electromagnetic shaker for modal testing of a micro-milling setup with an AMB spindle". After completing his MSc study, he worked as a video game designer for Capcom co., ltd., Japan, from 2007-2010. From May/2010 till May/2014 he worked as a doctoral candidate at Delft University of Technology, the Netherlands under the supervision of Prof.ir. R.H. Munnig Schmidt, Prof.dr.ir. J. van Eijk, and Dr.ir. R.A.J. van Ostayen. His doctoral research topic is the study of thermal errors in precision systems and the development of guidelines for the thermal design of those systems using industrial inkjet printing systems with hot melt ink as the main test bed for this research.

Since July/2014, he started working at ASML Netherlands B.V. as a Technical Business Analyst in the Corporate Intellectual Property department.

Publications

- Takeshi Morishima, Ron van Ostayen, Jan van Eijk, Robert-H. Munnig Schmidt, "Thermal displacement error compensation in temperature domain", Precision Engineering, Vol.42, pp.66-72, 2015.
- T. Morishima, R. van Ostayen, J. van Eijk, R. M. Schmidt, "Development of Transient Thermal Deformation Control Techniques Using Thermal Modal Analysis Based Design Methods", Key Engineering Materials, Vols. 523-524, pp. 750-755, 2012.
- T. Morishima, R. van Ostayen, J. van Eijk, R. Munnig Schmidt, "Reduction of transient thermal deformation in a this plate under moving heat load using thermal modal analysis based control methods",12th int. conf. of Euspen, Stockholm, Sweden, vol.1. pp.448-452, 2012.
- T. Morishima, R. van Ostayen, J. van Eijk, "Reduction of transient thermal errors in precision machines using thermal modal analysis based design methods", JSPE Autumn conf. proc., KAnazawa, Japan, 2011.